Morpho-functional analyses of the primate skeleton: applying 3D geometric morphometrics, finite element analysis and phylogenetic comparative methods to assess ecomorphological questions in extant and extinct anthropoids

A thesis submitted to the University of Manchester for the degree of Doctor of Philosophy in the Faculty of Science and Engineering.

2017

Thomas Puschel Rouliez

School of Earth and Environmental Sciences

TABLE OF CONTENTS

CHAPTER 3:

Analyzing the Sclerocarpy Adaptations of the Pitheciidae

Mandible using Finite Element Analysis and Geometric

Morphometrics   **105**

CHAPTER 4:

The evolution of the platyrrhine talus: A comparative analysis of

the phenetic affinities of the Miocene platyrrhines with their

modern relatives   **147**

CHAPTER 5:

Inferring locomotor behaviours in Miocene New World monkeys using Finite Element Analysis, Geometric Morphometrics and

Word count: 59,758 (including tables)

LIST OF FIGURES

CHAPTER 1:

Introduction

CHAPTER 2:

Standing on the Shoulders of Apes: Analyzing the Form and Function of the Hominoid Scapula using Geometric Morphometrics and Finite Element Analysis

CHAPTER 3:

Analyzing the Sclerocarpy Adaptations of the Pitheciidae Mandible using Finite Element Analysis and Geometric Morphometrics

CHAPTER 4:

The evolution of the platyrrhine talus: A comparative analysis of the phenetic affinities of the Miocene platyrrhines with their modern relatives

CHAPTER 5:

Inferring locomotor behaviours in Miocene New World monkeys using Finite Element Analysis, Geometric Morphometrics and Machine-learning classification techniques applied to talar morphology

LIST OF TABLES

CHAPTER 5:

Inferring locomotor behaviours in Miocene New World monkeys using Finite Element Analysis, Geometric Morphometrics and Machine-learning classification techniques applied to talar morphology

ABSTRACT

Thesis Title: *Morpho-functional analyses of the primate skeleton: applying 3D geometric morphometrics, finite element analysis and phylogenetic comparative methods to assess ecomorphological questions in extant and extinct anthropoids*

Name: Thomas Puschel Rouliez

Institution: University of Manchester

Degree Title: Doctor of Philosophy

Date: December 2017

The overarching objective of this dissertation is to understand the relationship between form and ecological function in diverse skeletal elements belonging to different primate clades using geometric morphometrics (GM), finite element analysis (FEA) and phylogenetic comparative methods (PCMs). GM provides a system for quantifying morphology; while FEA allows measuring biomechanical performance and PCMs are used to model how phenotypic traits have evolved through time. Most chapters in this thesis focus on the association between locomotion and morphology and how to apply this information in the fossil record, while one analyses the form–function relationship in a dietary context. Firstly, a combined approach using FEA and GM is applied to analyse different hominoid scapulae. The obtained results show that there is a significant relationship between scapular shape and its biomechanical performance. Hence at least part of scapular shape variation is due to non-phylogenetic factors. Secondly, it is tested whether there is a sclerocarpic specialization gradient in the mandibular morphology of pitheciids. The results show that there is indeed a relative specialization continuum for some aspects of shape, although the story is more complex from a biomechanical perspective. Subsequently, an analysis of the phenetic affinities of extant platyrrhine tali and their Miocene counterparts is carried out to explain the evolution of talar shape and size in platyrrhines. The results suggest that talar shape diversification can be explained by invoking a model representing a phylogenetic hypothesis in which each platyrrhine family occupied a separate adaptive optimum. Moreover, talar size diversification can be characterised by a multidimensional niche model. Finally, the main locomotor mode of different platyrrhine fossils is inferred by applying a combination of GM, FEA and machine-learning (ML) classification techniques. The ML algorithm applied to both biomechanical and morphometric data categorised most of the fossil sample as arboreal quadrupeds, which is consistent with previous studies. Thus, it is expected to contribute to the understanding of the correlation between form and ecological function, which is not only relevant to appreciate the morphological diversity in extant species, but also because it allows to infer past behaviours in fossil taxa.

DECLARATION

No portion of the work referred to in this thesis has been submitted in support of an application for another degree or qualification of this or any other university or other institute of learning.

COPYRIGHT STATEMENT

I.   The author of this thesis (including any appendices and/or schedules to this thesis) owns certain copyright or related rights in it (the "Copyright") and she has given the University of Manchester certain rights to use such Copyright, including for administrative purposes.

II. Copies of this thesis, either in full or in extracts and whether in hard or electronic copy, may be made only in accordance with the Copyright, Designs and Patents Act 1988 (as amended) and regulations issued under it or, where appropriate, in accordance with licensing agreements which the University has from time to time. This page must form part of any such copies made.

III. The ownership of certain Copyright, patents, designs trade marks and other intellectual property (the "Intellectual Property") and any reproductions of copyright works in this thesis, for example graphs and tables ("Reproductions"), which may be described in this thesis, may not be owned by the author and may be owned by third parties. Such Intellectual Property and Reproductions cannot and must bot be made available for use without the prior written permission of the owner(s) of the relevant Intellectual Property and/or Reproductions.

IV. Further information on the conditions under which disclosure, publication and commercialisation of this thesis, the Copyright and any Intellectual Property and/or Reproductions described in it may take place is available in the University IP Policy (see

http://documents.manchester.ac.uk/_DocuInfo.aspx?DocID=2442), in any relevant Thesis restriction declarations deposited in the University Library, The University Library's regulations (see http://www.manchester.ac.uk/library/aboutus/regulations/) and in the University's policy on Presentation of Theses.

ACKNOWLEDGMENTS

THE AUTHOR

Thomas A. Püschel

Research Interests

My main research focus is primate functional and evolutionary morphology. I apply geometric morphometrics, virtual biomechanical techniques, phylogenetic comparative methods and field research to reconstruct and compare the palaeobiology of extinct primates to their living ecological relatives.

Education

Academic Degree: PhD in Adaptive Organismal Biology

School of Earth and Environmental Sciences, University of Manchester, UK.

Topic: Primate Evolutionary and Functional Morphology

Supervisor: Prof. William I. Sellers

2014-2018

Academic Degree: MSc in Human Evolution with Distinction.

Hull York Medical School, University of York, UK.

Topic: Biomechanics and Geometric Morphometrics

Supervisor: Prof. Paul O'Higgins.

2012-2013

Academic Degree: BSc in Biological Anthropology with Distinction.

Department of Anthropology, Universidad de Chile, Chile.

Topic: Geometric Morphometrics.

Supervisor: Dr. Germán Manríquez.

2007-2011

Scholarships and Grants

1. ECOS-CONICYT scholarship for an Internship in the context of the bilateral cooperation project Ecos-Conicyt "Les découvertes archéologiques de la mission scientifique de Georges de Créqui-Montfort et d'Eugène

Sénéchal de la Grange (1903) dans la nécropole de Calama (Désert d'Atacama), Chili". Laboratory of Dr. Martin Friess, Musée de l'Homme, Muséum d'Histoire Naturelle, Paris. June 2012.

2. Becas Chile. Full Master Scholarship for studies in the MSc in Human Evolution, Hull York Medical School. 2012-2013.

3. Becas Chile. Full PhD Scholarship for studies in the PhD in Adaptive Organismal Biology, University of Manchester. 2014-2018.

4. Synthesis Access Project (European Union-funded Integrated Activities grant). BE-TAF-4459 grant for access to the Royal Museum for Central Africa, Tervuren (BE-TAF) under the SYNTHESYS Project. March 2015.

Refereed Journal Publications

1. Benítez, H.A., Lemic, D., Bažo k, R., Bravi, R., Buketa, M., **Püschel, T.**, 2014a. Morphological integration and modularity in Diabrotica virgifera virgifera LeConte (Coleoptera: Chrysomelidae) hind wings. Zoologischer Anzeiger - A Journal of Comparative Zoology. 253, 461–468.

2. Benítez, H.A., **Püschel, T**., Lemic, D., Čači ja, M., Kozina, A., Bažo k, R., 2014b. Ecomorphological Variation of the Wireworm Cephalic Capsule: Studying the Interaction of Environment and Geometric Shape. PLoS ONE. 9, e102059.

3. Benítez, H.A., **Püschel, T.A.**, 2014. Modelando la Varianza de la Forma: Morfometría Geométrica Aplicaciones en Biología Evolutiva. International Journal of Morphology. 32, 998–1008.

4. Benítez, H.A., Vargas, H.A., **Püschel, T.A.**, 2015. Left–right asymmetry and morphological consequences of a host shift in the oligophagous Neotropical moth Macaria mirthae (Lepidoptera: Geometridae). Journal of Insect Conservation. 1–10.

5. Bucchi, A., **Püschel, T.A.**, Manríquez, G., 2016. Artificial Cranial Modification in San Pedro de Atacama and the Loa Basin: A

Quantitative Approach to Its Role as a Marker of Social Identity. Revista Chilena de Antropología. 34, 19–30.

6. Marcé-Nogué, J., **Püschel, T.A**., Kaiser, T.M., 2017. A biomechanical approach to understand the ecomorphological relationship between primate mandibles and diet. Scientific Reports. 7, 8364.

7. Marcé-Nogué, J., Esteban-Trivigno, S.D., **Püschel, T.A.**, Fortuny, J., 2017. The intervals method: a new approach to analyse finite element outputs using multivariate statistics. PeerJ. 5, e3793.

8. Püschel, H.P., **Püschel, T.A**., Rubilar-Rogers, D., 2017. Taxonomic Comments of a Glossotherium Specimen from the Pleistocene of Central Chile. Boletín del Museo Nacional de Historia Natural, Chile. 66, 223–262.

9. **Püschel, T**., 2014. Modularidad e Integración Morfológica en Cráneos Humanos: un Enfoque Morfométrico Geométrico. International Journal of Morphology. 32, 299–304.

10. **Püschel, T.A**., Benítez, H.A., 2014. Femoral Functional Adaptation: A Comparison Between Hunter Gatherers and Agriculturalists Using Geometric Morphometrics. International Journal of Morphology. 32, 627–633.

11. **Püschel, T.A**., Espejo, J., Sanzana, M.-J., Benítez, H.A., 2014. Analysing the Floral Elements of the Lost Tree of Easter Island: A Morphometric Comparison between the Remaining Ex-Situ Lines of the Endemic Extinct Species Sophora toromiro. PLoS ONE. 9, e115548

12. **Püschel, T.A.**, Gladman, J.T., Bobe, R., Sellers, W.I., 2017. The evolution of the platyrrhine talus: A comparative analysis of the phenetic affinities of the Miocene platyrrhines with their modern relatives. Journal of Human Evolution. 111, 179–201.

13. **Püschel, T.A**., Sellers, W.I., 2016. Standing on the shoulders of apes: Analyzing the form and function of the hominoid scapula using geometric morphometrics and finite element analysis. American Journal of Physical Anthropology. 159, 325–341.

14. **Püschel**, TA, Marcé-Nogué J, Kaiser T, Brocklehurst R, Sellers, WI. Under review. Sclerocarpy Adaptations of the Pitheciidae Mandible: Analyzing the Morpho-functional Consequences of Seed Predation in

the Pitheciid lower Jaw using Finite Element Analysis and Geometric Morphometrics.

Book Chapters

1. Manríquez, G., **Püschel, T.A.**, Flores, S., González, T., Moraga, M., Rothhammer, F., 2016. Origen y evolución de la población chilena: el punto de vista biológico. In: Fallabela, F., Uribe, M., Aldunate, C., Hidalgo, J. (Eds.), Prehistoria en Chile: Desde sus Primeros Habitantes hasta los Incas. Editorial Universitaria.

"Parts and wholes evolve in consequence of their relationship, and the relationship itself evolves. These are the properties of things that we call dialectical: that one thing cannot exist without the other, that one acquires its properties from its relation to the other, that the properties of both evolve as a consequence of their interpenetration".

Richard Levins and Richard Lewontin, *The Dialectical Biologist* (1985)

CHAPTER 1

Introduction

INTRODUCTION

Understanding the evolution and ecology of animals and advancing predictions regarding particular behaviours in extant and extinct taxa involves an appreciation of the exact relationship between form and function which has always been challenging to ascertain (Benton, 2010). For a long time many authors have attempted to predict function from form in biological contexts (Borelli, 1680; Thompson, 1942; Alexander, 1971, 1983; Lauder, 1995; Alexander, 2006; Hutchinson, 2012; O'Higgins et al., 2017) and yet even nowadays there is no straightforward answer available (Pearson and Lieberman, 2004; Riggs et al., 2004). This is partly because there is no univocal relationship between the form and function of a biological structure, but also due to the many factors that interplay in this relationship (Bertram and Swartz, 1991; Pearson and Lieberman, 2004; Ruff et al., 2006; Barak et al., 2011). Given the inherent difficulty of this topic, to elucidate the association between form and function in an ecological and evolutionary context it is necessary to coherently apply a combination of diverse methods derived from several disciplines such as evolutionary biology, quantitative genetics, biomechanics, phylogenetic comparative techniques, multivariate statistics, ecology, among others (Polly et al., 2016).

Analysing the correlation between form and ecological function is not only relevant to understand the morphological diversity observed in extant species, but also because it allow us to infer past behaviours in palaeobiological contexts (Elton et al., 2016). This is particularly important when analysing skeletal morphology since any behavioural reconstruction derived from osteological data relies in the idea that bone is functionally adapted to its mechanical environment during life and that its shape also reflect evolutionary functional adaptations (Lieberman, 1997). So far, several approaches have been applied to understand the relationship between form and function in skeletal structures (e.g. Harcourt-Smith, 2002; Carter and Beaupre, 2007; Curtis et al., 2011; Bookstein, 2013; O'Higgins and Milne, 2013; Esteve-Altava and Rasskin-Gutman, 2014). Among them, the combined approach of geometric morphometrics (GM) and finite element analysis (FEA) is considered among the most promising ones (Pierce et al., 2008; Cox et al., 2011; O'Higgins et al., 2011; Parr et al., 2012; O'Higgins and Milne, 2013; Tseng, 2013; Toro-Ibacache et al.,

2016; O'Higgins et al., 2017). However, it still unclear how to properly combine or jointly apply these two methods in evolutionary contexts (Bookstein, 2013; Polly et al., 2016).

Although the present dissertation does not provide a definite answer to this question it advances some possible approaches by developing different examples of how to combine GM and FEA in evolutionary contexts using primate skeletal elements as biological case studies. Primates are arboreal, terrestrial, nocturnal, diurnal, and cathemeral, and live in several biomes from rainforests to deserts (Napier and Napier, 1967; Strier, 2006). As a result of the broadly varying demands and constraints of these diverse ecological niches, primate behaviours are congruently complex, plastic and diverse (Napier and Napier, 1967; Fleagle, 1998; Strier, 2006; Thorpe, 2016), which means that the relationship between a particular morphology and certain behaviour might not be that straightforward. Therefore, it is particularly relevant to understand how primate form reflects adaptation to specific environmental contexts and how these particular morphologies evolved, since they represent a particularly challenging and interesting case study (Thorpe, 2016).

Consequently, the overall objective of this dissertation is to understand the relationship between form and ecological function in diverse skeletal elements belonging to different primate clades taking into account their phylogenetic relatedness and using state-of-the-art *in silico* techniques. The different chapters of this thesis all aim to provide an understanding of the role of functional performance in the evolution of morphological form in different anthropoid groups and ascertain the influence of ecological function on skeletal morphology. My approach is characterised by the combination of GM to quantify shape, FEA to analyse function, and phylogenetic comparative methods (PCMs) to contextualise the obtained results in an evolutionary and ecomorphological framework. This allows me to explicitly test hypotheses regarding the role of functional factors in the evolution of morphological diversity. Most chapters in this thesis focus on the association between locomotion and morphology and how to apply this information to the fossil record, while one of them examines the form–function relationship in a dietary context. In addition, there is one chapter that also deals with the application

of machine-learning (ML) classification algorithms to infer fossil locomotion.

The objective of the Second Chapter is to explore a combined approach using FEA and GM to analyse the biomechanical performance of different hominoid scapulae. It has been shown that the evolution of shoulder mobility can be regarded as an important evolutionary process generating locomotor diversity in primates (Larson, 1998; Chan, 2007). This is of particular relevance among hominoids because within this group five divergent locomotion modes and associated body plans have evolved (Preuschoft, 2004). Provided that the scapula is both biomechanically and anatomically involved in the function of the shoulder and the movement of the arm (Kibler and McMullen, 2003), in this first chapter some basic biomechanical scenarios are simulated. In addition, scapular morphology is quantified and the association between form and function is analysed using phylogenetic comparative methods. This approach could provide a better understanding of the association between hominoid scapular morphology and its biomechanical performance.

In the Third Chapter, the aim is to investigate a specific dietary specialization observed in a lineage of New World monkeys, which are the Pitheciids. This group stands out among platyrrhines because they specifically predate seeds (Kay et al., 2013). This dietary specialization is known as sclerocarpy and involves using anterior dentition to separate seeds from the surrounding hard tissues, followed by their mastication (Kinzey, 1992). It has been proposed that *Callicebus–Pithecia–Chiropotes-Cacajao* represent a morphocline of increasingly specialized anatomical traits for sclerocarpic foraging (Kay, 1990; Kinzey, 1992; Rosenberger, 1992; Meldrum and Kay, 1997). However, this has neither been biomechanically tested in this lineage, nor has the association between mandibular shape and mastication performance been analysed. Using FEA and GM it is tested whether there is a sclerocarpic specialization gradient in the mandibular morphology of pitheciids as it has been previously suggested.

The Fourth Chapter focuses on the morphological evolution of the platyrrhine talus. New World monkeys are a diverse group of primates that inhabit a broad range of tropical-equatorial environments in the Americas (Rylands and Mittermeier, 2009). Whilst the modern day success of the group is clear, the

evolutionary history of these lineages is still highly debated (Youlatos and Meldrum, 2011). Even though the fossil record of New World monkeys has improved considerably in recent years (e.g. Bond et al., 2015; Bloch et al., 2016; Marivaux et al., 2016b, 2016a), tracing the origin of major modern clades is still a difficult task. The most commonly preserved post-cranial element in the platyrrhine record is the talus (Tejedor, 2008), hence its importance. Additionally, it has been shown that its morphology could reflect postural and locomotor adaptations based on its central position in the foot as well as its functional relationship with other foot bones (Lisowski et al., 1974; Yapuncich and Boyer, 2014; Yapuncich et al., 2015). For this reason, the Third Chapter analyses the phenetic affinities of extant platyrrhine tali and their Miocene counterparts, which is carried out using GM, extant locomotor data and a series of phylogenetic comparative analyses. All this allows understanding the evolution of talar shape and size in platyrrhines. Additionally, body mass predictions for the analysed fossil sample were also computed using the available articular surfaces. The results obtained from these analyses allowed advancing possible evolutionary mechanisms involved in talar shape and size evolution, as well as to infer locomotor behaviours and body mass in the fossil sample.

As outlined above, talar morphology can provide information about postural adaptations because it is the anatomical structure responsible for transmitting body mass forces from the leg to the foot, as well as providing stability and mobility throughout most postural and locomotor behaviours (Boyer et al., 2015). Therefore, the aim of the Fifth Chapter is to test whether the locomotor behaviour of fossil platyrrhines could be inferred from their talus morphology and biomechanical performance. To test this possibility the same extant sample of platyrrhines was classified into three different locomotor categories and then talar strength was compared between the different locomotion categories using FEA to simulate a static scenario. Subsequently, talar morphometric data was collected and analysed using GM to distinguish between locomotor modes. The association between talar shape and biomechanical function was tested using a phylogenetic version of partial least squares analysis. Finally, several ML algorithms were trained using both the biomechanical and morphometric data from the extant sample in order to infer the possible locomotor behaviour of the Miocene fossil sample. This Chapter shows that a combined approach using FEA, GM and ML algorithms, can contribute in

the understanding of platyrrhine talar morphology and its relationship with locomotion. Furthermore, it is proposed that this approach is likely to be beneficial for determining locomotor habits in other vertebrate taxa.

Finally, the following subsection is devoted to provide some key terminology necessary as background information, such as defining ecomorphology, as well as succinctly introducing the group under study (i.e. primates and more specifically anthropoids) and summarising the different methods used in the present dissertation.

1.1 Ecomorphology

Ecomorphology or ecological morphology can be defined as the characterisation of the adaptive relationship between the morphology of an organism and its ecological role (Soligo and Smaers, 2016). Ecomorphological studies try to relate the function and structure of organisms with relevant aspects of their environment (Losos and Miles, 1994), while their scope encompasses adaptation, morpho-functional evolution, convergence, form-function correlations and community organization (Wainwright and Reilly, 1994). Since its conception as a sub-discipline, several studies have shown different relationships between form, function and ecology in numerous animal groups (e.g. Williams, 1972; Losos, 1990; Leisler and Winkler, 1991; Motta and Kotrschal, 1991; Winemiller, 1991; Bock, 1994; Wainwright and Reilly, 1994; Fortuny et al., 2011; Vizcaíno et al., 2011), including primates (e.g. Cartmill, 1972; Fleagle, 1977; Rodman, 1984; Hunt, 1991, 2004; Sussman, 1991; Norconk et al., 2013).

The ecomorphological framework is based on the idea that morphology is an accurate and predictable reflection of an animal's behaviours and ecology (Thorpe, 2016). The general notion that mechanical loadings influence bone structure has been acknowledged for almost a century in what is commonly referred as 'Wolff's Law', even though several later authors have pointed out that its original meaning was to certain extent different (Lieberman et al. 2004; Ruff et al. 2006; Ruff 2008). For this reason, it has been proposed to replace the term with the more precise 'bone functional adaptation' (Ruff et al. 2006). It is now accepted that the ultimate

form of a bone is dependent upon extra constraints, in addition to the mechanical loadings to which it is subjected (Pearson and Lieberman, 2004). Non-functional influences acting on skeletal form such as disease, age, circulating hormones, genetic drift, phylogeny, etc. might obscure the relationship between ecological function and morphology (Pearson and Lieberman, 2004; Ruff et al., 2006; Barak et al., 2011). However, it is also known that there are also many frequently interacting functional demands such as postural behaviour, locomotion, diet, thermoregulation, social behaviour, among others, which certainly influence bone shape and size (Elton et al., 2016), thus enabling the 'ecomorphological agenda'.

Consequently, it is particularly interesting to examine how morphology reflects adaptation to a specific environmental context (i.e. the functional consequences which are enabled by a specific morphology), but also to understand how these specific morphologies influence the environment where they are being expressed (i.e. the ecological role an organism in its environment given its phenotype) (Soligo and Smaers, 2016). Morphological evolution results from both selective and random processes acting on a certain phenotype, which are channelled by genetic, developmental, mechanical, and physical constrains (Raff, 1996). Analysing function is crucial as it influences selection, since fitness is at least partially determined by the overall functional performance of a certain morphology in a particular ecological context (Endler, 1986; Arnold, 2003; McGill et al., 2006; Charmantier et al., 2014).

All chapters of the present dissertation analyse ecomorphological questions in different primate skeletal elements. Most of them deal with the association between form and function in locomotor contexts. Chapter 2 focuses on hominoid scapular functional morphology, while Chapters 4 and 5 analyse the evolution of the platyrrhine talus and the link between its morphology, locomotor behaviour and biomechanical performance. Chapter 3 does not focus on locomotion, but it analyses a specific dietary ecomorphological adaptation by studying the mandibular morphology of the Pitheciidae and its association with stress data.

1.2 Primates

The animal group under study in this dissertation is the order Primates and more specifically anthropoids. Therefore the following section briefly characterises both primates and anthropoids to provide a basic context.

1.2.1 Primate classification

The mammalian order Primates has always captivated our imagination as humans, probably because it is quite easy to notice morphological and behavioural similarities that evidence our shared ancestry (Aiello and Dean, 1990; Fleagle, 2013). Extant primates are quite diverse, with more than ~ 600 species recognised by the IUCN https://www.iucn.org/ (Rowe and Myers, 2016), ranging in size from minuscule mouse lemurs (30 g) to large gorilla silverbacks (200,000 g) (Jungers, 2013). Primates are relatively well-defined when compared to other mammalian orders, with some key sets of traits considered to be exclusive of this group (Silcox et al., 2015). This includes features such as grasping hands with nails on all or most digits (i.e. relatively long hand and foot phalanges, divergent thumb and big toe), common leaping specializations (e.g. long hind limbs ending in modified ankle bones), developed visual system (i.e. large eyes, convergent orbits, postorbital bar, increased visual cortex), decreased olfactory capabilities, and dental characters mostly associated with frugivory (e.g. bunodont molars) (Aiello and Dean, 1990; Fleagle, 2013a; Gebo, 2014).

Extant primates are currently classified into two main groups: the Strepsirrhini, comprising lemurs, galagos, and lorises, and the Haplorrhini containing tarsiers and anthropoids (i.e. New and Old World monkeys and apes) (Fleagle, 2013a). Fossil primates were also extremely diverse, with some species smaller than mouse lemurs (e.g. middle Eocene Shanghuang primate species; Gebo et al., 2000) (or larger than any living primate (e.g. *Gigantopithecus blacki*; Simons and Ettel, 1970). Many of these fossils have been classified into the current taxonomic consensus, thus providing highly relevant information about the particular evolution of different lineages within this order. However, there are still many fossil taxa that have not been classified, hence sparking intense debates about their possible phyletic relationships

(Cachel, 2015). The earliest stage of the evolution of primates is still subject of intense research, with studies constantly carried out and new materials being discovered with relatively high frequency. Diverse review articles offer background information regarding primate's early evolution (e.g. Cartmill, 1992; Ross, 2000; Sussman et al., 2013; Silcox et al., 2015), but it is such an active area of research that most of those reviews cannot keep up with the pace of investigations and volume of new discoveries. For this reason, the following summary will be based mostly on consensus ideas.

1.2.3 Primates within Mammalia

The use of modern phylogenetic inference tools using genetic data has revolutionised our understanding about the inter-ordinal relationships among Mammalia. Molecular analyses tend to show that the order Primate seems to be closely related to Scandentia and Dermoptera, thus comprising a group known as Euarchonta (Waddell et al., 1999), which is closely related to Glires (i.e. the supraordinal grouping including rodents and lagomorphs), hence conforming a group now recognised as Euarchontoglires (Murphy et al., 2001). It is important to point out that even though most of these new taxonomic classifications are based on molecular data and analyses, one of the largest studies carried out analysing mammalian morphological data found mostly consistent relationships with the molecular classification mentioned above (O'Leary et al., 2013).

1.2.4 Earliest primates
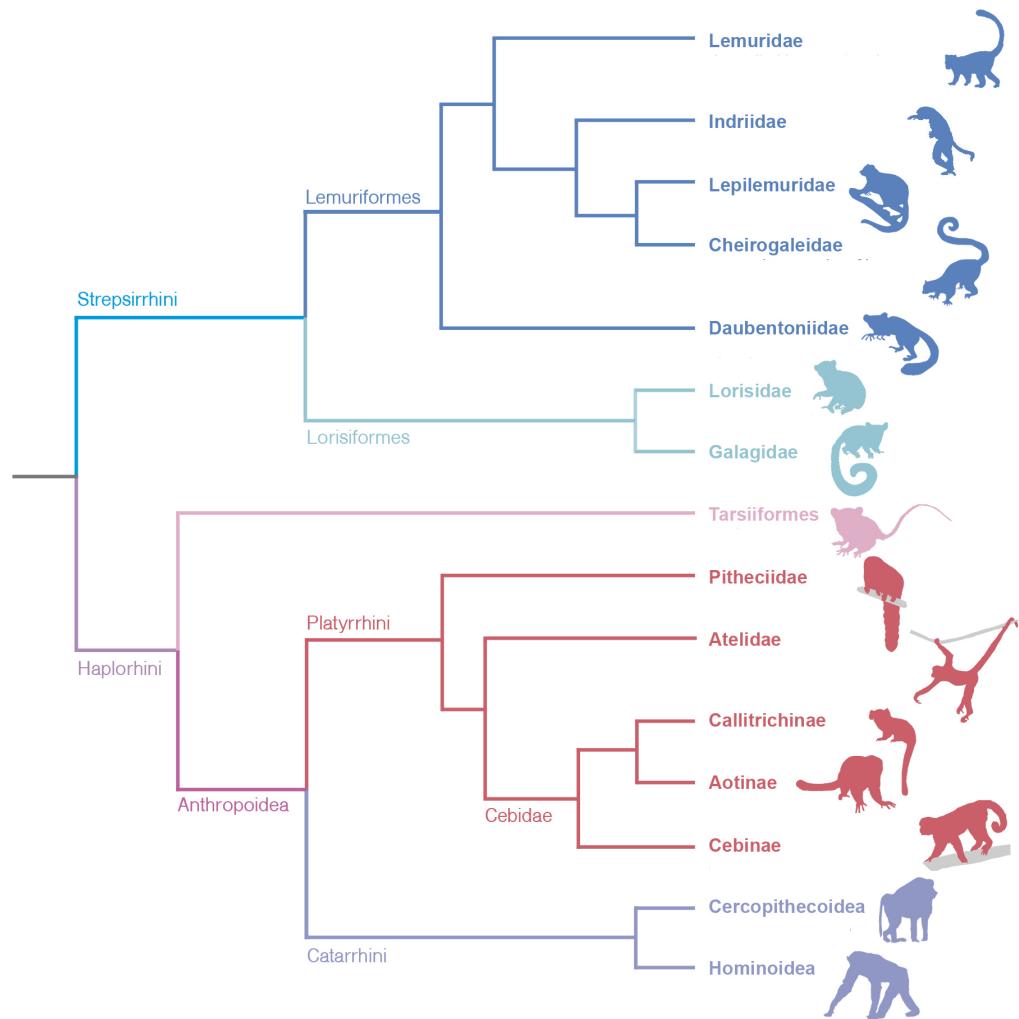
Fossil record

Omomyoidea and Adapoidea are two fossil groups that appear near the start of the Eocene ∼55.8 million mya across Laurasia (Ni et al., 2004; Smith et al., 2006; Beard, 2008; Rose et al., 2011, 2012). They exhibit all (or most) of the diagnostic traits of living primates including features such as the postorbital bar and digits tipped with nails. There is still a lively debate regarding the relationships between these two groups and with respect to Primates (e.g. Franzen et al., 2009;

Gingerich et al., 2010; Williams et al., 2010). Nonetheless, there is relative consensus that they both are within Primates or Euprimates (Robert Hoffstetter, 1977). Omomyoids have been broadly characterised as tarsier- or galago-like (i.e., nocturnal animals with leaping specializations), whilst adapoids have been interpreted as being relatively lemur-like (i.e. frequently larger and showing a diversity of arboreal locomotor behaviours) (Fleagle, 2013a).

Molecular analyses

Several molecular studies (e.g. Springer et al. 2003, Meredith et al. 2011) suggest an origin of Primates well back in the Cretaceous, much earlier than the earliest primate or euprimate fossil. A possible cause for this conflict is that earlier primates are simply not being recognized because of their primitive morphology (Silcox et al., 2015). However, as molecular clock estimates have been refined, the estimates for the origin of Euprimates have come closer to the dates from the fossil record. Indeed, Springer et al. (2012) put the age of the last common ancestor of living primates between 71 and 63 mya, implying that the group could have originated in the Paleogene, which is more concordant with the fossil record. Figure 1.1 provides a phylogenetic hypothesis of the order Primates based on Springer et al. (2012), while the taxonomic groupings are displayed according to Fleagle (2013).

Figure 1.1 Phylogeny for extant primates based on Springer et al. (2012).

1.2.5 Anthropoidea

Anthropoidea (i.e. simians, infraorder Simiiformes) was recognized as a natural group by Carl von Linné (1707-1778) who classified Simia (monkeys and apes) as one of four divisions of his first mammalian order Primates (i.e. animals with four parallel upper incisors and two pectoral mammae). Several morphological, behavioural and ecological traits distinguish the anthropoids from the rest of the primates. These features are currently interpreted as synapomorphies defining this clade. Furthermore, diverse functional and/or adaptive interpretations of these synapomorphies have been advanced in order to propose explanations regarding the origins of the anthropoids (Cartmill, 1980; Ross, 1996; Kay et al., 1997). Diverse investigations have provided new evidence about the phylogenetic relationships of early anthropoids, as well as about the functional significance of the different anthropoid synapomorphies (Gebo, 1986; Fleagle and Kay, 1994; Kay et al., 1997; Ross, 2000; Gunnell and Miller, 2001).

Anthropoid monophyly is pretty much universally accepted (Delson and Rosenberger, 1980; Hoffstetter, 1980; Rosenberger, 1986; Martin, 1993; Kay et al., 1997; Ross et al., 1998; Gunnell and Miller, 2001; Szalay and Delson, 2013), and the Early Oligocene Parapithecidae are considered by most to represent a sister taxon of the crown group of the anthropoids (Delson, 1975; Hoffstetter, 1977; Fleagle and Kay, 1987; Harrison, 1987). The late Eocene–early Oligocene Oligopithecidae are considered by some researchers to represent early catarrhines (e.g. Miller and Simons, 1997; Simons et al., 1999), while others (e.g. Ross et al., 1998) place them further down the anthropoid stem. There is still no consensus regarding the phylogenetic relationship and position of Pondaungidae (Ducrocq, 1999), because some researchers consider this group to be located between the Oligopithecidae and the Parapithecidae (Ross, 2000), while others regard them as crown anthropoids (Chaimanee et al., 1997; Ducrocq, 1999). Until it is resolved which is the phylogenetic position of this group, the current consensus position regards the Propliopithecidae as the oldest definitive catarrhines (Harrison, 2013).

There still disagreement when it comes to the phylogenetic relationship between the Oligopithecidae and Parapithecidae in relation to platyrrhines and catarrhines (Ross

et al., 1998; Ross, 2000). Two main monophyletic groups are widely recognised, the Propliopithecidae and the Parapithecidae (Ross, 2000). Oligopithecids are considered to either represent primitive members of the Propliopithecidae, thus true catarrhines, possibly ancestral to later cercopithecoids and hominoids (Simons and Rasmussen, 1994). Others think that they are actually stem anthropoids (Ross et al., 1998). The Parapithecidae are now regarded by most as being a sister clade of all anthropoids (i.e. extant and extinct) (Hoffstetter, 1977; Fleagle and Kay, 1987; Harrison, 1987).

Platyrrhines

Currently, a source of difficulties in platyrrhine palaeontology is the scarcity of available data from the Eocene and Oligocene. Most platyrrhine fossils have been dated to the Miocene or the Pleistocene of South America and the Caribbean (Rímoli, 1977; MacPhee et al., 2003; Kay and Cozzuol, 2006; Tejedor et al., 2006; Fleagle et al., 2012; Perkins et al., 2012). Nevertheless, there are remarkable exceptions from Bolivia and Peru (Hoffstetter, 1969, p. 19; Wolff, 1984; Rosenberger et al., 1991; Takai and Anaya, 1996; Takai et al., 2000; Kay et al., 2002; Bond et al., 2015). Most of the fossils are composed of fragmentary dental remains, with several species such as *Branisella boliviana* (Hoffstetter, 1969), *Mohanimico hershkovitzi* (Luchterhand et al., 1986), *Szalatavus attricuspis* (Rosenberger et al., 1991), *Solimoea acrensis* (Kay and Cozzuol, 2006), *Insulacebus toussainatiana* (Cooke et al., 2011), *Perupithecus ucayaliensis* (Bond et al., 2015), *Panamacebus transitus* (Bloch et al., 2016) and *Canaanimico amazonensis* (Marivaux et al., 2016a), being classified based on limited dental traits. Interestingly, the Eocene species *Perupithecus ucayaliensis* found in Peru bear striking resemblances to Eocene African anthropoids (Bond et al., 2015). Bond et al. (2015) suggest that *Perupithecus* would be nested within a Late Eocene (38 to 34 mya) African anthropoid group comprising *Catopithecus, Proteopithecus,* and *Talahpithecus.* However, in spite of their morphological resemblance, others have disputed this proposal (see Kay, 2015 for a discussion) since *Proteopithecus* is normally classified as a parapithecoid, while *Catopithecus* and *Talahpithecus* are recognised most of the time as oligopithecids. Despite this controversy, most of the available evidence including molecular analyses strongly points that Africa was the most likely source of the protoplatyrrhine immigration. Modelling approaches have

suggest that somewhere between 40 and 30 myr, the time when the Fayum sediments were being laid down, a primate of ~1,000 g could have crossed the Atlantic on a 'floating island' (Houle, 1999).

Extant platyrrhines or New World Monkeys (NWM) inhabit a diverse range of habitats in the Americas (Fleagle, 2013b). The occupation of these niches has been accompanied by distinct behavioural, locomotor, morphological, and ecological adaptations in each one of the main platyrrhine clades (Ford and Davis, 1992; Rosenberger, 1992; Fleagle and Reed, 1996; Fleagle et al., 1999; Rosenberger, 2002; Youlatos, 2004; Rosenberger et al., 2009). The Pitheciidae (*Callicebus, Pithecia, Chiropotes, Cacajao*) are characterized by their peculiar adaptions to sclerocarpy, exhibiting evident modifications of the cranium, mandible, dentition, cranial musculature and viscera to predate seeds (Kinzey, 1992; Norconk and Veres, 2011; Kay et al., 2013; Ledogar et al., 2013; Norconk et al., 2013), as well as being canopy dwellers, which move mostly quadrupedally with variable rates of suspension and leaping (Youlatos and Meldrum, 2011). The Atelidae (*Ateles, Alouatta, Lagothrix, Brachyteles*), comprise the largest NWM which are characterized by their occupation of the upper canopy layers and their diet being composed mostly by fruits and leaves (Campbell, 2008). One of their most distinct traits is their highly specialized locomotion that often employs climb/clambering and suspensory behaviours, frequently aided by the use of their prehensile tails (Rosenberger and Strier, 1989; Strier, 1992). The Cebidae encompass two morphologically and behaviourally distinct groups. The Cebinae (*Cebus, Saimiri*) correspond to medium-sized inhabitants of all forest strata. They represent the most encephalized NWM, showing particularly complex behaviours, foraging on both fruits and animal preys via manipulative behaviours, and moving via quadrupedalism and leaping (Janson and Boinski, 1992; Fragaszy et al., 2004). Finally, the Callitrichinae (*Callithrix, Cebuella, Leontopithecus, Saguinus, Callimico, Mico*) are miniature monkeys characterized by several unusual traits, such as being the only primate group that often gives birth to twins, as well as exhibiting high levels of male parental care (Ford, 1980). Besides their extremely reduced size, they also show other uncommon morphological features, such as claws instead of nails and the loss of their third molar (excepting *Callimico*) (Ford et al., 2009). Callitrichines occupy diverse levels of strata and many

forests types, exhibiting a diet based on gums and arthropods and moving along using quadrupedalism, leaping and clawed scansorial locomotion (Garber, 1992).

In the present dissertation both extant and extinct platyrrhines are the group under study in the Fourth and Fifth Chapters, where different analyses are applied to study their talar morphological data to get an insight into the evolution of this anatomical structure, as well as its relationship with locomotion. In the Third Chapter the Pitheciidae mandible is analysed to biomechanically test hypotheses regarding a particular ecomorphological adaptation to seed predation known as sclerocarpy.

Catarrhines

From paleontological evidence it has been suggested that the first appearance of early catarrhines occurred in Afro-Arabia during the Early Oligocene (dating to about 29–32 mya), before their migration to Eurasia during the Miocene (~17-18 mya) (Andrews et al., 1996; Harrison and Yumin, 1999; Harrison, 2005). For catarrhines and platyrrhines, the estimated molecular divergence date suggests that catarrhines may have had an even earlier phylogenetic history that can be traced back to the Middle Eocene (~40-44 mya) (Chatterjee et al., 2009). During this period numerous clades of catarrhines originated, including the Propliopithecoidea, Pliopithecoidea, Saadanioidea, Dendropithecoidea, Cercopithecoidea and Hominoidea.

These lineages separated before the last common ancestor of hominoids and cercopithecoids, being commonly known as stem catarrhines (Harrison, 2013). Except Eurasian Pliopithecoidea, all of them were confined to Afro-Arabia, and range in age from 32 to 7 mya (late Oligocene to late Miocene). In the past, some Eocene and Early Oligocene anthropoids from the same region were proposed as early catarrhines (Rasmussen, 2002), such as for instance the parapithecoids and oligopithecids. Nevertheless, new evidence suggests that these taxa are in fact stem anthropoids which diverged before the last common ancestor of both platyrrhines and catarrhines (Fleagle and Kay, 1987; Harrison, 1987; Kay et al., 1997; Ross et al., 1998; Beard, 2002; Kay et al., 2004; Seiffert et al., 2005, 2010). The earliest widely

accepted record of fossil catarrhines is represented by the propliopithecoids from the Early Oligocene (~ 29–32 mya) of Egypt (Zalmout et al., 2010).

Extant catarrhines are the result of two distinct radiations with their own characteristic evolutionary histories (i.e. cercopithecoids and hominoids) (Raaum et al., 2005; Pozzi et al., 2014). In taxonomical terms Cercopithecoidea (i.e. Old World monkeys) are the more diverse and successful of extant catarrhines at least in view of the number of species and its diversity (Whitehead and Jolly, 2000; Fleagle, 2013). Cercopithecoid monkeys currently inhabit most of Africa and Asia, however it is now also clear that they also occupied some parts of Europe in the recent past (Modolo et al., 2005). The Old World monkeys can be characterise in two very distinct groups which are classified into two subfamilies: the cercopithecines and the colobines (Napier and Napier, 1967). It has been argued that when compared to either platyrrhines or strepsirrhines, catarrhines seem to be a comparatively uniform group regarding a variety of morphological and behavioural aspects, probably due to the recentness of their adaptive radiation (Harrison, 2013). Nonetheless, both lineages have experienced extensive adaptive radiations and are also composed of numerous genera and species (Herrera, 2017). The colobines are predominantly leaf and seed eaters of Africa and Asia, represented by two major groups: the colobus monkeys of Africa (Colobini) and the langurs of Asia (Presbytini) (Davies and Oates, 1994; Kirkpatrick, 2016). Yet genetic and phylogenetic relationships within and between African and Asian colobines are very intricate, probably reflecting a complex history of hybridization (Roos et al., 2011; Wang et al., 2012). The cercopithecines on the other hand, are a predominantly African group of fruit eaters represented by a single extremely successful genus in Asia and Europe (i.e. *Macaca*) (Morales and Melnick, 1998) and two distinct clades of African cercopithecines: the larger papionins (i.e. macaques, mangabeys, mandrills, geladas, and baboons) (Zinner et al., 2011, 2013) and the smaller cercopithecines (i.e. guenons, vervets, grivets, patas and talapoin monkeys) (Glenn and Cords, 2002). They exhibit a complex phylogenetic history that is reflected in the variety of alternative taxonomies proposed to resolve these relationships (Tosi et al., 2005; Sargis et al., 2008).

Hominoids are the less taxonomically diverse group of living catarrhines (Fleagle, 2013), being distinguished from the rest of the Old World monkeys by a variety of both primitive catarrhine features and unique specializations, particularly in aspects related to many aspects of their behaviour and ecology, as well as their life history (Hill and Ward, 1988; Hunt, 1991b; Benefit and McCrossin, 1995). There are only five genera of extant hominoids that are categorised in two families: hylobatids (i.e. siamangs and gibbons) and hominids (i.e. orang-utans, gorillas, chimpanzees, bonobos and humans) (Pilbeam, 1996). They have an interesting fossil record that starts probably around the latest part of the Oligocene and Early to Middle Miocene, with evidence of an extensive radiation of ape-like catarrhines that have been traditionally placed in one superfamily known as the proconsuloids (Fleagle, 2013). Subsequently, there is dissimilar fossil record for the different hominoid groups with an increasingly complex evolutionary history (Begun, 2015). Even though the phylogenetic relationships among the extant taxa are mostly well resolved since there is high quality genomic data for the majority of the hominoid genera (Costa et al., 2016).

Hominoids are the group under study in the Second Chapter of this thesis, which aims to analyse the association between scapular form and function in hominoids. This is relevant because it has been proposed that the evolution of shoulder mobility is one of the important evolutionary processes generating the locomotor diversity observed in different primate lineages.

1.3 Methods applied in the present dissertation

Since an important part of the present dissertation deals with how to jointly apply GM, FEA and PCMs in ecomorphological contexts, a brief description of these methods will be provided in the following subsection. In addition, the Fifth chapter of this dissertation also applies ML techniques to infer locomotion in a fossil platyrrhine sample, so a succinct characterisation of this group of methods is also included.

1.3.1 Finite element analysis

Finite Element Analysis (FEA) is a general modelling technique that can be used for structural, thermal, fluid, and acoustic analyses, amongst others (Zienkiewicz et al., 2005). It is a computational technique which applies the finite element method that when used to deal with structural problems, allows the computation of the mechanical response of a structure to different simulated loads and constraints and with defined material properties (Zienkiewicz et al., 2005). FEA acts by dividing a structure into a finite number (normally thousands or millions) of discrete elements with well-known mathematical properties (e.g., triangles, tetrahedrons or cubes) (Beaupré and Carter, 1992). If the geometry of an object is simple enough, applying analytical solutions can solve strain and stress (Richmond et al., 2005). However, more complex shapes (such as the ones observed in most biological cases) might be difficult or even impossible to solve using analytical means, especially if the loading scenarios or material properties are complex (Richmond et al., 2005). Therefore, FEA offers an alternative approach by approximating the solution via the subdivision of complex geometries into multiple finite elements of simpler geometry. After virtually applying forces to the structure under analysis the displacements of the nodes are computed, which are are then converted into strains, and ultimately used to calculate stresses (Marcé-Nogué et al., 2017a).

FEA has been used in engineering (with particular emphasis in mechanical engineering) for a long time, with applications to biological structures particularly in the field of bioengineering, implantology and orthopaedic medicine (e.g. Huiskes and Chao, 1983; Geng et al., 2001; Trivedi, 2014; Taylor and Prendergast, 2015). FEA has attracted attention of organismal biologists and especially palaeontologists, as it allows analysing the mechanical behaviour and performance under simulated biomechanical scenarios of not only extant species, but also fossils, as well as modern species in which experimentation is not allowed due to ethical, conservation and/or access reasons (Spears and Crompton, 1994; Richmond et al., 2005; Rayfield, 2007; Panagiotopoulou, 2009; Bright, 2014). Most of the studies in organismal biology have focused in the vertebrate skull, jaw and teeth (e.g. Kupczik et al., 2007; Pierce et al., 2009; Gröning et al., 2011; Rayfield, 2011; Tseng, 2013; Figueirido et al., 2014), although more recently several studies have applied FEA to

analyse aspects of the postcranial skeleton (Ogihara et al., 2003; Piras et al., 2012, 2015; Püschel and Sellers, 2016).

The FEA workflow starts by capturing the geometry of the structure under analysis, in 2D or 3D, but planar models have been also used (i.e. '2D model' with constant thickness) (Marcé Nogué et al., 2013). Depending on the desired dimensionality different methods are available to capture morphological data. 2D FE models are commonly generated using photographs, outlines or even drawings (Marcé Nogué et al., 2013), whilst 3D FE models are usually obtained from CT-scans, magnetic resonance imaging, photogrammetry, among other options (Ross, 2005). In cases with a limited access to the specimen of interest or when it is not possible to scan it due to any limitations, it has been even proposed that models could be generated from simple shapes and then CAD software could be used to modify these shapes until the desired morphology is achieved (i.e. Box modelling) (Rahman and Lautenschlager, 2016). 3D volumetric models obtained from methods that allow obtaining internal geometry have the advantage of enabling modelling of both the external and internal morphology of the structure under analysis (e.g. trabecular structure, cavities, sinuses, osteological thickness), which are factors that might influence the mechanical behaviour of an structure or might be relevant for certain studies (Fagan et al., 2007). However, it has been shown that when FEA is applied to specimens with unknown internal architecture, it still can produce reliable results, even when the internal bone architecture cannot be modelled in detail, because probably most of the stiffness in a structure depends on its external morphology (Fitton et al., 2015).

After obtaining the model, the digital area (2D) or volume (3D) is transformed into a finite number of simpler geometric shapes called 'elements', which are joined by nodes, thus conforming a mesh (Bright, 2014). Meshes can be comprised of different numbers and shapes of elements (Zienkiewicz et al., 2005). Increasing the number of elements usually generates better models, but it does not necessarily increase the accuracy of the solution, whereas it substantially increases computing time (Brassey et al., 2013). Therefore, it is a quite common procedure to perform sensitivity studies testing models that exclusively vary in the number of elements to determine the number elements required for the convergence of the results

(Kupczik et al., 2007; Brassey et al., 2013). The following step is to assign material properties to the mesh elements (Bhatti, 2005). Depending on the specific purpose of the analyses, just one or several material properties can be assigned to different elements representing, for instance, different tissues (e.g., cortical and trabecular bone, ligaments, dentine, cement, enamel, etc.) (Gröning et al., 2011). It is quite common for biological contexts to just specify the Young's modulus of elasticity and Poisson's ratio of compressibility, which can vary in magnitude or orientation to reflect heterogeneous or anisotropic properties of the source material, respectively (Williams and Lewis, 1982; Chen and Povirk, 1996; Rho et al., 2001). Nonetheless, most of the studies assume a linear, isotropic behaviour to simplify the analyses unless the actual objective of the study is to see how this decision influences the obtained results (Chen and Povirk, 1996). Although bone generally behaves anisotropically, it is usually modelled as a linear elastic and isotropic material for simplicity, because it has been shown that isotropic modelling seems to have little effect compared to anisotropic modelling on the pattern of stress (Chen and Povirk, 1996; Strait et al., 2005). Material properties can be determined using experimental approaches for extant species (Peterson and Dechow, 2003; Daegling et al., 2009), but for extinct taxa the material properties are typically established using some comparative criterion such as the extant phylogenetic bracket (Witmer, 1995), phylogenetic distance/relatedness (Wroe et al., 2007) or by comparing bone histological morphology in a series of taxa (Rayfield et al., 2001). However, in most studies comparing different specimens FEA is applied as a structural comparative technique and the objective is not necessarily to recreate exactly the way an anatomical structure is loaded during life and/or to estimate exact strain/stress values, but rather to compare a general measure of mechanical performance (Püschel and Sellers, 2016). In other words, in comparative studies the idea is to assess how different shapes affect mechanical performance under comparable loading scenarios, with no need of validating the obtained results against experimental data and/or obtain *in vivo*-like stress or strain values (at least not necessarily) (Marcé-Nogué et al., 2017b).

The following step is to define boundary conditions, constraints and loads (wich specify magnitudes and orientations) in order to simulate the desired biomechanical scenarios (e.g. unilateral biting, striding, jumping, climbing, standing, etc.)

(Richmond et al., 2005; Rayfield, 2007). In most cases extra constraints are required to prevent rigid body motions of the geometry and counteract residual moments (e.g. from errors when applying the loadings), although caution is required when placing constraints in order to avoid over-constraining the model under analysis (Ross, 2005). The applied loads are used to simulate either an external force (e.g. ground reaction forces, impacts, etc.) or intrinsic loads, such as muscle actions or joint reaction forces (Rayfield, 2007). Depending on the specific purpose of the study, loads can be more realistically derived by estimating them using experimental data (i.e. by measuring the performance of a certain action both *in vivo* or *ex vivo*) (Anderson et al., 2007; Ellis et al., 2008), soft tissue data obtained from dissections (Toro-Ibacache et al., 2016), or contrast enhanced CT-scanning (Cox et al., 2011; Bribiesca-Contreras and Sellers, 2017). Since most of the above mentioned information is not available for extinct taxa, similar criteria as the ones mentioned for material properties can be applied to determine which values to apply (Bright, 2014). Extant phylogenetic bracket can be used to reconstruct muscle position and forces (Witmer, 1995), or muscle or fascia insertion marks can be used to establish muscle attachment areas to compute muscle volume and cross-sectional area (i.e. anatomical cross-sectional area) (Demes and Creel, 1988; Christiansen and Adolfssen, 2005; Ellis et al., 2008). However, as it was previously mentioned, in several studies the objective is not to obtain the absolute forces or loads, but to analyse the performance in relation to shape in a comparative framework (Piras et al., 2013).

One important consideration to take into account when analysing different individuals using FEA is how to make the obtained results comparable. Strain energy is proportional to the square of the load and to volume (Dumont et al., 2009), hence it is important to account for size differences when performing strain or stress comparisons. Several solutions have been proposed to compare total strain or stress between different specimens. Suggestions include scaling the loads to yield similar force:surface area ratios or scaling them to a relevant biological measurement (e.g. bite force, moment arm, animal weight) (Fitton et al., 2012; Parr et al., 2012; Brassey et al., 2013). Another possibility is to scale the models to achieve the same surface area or same volume, or to simply scale the obtained results from the analysis with respect to a sensible measure (Dumont et al., 2009).

In a structural analysis, typical mechanical parameters of interest are strain, which is the deformation within a structure (Δlength/length; unitless) and stress, the applied force per unit area (Nm^{-2}), which are obtainable as result of FEA (Kupczik, 2008). Therefore FEA calculate the deformation at the nodes within the FE models as affected by the applied simulation conditions, thus providing values of nodal strains, element stress, and strain energy (Zienkiewicz et al., 2005). Subsequently, these values are used as indicators of the mechanical performance of a structure (Marcé-Nogué et al., 2013). Earlier studies assumed that in most cases natural selection acted to increase the mechanical efficiency of anatomical structures (e.g. decreased strain and stress under the typical behaviour of an animal would be indicative of adaptation for structural strength) (e.g. Preuschoft and Witzel, 2005; Wroe et al., 2005, 2007; Dumont et al., 2011). However, more recent studies analysing several taxa have shown that the picture is not as simple as initially thought. For example, a study addressing adaptation hypotheses using FEA derived data from large-enough clades with well-documented phylogenies has shown that there is no straightforward evidence of low stress selection in hard-food eating species (Dumont et al., 2014), although the expected pattern has been found in other clades (Marcé-Nogué et al., 2017b). In part, this is related to the fact that in many of these structures several different functions are performed (e.g. the cranium is involved in feeding, hearing, vocalization, etc.) (Lieberman, 2011) and consequently, several selection pressures could be acting simultaneously. Additionally, the role of morphological integration in the development of these structures could also influence the final morphology and as a result, some morphological aspects could not be functionally related, but instead arise as result of the developmental covariation between modules (Klingenberg, 2008).

Finally, in some cases when necessary, FE models can be validated experimentally by measuring strains and stress in an experimental setting and comparing those values against the ones obtained *in silico* (Kupczik et al., 2007; Panagiotopoulou et al., 2011; Rayfield, 2011; Toro-Ibacache et al., 2016). There are several ways in which the validation procedure can be performed, ranging from *in vivo* recordings using strain gauges or force transducers to *ex vivo* measurements using digital speckle interferometry, photoelastic materials, etc. (Toro-Ibacache et al., 2016). Validation

studies are important not only to validate the specific models (Kupczik et al., 2007), but also to test how accurate the discretised models are, or how changing parameters affects their performance (Panagiotopoulou et al., 2011), as well as how they can be simplified until they are no longer realistic (Fitton et al., 2015). Another available approach is sensitivity analysis, which in its basic form enables us to assess how variation in the FEA input parameters or model geometry affects the obtained results (the ideal is to reach convergence, which means the point in which variation in the parameters does not affect significantly the outcomes) (Brassey et al., 2013).

1.3.2 Geometric morphometrics

Geometric morphometrics (GM) comprise a set of techniques for the analysis of form (i.e. shape and size) that utilise as primary data Cartesian coordinates rather than linear distances, angles, ratios or other measurements (Adams et al., 2013). These techniques focus their analyses on homologous coordinates instead of linear measurements, thus allowing a consistent partition of the mathematical effects of size, as well as providing results that can be visualized as graphical transformations of the shape under analysis (Slice, 2007). The primary data for geometric morphometric analysis are landmarks (i.e. 2D or 3D discrete anatomical loci on the specimens of interest) or semi-landmarks (i.e. series of points that are located relative to one another by some consistent rule along a curve or across a surface), which from a mathematical perspective correspond to homologous points between different specimens (Dryden and Mardia, 1998).

Coordinate data collection will vary primarily depending on the required dimensionality (i.e. 2D or 3D), as well as depending on the structure of interest. 2D landmarks can be simply collected from digital photographs using standard geometric software (e.g. TPS series) or using custom written scripts or R functions (Zelditch et al., 2012; Adams and Otárola-Castillo, 2013; Rohlf, 2015). In general, collecting 3D landmarks requires some more specialized equipment such as point digitizers (e.g., Microscribe 3D), laser or structured-light surface scanners (e.g., NextEngine, David), CT-scans or MRIs, among other equipment (Weber and Bookstein, 2011). Nonetheless, a simpler and non-expensive solution can be achieved by using photogrammetry to generate 3D models from several digital

photos taken from different angles and positions (Falkingham, 2012) or by using at least two photographic cameras to set up a stereo camera that allows the collection of 3D points (Olsen and Westneat, 2015).

Even though linear measurements do not allow a separation of size as coherent as the one achieved by using GM techniques, they have the advantage that distances are invariant with respect to rotation and translation, whereas coordinate data is not (Bookstein, 1991). Since landmark coordinates have no intrinsic scale or orientation, they have to be collected in way that makes the coordinates of one specimen comparable to rest of the sample (Kendall, 1977). The most popular method to achieve this is the Generalized Procrustes Analysis (GPA) that basically consists in an algorithmic procedure that rescales a set of landmarks and then aligns them with other sets at their geometric centres (i.e. centroids), to finally rotate them until the sum of squared distances between them is minimized (Gower, 1975; Rohlf and Slice, 1990). Several variations of the traditional Procrustes superimposition that are available differ in the manner in which size is computed to be rescaled, the coordinates used to rotate the structure of interest and if shapes are fit one another or with respect to the sample mean (Zelditch et al., 2012). For instance, most standard GM packages (e.g. TPS series, 'geomorph' R package) perform a partial Procrustes superimposition (i.e. configurations are scaled to unit centroid size during the scaling step) (Rohlf, 1999), where there is an additional step that projects the aligned specimens onto the tangent space (Adams and Otárola-Castillo, 2013; Rohlf, 2015), while others (e.g. MorphoJ) carry out a full Procrustes superimposition (i.e. configurations are scaled to $\cos(\rho)$ during the scaling step, where ρ are Procrustes distances, so that the total sum of squares is minimised) (Dryden and Mardia, 1998; Klingenberg, 2011). Nevertheless, the differences due to the application of slightly dissimilar Procrustes superimposition procedures are expected to be insignificant or almost negligible depending on the dataset under analysis (unless there is unusual large variation or extreme outliers) (Dryden and Mardia, 1998).

It is also important to consider that by removing the effects of size, orientation and translation, there is consequent reduction in the degrees of freedom of the Procrustes residuals (i.e. four degrees of freedom in 2D and seven in 3D

configurations, respectively). This reduced dimensionality implies that variation is constrained so that shapes are distributed in a hyperdimensional sphere, which is a non-Euclidean mathematical space (Kendall, 1984). Consequently, shapes are often projected to a Euclidean tangent space to allow the use of traditional multivariate statistics. Although routinely performed, this step is not strictly necessary since most biological shape variation is sufficiently constrained due to factors such integration that the non-Euclidean curvatures of shape space are negligible (Rohlf and Slice, 1990), unless comparing astoundingly dissimilar structures.

The coordinates transformed after the Procrustes superimposition can be used as shape variables themselves, but their covariances and reduced degrees of freedom have to be considered when computing p-values or other statistics (Zelditch et al., 2012). Frequently these coordinates are converted into other two kinds of variables commonly seen in the morphometric literature so that they have the proper number of degrees of freedom (Bookstein, 1991). One option is to simply carry out a principal component analysis (PCA) so that the Procrustes coordinates are projected onto their principal component axes (PCs) (Rohlf, 1993). Therefore, each PC corresponds to a new variable of correlated variation in landmark coordinates that is orthogonal to the other PCs (Polly et al., 2013). The scores of the objects on the PC axes are then shape variables that have both the proper number of degrees of freedom and are uncorrelated (Hotelling, 1933; Zelditch et al., 2012). The other commonly used option is to apply the thin-plate spline decomposition method to factor the coordinates into partial warp and uniform component scores (Bookstein, 1991; Bookstein et al., 2003). Carrying out a PCA using the partial warp and uniform component scores (i.e., relative warps analysis *sensu* Bookstein) is identical to performing a PCA using Procrustes residuals (i.e. if the partial warp and uniform component scores are weighted equally) (Rohlf, 1993). Subsequently, the standard multivariate toolkit can be applied on these different shape variables, using standard multivariate techniques (e.g. regression, MANOVA, partial-least squares, etc.) with the precaution of preferring non-parametric permutation tests since shape variation infrequently meets normality assumptions and sample sizes are often unbalanced (Zelditch et al., 2012).
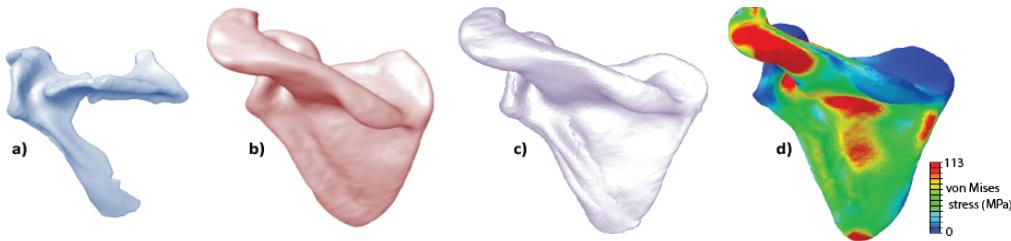
One of the greatest features of geometric morphometrics is that it allows a graphic and more intuitive visualization of the obtained results (Klingenberg, 2013). Whilst in linear morphometrics most results are summarised in the form of tables and/or traditional graphs, the application of the thin-plate spline method allows us to visualize shape changes by morphing one digital object into the shape of another or into hypothetical morphologies resulting from multivariate analyses (Weber and Bookstein, 2011). The thin-plate spline also can also be applied to decompose shape differences into different geometric components (i.e., the uniform component that corresponds shape differences across a whole target specimen and the non-uniform component that describes local shape differences) (Bookstein, 1989).

GM has become the standard tool to quantify morphology in organismal biology and vertebrate palaeontology. Many examples are available with applications to development, integration, sexual dimorphism, intra and inter-specific variation, functional morphology, taxonomy, phylogenetics, ecomorphology, palaeoecology, among others.

1.3.3 Approaches combining FEA and GM

Recent developments in the study of geometric shape and biomechanical modelling have proposed that using both GM and FEA could provide a better understanding of the existing relationship between the shape of skeletal elements and their mechanical performance (Pierce et al., 2008; Piras et al., 2012, 2013; Tseng, 2013). Even though there has been some controversy regarding how to properly combine FEA and GM data (Bookstein, 2013), there is relatively uniform agreement that bridging these two techniques could provide interesting insights about the relationship between form and function (O'Higgins et al., 2011; Parr et al., 2012; Polly et al., 2016). For this reason, different approaches have been proposed to combine FEA and GM data, such as for instance landmark-based analysis in the size-and-shape space of the deformations obtained as result of FEA (Cox et al., 2011; Gröning et al., 2011; O'Higgins et al., 2011; Milne and O'Higgins, 2012; O'Higgins and Milne, 2013), the analysis of finite element models based on warped and target surface meshes (Stayton, 2009; Parr et al., 2012), and the construction of regressions for strain energy density on the largest-scale relative warps (Bookstein,

2013), among others. Since several approaches have been proposed to combine these two tools in the context of the virtual functional morphology toolkit, a brief summary and classification of the most popular ones is provided below:
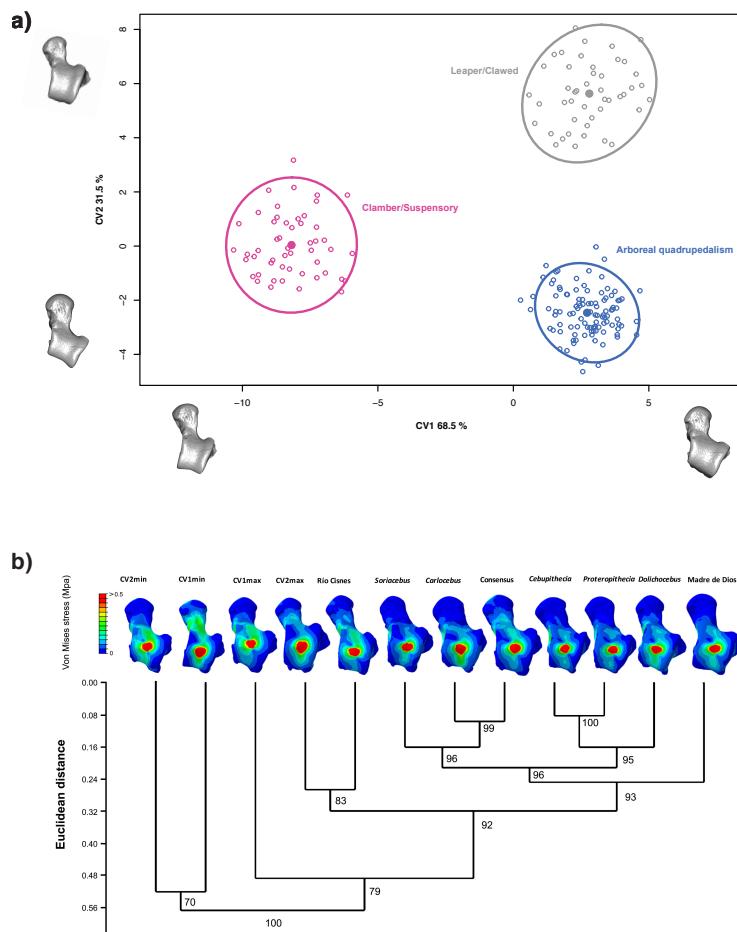
Figure 1.2 a) Virtual representation of the original Neanderthal scapula (Krapina 132), b) Female *Homo sapiens* scapula used as reference to warp the fossil using the thin-plate spline function, c) final result of the virtual reference-based reconstruction process and d) FEA analysis of the reconstructed model.

GM as data generation/manipulation tool for FEA

One of the simplest options is to just use the reconstruction techniques derived from GM (e.g. TPS, multivariate regression, PLS, etc.) (see Figure 1.2 for an example) to reconstruct missing portions of a model or to correct deformed or distorted aspects of its anatomy, and then to carry out an FEA of the resulting reconstructed model (Zollikofer and Ponce de León, 2005; Weber and Bookstein, 2011). Another similar approach implies warping a model to represent some of the results obtained from analyses such as PCAs, CVAs, or multivariate regressions (i.e., hypothetical morphologies) and then to perform an FEA of these theoretical morphologies (Fig. 1.3). This approach has the advantage that starting from just one model (e.g., a warped model representing the multivariate mean of a sample) it is possible to efficiently and quickly generate a dataset of hypothetical morphologies representing the variation observed in a particular morphospace (Stayton, 2009). With this approach, landmark data can be used to warp an FE mesh generated from one particular individual into several different target shapes that could be hypothetical morphologies, or real specimens whose mechanical performance can then be studied (Parr et al., 2012). It is important to consider that warped morphologies depend on the initial landmark selection and if only surface

landmarks were collected then the internal anatomy of the model is likely to be severely distorted since the internal architecture of the bone (e.g., cortical thickness, trabecular organization) would not be accurately represented. One solution is to analyse only filled models or to collect representative landmark all over the model. However, the latter still needs to be properly explored to define a well-established workflow.

Figure 1.3 a) Canonical variate analyses (CVA) of talar shape using locomotor classifications. The circles represent 90% confidence intervals, while the filled dots correspond to the group means. One of the models closest to the mean shape was warped to match the multivariate mean using the thin plate spline method, then the obtained average model was warped to represent the variation along the two plotted CV axes in both analyses. These warped models were then used to b) perform a FEA of these hypothetical extreme locomotor morphologies and compare them against a fossil sample using a UPGMA clustering method. Bootstrap values at nodes were calculated after 10,000 permutations.

GM as a tool to analyse deformations after FEA analysis

GM has been applied to analyse strain deformation, particularly in the context of sensitivity analysis (i.e., how changing certain parameters, such as for instance material properties or load forces, affect the obtained outputs) (Cox et al., 2011). This has been done by collecting a series of easy identifiable landmarks on the model and then comparing the strain values at those locations (Parr et al., 2012) and also by using GM itself to analyse the global deformation before and after FEA, and depending on different loading scenarios (Cox et al., 2011; O'Higgins et al., 2011; Toro-Ibacache et al., 2016; O'Higgins et al., 2017). Although initially promising, it remains still unclear how the representations of these shape differences (measured in Procrustes distances) relate to the strain/stress patterns obtained from FEA, in particular when shape changes are obtained via interpolation (e.g., when using the TPS method) (Bookstein, 2013). Furthermore, there are concerns regarding certain incompatibilities of the differential equation implementation between the two techniques, along with incompatibilities of graphical semiotics (i.e. how to compare stress/strain maps from different specimens in FEA) (Bookstein, 2013). All these unresolved questions perhaps explain why this approach has not been widely adopted among researchers.

GM and FEA combined by analysing their results using multivariate statistical tools

FEA and GM outputs have been used to explore questions in functional morphology, ecomorphology, macroevolution, among others, by applying standard statistical methods such as multivariate regressions, ANOVAs or PLSs. Diverse authors have tried to link functional performance (i.e., measured as a strain or stress) and shape data (i.e., PC axes, or Procrustes coordinates) (e.g. Pierce et al., 2008, 2009, Piras et al., 2012, 2013; Püschel and Sellers, 2016). Furthermore, using the results obtained from both techniques, evolutionary hypotheses can be tested in order to understand the possible underlying mechanisms explaining the observed phenotypic differences (Polly et al., 2016). For example, by combining these results

with a well-resolved phylogeny, it is possible to test different evolutionary models (e.g. Brownian motion, adaptive radiation, directional selection, stasis, Ornstein-Uhlenbeck models) for congruence with the phenotypic data models using a maximum-likelihood framework in order to assess which possible evolutionary scenario better explains the distribution of shape and function on a phylogeny (Young et al., 2011). In addition, some other studies have also generated several FE models representing a range of morphologies corresponding to a set of consistently spaced points from a particular morphospace and then assigned to each point in the set its stress or strain values and by using interpolation functions generate a continuous surface showing expected performance for all possible shapes in that morphospace (Stayton, 2011; Dumont et al., 2014; Polly et al., 2016). For example, Polly et al. (2016), combined FEA and GM by generating performance surfaces describing a quantitative adaptive landscape that was used to predict the direction of morphological evolution (assuming that shapes were being selected for functional performance). Then they proposed to test the obtained evolutionary paths against evolutionary pathways documented by either phylogenies or fossil sequences (Polly et al., 2016). The present dissertation can be regarded as being within this latter approach to bridge GM and FEA using multivariate tools, but it differs from previous approaches in some ways that will be explained in the general discussion section.

1.3.4 Phylogenetic comparative methods

Modern phylogenetic comparative methods (PCMs) consist of a series of statistical procedures applied to analyse phylogenetic trees, and frequently, their association with trait/phenotypic data (Paradis 2014). The overall objective of most modern phylogenetic comparative tools is to elucidate how evolution has generated the observed biodiversity patterns through time (O'Meara, 2012; Pennell and Harmon, 2013). The first PCMs were developed to test if two or more traits evolved in a correlated fashion taking into account the inherent non-independence of phylogenetic data (Felsenstein, 1985; Grafen, 1989), but they have now expanded to also test hypotheses about the evolutionary tempo and mode of different phenotypes (Butler and King, 2004; O'Meara et al., 2006), as well as to analyse clade diversification dynamics.

Currently there are two main sub-families of methods within the PCMs, which can be broadly classified as those focused on trait evolution and those used to investigate lineage diversification (Cornwell and Nakagawa, 2017). Since the present dissertation exclusively applies trait-evolution PCMs, the following section explains these methods in more detail than those focused on lineage diversification, which are just briefly presented.

Trait-evolution PCMs

One of the main goals of trait-evolution PCMs is to model evolutionary tempo and mode (i.e. speed and manner of evolution) (Simpson, 1944). Consequently, phylogeny is used as a historical framework that can be used to model trait evolution along its branches (Smaers et al., 2016). Trait-evolution PCMs commonly apply different models of evolution that define how to map trait variation in observed taxonomic units onto the branches of a phylogenetic tree. There are two main standard models commonly applied to characterise trait evolution: Brownian motion (BM) and Ornstein–Uhlenbeck (OU). However, they have been adapted and modified to model other possible evolutionary scenarios, which were not possible to describe with the most basic formulations (Butler and King, 2004; O'Meara, 2012; Ho and Ané, 2014; Smaers et al., 2016; Cornwell and Nakagawa, 2017).

Under BM, trait evolution is simulated as a random walk through trait space, and phenotypic difference between sister taxa is expected to grow proportional to the sum of branch lengths between them. Support for a BM model suggests that trait disparity uniformly increases over time. An extension of the BM model applied to adaptive radiation scenarios is the Early Burst (EB) model, where the rates of Brownian evolution decay exponentially with time, thus use to represent niche-filling scenarios (Harmon et al., 2010). Support for EB models suggests that most of the trait disparity of a particular clade is partitioned early in their evolutionary history (Harmon et al., 2010). It is important to keep in mind that BM represents random change that can arise as result of several distinct evolutionary processes such as genetic drift (i.e. a BM process that generally affects smaller populations since results from chance sampling of one generation from the previous one, thus being related to population size) or selective drift (i.e. a BM process

randomly changing directional selection). Although these two different phenomena can be modelled using a BM process, they can be distinguished by estimating evolutionary change rates (i.e. fast rates for selective drift, whereas slower rates for genetic drift) (Harmon et al., 2003). The traditional BM model has been now expanded to allow multi-rate BM models using reversible-jump Markov chain Monte Carlo procedures in order to estimate how rates change across a phylogeny, and to test specific hypotheses about where rate shifts happen (O'Meara et al., 2006; Eastman et al., 2011; Venditti et al., 2011; Revell et al., 2012). In addition, recent developments in BM models have allowed the estimation of branch-specific rates of evolution in a deterministic manner using the available phylogenetic and phenotypic information (Smaers et al., 2016). The obtained evolutionary rates are successively used to parameterize a multiple variance BM model, in which it is possible to stochastically infer the phenotypic values for all internal nodes using a Bayesian Markov chain Monte Carlo approach (Smaers et al., 2016).

On the other hand, OU models allow us to model processes that are not possible to describe using the unconstrained random walk of BM (Bookstein, 1987; Gingerich, 1993; Butler and King, 2004; Hunt, 2006; Cressler et al., 2015). OU models describe trait evolution under stabilizing selection, so in addition to a random walk component there is attraction to a selective optimum (θ), and the strength of attraction to this selective optimum (i.e., the strength of selection) is measured using the α parameter (Butler and King, 2004). The OU framework has been expanded to consider not only single peak models (which in most cases would be highly unrealistic), but to also consider 'multi-regime' scenarios that enable the OU parameters to vary across the phylogeny (Butler and King, 2004; Beaulieu et al., 2012; Ingram and Mahler, 2013; Uyeda and Harmon, 2014; Khabbazian et al., 2016). These 'multi-regime' OU models are extremely useful when testing different evolutionary hypotheses (i.e. when selecting among different model parameterizations, where each parameterization describes an alternative evolutionary scenario characterising the structure of the adaptive landscape throughout time) (Butler and King, 2004).

It has to be noted that these different evolutionary models are generated to facilitate the understanding of possible underlying evolutionary processes, but they do not

necessarily represent complete explanations (i.e., model selection is not an end in itself but a helpful approach in contributing to reasoning about the evolutionary mechanisms that might explain the observed variation in the analysed traits) (Ho and Ané, 2014; Cressler et al., 2015). In fact the manner in which both BM and OU model parameters are connected to more commonly tested biological scenarios, such as 'adaptive radiations', 'key innovations', 'niche-filling situations', etc., is not necessarily straightforward (Pennell and Harmon, 2013; Pennell, 2015; Pyron, 2015). For instance, model selection among poor alternatives will unavoidably provide a best candidate, which might be in any case a poor explanation of the evolutionary phenomenon under study (Aho et al., 2014). Furthermore, the evolutionary scenarios of interest may be not well-described by current models and methods (Harmon et al., 2010; Pennell, 2015). The OU assumption of clade-wide stabilizing selection might be unrealistic, since particular lineages within a clade may have experienced their own specific evolutionary histories that could differ strikingly from the history of the rest of the clade (Pennell, 2015). Likewise, the BM assumption that trait change is proportional to the square root of time and constant along all branches has long been considered to be discordant with how many traits evolve (although as explained above new models can at least consider different rates in different branches) (Harvey and Purvis, 1991; Smaers et al., 2016).

Nonetheless, the application of BM and OU models continues to be highly useful and is supported by their efficacy to detect patterns of change through time, their interpretative value in terms of evolutionary processes (i.e. it allows describe trait evolution as wished by Simpson [1944]) and being at least loosely connected to biological concepts, such as 'adaptive radiation', 'niche-filling scenarios', among others (Pennell, 2015). In fact, it can be argued that trait-evolution PCMs aim to detect patterns of trait change through time, irrespective of the underlying microevolutionary processes that might explain the observed pattern (Pennell, 2015). Further studies connecting PCMs with quantitative genetic models might help to properly connect the macroevolutionary explanations derived from trait-evolution phylogenetic comparative techniques with the underlying microevolutionary processes (Lynch, 1991; Housworth et al., 2004; Hadfield and Nakagawa, 2010).

Lineage diversification PCMs

The second sub-family of PCMs is focused on answering questions about taxa number and distribution across the tree of life (Cornwell and Nakagawa, 2017). There is evidence for shifts in speciation and extinction rates in different groups from both the fossil record and also based on the relative diversity of extant lineages, therefore the main goal of this group of PCMs is to test for changes in speciation and/or extinction rates through time and across different groups (Alfaro et al., 2009; Morlon et al., 2011; Stadler, 2011; Etienne and Haegeman, 2012; Condamine et al., 2013). Lineage diversification PCMs can be further divided between those using a) tree topology and those that are b) model-based.

a) Methods using tree topology to investigate lineage diversification: The topology of any phylogeny contains information about historical patterns of diversity dynamics (Pennell and Harmon, 2013). This approach used different tree metrics measuring how balanced a trees was in order to get insight about diversification dynamics. In brief terms, these metrics compare the number of species in sister clades and the obtained differences are compare against a null model (usually a birth-death one) (Slowinski and Guyer, 1989). Thus, high differences in the number of species between sister clades were considered as a sign of different diversification rates (Slowinski and Guyer, 1993). One limitation of this approach is that the birth-death model requires dramatic differences in diversity between clades in order to find significant results (Slowinski and Guyer, 1989). Yet more recent methods used either a maximum-likelihood or Bayesian framework in their tree balance tests to counteract this limitation (Chan and Moore, 2005; Moore and Donoghue, 2009).

b) Model-based methods to assess rates of diversification: It is also possible to directly fit a birth-death model to a phylogenetic tree by using likelihood equations for phylogenetic trees of extant taxa generated under a birth–death process (Nee et al., 1992). This approach has been expanded to allow more complex hypotheses testing, such as to find clades that have unusual rates of speciation and/or extinction (Alfaro et al., 2009), or to test how patterns of diversification rates change through time (Morlon et al., 2010; FitzJohn, 2012).

1.3.5 Machine Learning

Machine-learning (ML) is a discipline at the crossroads between statistics, artificial intelligence, data and computer sciences, being also known as predictive analytics/modelling or statistical learning (Kuhn and Johnson, 2013a). ML deals with topics such as developing and assessing algorithms for classification, prediction and pattern recognition based on models derived from existing data (Tarca et al., 2007). This means that both the generation of the algorithm and its object classification process or event prediction are to be based on observable data. There is a long and complex history between biology and ML, since some of the first ML algorithms were developed to tackle questions in the cognitive sciences (Wilson and Kehr, 2001). For example, an early ML technique called the perceptron constituted one of the first attempts to model neuronal behaviour, and the field of artificial neural network (ANN) arose from this initiative (Tarca et al., 2007). Currently, the application of ML techniques has become ubiquitous in different fields within biology, although its application has been mostly concentrated in certain areas. Some well-known algorithms (e.g. Bayesian and Gaussian networks, random forests, hidden Markov models, support vector machines, etc.) have been successfully used in genomics, transcriptomics, proteomics, systems biology and numerous other domains (Larrañaga et al., 2006). Even so, in the areas of ecology and evolution it has been mostly applied to tackle problems of automated taxon identification, comparative genomics and phylogenetic inference (Larrañaga et al., 2006; MacLeod, 2007; Libbrecht and Noble, 2015).
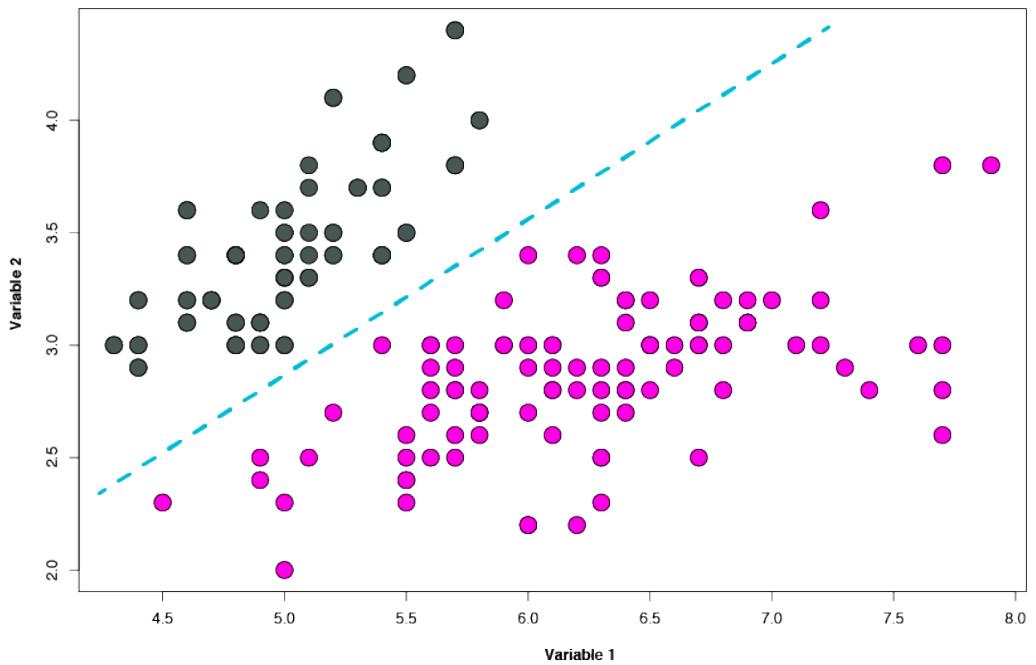
It has been only recently that several ML methods have started to be applied more frequently in the field of functional evolutionary morphology (Dobigny et al., 2002; Feldesman, 2002; Mendoza et al., 2002; Baylac et al., 2003; Bignon et al., 2005; MacLeod, 2007; Van Bocxlaer and Schultheiß, 2010; Brink and Bokma, 2011; Santos et al., 2014; Navega et al., 2015; Sonnenschein et al., 2015; Li et al., 2016; Hanot et al., 2017; MacLeod, 2017). While some of these techniques (e.g. support vector machines, random forests) are based on mathematics, which are quite different to those regularly applied in standard morphometric studies, other approaches (e.g., logistic regression, Bayesian networks) are related to methods that have been previously applied in morphometrics or in other related biological fields

(MacLeod, 2017). Although there are available publications using ML techniques to classify observations using morphometric data (e.g. Dobigny et al., 2002; Feldesman, 2002; Mendoza et al., 2002; Baylac et al., 2003; Bignon et al., 2005; MacLeod, 2007; Van Bocxlaer and Schultheiß, 2010; Brink and Bokma, 2011; Santos et al., 2014; Navega et al., 2015; Sonnenschein et al., 2015; Li et al., 2016; Hanot et al., 2017; MacLeod, 2017), they are still not commonly adopted by the morphometrics or functional morphology community, probably due to the lack of familiarity regarding these techniques among the practitioners of these disciplines. Consequently, the idea of this section is to briefly describe some of the most common concepts in ML, as well as to characterise some of the most widespread practices. One of the most common ways to classify ML algorithms is based on whether they require prior information about the output, or whether they are able to define their classification criteria without this additional information.

Supervised learning

The ML algorithms applied in supervised learning are those that automate decision-making processes by making generalisations from known examples (Wilson and Kehr, 2001). When using supervised ML techniques, the user feeds the algorithm with inputs and expected outputs, and the algorithm seeks a manner to generate the expected output given an input (Hastie et al., 2017). ML algorithms that learn in this way are known as supervised learners because a 'teacher' supervises the algorithms by providing the expected outputs for each example that they learn from (Raschka and Mirjalili, 2017). While organising a dataset of inputs and outputs is frequently an arduous procedure, supervised learning algorithms are well understood and their performance is relatively simple to measure and compare (Kuhn, 2008). In any case, the objective of supervised learning is to generate a system that allows an accurate prediction of the category/classification of new observations based on the available variables (Tarca et al., 2007). As well as predicting categorical attributes such as class/category membership, supervised techniques can also be applied to predict continuous features of the observations (Raschka and Mirjalili, 2017).
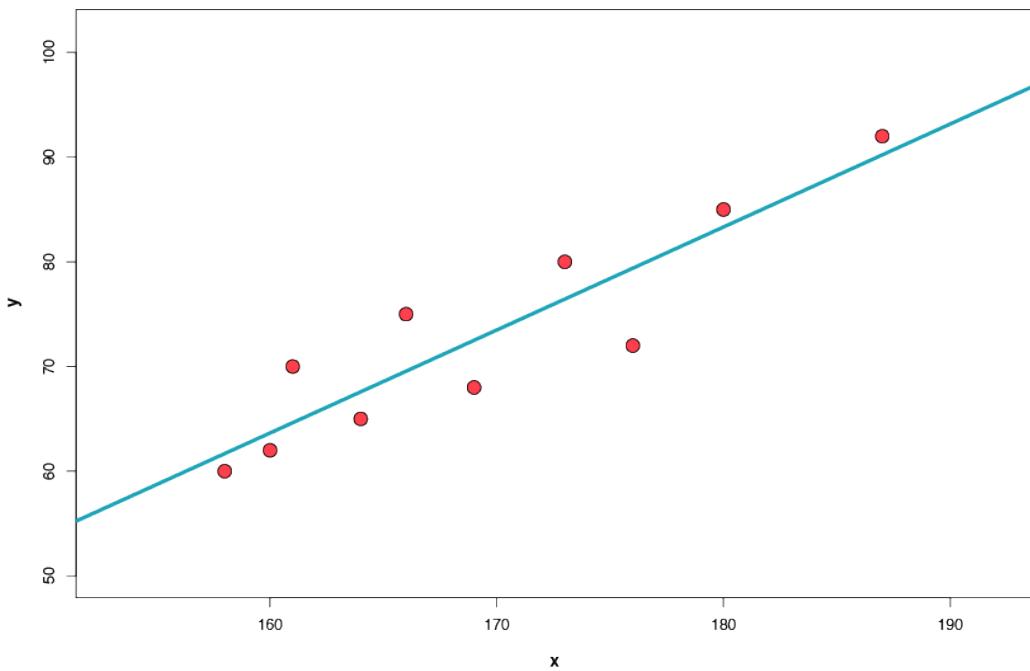
Classification for predicting class labels: Classification is a subcategory of supervised learning where the ultimate objective is to predict the categorical class labels of new observations, based on past instances. The class labels or categories are discrete, unordered values that can be understood as the group memberships of the observations (Raschka and Mirjalili, 2017). Labels or categories can be either binary or multiclass, which means that a supervised learning algorithm can assign any class membership in the training dataset to a new, unlabelled observation. The following figure illustrates the concept of a binary classification task (Fig. 1.4). Given two variables in a two dimensional dataset (i.e. each sample has two values associated), a supervised ML algorithm will try to learn a rule (i.e. the decision boundary represented as a dashed line) that can separate those two classes and classify new data into each of those two categories given its values in the two variables.

Figure 1.4 Example of a classification task that can be modelled using supervised learning techniques. See text for an explanation.

Regression for predicting continuous outcomes: Another kind of supervised learning is the prediction of continuous results, which is also known as regression analysis, although it is important not to confuse this type of supervised learning with

linear regression analysis, which is only one technique among several others that can be applied to predict a continuous outcome (Kuhn and Johnson, 2013a). In regression analysis, a number of predictor (explanatory) variables are used to predict a continuous response variable (outcome or target) by finding a relationship that allows the prediction of the outcome. Depending on the dataset under analysis these relationships can be either linear or non-linear. Figure 1.5 illustrates the concept by showing a classic linear regression. Given a predictor variable x and a response variable y, a straight line can be fitted to this data by minimising the average squared distance between the sample points and the fitted line. Subsequently, the intercept and slope learned from this data can be applied to predict the outcome variable of new observations.
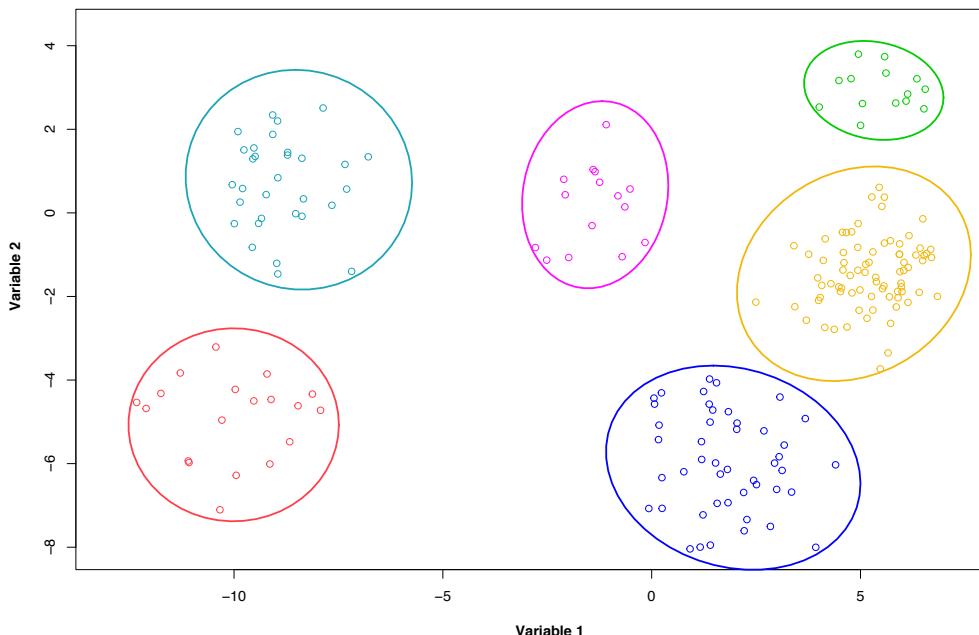
Figure 1.5 Example of a regression task that can be modelled using supervised learning techniques. See text for an explanation.

Unsupervised learning

Unsupervised learning algorithms work in a different way, since no known output data is provided to the algorithm (i.e. no *a priori* class labels are available for the observations under study), and only the input data is known (Kuhn and Johnson, 2013a). In brief terms, the goal in unsupervised learning is to find 'natural' groupings in the data by discovering similarities between observations (Cui et al.,

2011). Similarities are computed to distinguish groups of objects, normally denoted as clusters (Tarca et al., 2007), thus many unsupervised learning algorithms (with certain shared characteristics) are classified under the term 'clustering'. Although highly used to explore data (especially when little is know about it), they are often more difficult to understand and assess as compared to a more standard supervised learning algorithm (Kuhn and Johnson, 2013a).

Clustering: This is a family of exploratory data analysis methods that allow to organize un-labelled information into meaningful sub-groups or clusters without having any prior knowledge regarding their group memberships (Tarca et al., 2007). Each cluster generated during the analysis defines a group of observations that share a certain degree of similarity based on a specific criterion, being at the same time more different with respect to the observations structured in other clusters (Raschka and Mirjalili, 2017). Clustering is a useful set of methods to structure information and extract meaningful relationships from the data itself, that are often not evident to the researcher prior to the analysis. Figure 1.6 shows how clustering can be used to organise unlabelled data into six distinct groups based on the similarity of their two variables.

Figure 1.6 Example of a clustering task that can be modelled using unsupervised learning techniques. See text for an explanation.

Dimensionality reduction: Although dimensionality reduction for data compression could be regarded as its own topic, several standard dimensionality reduction techniques are routinely used in ML and can be considered as a sub-category within the unsupervised methods. It is quite common (especially nowadays in the era of Big Data), that each observation (e.g. species) is described by a high number of features (i.e. variables), which can be challenging in term of storage space, computational performance and visualization. Unsupervised dimensionality reduction is commonly applied during pre-processing to remove noise from data, or to reduce the number of variables to work with, thus compressing the data onto a smaller dimensional subspace while retaining most of the relevant information (Kuhn and Johnson, 2013b).

Reinforcement learning

These kinds of algorithms need an evaluation signal that specifies some measure of progress without intrinsically giving an example of correct behaviour (Wilson and Kehr, 2001). Reinforcement learning research has had an especial emphasis on temporal learning tasks, in which the assessment is given following a sequence of responses. Reinforcement learning is distinguished from typical supervised learning in that precise input/output pairs are not provided at all, nor sub-optimal actions explicitly amended. Instead the attention is on online performance, which implies finding the correct balance between exploration (of unknown terrain) and exploitation (of available knowledge) (Kaelbling et al., 1996). In other words, in reinforcement learning the aim is to develop a system (i.e. agent) that improves its performance based on its interactions with the environment. The information about the current state of the environment typically includes a reward signal, which is not the correct label or value (as it would be in supervised learning), but a performance measure of how well the action was calculated by a reward function (Raschka and Mirjalili, 2017). The latter is an extremely brief and simplified description of reinforcement learning, since a detailed overview is beyond the scope of this dissertation.

Modern biology can greatly profit from the developments made in the area of ML (Tarca et al., 2007). In the present dissertation different supervised ML algorithms
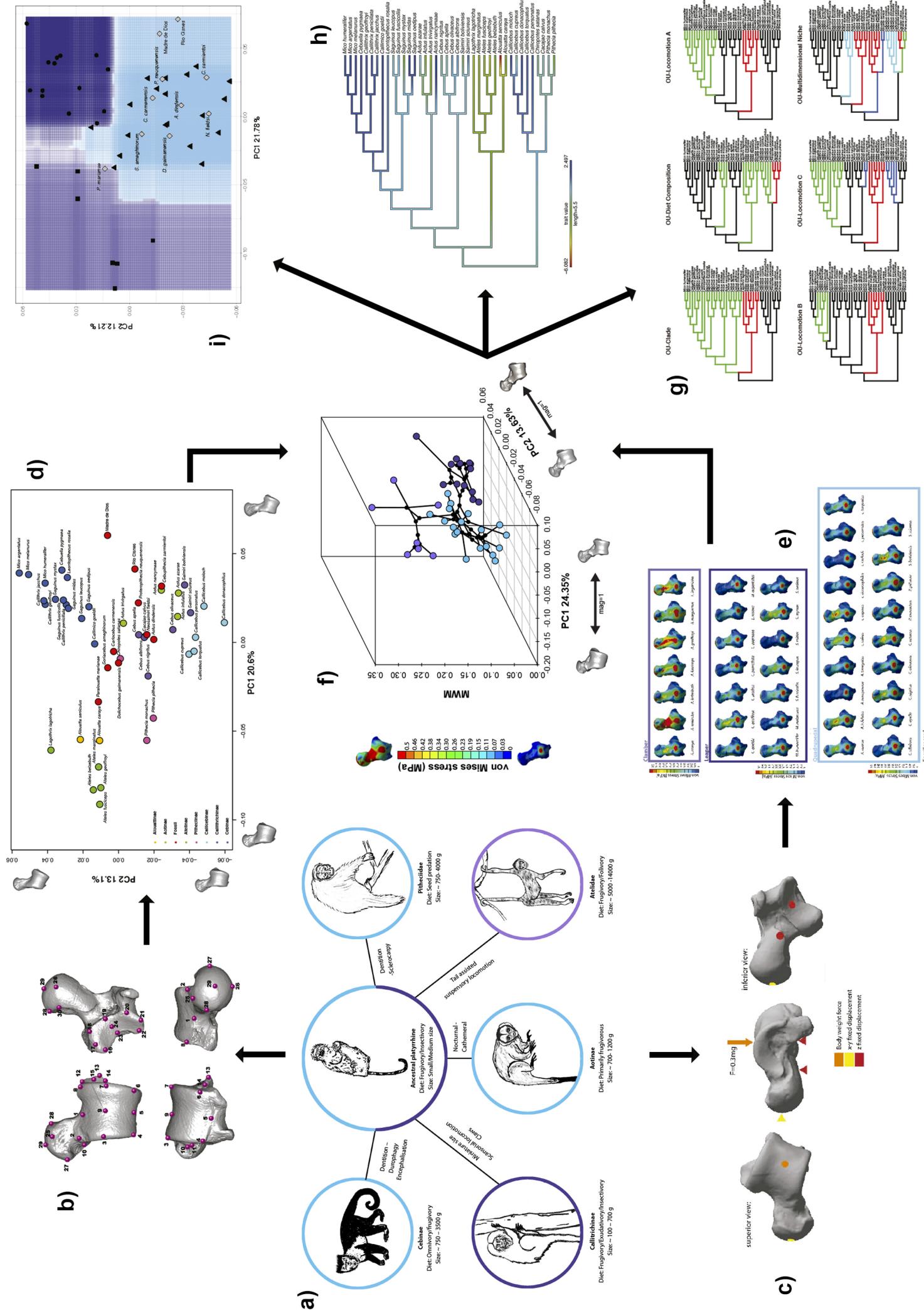
were used to address problems of group analysis and classifications using morphometric and biomechanical data. The application of these algorithms to at least some types of morphometric and biomechanical problems can be regarded as a contribution that could improve the traditional way in which classification tasks have been undertaken in these fields. One of the advantages is the flexibility that allows the use of several different algorithms which can have dissimilar performance depending on the specific problem, rather than the use of only one classification approach (e.g., linear discriminant analysis) without comparing its performance against alternative approaches that might be more suitable for a particular task. The potential is enormous when it comes to the possible applications of ML algorithms in the field of functional morphology. For example, the ability of some of these algorithms to deal with image identification could provide a complementary approach to traditional morphometrics that cannot typically deal with some visual information other than shape (e.g. texture, colour, etc.). This could prove highly useful when carrying out classification tasks. Incorporating the predictive modelling techniques derived from ML into the standard virtual functional morphology toolkit can result in a useful addition that offers further flexibility and predictive power when analysing data and dealing with classification problems.

1.4 Workflow applied in the present dissertation

Figure 1.7 schematises how the above-mentioned methods were used and combined in the dissertation. In the different chapters, diverse sections of this workflow were applied. The tested dataset is a real example comprising talar 3D morphological data representing several extant and extinct platyrrhines, which was analysed in Chapters 4 and 5.

a) Firstly, morpho-functional or ecomorphological questions were identified. For example: How did talar shape evolved during platyrrhine evolution? Is talar morphology related to biomechanical performance and/or locomotion? What was the locotomor behaviour of fossil platyrrhines? b) landmark data was collected to quantify morphology (i.e. talar shape), while c) FEA was used to simulate a functional/locomotor/postural scenario to analyse biomechanical performance (in this case quadrupedal standing); d) a data dimensionality reduction technique was

applied (i.e. PCA) to generate a morphospace that displays the main aspects of shape variation; e) stress and strain data were obtained from the FEA simulation, thus characterising biomechanical performance among several taxa; f) a combined biomechanical-phylomorphospace can be computed to ordinate the data according to both morphology and biomechanics (i.e. x and y are shape PCs, while z is an average stress value); g) evolutionary modelling techniques can be used to test different evolutionary hypotheses for congruence with the phenotypic data using BM, OU, EB, among other possible processes; h) phenotypic data can be mapped onto the phylogeny and ancestral states can be estimated according to a defined mode of evolution; and i) ML approaches can be used to classify new observations (e.g. fossils) into taxonomic, functional, phenetic, etc. categories (e.g. locomotor classes).

Figure 1.7 Proposed workflow to combine GM and FEA in this dissertation. See text for an explanation.

1.5 Journal format

The thesis is being presented in the alternative format in accordance with the rules and regulations of the University of Manchester. Chapters 2 and 4 presented herein have been published as articles in peer-reviewed journals during the course of my PhD. These chapters have been inserted in their final typeset as specified by the individual journals. As such, each chapter differs in layout and referencing style. Chapter 3 is currently undergoing revisions for *The American Journal of Primatology*, while Chapter 5 will be submitted in soon to the *Journal of the Royal Society INTERFACE*, so they have been included here as a manuscripts.

Listed below are the details of each article, its final journal destination and the contribution of each author to the work presented.

Chapter 2. Standing on the shoulders of apes: Analyzing the form and function of the hominoid scapula using geometric morphometrics and finite element analysis.

Authors: **Püschel, T.A**., Sellers, W.I.
Destination: American Journal of Physical Anthropology. 2016. 159, 325–341.

Author contribution: T.A.P and W.I.S. designed the study. T.A.P collected and analysed the data. T.A.P. interpreted the data and wrote the paper, while W.I.S. advised and provided feedback and interpretation at all stages.

Chapter 3. Analyzing the Sclerocarpy Adaptations of the Pitheciidae Mandible using Finite Element Analysis and Geometric Morphometrics

Authors: **Püschel, T.A**., Marcé-Nogué J., Kaiser T., Brocklehurst R., Sellers, W.I.
Destination: American Journal of Primatology. Under review.

Author contribution: T.A.P, R. B. and W.I.S. designed the study. R.B segmented the CT-scan data. T.A.P and J.M-N carried out the simulations. T.A.P analysed the data.

T.A.P. interpreted the data and wrote the paper, while R.B, J. M-N, T.K and W.I.S. advised and provided feedback and interpretation at all stages

Chapter 4. The evolution of the platyrrhine talus: A comparative analysis of the phenetic affinities of the Miocene platyrrhines with their modern relatives.

Authors: **Püschel, T.A**., Gladman, J.T., Bobe, R., Sellers, W.I.
Destination: Journal of Human Evolution. 2017. 111, 179–201.

Author contribution: T.A.P, R. B and W.I.S designed the study. T.A.P and J.T.G collected the primary data. T.A.P carried out the different analyses. T.A.P interpreted the data and wrote the paper, while J.T.G, R.B and W.I.S advised and provided feedback and interpretation at all stages.

Chapter 5. Inferring locomotor behaviours in Miocene New World monkeys using Finite Element Analysis, Geometric Morphometrics and Machine-Learning classification techniques applied to talar morphology

Authors: **Püschel, T.A**., Marcé-Nogué J., Gladman, J.T., Bobe, R., Sellers, W.I.
Destination: Journal of the Royal Society INTERFACE. In preparation.

Author contribution: T.A.P and W.I.S. designed the study. T.A.P and J.T.G collected the primary data. T.A.P and J.M-N carried out the simulations. T.A.P analysed the data. T.A.P interpreted the data and wrote the paper, whilst J.M-N, J.T.G, R.B and W.I.S advised and provided feedback and interpretation at all stages

1.6 References

Adams, D.C., Otárola-Castillo, E., 2013. geomorph: an r package for the collection and analysis of geometric morphometric shape data. Methods in Ecology and Evolution. 4, 393–399.

Adams, D.C., Rohlf, F.J., Slice, D.E., 2013. A field comes of age: geometric morphometrics in the 21st century. Hystrix the Italian Journal of Mammalogy. 21, 7–14.

Aho, K., Derryberry, D., Peterson, T., 2014. Model selection for ecologists: the worldviews of AIC and BIC. Ecology. 95, 631–636.

Aiello, L., Dean, C., 1990. An introduction to human evolutionary anatomy. Academic Press, London; San Diego.

Alexander, R.M., 1971. Size and shape. Hodder Arnold, London.

Alexander, R.M., 1983. Animal mechanics. Blackwell Scientific, London.

Alexander, R.M., 2006. Dinosaur biomechanics. Proceedings of the Royal Society B: Biological Sciences. 273, 1849–1855.

Alfaro, M.E., Santini, F., Brock, C., Alamillo, H., Dornburg, A., Rabosky, D.L., Carnevale, G., Harmon, L.J., 2009. Nine exceptional radiations plus high turnover explain species diversity in jawed vertebrates. Proceedings of the National Academy of Sciences. 106, 13410–13414.

Anderson, D.D., Goldsworthy, J.K., Li, W., James Rudert, M., Tochigi, Y., Brown, T.D., 2007. Physical validation of a patient-specific contact finite element model of the ankle. Journal of Biomechanics. 40, 1662–1669.

Andrews, P., Harrison, T., Delson, E., Bernor, R.L., Martin, L., 1996. Distribution and biochronology of European and Southwest Asian Miocene catarrhines. The evolution of western eurasian neogene mammal faunas. Columbia University Press, New York. 168–207.

Arnold, S.J., 2003. Performance surfaces and adaptive landscapes. Integrative and Comparative Biology. 43, 367–375.

Barak, M.M., Lieberman, D.E., Hublin, J.-J., 2011. A Wolff in sheep's clothing: Trabecular bone adaptation in response to changes in joint loading orientation. Bone. 49, 1141–1151.

Beard, K.C., 2002. Basal anthropoids. In: Hartwig, W. C. (Ed.), The Primate Fossil Record. Cambridge University Press, Cambridge, pp. 133–149.

Beard, K.C., 2008. The oldest North American primate and mammalian biogeography during the Paleocene–Eocene Thermal Maximum. Proceedings of the National Academy of Sciences. 105, 3815–3818.

Beaulieu, J.M., Jhwueng, D.-C., Boettiger, C., O'Meara, B.C., 2012. Modeling Stabilizing Selection: Expanding the Ornstein–Uhlenbeck Model of Adaptive Evolution. Evolution. 66, 2369–2383.

Beaupré, G.S., Carter, D.R., 1992. Finite element analysis in biomechanics. In: Biewener, A.A. (Ed.), Biomechanics-Structures and Systems: A Practical Approach. RL Press at Oxford University Press, Oxford, pp. 149-174.

Begun, D.R., 2015. Fossil Record of Miocene Hominoids. In: Henke, W., Tattersall, I. (Eds.), Handbook of Paleoanthropology. Springer Berlin Heidelberg, pp. 1261–1332.

Benefit, B.R., McCrossin, M.L., 1995. Miocene Hominoids and Hominid Origins. Annual Review of Anthropology. 24, 237–256.

Benton, M.J., 2010. Studying Function and Behavior in the Fossil Record. PLOS Biology. 8, e1000321.

Bertram, J.E., Swartz, S.M., 1991. The "law of bone transformation": a case of crying Wolff? Biological Reviews of the Cambridge Philosophical Society. 66, 245–273.

Bhatti, M.A., 2005. Fundamental Finite Element Analysis and Applications: with Mathematica and Matlab Computations, 1 edition. ed. John Wiley & Sons, Hoboken, NJ.

Bloch, J.I., Woodruff, E.D., Wood, A.R., Rincon, A.F., Harrington, A.R., Morgan, G.S., Foster, D.A., Montes, C., Jaramillo, C.A., Jud, N.A., Jones, D.S., MacFadden, B.J., 2016. First North American fossil monkey and early Miocene tropical biotic interchange. Nature. 533, 243–246.

Bock, W.J., 1994. Concepts and methods in ecomorphology. Journal of Biosciences. 19, 403–413.

Bond, M., Tejedor, M.F., Campbell Jr, K.E., Chornogubsky, L., Novo, N., Goin, F., 2015. Eocene primates of South America and the African origins of New World monkeys. Nature. 520, 538–541.

Bookstein, F.L., 1989. Principal warps: Thin-plate splines and the decomposition of deformations. IEEE Transactions on pattern analysis and machine intelligence. 11, 567–585.

Bookstein, F.L., 1991. Morphometric Tools for Landmark Data: Geometry and Biology. Cambridge University Press, Cambridge.

Bookstein, F.L., 2013. Allometry for the Twenty-First Century. Biological Theory. 7, 10–25.

Bookstein, F.L., Gunz, P., Mitteroecker, P., Prossinger, H., Schaefer, K., Seidler, H., 2003. Cranial integration in Homo: singular warps analysis of the midsagittal plane in ontogeny and evolution. Journal of Human Evolution. 44, 167–187.

Borelli, G.A., 1680. De motu animalium. Ex typographia Angeli Bernabò, Romae.

Boyer, D.M., Yapuncich, G.S., Butler, J.E., Dunn, R.H., Seiffert, E.R., 2015. Evolution of postural diversity in primates as reflected by the size and shape of the medial tibial facet of the talus. American Journal of Physical Anthropology. 157, 134–177.

Brassey, C.A., Margetts, L., Kitchener, A.C., Withers, P.J., Manning, P.L., Sellers, W.I., 2013. Finite element modelling versus classic beam theory: comparing methods for stress estimation in a morphologically diverse sample of vertebrate long bones. Journal of the Royal Society, Interface / the Royal Society. 10, 20120823.

Bright, J.A., 2014. A review of paleontological finite element models and their validity. Journal of Paleontology. 88, 760–769.

Butler, M.A., King, A.A., 2004. Phylogenetic comparative analysis: a modeling approach for adaptive evolution. The American Naturalist. 164, 683–695.

Cachel, S., 2015. Fossil Primates. Cambridge University Press, Cambridge.

Campbell, C.J., 2008. Spider Monkeys: The Biology, Behavior and Ecology of the Genus Ateles. Cambridge University Press, Cambridge.

Carter, D.R., Beaupre, G.S., 2007. Skeletal Function and Form: Mechanobiology of Skeletal Development, Aging, and Regeneration. Cambridge University Press, Cambridge; New York.

Cartmill, M., 1972. Arboreal adaptations and the origin of the order Primates. In Tuttle R. (Ed.), The function and evolutionary biology of primates, pp.97–122.

Cartmill, M., 1980. Morphology, function, and evolution of the anthropoid postorbital septum. In: Ciochon, Russell L. (Ed.), Evolutionary Biology of the New World Monkeys and Continental Drift. Springer, pp. 243–274.

Cartmill, M., 1992. New views on primate origins. Evolutionary Anthropology: Issues, News, and Reviews. 1, 105–111.

Chaimanee, Y., Suteethorn, V., Jaeger, J.-J., Ducrocq, S., 1997. A new late Eocene anthropoid primate from Thailand. Nature. 385, 429–431.

Chan, K.M.A., Moore, B.R., 2005. SYMMETREE: whole-tree analysis of differential diversification rates. Bioinformatics. 21, 1709–1710.

Chan, L.K., 2007. Glenohumeral Mobility in Primates. Folia Primatologica. 78, 1–18.

Charmantier, A., Garant, D., Kruuk, L.E., 2014. Quantitative genetics in the wild. Oxford University Press, Oxford.

Chatterjee, H.J., Ho, S.Y., Barnes, I., Groves, C., 2009. Estimating the phylogeny and divergence times of primates using a supermatrix approach. BMC Evolutionary Biology. 9, 259.

Chen, X., Povirk, G., 1996. Assessing errors introduced by modeling the anisotropic human mandible isotropically with the finite element method. American Journal of Physical Anthropology. 22 (Suppl.).

Christiansen, P., Adolfssen, J.S., 2005. Bite forces, canine strength and skull allometry in carnivores (Mammalia, Carnivora). Journal of Zoology. 266, 133–151.

Condamine, F.L., Rolland, J., Morlon, H., 2013. Macroevolutionary perspectives to environmental change. Ecology Letters. 16, 72–85.

Cooke, S.B., Rosenberger, A.L., Turvey, S., 2011. An extinct monkey from Haiti and the origins of the Greater Antillean primates. Proceedings of the National Academy of Sciences. 108, 2699–2704.

Cornwell, W., Nakagawa, S., 2017. Phylogenetic comparative methods. Current Biology. 27, R333–R336.

Costa, I.R., Prosdocimi, F., Jennings, W.B., 2016. In silico phylogenomics using complete genomes: a case study on the evolution of hominoids. Genome Research. 26, 1257–1267.

Cox, P.G., Fagan, M.J., Rayfield, E.J., Jeffery, N., 2011. Finite element modelling of squirrel, guinea pig and rat skulls: using geometric morphometrics to assess sensitivity. Journal of Anatomy. 219, 696–709.

Cressler, C.E., Butler, M.A., King, A.A., 2015. Detecting Adaptive Evolution in Phylogenetic Comparative Analysis Using the Ornstein–Uhlenbeck Model. Systematic Biology. 64, 953–968.

Cui, H., Singaram, S., Janning, A., 2011. Combine unsupervised learning and heuristic rules to annotate organism morphological descriptions. Proceedings of the American Society for Information Science and Technology. 48, 1–9.

Curtis, N., Jones, M.E.H., Shi, J., O'Higgins, P., Evans, S.E., Fagan, M.J., 2011. Functional Relationship between Skull Form and Feeding Mechanics in Sphenodon, and Implications for Diapsid Skull Development. PLoS ONE. 6.

Daegling, D.J., Hotzman, J.L., McGraw, W.S., Rapoff, A.J., 2009. Material property variation of mandibular symphyseal bone in colobine monkeys. Journal of Morphology. 270, 194–204.

Davies, G., Oates, J., 1994. Colobine Monkeys: Their Ecology, Behaviour and Evolution. Cambridge University Press, Cambridge.

Delson, E., 1975. Toward the origin of the Old World monkeys. Evolution des Vertébrès-Problèms Actuels de Paléontologie. Actes CNRS Coll. Int. 218, 839–850.

Delson, E., Rosenberger, A.L., 1980. Phyletic perspectives on platyrrhine origins and anthropoid relationships. In: Evolutionary Biology of the New World Monkeys and Continental Drift. Springer, pp. 445–458.

Demes, B., Creel, N., 1988. Bite force, diet, and cranial morphology of fossil hominids. Journal of Human Evolution. 17, 657–670.

Dryden, I.L., Mardia, K.V., 1998. Statistical Shape Analysis. Wiley-Blackwell, Chichester ; New York.

Ducrocq, S., 1999. Siamopithecus eocaenus, a late Eocene anthropoid primate from Thailand: its contribution to the evolution of anthropoids in Southeast Asia. Journal of Human Evolution. 36, 613–635.

Dumont, E.R., Davis, J.L., Grosse, I.R., Burrows, A.M., 2011. Finite element analysis of performance in the skulls of marmosets and tamarins. Journal of Anatomy. 218, 151–162.

Dumont, E.R., Grosse, I.R., Slater, G.J., 2009. Requirements for comparing the performance of finite element models of biological structures. Journal of Theoretical Biology. 256, 96–103.

Dumont, E.R., Samadevam, K., Grosse, I., Warsi, O.M., Baird, B., Davalos, L.M., 2014. Selection for Mechanical Advantage Underlies Multiple Cranial Optima in New World Leaf-Nosed Bats. Evolution. 68, 1436–1449.

Eastman, J.M., Alfaro, M.E., Joyce, P., Hipp, A.L., Harmon, L.J., 2011. A Novel Comparative Method for Identifying Shifts in the Rate of Character Evolution on Trees. Evolution. 65, 3578–3589.

Ellis, J.L., Thomason, J.J., Kebreab, E., France, J., 2008. Calibration of estimated biting forces in domestic canids: comparison of post-mortem and in vivo measurements. Journal of Anatomy. 212, 769–780.

Elton, S., Jansson, A.-U., Meloro, C., Louys, J., Plummer, T., Bishop, L.C., 2016. Exploring morphological generality in the Old World monkey postcranium using an ecomorphological framework. Journal of Anatomy. 228, 534–560.

Endler, J.A., 1986. Natural selection in the wild. Princeton University Press.

Esteve-Altava, B., Rasskin-Gutman, D., 2014. Beyond the functional matrix hypothesis: a network null model of human skull growth for the formation of bone articulations. Journal of Anatomy. 225, 306–316.

Etienne, R.S., Haegeman, B., 2012. A conceptual and statistical framework for adaptive radiations with a key role for diversity dependence. The American Naturalist. 180, E75-89.

Fagan, M.J., Curtis, N., Dobson, C.A., Karunanayake, J.H., Kitpczik, K., Moazen, M., Page, L., Phillips, R., O'Higgins, P., 2007. Voxel-based finite element analysis - Working directly with microCT scan data. Journal of morphology. 268, 1071–1071.

Falkingham, P., 2012. Acquisition of high resolution three-dimensional models using free, open-source, photogrammetric software. Palaeontologia Electronica. 15.1.1T.

Figueirido, B., Tseng, Z.J., Serrano-Alarcón, F.J., Martín-Serra, A., Pastor, J.F., 2014. Three-dimensional computer simulations of feeding behaviour in red and giant pandas relate skull biomechanics with dietary niche partitioning. Biology Letters. 10, 20140196.

Fitton, L.C., Prôa, M., Rowland, C., Toro-Ibacache, V., O'Higgins, P., 2015. The impact of simplifications on the performance of a finite element model of a Macaca fascicularis cranium. Anatomical Record (Hoboken, N.J.: 2007). 298, 107–121.

Fitton, L.C., Shi, J.F., Fagan, M.J., O'Higgins, P., 2012. Masticatory loadings and cranial deformation in Macaca fascicularis: a finite element analysis sensitivity study. Journal of Anatomy. 221, 55–68.

FitzJohn, R.G., 2012. Diversitree: comparative phylogenetic analyses of diversification in R. Methods in Ecology and Evolution. 3, 1084–1092.

Fleagle, J.G., 1977. Locomotor behavior and muscular anatomy of sympatric Malaysian leaf-monkeys (Presbytis obscura and Presbytis melalophos). American Journal of Physical Anthropology. 46, 297–307.

Fleagle, J.G., 1998. Primate adaptation and evolution. 1st edition. Academic Press, London.

Fleagle, J.G., 2013. Primate Adaptation and Evolution, 3rd Revised edition edition. Academic Press, Amsterdam ; Boston.

Fleagle, J.G., Janson, C., Reed, K., 1999. Primate Communities. Cambridge University Press.

Fleagle, J.G., Kay, R.F., 1987. The phyletic position of the Parapithecidae. Journal of Human Evolution. 16, 483–532.

Fleagle, J.G., Kay, R.F., 1994. Anthropoid Origins. In: Fleagle, J.G., Kay, R.F. (Eds.), Anthropoid Origins, Advances in Primatology. Springer US, pp. 675–698.

Fleagle, J.G., Perkins, M.E., Heizler, M.T., Nash, B., Bown, T.M., Tauber, A.A., Dozo, M.T., Tejedor, M.F., 2012. Absolute and relative ages of fossil localities in the Santa Cruz and Pinturas Formations. In: Vizcaíno, S.F., Kay, R.F., Bargo S.M. (Eds.), Early Miocene Paleobiology in Patagonia. Cambridge University Press, pp. 41-58.

Fleagle, J.G., Reed, K.E., 1996. Comparing primate communities: a multivariate approach. Journal of Human Evolution. 30, 489–510.

Ford, S.M., 1980. Callitrichids as phyletic dwarfs, and the place of the callitrichidae in platyrrhini. Primates. 21, 31–43.

Ford, S.M., Davis, L.C., 1992. Systematics and body size: implications for feeding adaptations in New World monkeys. American Journal of Physical Anthropology. 88, 415–468.

Ford, S.M., Porter, L.M., Davis, L.C., 2009. The Smallest Anthropoids: The Marmoset/Callimico Radiation. Springer Science & Business Media.

Fortuny, J., Marcé-Nogué, J., De Esteban-Trivigno, S., Gil, L., Galobart, À., 2011. Temnospondyli bite club: ecomorphological patterns of the most diverse group of early tetrapods. Journal of Evolutionary Biology. 24, 2040–2054.

Fragaszy, D.M., Visalberghi, E., Fedigan, L.M., 2004. The Complete Capuchin: The Biology of the Genus Cebus. Cambridge University Press.

Franzen, J.L., Gingerich, P.D., Habersetzer, J., Hurum, J.H., von Koenigswald, W., Smith, B.H., 2009. Complete primate skeleton from the middle Eocene of Messel in Germany: morphology and paleobiology. PLoS one. 4, e5723.

Garber, P.A., 1992. Vertical clinging, small body size, and the evolution of feeding adaptations in the Callitrichinae. American Journal of Physical Anthropology. 88, 469–482.

Gebo, D.L., 1986. Anthropoid origins—the foot evidence. Journal of Human Evolution. 15, 421–430.

Gebo, D.L., 2014. Primate Comparative Anatomy, 1 edition. ed. Johns Hopkins University Press, Baltimore.

Gebo, D.L., Dagosto, M., Beard, K.C., Qi, T., 2000. The smallest primates. Journal of human evolution. 38, 585–594.

Geng, J.-P., Tan, K.B.C., Liu, G.-R., 2001. Application of finite element analysis in implant dentistry: A review of the literature. The Journal of Prosthetic Dentistry. 85, 585–598.

Gingerich, P.D., Franzen, J.L., Habersetzer, J., Hurum, J.H., Smith, B.H., 2010. Darwinius masillae is a Haplorhine — Reply to Williams et al. (2010). Journal of Human Evolution. 59, 574–579.

Glenn, M.E., Cords, M., 2002. The guenons: Diversity and adaptation in African monkeys. Springer Science & Business Media.

Gower, J.C., 1975. Generalized procrustes analysis. Psychometrika. 40, 33–51.

Gröning, F., Fagan, M.J., O'Higgins, P., 2011. The effects of the periodontal ligament on mandibular stiffness: a study combining finite element analysis and geometric morphometrics. Journal of Biomechanics. 44, 1304–1312.

Gröning, F., Liu, J., Fagan, M.J., O'Higgins, P., 2011. Why do humans have chins? Testing the mechanical significance of modern human symphyseal morphology with finite element analysis. American Journal of Physical Anthropology. 144, 593–606.

Gunnell, G.F., Miller, E.R., 2001. Origin of anthropoidea: Dental evidence and recognition of early anthropoids in the fossil record, with comments on the Asian anthropoid radiation. American Journal of Physical Anthropology. 114, 177–191.

Hadfield, J.D., Nakagawa, S., 2010. General quantitative genetic methods for comparative biology: phylogenies, taxonomies and multi-trait models for continuous and categorical characters. Journal of Evolutionary Biology. 23, 494–508.

Harcourt-Smith, W., 2002. Form and function in the hominoid tarsal skeleton. PhD Dissertation. University College London.

Harmon, L.J., Losos, J.B., Jonathan Davies, T., Gillespie, R.G., Gittleman, J.L., Bryan Jennings, W., Kozak, K.H., McPeek, M.A., Moreno-Roark, F., Near, T.J., Purvis, A., Ricklefs, R.E., Schluter, D., Schulte II, J.A., Seehausen, O., Sidlauskas, B.L., Torres-Carvajal, O., Weir, J.T., Mooers, A.Ø., 2010. Early Bursts of Body Size and Shape Evolution Are Rare in Comparative Data. Evolution. 64, 2385–2396.

Harrison, T., 1987. The phylogenetic relationships of the early catarrhine primates: a review of the current evidence. Journal of Human Evolution. 16, 41–80.

Harrison, T., 2005. The zoogeographic and phylogenetic relationships of early catarrhine primates in Asia. Anthropological Science. 113, 43–51.

Harrison, T., 2013. Catarrhine Origins. In: Begun, D.R. (Ed.), A Companion to Paleoanthropology. Blackwell Publishing Ltd, pp. 376–396.

Harrison, T., Yumin, G., 1999. Taxonomy and phylogenetic relationships of early Miocene catarrhines from Sihong, China. Journal of human evolution. 37, 225–277.

Harvey, P.H., Purvis, A., 1991. Comparative methods for explaining adaptations. Nature. 351, 351619a0.

Hastie, T., Tibshirani, R., Friedman, J., 2017. The Elements of Statistical Learning: Data Mining, Inference, and Prediction, Second Edition, 2nd ed. 2009, Corr. 9th printing 2017 edition. ed. Springer, New York, NY.

Herrera, J.P., 2017. Primate diversification inferred from phylogenies and fossils. Evolution. Early view.

Hill, A., Ward, S., 1988. Origin of the hominidae: The record of african large hominoid evolution between 14 my and 4 my. American Journal of Physical Anthropology. 31, 49–83.

Ho, L.S.T., Ané, C., 2014. Intrinsic inference difficulties for trait evolution with Ornstein-Uhlenbeck models. Methods in Ecology and Evolution. 5, 1133–1146.

Hoffstetter, R., 1969. Un primate de l'Oligocene inférieur sudamericain: Branisella boliviana gen. et sp. nov. CR Acad. Sci. Paris. 269, 434–437.

Hoffstetter, R., 1977. Phylogénie des primates. Confrontation des resultats obtenus par les diverses voies d'approche du probleme. Bulletins et Mémoires de la Société d'Anthropologie de Paris. 4, 327–346.

Hoffstetter, R., 1977. Primates: Filogenia e historia biogeographica. Stud. Geol. 13, 211–53.

Hoffstetter, R., 1980. Origin and Deployment of New World Monkeys Emphasizing the Southern Continents Route. In: Ciochon, R.L., Chiarelli, A.B. (Eds.), Evolutionary Biology of the New World Monkeys and Continental Drift, Advances in Primatology. Springer US, pp. 103–122.

Hotelling, H., 1933. Analysis of a complex of statistical variables into principal components. Journal of educational psychology. 24, 417.

Houle, A., 1999. The origin of platyrrhines: an evaluation of the Antarctic Scenario and the Floating Island Model. American journal of physical anthropology. 109, 541–59.

Housworth, E.A., Martins, E.P., Lynch, M., 2004. The phylogenetic mixed model. The American Naturalist. 163, 84–96.

Huiskes, R., Chao, E.Y.S., 1983. A survey of finite element analysis in orthopedic biomechanics: The first decade. Journal of Biomechanics. 16, 385–409.

Hunt, K.D., 1991a. Mechanical implications of chimpanzee positional behavior. American Journal of Physical Anthropology. 86, 521–536.

Hunt, K.D., 1991b. Positional behavior in the Hominoidea. International Journal of Primatology. 12, 95–118.

Hunt, K.D., 2004. The special demands of great ape locomotion and posture. In: Russon, A.E., David R. Begun (Eds.), The Evolution of Thought. Cambridge University Press, Cambridge.

Hutchinson, J.R., 2012. On the inference of function from structure using biomechanical modelling and simulation of extinct organisms. Biology Letters. 8, 115–118.

Ingram, T., Mahler, D.L., 2013. SURFACE: detecting convergent evolution from comparative data by fitting Ornstein-Uhlenbeck models with stepwise Akaike Information Criterion. Methods in Ecology and Evolution. 4, 416–425.

Janson, C.H., Boinski, S., 1992. Morphological and behavioral adaptations for foraging in generalist primates: the case of the cebines. American Journal of Physical Anthropology. 88, 483–498.

Jungers, W.J., 2013. Size and Scaling in Primate Biology. Springer Science & Business Media.

Kaelbling, L.P., Littman, M.L., Moore, A.W., 1996. Reinforcement Learning: A Survey. J. Artif. Int. Res. 4, 237–285.

Kay, R.F., 1990. The Platyrrhine Fossil RecordThe phyletic relationships of extant and fossil Pitheciinae (Platyrrhini, Anthropoidea). Journal of Human Evolution. 19, 175–208.

Kay, R.F., 2015. New World monkey origins. Science. 347, 1068–1069.

Kay, R.F., Cozzuol, M.A., 2006. New platyrrhine monkeys from the Solimões Formation (late Miocene, Acre State, Brazil). Journal of Human Evolution. 50, 673–686.

Kay, R.F., Meldrum, D.J., Takai, M., 2013. Pitheciidae and other platyrrhine seed predators. In: Veiga, L.M., Barnett, A.A., Ferrari, S.F., Norconk, M.A. (Eds.), Evolutionary Biology and Conservation of Titis, Sakis and Uacaris, Cambridge Studies in Biological and Evolutionary Anthropology. Cambridge University Press, Cambridge.

Kay, R.F., Ross, C., Williams, B.A., 1997. Anthropoid Origins. Science. 275, 797–804.

Kay, R.F., Williams, B.A., Anaya, F., 2002. The Adaptations of Branisella boliviana, the Earliest South American Monkey. In: Plavcan, J.M., Kay, R.F., Jungers, W.L., Schaik, C.P. van (Eds.), Reconstructing Behavior in The Primate Fossil Record, Advances in Primatology. Springer US, pp. 339–370.

Kay, R.F., Williams, B.A., Ross, C.F., Takai, M., Shigehara, N., 2004. Anthropoid Origins: A Phylogenetic Analysis. In: Ross, C.F., Kay, R.F. (Eds.),

Anthropoid Origins, Developments in Primatology: Progress and Prospects. Springer US, pp. 91–135.

Kendall, D.G., 1977. The diffusion of shape. Advances in Applied Probability. 9, 428–430.

Kendall, D.G., 1984. Shape manifolds, procrustean metrics, and complex projective spaces. Bulletin of the London Mathematical Society. 16, 81–121.

Khabbazian, M., Kriebel, R., Rohe, K., Ané, C., 2016. Fast and accurate detection of evolutionary shifts in Ornstein–Uhlenbeck models. Methods in Ecology and Evolution. 7, 811–824.

Kibler, W.B., McMullen, J., 2003. Scapular dyskinesis and its relation to shoulder pain. The Journal of the American Academy of Orthopaedic Surgeons. 11, 142–151.

Kinzey, W.G., 1992. Dietary and dental adaptations in the Pitheciinae. American Journal of Physical Anthropology. 88, 499–514.

Kirkpatrick, C., 2016. Asian Colobines. In: The International Encyclopedia of Primatology. John Wiley & Sons, Inc.

Klingenberg, C.P., 2008. Morphological Integration and Developmental Modularity. Annual Review of Ecology, Evolution, and Systematics. 39, 115–132.

Klingenberg, C.P., 2011. MorphoJ: an integrated software package for geometric morphometrics. Molecular Ecology Resources. 11, 353–357.

Klingenberg, C.P., 2013. Visualizations in geometric morphometrics: how to read and how to make graphs showing shape changes. Hystrix, the Italian Journal of Mammalogy. 24, 15–24.

Kuhn, M., Johnson, K., 2013a. Applied Predictive Modeling, 2013 edition. ed. Springer, New York.

Kuhn, M., Johnson, K., 2013b. Data Pre-processing. In: Applied Predictive Modeling. Springer, New York, pp. 27–59.

Kupczik, K., 2008. Virtual biomechanics: basic concepts and technical aspects of finite element analysis in vertebrate morphology. Journal of Anthropological Sciences. 86, 193–198.

Kupczik, K., Dobson, C.A., Fagan, M.J., Crompton, R.H., Oxnard, C.E., O'Higgins, P., 2007. Assessing mechanical function of the zygomatic region in macaques: validation and sensitivity testing of finite element models. Journal of Anatomy. 210, 41–53.

Larrañaga, P., Calvo, B., Santana, R., Bielza, C., Galdiano, J., Inza, I., Lozano, J.A., Armañanzas, R., Santafé, G., Pérez, A., Robles, V., 2006. Machine learning in bioinformatics. Briefings in Bioinformatics. 86–112.

Larson, S.G., 1998. Parallel evolution in the hominoid trunk and forelimb. Evolutionary Anthropology: Issues, News, and Reviews. 6, 87–99.

Lauder, G.V., 1995. On the inference of function from structure. pp. 1–18.

Ledogar, J.A., Winchester, J.M., St. Clair, E.M., Boyer, D.M., 2013. Diet and dental topography in pitheciine seed predators. American Journal of Physical Anthropology. 150, 107–121.

Leisler, B., Winkler, H., 1991. Ergebnisse und Konzepte ökomorphologischer Untersuchungen an Vögeln. Journal für Ornithologie. 132, 373–425.

Libbrecht, M.W., Noble, W.S., 2015. Machine learning applications in genetics and genomics. Nature Reviews Genetics. 16, 321–332.

Lieberman, D.E., 2011. Evolution of the Human Head, 1 edition. ed. Harvard University Press, Cambridge, Mass.

Lisowski, F.P., Albrecht, G.H., Oxnard, C.E., 1974. The form of the talus in some higher primates: A multivariate study. American Journal of Physical Anthropology. 41, 191–215.

Losos, J.B., 1990. Ecomorphology, Performance Capability, and Scaling of West Indian Anolis Lizards: An Evolutionary Analysis. Ecological Monographs. 60, 369–388.

Losos, J.B., Miles, D.B., 1994. Adaptation, constraint, and the comparative method: phylogenetic issues and methods. Ecological morphology: Integrative organismal biology. 60–98.

Luchterhand, K., Kay, R.F., Madden, R.H., 1986. Mohanamico hershkovitzi, gen. et sp. Nov., un primate du Miocène moyen d'Amérique du Sud. Comptes Rendus de l'Académie de Sciences, Paris. Ser. II, 303, 1753–1758.

Lynch, M., 1991. Methods for the analysis of comparative data in evolutionary biology. Evolution. 45, 1065–1080.

MacLeod, N., 2007. Automated Taxon Identification in Systematics: Theory, Approaches and Applications. CRC Press.

MacPhee, R.D.E., Iturralde-Vinent, M., Gaffney, E.S., 2003. Domo de Zaza, an Early Miocene Vertebrate Locality in South-Central Cuba: With Notes on

the Tectonic Evolution of Puerto Rico and the Mona Passage. American Museum of Natural History.

Marcé Nogué, J., DeMiguel, D., Fortuny Terricabras, J., Trivigno, E., Gil Espert, L., others, 2013. Quasi-homothetic transformation for comparing the mechanical performance of planar models in biological research. Palaeontologia electronica. 16, 1–15.

Marcé-Nogué, J., Esteban-Trivigno, S.D., Püschel, T.A., Fortuny, J., 2017a. The intervals method: a new approach to analyse finite element outputs using multivariate statistics. PeerJ. 5, e3793.

Marcé-Nogué, J., Püschel, T.A., Kaiser, T.M., 2017b. A biomechanical approach to understand the ecomorphological relationship between primate mandibles and diet. Scientific Reports. 7, 8364.

Marivaux, L., Adnet, S., Altamirano-Sierra, A.J., Boivin, M., Pujos, F., Ramdarshan, A., Salas-Gismondi, R., Tejada-Lara, J.V., Antoine, P.-O., 2016a. Neotropics provide insights into the emergence of New World monkeys: New dental evidence from the late Oligocene of Peruvian Amazonia. Journal of Human Evolution. 97, 159–175.

Marivaux, L., Adnet, S., Altamirano-Sierra, A.J., Pujos, F., Ramdarshan, A., Salas-Gismondi, R., Tejada-Lara, J.V., Antoine, P.-O., 2016b. Dental remains of cebid platyrrhines from the earliest late Miocene of Western Amazonia, Peru: Macroevolutionary implications on the extant capuchin and marmoset lineages. American Journal of Physical Anthropology. 161, 478–493.

Martin, R.D., 1993. Primate origins: plugging the gaps. Nature. 363, 223–234.

McGill, B.J., Enquist, B.J., Weiher, E., Westoby, M., 2006. Rebuilding community ecology from functional traits. Trends in ecology & evolution. 21, 178–185.

Meldrum, D.J., Kay, R.F., 1997. Nuciruptor rubricae, a new Pitheciin seed predator from the Miocene of Colombia. American Journal of Physical Anthropology. 102, 407–427.

Miller, E.R., Simons, E.L., 1997. Dentition of Proteopithecus sylviae, an archaic anthropoid from the Fayum, Egypt. Proceedings of the National Academy of Sciences. 94, 13760–13764.

Milne, N., O'Higgins, P., 2012. Scaling of form and function in the xenarthran femur: a 100-fold increase in body mass is mitigated by repositioning of the

third trochanter. Proceedings of the Royal Society B: Biological Sciences. 279, 3449–3456.

Modolo, L., Salzburger, W., Martin, R.D., 2005. Phylogeography of Barbary macaques (Macaca sylvanus) and the origin of the Gibraltar colony. Proceedings of the National Academy of Sciences of the United States of America. 102, 7392–7397.

Moore, B.R., Donoghue, M.J., 2009. A Bayesian approach for evaluating the impact of historical events on rates of diversification. Proceedings of the National Academy of Sciences. 106, 4307–4312.

Morales, J.C., Melnick, D.J., 1998. Phylogenetic relationships of the macaques (Cercopithecidae:Macaca), as revealed by high resolution restriction site mapping of mitochondrial ribosomal genes. Journal of Human Evolution. 34, 1–23.

Morlon, H., Parsons, T.L., Plotkin, J.B., 2011. Reconciling molecular phylogenies with the fossil record. Proceedings of the National Academy of Sciences. 108, 16327–16332.

Morlon, H., Potts, M.D., Plotkin, J.B., 2010. Inferring the Dynamics of Diversification: A Coalescent Approach. PLOS Biology. 8, e1000493.

Motta, P.J., Kotrschal, K.M., 1991. Correlative, experimental, and comparative evolutionary approaches in ecomorphology. Netherlands Journal of Zoology. 42, 400–415.

Murphy, W.J., Eizirik, E., O'Brien, S.J., Madsen, O., Scally, M., Douady, C.J., Teeling, E., Ryder, O.A., Stanhope, M.J., Jong, W.W. de, Springer, M.S., 2001. Resolution of the Early Placental Mammal Radiation Using Bayesian Phylogenetics. Science. 294, 2348–2351.

Napier, J.R., Napier, P.H., 1967. A handbook of living primates: morphology, ecology and behaviour of nonhuman primates. Academic Press, London.

Nee, S., Mooers, A.O., Harvey, P.H., 1992. Tempo and mode of evolution revealed from molecular phylogenies. Proceedings of the National Academy of Sciences. 89, 8322–8326.

Ni, X., Wang, Y., Hu, Y., Li, C., 2004. A euprimate skull from the early Eocene of China. Nature. 427, 65–68.

Norconk, M.A., Grafton, B.W., McGraw, W.S., 2013. Morphological and ecological adaptations to seed predation - a primate-wide perspective. In: Veiga, L.M.,

Barnett, A.A., Ferrari, S.F., Norconk, M.A. (Eds.), Evolutionary Biology and Conservation of Titis, Sakis and Uacaris, Cambridge Studies in Biological and Evolutionary Anthropology. Cambridge University Press.

Norconk, M.A., Veres, M., 2011. Physical Properties of Fruit and Seeds Ingested by Primate Seed Predators with Emphasis on Sakis and Bearded Sakis. The Anatomical Record: Advances in Integrative Anatomy and Evolutionary Biology. 294, 2092–2111.

Ogihara, N., Yamanaka, A., Masato, N., Ishida, H., 2003. Functional Morphology of Primate Scapula Based on Finite Element Analysis. Primate Research. 19, 203–215.

O'Higgins, P., Cobb, S.N., Fitton, L.C., Gröning, F., Phillips, R., Liu, J., Fagan, M.J., 2011. Combining geometric morphometrics and functional simulation: an emerging toolkit for virtual functional analyses. Journal of Anatomy. 218, 3–15.

O'Higgins, P., Fitton, L.C., Godinho, R.M., 2017. Geometric morphometrics and finite elements analysis: Assessing the functional implications of differences in craniofacial form in the hominin fossil record. Journal of Archaeological Science.

O'Higgins, P., Milne, N., 2013. Applying geometric morphometrics to compare changes in size and shape arising from finite elements analyses. Hystrix the Italian Journal of Mammalogy. 24, 126–132.

O'Leary, M.A., Bloch, J.I., Flynn, J.J., Gaudin, T.J., Giallombardo, A., Giannini, N.P., Goldberg, S.L., Kraatz, B.P., Luo, Z.-X., Meng, J., Ni, X., Novacek, M.J., Perini, F.A., Randall, Z.S., Rougier, G.W., Sargis, E.J., Silcox, M.T., Simmons, N.B., Spaulding, M., Velazco, P.M., Weksler, M., Wible, J.R., Cirranello, A.L., 2013. The Placental Mammal Ancestor and the Post–K-Pg Radiation of Placentals. Science. 339, 662–667.

Olsen, A.M., Westneat, M.W., 2015. StereoMorph: an R package for the collection of 3D landmarks and curves using a stereo camera set-up. Methods in Ecology and Evolution. 6, 351–356.

O'Meara, B.C., 2012. Evolutionary Inferences from Phylogenies: A Review of Methods. Annual Review of Ecology, Evolution, and Systematics. 43, 267–285.

O'Meara, B.C., Ané, C., Sanderson, M.J., Wainwright, P.C., Hansen, T., 2006. Testing for different rates of continuous trait evolution using likelihood. Evolution. 60, 922–933.

Panagiotopoulou, O., 2009. Finite element analysis (FEA): applying an engineering method to functional morphology in anthropology and human biology. Annals of human biology. 36, 609–623.

Panagiotopoulou, O., Kupczik, K., Cobb, S.N., 2011. The mechanical function of the periodontal ligament in the macaque mandible: a validation and sensitivity study using finite element analysis. Journal of Anatomy. 218, 75–86.

Parr, W.C.H., Wroe, S., Chamoli, U., Richards, H.S., McCurry, M.R., Clausen, P.D., McHenry, C., 2012. Toward integration of geometric morphometrics and computational biomechanics: New methods for 3D virtual reconstruction and quantitative analysis of Finite Element Models. Journal of Theoretical Biology. 301, 1–14.

Pearson, O.M., Lieberman, D.E., 2004. The aging of Wolff's "law": Ontogeny and responses to mechanical loading in cortical bone. American Journal of Physical Anthropology. 125, 63–99.

Pennell, M.W., 2015. Modern Phylogenetic Comparative Methods and Their Application in Evolutionary Biology: Concepts and Practice. — Edited by László Zsolt Garamszegi. Systematic Biology. 64, 161–163.

Pennell, M.W., Harmon, L.J., 2013. An integrative view of phylogenetic comparative methods: connections to population genetics, community ecology, and paleobiology. Annals of the New York Academy of Sciences. 1289, 90–105.

Perkins, M.E., Fleagle, J.G., Heizler, M.T., Nash, B., Bown, T.M., Tauber, A.A., Dozo, M.T., 2012. Tephrochronology of the Miocene Santa Cruz and Pinturas Formations, Argentina. In: Vizcaíno, S.F., Kay, R.F., Bargo S.M. (Eds.), Early Miocene Paleobiology in Patagonia. Cambridge University Press.

Peterson, J., Dechow, P.C., 2003. Material properties of the human cranial vault and zygoma. The Anatomical Record Part A: Discoveries in Molecular, Cellular, and Evolutionary Biology. 274A, 785–797.

Pierce, S.E., Angielczyk, K.D., Rayfield, E.J., 2008. Patterns of morphospace occupation and mechanical performance in extant crocodilian skulls: A

combined geometric morphometric and finite element modeling approach. Journal of Morphology. 269, 840–864.

Pierce, S.E., Angielczyk, K.D., Rayfield, E.J., 2009. Shape and mechanics in thalattosuchian (Crocodylomorpha) skulls: implications for feeding behaviour and niche partitioning. Journal of Anatomy. 215, 555–576.

Pilbeam, D., 1996. Genetic and Morphological Records of the Hominoidea and Hominid Origins: A Synthesis. Molecular Phylogenetics and Evolution. 5, 155–168.

Piras, P., Maiorino, L., Teresi, L., Meloro, C., Lucci, F., Kotsakis, T., Raia, P., 2013. Bite of the Cats: Relationships between Functional Integration and Mechanical Performance as Revealed by Mandible Geometry. Systematic Biology. 62, 878–900.

Piras, P., Sansalone, G., Teresi, L., Kotsakis, T., Colangelo, P., Loy, A., 2012. Testing convergent and parallel adaptations in talpids humeral mechanical performance by means of geometric morphometrics and finite element analysis. Journal of Morphology. 273, 696–711.

Piras, P., Sansalone, G., Teresi, L., Moscato, M., Profico, A., Eng, R., Cox, T.C., Loy, A., Colangelo, P., Kotsakis, T., 2015. Digging adaptation in insectivorous subterranean eutherians. The enigma of Mesoscalops montanensis unveiled by geometric morphometrics and finite element analysis. Journal of Morphology. 276, 1157–1171.

Polly, D.P., Lawing, M.A., Fabre, A.-C., Goswami, A., 2013. Phylogenetic Principal Components Analysis and Geometric Morphometrics. Hystrix the Italian Journal of Mammalogy. 24.

Polly, P.D., Stayton, C.T., Dumont, E.R., Pierce, S.E., Rayfield, E.J., Angielczyk, K.D., 2016. Combining geometric morphometrics and finite element analysis with evolutionary modeling: towards a synthesis. Journal of Vertebrate Paleontology. 0, e1111225.

Pozzi, L., Hodgson, J.A., Burrell, A.S., Sterner, K.N., Raaum, R.L., Disotell, T.R., 2014. Primate phylogenetic relationships and divergence dates inferred from complete mitochondrial genomes. Molecular Phylogenetics and Evolution. 75, 165–183.

Preuschoft, H., 2004. Mechanisms for the acquisition of habitual bipedality: are there biomechanical reasons for the acquisition of upright bipedal posture? Journal of Anatomy. 204, 363–384.

Preuschoft, H., Witzel, U., 2005. Functional shape of the skull in vertebrates: Which forces determine skull morphology in lower primates and ancestral synapsids? The Anatomical Record Part A: Discoveries in Molecular, Cellular, and Evolutionary Biology. 283A, 402–413.

Püschel, T.A., Sellers, W.I., 2016. Standing on the shoulders of apes: Analyzing the form and function of the hominoid scapula using geometric morphometrics and finite element analysis. American Journal of Physical Anthropology. 159, 325–341.

Pyron, R.A., 2015. Post-molecular systematics and the future of phylogenetics. Trends in Ecology & Evolution. 30, 384–389.

Raaum, R.L., Sterner, K.N., Noviello, C.M., Stewart, C.-B., Disotell, T.R., 2005. Catarrhine primate divergence dates estimated from complete mitochondrial genomes: concordance with fossil and nuclear DNA evidence. Journal of Human Evolution. 48, 237–257.

Raff, R.A., 1996. The shape of life: genes, development, and the evolution of animal form. University of Chicago Press.

Rahman, I.A., Lautenschlager, S., 2016. Applications of three-dimensional box modeling to paleontological functional analysis. The Paleontological Society Papers. 22, 119–132.

Raschka, S., Mirjalili, V., 2017. Python Machine Learning: Machine Learning and Deep Learning with Python, scikit-learn, and TensorFlow, 2nd Edition. Packt Publishing, Birmingham.

Rasmussen, D.T., 2002. Early catarrhines of the African Eocene and Oligocene. In: Hartwig, W.C., The Primate Fossil Record. Cambridge University Press.

Rayfield, E.J., 2007. Finite Element Analysis and Understanding the Biomechanics and Evolution of Living and Fossil Organisms. Annual Review of Earth and Planetary Sciences. 35, 541–576.

Rayfield, E.J., 2011. Strain in the ostrich mandible during simulated pecking and validation of specimen-specific finite element models. Journal of anatomy. 218, 47–58.

Rayfield, E.J., Norman, D.B., Horner, C.C., Horner, J.R., Smith, P.M., Thomason, J.J., Upchurch, P., 2001. Cranial design and function in a large theropod dinosaur. Nature. 409, 1033–1037.

Revell, L.J., Mahler, D.L., Peres-Neto, P.R., Redelings, B.D., 2012. A new phylogenetic method for identifying exceptional phenotypic diversification. Evolution; International Journal of Organic Evolution. 66, 135–146.

Rho, J.Y., Currey, J.D., Zioupos, P., Pharr, G.M., 2001. The anisotropic Young's modulus of equine secondary osteones and interstitial bone determined by nanoindentation. Journal of Experimental Biology. 204, 1775–1781.

Richmond, B.G., Wright, B.W., Grosse, I., Dechow, P.C., Ross, C.F., Spencer, M.A., Strait, D.S., 2005. Finite element analysis in functional morphology. The Anatomical Record Part A: Discoveries in Molecular, Cellular, and Evolutionary Biology. 283A, 259–274.

Riggs, B.L., Melton Iii, L.J., Robb, R.A., Camp, J.J., Atkinson, E.J., Peterson, J.M., Rouleau, P.A., McCollough, C.H., Bouxsein, M.L., Khosla, S., 2004. Population-based study of age and sex differences in bone volumetric density, size, geometry, and structure at different skeletal sites. Journal of Bone and Mineral Research: The Official Journal of the American Society for Bone and Mineral Research. 19, 1945–1954.

Rímoli, R.O., 1977. Una nueva especie de monos (Cebidae: Saimirinae: Saimiri) de la Hispaniola. Universidad Autónoma de Santo Domingo.

Rodman, P., 1984. Foraging and social systems of orangutans and chimpanzees. In: Rodman, P., Cant, J.G. (Eds.), Adaptations for Foraging in Nonhuman Primates. Columbia University Press, New York, pp. 134–160.

Rohlf, F., 1993. Relative-warp analysis and an example of its application to mosquito wings. In: Contributions Morphometrics. pp. 131–159.

Rohlf, F., 2015. The Tps series of software. Hystrix. 26, 1–4.

Rohlf, F.J., 1999. Shape Statistics: Procrustes Superimpositions and Tangent Spaces. Journal of Classification. 16, 197–223.

Rohlf, F.J., Slice, D., 1990. Extensions of the Procrustes Method for the Optimal Superimposition of Landmarks. Systematic Zoology. 39, 40–59.

Roos, C., Zinner, D., Kubatko, L.S., Schwarz, C., Yang, M., Meyer, D., Nash, S.D., Xing, J., Batzer, M.A., Brameier, M., Leendertz, F.H., Ziegler, T., Perwitasari-Farajallah, D., Nadler, T., Walter, L., Osterholz, M., 2011.

Nuclear versus mitochondrial DNA: evidence for hybridization in colobine monkeys. BMC Evolutionary Biology. 11, 77.

Rose, K.D., Chester, S.G., Dunn, R.H., Boyer, D.M., Bloch, J.I., 2011. New fossils of the oldest North American euprimate Teilhardina brandti (Omomyidae) from the Paleocene–Eocene thermal maximum. American journal of physical anthropology. 146, 281–305.

Rose, K.D., Chew, A.E., Dunn, R.H., Kraus, M.J., Fricke, H.C., Zack, S.P., 2012. Earliest Eocene mammalian fauna from the Paleocene-Eocene thermal maximum at sand creek divide, southern Bighorn Basin, Wyoming.

Rosenberger, A.L., 1986. Platyrrhines, catarrhines and the anthropoid transition. Cambridge University Press, Cambridge.

Rosenberger, A.L., 1992. Evolution of feeding niches in new world monkeys. American Journal of Physical Anthropology. 88, 525–562.

Rosenberger, A.L., 2002. Platyrrhine paleontology and systematics: the paradigm shifts. In: Hartwig, W.C. (Ed.), The Primate Fossil Record. Cambridge University Press.

Rosenberger, A.L., Hartwig, W.C., Wolff, R.G., 1991. Szalatavus attricuspis, an early platyrrhine primate. Folia Primatologica. 56, 225–233.

Rosenberger, A.L., Strier, K.B., 1989. Adaptive radiation of the ateline primates. Journal of Human Evolution. 18, 717–750.

Rosenberger, A.L., Tejedor, M.F., Cooke, S.B., Pekar, S., 2009. Platyrrhine Ecophylogenetics in Space and Time. In: Garber, P.A., Estrada, A., Bicca-Marques, J.C., Heymann, E.W., Strier, K.B. (Eds.), South American Primates, Developments in Primatology: Progress and Prospects. Springer New York, pp. 69–113.

Ross, C., 1996. Adaptive explanation for the origins of the Anthropoidea (Primates). American Journal of Primatology. 40, 205–230.

Ross, C., Williams, B., Kay, R.F., 1998. Phylogenetic analysis of anthropoid relationships. Journal of Human Evolution. 35, 221–307.

Ross, C.F., 2000. Into the Light: The Origin of Anthropoidea. Annual Review of Anthropology. 29, 147–194.

Ross, C.F., 2005. Finite element analysis in vertebrate biomechanics. The Anatomical Record Part A: Discoveries in Molecular, Cellular, and Evolutionary Biology. 283A, 253–258.

Rowe, N., Myers, M. (Eds.), 2016. All the Worlds Primates, UK ed. edition. Pogonias Press, Charlestown, RI.

Ruff, C., Holt, B., Trinkaus, E., 2006. Who's afraid of the big bad Wolff?: "Wolff's law" and bone functional adaptation. American Journal of Physical Anthropology. 129, 484–498.

Rylands, A.B., Mittermeier, R.A., 2009. The Diversity of the New World Primates (Platyrrhini): An Annotated Taxonomy. In: South American Primates, Developments in Primatology: Progress and Prospects. Springer, New York, pp. 23–54.

Sargis, E.J., Terranova, C.J., Gebo, D.L., 2008. Evolutionary morphology of the guenon postcranium and its taxonomic implications. Mammalian Evolutionary Morphology. 361–372.

Seiffert, E.R., Simons, E.L., Clyde, W.C., Rossie, J.B., Attia, Y., Bown, T.M., Chatrath, P., Mathison, M.E., 2005. Basal Anthropoids from Egypt and the Antiquity of Africa's Higher Primate Radiation. Science. 310, 300–304.

Seiffert, E.R., Simons, E.L., Fleagle, J.G., Godinot, M., 2010. Paleogene anthropoids. Cenozoic mammals of Africa. Berkeley: University of California Press. p. 369–391.

Silcox, M.T., Sargis, E.J., Bloch, J.I., Boyer, D.M., 2015. Primate Origins and Supraordinal Relationships: Morphological Evidence. In: Henke, W., Tattersall, I. (Eds.), Handbook of Paleoanthropology. Springer Berlin Heidelberg, pp. 1053–1081.

Simons, E.L., Ettel, P.C., 1970. Gigantopithecus. Scientific American. 222, 76–87.

Simons, E.L., Plavcan, J.M., Fleagle, J.G., 1999. Canine sexual dimorphism in Egyptian Eocene anthropoid primates: Catopithecus and Proteopithecus. Proceedings of the National Academy of Sciences. 96, 2559–2562.

Simons, E.L., Rasmussen, T., 1994. A whole new world of ancestors: Eocene anthropoideans from Africa. Evolutionary Anthropology: Issues, News, and Reviews. 3, 128–139.

Simpson, G.G., 1944. Tempo and mode in evolution. Columbia University Press.

Slice, D.E., 2007. Geometric Morphometrics. Annual Review of Anthropology. 36, 261–281.

Slowinski, J.B., Guyer, C., 1989. Testing the Stochasticity of Patterns of Organismal Diversity: An Improved Null Model. The American Naturalist. 134, 907–921.

Slowinski, J.B., Guyer, C., 1993. Testing Whether Certain Traits have Caused Amplified Diversification: An Improved Method Based on a Model of Random Speciation and Extinction. The American Naturalist. 142, 1019–1024.

Smaers, J.B., Mongle, C.S., Kandler, A., 2016. A multiple variance Brownian motion framework for estimating variable rates and inferring ancestral states. Biological Journal of the Linnean Society. 118, 78–94.

Smith, T., Rose, K.D., Gingerich, P.D., 2006. Rapid Asia–Europe–North America geographic dispersal of earliest Eocene primate Teilhardina during the Paleocene–Eocene thermal maximum. Proceedings of the National Academy of Sciences. 103, 11223–11227.

Soligo, C., Smaers, J.B., 2016. Contextualising primate origins – an ecomorphological framework. Journal of Anatomy. 228, 608–629.

Spears, I.R., Crompton, R.H., 1994. Finite Elements Stress Analysis as a possible tool for reconstruction of hominid dietary mechanics. Zeitschrift für Morphologie und Anthropologie. 80, 3–17.

Springer, M.S., Meredith, R.W., Gatesy, J., Emerling, C.A., Park, J., Rabosky, D.L., Stadler, T., Steiner, C., Ryder, O.A., Janečka, J.E., 2012. Macroevolutionary dynamics and historical biogeography of primate diversification inferred from a species supermatrix. PloS one. 7, e49521.

Stadler, T., 2011. Mammalian phylogeny reveals recent diversification rate shifts. Proceedings of the National Academy of Sciences of the United States of America. 108, 6187–6192.

Stayton, C.T., 2009. Application of Thin-Plate Spline Transformations to Finite Element Models, or, How to Turn a Bog Turtle into a Spotted Turtle to Analyze Both. Evolution. 63, 1348–1355.

Stayton, C.T., 2011. Biomechanics on the half shell: functional performance influences patterns of morphological variation in the emydid turtle carapace. Zoology. 114, 213–223.

Strier, K.B., 1992. Atelinae adaptations: Behavioral strategies and ecological constraints. American Journal of Physical Anthropology. 88, 515–524.

Strier, K.B., 2006. Primate behavioral ecology. Prentice Hall, Upper Saddle River, N.J.

Sussman, R.W., 1991. Primate origins and the evolution of angiosperms. American Journal of Primatology. 23, 209–223.

Sussman, R.W., Tab Rasmussen, D., Raven, P.H., 2013. Rethinking primate origins again. American journal of primatology. 75, 95–106.

Szalay, F.S., Delson, E., 2013. Evolutionary History of the Primates. Academic Press.

Takai, M., Anaya, F., 1996. New specimens of the oldest fossil platyrrhine, Branisella boliviana, from Salla, Bolivia. American Journal of Physical Anthropology. 99, 301–317.

Takai, M., Anaya, F., Shigehara, N., Setoguchi, T., 2000. New fossil materials of the earliest new world monkey, Branisella boliviana, and the problem of platyrrhine origins. American Journal of Physical Anthropology. 111, 263–281.

Tarca, A.L., Carey, V.J., Chen, X., Romero, R., Drăghici, S., 2007. Machine Learning and Its Applications to Biology. PLOS Computational Biology. 3, e116.

Taylor, M., Prendergast, P.J., 2015. Four decades of finite element analysis of orthopaedic devices: Where are we now and what are the opportunities? Journal of Biomechanics, In Memory of Rik Huiskes. 48, 767–778.

Tejedor, M.F., 2008. The origin and evolution of Neotropical Primates. Arquivos do Museu Nacional, Rio de Janeiro. 66, 251–269.

Tejedor, M.F., Tauber, A.A., Rosenberger, A.L., Swisher, C.C., Palacios, M.E., 2006. New primate genus from the Miocene of Argentina. Proceedings of the National Academy of Sciences. 103, 5437–5441.

Thompson, D.W., 1942. On growth and form. Cambridge University Press.

Thorpe, S.K.S., 2016. Symposium on Primate Ecomorphology: introduction. Journal of Anatomy. 228, 531–533.

Toro-Ibacache, V., Fitton, L.C., Fagan, M.J., O'Higgins, P., 2016. Validity and sensitivity of a human cranial finite element model: implications for comparative studies of biting performance. Journal of Anatomy. 228, 70–84.

Tosi, A.J., Detwiler, K.M., Disotell, T.R., 2005. X-chromosomal window into the evolutionary history of the guenons (Primates: Cercopithecini). Molecular phylogenetics and evolution. 36, 58–66.

Trivedi, S., 2014. Finite element analysis: A boon to dentistry. Journal of Oral Biology and Craniofacial Research. 4, 200–203.

Tseng, Z.J., 2013. Testing Adaptive Hypotheses of Convergence with Functional Landscapes: A Case Study of Bone-Cracking Hypercarnivores. PLoS ONE. 8, e65305.

Uyeda, J.C., Harmon, L.J., 2014. A novel Bayesian method for inferring and interpreting the dynamics of adaptive landscapes from phylogenetic comparative data. Systematic Biology. 63, 902–918.

Venditti, C., Meade, A., Pagel, M., 2011. Multiple routes to mammalian diversity. Nature. 479, 393–396.

Vizcaíno, S.F., Cassini, G.H., Fernicola, J.C., Bargo, M.S., 2011. Evaluating Habitats and Feeding Habits Through Ecomorphological Features in Glyptodonts (Mammalia, Xenarthra). Ameghiniana. 48, 305–319.

Waddell, P.J., Okada, N., Hasegawa, M., 1999. Towards resolving the interordinal relationships of placental mammals. Systematic Biology. 48, 1–5.

Wainwright, P.C., Reilly, S.M., 1994. Ecological morphology: integrative organismal biology. University of Chicago Press.

Wang, X.P., Yu, L., Roos, C., Ting, N., Chen, C.P., Wang, J., Zhang, Y.P., 2012. Phylogenetic Relationships among the Colobine Monkeys Revisited: New Insights from Analyses of Complete mt Genomes and 44 Nuclear Non-Coding Markers. PLOS ONE. 7, e36274.

Weber, G.W., Bookstein, F.L., 2011. Virtual anthropology: a guide to a new interdisciplinary field. Springer, Wien; London.

Whitehead, P.F., Jolly, C.J. (Eds.), 2000. Old World Monkeys, 1 edition. ed. Cambridge University Press, Cambridge.

Williams, B.A., Kay, R.F., Kirk, E.C., Ross, C.F., 2010. Darwinius masillae is a strepsirrhine--a reply to Franzen et al. (2009). Journal of Human Evolution. 59, 567-573; discussion 574-579.

Williams, E.E., 1972. The Origin of Faunas. Evolution of Lizard Congeners in a Complex Island Fauna: A Trial Analysis. Evolutionary Biology. In: Dobzhansky T., Hecht M.K., Steere W.C. (Eds), Evolutionary Biology. Springer, Boston, MA, pp. 47–89.

Williams, J.L., Lewis, J.L., 1982. Properties and an anisotropic model of cancellous bone from the proximal tibial epiphysis. Journal of biomechanical engineering. 104, 50–56.

Wilson, R.A., Kehr, F.C. (Eds.), 2001. The MIT Encyclopedia of the Cognitive Sciences, New Ed edition. MIT Press, Cambridge.

Winemiller, K.O., 1991. Ecomorphological diversification in lowland freshwater fish assemblages from five biotic regions. Ecological Monographs. 61, 343–365.

Witmer, L.M., 1995. The extant phylogenetic bracket and the importance of reconstructing soft tissues in fossils. Functional morphology in vertebrate paleontology. 1, 19–33.

Wolff, R.G., 1984. New specimens of the primate Branisella boliviana from the early oligocene of Salla, Bolivia. Journal of Vertebrate Paleontology. 4, 570–574.

Wroe, S., McHenry, C., Thomason, J., 2005. Bite club: comparative bite force in big biting mammals and the prediction of predatory behaviour in fossil taxa. Proceedings of the Royal Society B: Biological Sciences. 272, 619–625.

Wroe, S., Moreno, K., Clausen, P., Mchenry, C., Curnoe, D., 2007. High-Resolution Three-Dimensional Computer Simulation of Hominid Cranial Mechanics. The Anatomical Record: Advances in Integrative Anatomy and Evolutionary Biology. 290, 1248–1255.

Yapuncich, G.S., Boyer, D.M., 2014. Interspecific scaling patterns of talar articular surfaces within primates and their closest living relatives. Journal of Anatomy. 224, 150–172.

Yapuncich, G.S., Gladman, J.T., Boyer, D.M., 2015. Predicting euarchontan body mass: A comparison of tarsal and dental variables. American Journal of Physical Anthropology. 157, 472–506.

Youlatos, D., 2004. Multivariate analysis of organismal and habitat parameters in two neotropical primate communities. American Journal of Physical Anthropology. 123, 181–194.

Youlatos, D., Meldrum, J., 2011. Locomotor Diversification in New World Monkeys: Running, Climbing, or Clawing Along Evolutionary Branches. The Anatomical Record: Advances in Integrative Anatomy and Evolutionary Biology. 294, 1991–2012.

Young, M.T., Bell, M.A., Brusatte, S.L., 2011. Craniofacial form and function in Metriorhynchidae (Crocodylomorpha: Thalattosuchia): modelling phenotypic evolution with maximum-likelihood methods. Biology Letters. 7, 913–916.

Zalmout, I.S., Sanders, W.J., MacLatchy, L.M., Gunnell, G.F., Al-Mufarreh, Y.A., Ali, M.A., Nasser, A.-A.H., Al-Masari, A.M., Al-Sobhi, S.A., Nadhra, A.O., Matari, A.H., Wilson, J.A., Gingerich, P.D., 2010. New Oligocene primate from Saudi Arabia and the divergence of apes and Old World monkeys. Nature. 466, 360–364.

Zelditch, M.L., Swiderski, D.L., Sheets, H.D., 2012. Geometric Morphometrics for Biologists, Second Edition: A Primer, 2 edition. ed. Academic Press, Amsterdam u.a.

Zienkiewicz, O.C., Taylor, R.L., Zhu, J.Z., 2005. The finite element method its basis and fundamentals. Elsevier Butterworth-Heinemann, Amsterdam; Boston.

Zinner, D., Buba, U., Nash, S., Roos, C., 2011. Pan-African Voyagers: The Phylogeography of Baboons. In: Primates of Gashaka, Developments in Primatology: Progress and Prospects. Springer, New York, NY, pp. 319–358.

Zinner, D., Wertheimer, J., Liedigk, R., Groeneveld, L.F., Roos, C., 2013. Baboon phylogeny as inferred from complete mitochondrial genomes. American Journal of Physical Anthropology. 150, 133–140.

Zollikofer, C.P., Leon, M.P. de, 2005. Virtual Reconstruction: A Primer in Computer-Assisted Paleontology and Biomedicine, 1 edition. ed. Wiley-Liss, Hoboken, N.J.

CHAPTER 2

Standing on the Shoulders of Apes: Analyzing the Form and Function of the Hominoid Scapula using Geometric Morphometrics and Finite Element Analysis

Standing on the Shoulders of Apes: Analyzing the Form and Function of the Hominoid Scapula Using Geometric Morphometrics and Finite Element Analysis

Thomas A. Püschel* and William I. Sellers

Computational and Evolutionary Biology Group, Faculty of Life Sciences, University of Manchester, Manchester, M13 9PT, UK

ABSTRACT

Objective: The aim was to analyze the relationship between scapular form and function in hominoids by using geometric morphometrics (GM) and finite element analysis (FEA).
Methods: FEA was used to analyze the biomechanical performance of different hominoid scapulae by simulating static postural scenarios. GM was used to quantify scapular shape differences and the relationship between form and function was analyzed by applying both multivariate-multiple regressions and phylogenetic generalized least-squares regressions (PGLS).
Results: Although it has been suggested that primate scapular morphology is mainly a product of function rather than phylogeny, our results showed that shape has a significant phylogenetic signal. There was a significant relationship between scapular shape and its biomechanical performance; hence at least part of the scapular shape variation is due to non-phylogenetic factors, probably related to functional demands.
Discussion: This study has shown that a combined approach using GM and FEA was able to cast some light regarding the functional and phylogenetic contributions in hominoid scapular morphology, thus contributing to a better insight of the association between scapular form and function. Am J Phys Anthropol 159:325–341, 2016.   © 2015 Wiley Periodicals, Inc.

Primates live in diverse environments, mastering both life in trees and in terrestrial locations (Fleagle, 1998). Because of the variable requirements of these diverse ecological niches, primate movements are consequently complex, exhibiting an impressively large locomotor repertoire. This locomotor complexity relies on the strong hind limbs and mobile forelimbs. The overall mobility of the forelimb depends on the structure and function of the shoulder region (Larson, 1995; Chan, 2007). Consequently, the evolution of shoulder mobility is one of the important evolutionary processes generating the locomotor diversity of primates. The latter is especially relevant among hominoids because within Hominoidea five divergent locomotion modes and associated body plans have evolved (Preuschoft, 2004): arm-swinging in gibbons; forelimb-dominated slow climbing in orangutans; quadrupedalism with climbing in the African apes; mixed bipedal climbing for australopithecines; and bipedal walking in humans. Although the anatomy of the upper limb of apes has been suggested to be adapted for suspensory behaviors (Aiello and Dean, 1990; Larson, 1993; Rose, 1993), some significant differences in limb morphology have also been described that could correspond to differences in locomotion. Even though the locomotor repertoires of non-human apes overlap to a certain extent, the proportions of the different locomotor behaviors and their related kinematics differ between species and hence it is logical to expect that these differences will be reflected in their shoulder morphology. One of the main behavioral dissimilarities is the amount of time that each species spends in arboreal locations. For instance, orangutans and gibbons are predominantly arboreal spending the majority of their time in the canopy (Rodman, 1984), while on the other hand African apes are primarily terrestrial

using knuckle-walking when travelling (Hunt, 2004), spending time in the forest canopy to almost exclusively sleep and feed (Hunt, 1992).

The shoulder is a region that in primates functions in rather dissimilar ways in different groups (Oxnard, 1967). It is a pivotal component of the locomotor system as it links the upper limb with the trunk and participates in several ways during different locomotion behaviors (e.g., grasping, climbing, brachiation, among others). Primates exhibit some specific morphological features in their shoulders that distinguish them with respect to other mammals, such as a well-developed clavicle, a dorsally shifted scapula with a prominent acromion and robust spine, and a relatively straight humerus with a globular head (Schultz, 1930, 1961). These traits have usually been related to the high mobility of the arm, and the wide

*Correspondence to: Thomas A. Püschel, Faculty of Life Sciences, University of Manchester, Michael Smith Building, Oxford Road, Manchester, M13 9PT, United Kingdom.
E-mail: thomas.puschel@postgrad.manchester.ac.uk

excursions of the forelimb. Earlier studies (Oxnard and Ashton, 1962; Ashton and Oxnard, 1963, 1964a,b) showed that forelimb function was related to the degree to which the limb is subject to tensile or compressive forces, being consequently classified based on these results: a) quadrupeds (shoulder subject to mainly compressive forces), b) brachiators (shoulder subject to mostly tensile forces), and c) semi-brachiators (shoulder intermittingly subject to both forces) (Oxnard, 1967, 1968, 1973; Feldesman, 1976; Corruccini and Ciochon, 1978). Following this trend, several authors attempted to relate the observed variability in the primate scapula and associate it with a priori defined locomotor categories by using morphometrics (Miller, 1932; Inman et al., 1944; Davis, 1949; Smith and Savage, 1956; Ashton and Oxnard, 1963, 1964a; Müller, 1967; Oxnard, 1973; Roberts, 1974; Corruccini and Ciochon, 1976; Fleagle, 1977; Kimes et al., 1981; Shea, 1986; Taylor, 1997; Young, 2004, 2006, 2008). These studies have shown that the primate scapular morphology mainly reflects its function; however these analyses do not provide any understanding about the underlying processes relating the scapular form with its function. Although valuable, most of the research about the shoulder girdle have been restricted to morphological comparisons and infrequently aimed to elucidate function from a biomechanical perspective (Preuschoft et al., 2010).

The scapula is anatomically and biomechanically involved in shoulder function and the movement of the arm (Kibler and McMullen, 2003). During daily activities, the shoulder and arm movements required to produce a change in the glenohumeral position are linked. Scapula, shoulder, and arm are either moved into or stabilize in a certain position in order to generate, absorb, and transfer forces that allow movement. Nonetheless, the specific biomechanical function of the shoulder is poorly known when compared to other anatomical locations (Preuschoft et al., 2010). Some classical studies have focused on estimating the force equilibrium for the glenoid cavity of chimpanzees (Preuschoft, 1973), defining basic conditions (Badoux, 1974; Roberts, 1974) and analyzing the functional loadings of the scapula by modeling it as a framework (Müller, 1967). In spite of the practical difficulties involved in observing the movements of the shoulder, some primate taxa have been analyzed (Schmidt and Fischer, 2000; Schmidt, 2005, 2008; Schmidt and Krause, 2011), complementing the observations made earlier by several authors (Stern and Oxnard, 1973; Rose, 1974, 1979; Larson, 1993; Whitehead and Larson, 1994). Preuschoft et al., (2010) applied both armchair biomechanics and 2D finite element models in order to understand the basic functional conditions that occur in the shoulder joint and shoulder girdle of primates. The stress distributions in their hypothetical scapula under the conditions of terrestrial versus suspensory behavior showed that during quadrupedalism the scapula concentrates stress along the cranial margin whereas during suspension generates higher stresses along the axillary border. This would mean that quadrupedal locomotion involves joint forces and muscle activities that would require a long scapula with axillar and cranial margins of a relatively similar length. On the other hand, suspensory behaviors would need a more extended axillary border and a relatively shorter cranial margin in order to provide longer lever arms to the active muscles. Based on their results, they suggested that the forces exerted on the scapula generate, at least partially, its shape (Preuschoft et al., 2010). Indeed,

arboreal monkeys seem to have concordant morphological features such as the reinforcement of the axillary border of the scapula and the extension of the infraspinatous fossa (Larson, 1993). This is coherent with all the evidence supporting the idea that bone is functionally adapted to the mechanical demands that are imposed during life (Wolff, 1892; Pearson and Lieberman, 2004).

Nevertheless, other lines of evidence regarding shoulder form and function have found that this relationship is not as clear or straightforward as initially thought (Taylor, 1997; Young, 2003, 2008; Larson and Stern, 2013). It has been found that locomotion differences are not well reflected at an intraspecific level in gorilla scapulae (Taylor, 1997) and that despite locomotion similarities, the scapulae of hylobatids are most similar to those of panids, rather than to those of orangutans (Young, 2008). Furthermore, comparative electromyography data recorded from different apes have shown that there are few differences in patterns of muscle activity among them, consequently suggesting that perhaps hominoids in general use basically similar shoulder mechanisms during locomotion (Larson and Stern, 2013). Unfortunately, there is no clear perspective about the relationship between scapular morphology and its function, in spite of its growing relevance due to recent finding of several hominin scapulae such as *Australopithecus afarensis* (Alemseged et al., 2006; Haile-Selassie et al., 2010; Green and Alemseged, 2012) or *Australopithecus sediba* (Berger et al., 2010; Churchill et al., 2013). In fact, the analyses of these fossils have shown that they tend to resemble the scapula of juvenile gorillas (Green and Alemseged, 2012) or orangutans (Churchill et al., 2013), instead of those of our closest phylogenetic relatives (i.e., panids). Because scapular form has been widely regarded to be primarily a product of shoulder function, it has been a central element in the interpretation of the primate fossil record (Larson, 2007). Understanding how scapular morphology is related to biomechanical performance is important in order to reconstruct the possible locomotor repertoires of extinct species and to appreciate the locomotor diversity observed in extant hominoids.

Nowadays it is possible to produce scientifically accurate virtual reconstructions of primates (Zollikofer and Leon, 2005; Sellers et al., 2010; Ogihara et al., 2011; Weber and Bookstein, 2011). Technological advances in 3D imaging allow the generation of virtual models based on skeletal morphology and comparative soft tissue data obtained from the literature. This is highly useful since the study of primate biomechanics is challenging because traditional experimental techniques are not easily applicable due to practical, conservation, and ethical reasons (Sellers et al., 2010; D'Août and Vereecke, 2011). Computer-based biomechanics comprise 3D quantitate image analysis and simulation techniques applied to musculo-skeletal systems such as finite element analysis (FEA) and multibody dynamics (Sellers and Crompton, 2004; Kupczik, 2008; O'Higgins et al., 2012). FEA is a technique that reconstructs stress, strain, and deformation in material structures and has its origin in mathematical and engineering problems, although it is been increasingly used in biological fields (Rayfield, 2007). This technique is a numerical analysis that acts by dividing a system into a finite number of discrete elements with well-known properties (e.g., triangles, tetrahedrons, or cubes) (Ross, 2005). Strain and stress can be solved by finding analytical solutions if the geometry of the object is simple enough. However, more complex forms may be difficult or even impossible to solve using analytical means, especially if the loading regimens and/or material

properties are complex (Beaupré and Carter, 1992). This situation is the most common when dealing with realistic representations of biological structures. FEA offers an alternative approach, approximating the solution by subdividing complex geometries into multiple finite elements of simple geometry. In a structural analysis, typical mechanical parameters of interest are strain, which is the deformation within a structure (Δlength/length; unitless) and stress, the applied force per unit area (Nm^{-2}), which are obtainable as result of FEA (Kupczik, 2008). FEA studies of the scapula have been mostly restricted to orthopedic studies focusing principally on the generation of models of the implanted glenoid (e.g., Friedman et al., 1992; Lacroix et al., 2000; Gupta and van der Helm, 2004; Gupta et al., 2004; Yongpravat et al., 2013; Campoli et al., 2014; Hermida et al., 2014). Even though other FEA studies have been used in comparative primatology and paleoanthropology, they have been predominantly devoted to the analysis of the craniofacial system during mastication (Kupczik et al., 2007; Wroe et al., 2007, 2010; Strait et al., 2009; Curtis et al., 2011; Dumont et al., 2011; O'Higgins et al., 2011; Fitton et al., 2012; Kupczik and Lev-Tov Chattah, 2014). There have been fewer attempts applying FEA to analyze different primate scapulae (Ogihara et al., 2003), so the present study probably represents one of the first analyses of this anatomical structure using an explicit comparative framework.

Morphometrics can be understood as the quantitative analysis of form (i.e., shape and size) and how it covaries with regard to other factors (e.g., biomechanics, development, ecology, genetics, etc.) (O'Higgins, 2000; Adams et al., 2004, 2013). More specifically, geometric morphometrics (GM) refers to the application of morphometrics to coordinate data (i.e., 2D or 3D Cartesian coordinates), normally defined as discrete anatomical loci that are homologous among all the individuals under analysis (Bookstein, 1991; Slice, 2007). GM allows the analysis of the association between morphometric and biomechanical data, which is really useful when studying the relationship between shape and function. There are many available methods to study the connection between morphological and biomechanical variables (e.g., canonical correlation, regression analysis, Mantel test, principal coordinate analysis, and partial least squares, among others). Recent developments in the study of geometric shape and biomechanical modeling have proposed that using both GM and FEA could provide a better understanding of the existing relationship between the shape of skeletal elements and their mechanical performance (Pierce et al., 2008; Piras et al., 2012, 2013; Tseng, 2013). Even though there has been some controversy regarding how to properly combine FEA and GM data (Bookstein, 2013), there is relative agreement that bridging these two techniques could provide interesting insights about the relationship between form and function (O'Higgins et al., 2011; Parr et al., 2012). Because of this reason, different approaches have been proposed to combine FEA and GM data, such as landmark-based analysis in the size-and-shape space of the deformations obtained as result of FEA (Cox et al., 2011; Gröning et al., 2011; O'Higgins et al., 2011; Milne and O'Higgins, 2012; O'Higgins and Milne, 2013), the analysis of finite element models based on warped and target surface meshes (Parr et al., 2012), and the construction of regressions for strain energy density on the largest-scale relative warps (Bookstein, 2013). Besides the issues of how to properly analyze both GM and FEA data, another problem arises when carrying out any biological study containing several species, due to the phy-

logenetic structure of the data (i.e., non-independence problem). Some approaches have been proposed to take into account phylogeny such as the application of phylogenetic generalized least squares models (PGLS) to fit regressions between matrices of functional/ecological variables and shape variables (Rüber and Adams, 2001; Clabaut et al., 2007; Meloro et al., 2008; Nogueira et al., 2009; Raia et al., 2010; Piras et al., 2013), the use of phylogenetic-independent contrasts estimated for each shape variable before associating them with contrasts derived from functional/ecological variables applying either partial least squares (Klingenberg and Ekau, 1996) or multivariate regressions (Figueirido et al., 2010) and the correlation between morphometric, functional/ecological, and phylogenetic matrices (Harmon et al., 2005; Young et al., 2007; Astúa, 2009; Monteiro and Nogueira, 2010). In the present study, PGLS was preferred because this method is considered more informative and powerful than other methods (e.g., distance matrix correlation) (Peres-Neto and Jackson, 2001).

In this work, FEA was used to analyze the biomechanical performance of different hominoid scapulae by simulating two basic static scenarios: a) quadrupedal standing and b) bimanual suspension. It is expected that scapular mechanical performances will vary depending on the principal locomotion mode of each species. Hence, it is expected that those species that are mostly quadrupedal (i.e., chimpanzees, bonobos, and gorillas) will better withstand the forces generated during quadrupedal standing, while more arboreal species (i.e., orangutans and gibbons) will better bear the forces generated during suspension, as previously proposed (Oxnard and Ashton, 1962; Ashton and Oxnard, 1964a; Roberts, 1974; Preuschoft et al., 2010). On the other hand, GM was used to quantify shape differences, thus comparing different scapular morphologies in relation to their known locomotion regimes. Based on preceding studies (Oxnard and Ashton, 1962; Ashton and Oxnard, 1964a; Young, 2008), scapular shape is expected to reflect mostly functional demands instead of phylogenetic relationships. Finally both FEA and GM were used to study the relationship between form and function by applying both multiple multivariate regressions and PGLS regressions. Our results are expected to contribute to a better insight of the association between hominoid scapular morphology and its biomechanical performance.

MATERIALS AND METHODS

Sample

CT-scan stacks of 11 different hominoid individuals obtained from online databases and two zoos were analyzed (Table 1; Fig. 1) (for further details about the sample see Supporting Information 1). The included species were *Hylobates lar, Pongo abelii, Pongo pygmaeus, Gorilla gorilla, Pan paniscus, Pan troglodytes*, and *Homo sapiens*. All the specimens were adult with no evident or reported pathologies associated with their shoulder girdles. Only left scapulae were modeled, although due to some CT artifacts, some right scapulae were reflected to be used in the subsequent analyses.

Finite element modeling

Segmentation. The first step to build a model from a CT stack is to carry out image segmentation. This procedure basically consists in extracting the material of
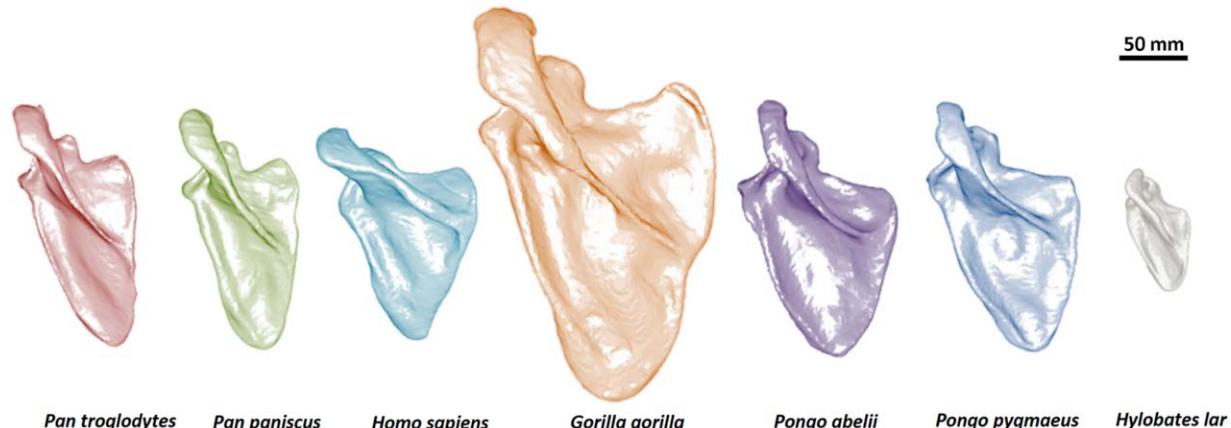
TABLE 1. Sample

Species	Common name	Accession number	Origin	Sex	Number of elements
Pan paniscus	Bonobo	Desmond	The Royal Zoological Society of Antwerp	Male	953156
Gorilla gorilla	Gorilla	Willie (GAIN 23)	Digital Morphology Museum (KUPRI)	Male	931087
Pan troglodytes	Chimpanzee	9266	Digital Morphology Museum (KUPRI)	Male	936693
Pan troglodytes	Chimpanzee	9783	Digital Morphology Museum (KUPRI)	Female	952156
Pan troglodytes	Chimpanzee	10048	Digital Morphology Museum (KUPRI)	Female	950295
Pongo pygmaeus	Bornean Orangutan	Satsuki (GAIN 37)	Digital Morphology Museum (KUPRI)	Female	996480
Pongo abelii	Sumatran Orangutan	9653	Digital Morphology Museum (KUPRI)	Male	935358
Homo sapiens	Human	Visible human female	The Visible Human Project	Female	962225
Homo sapiens	Human	Visible human male	The Visible Human Project	Male	985562
Hylobates lar	White-handed Gibbon	3308	National Museum of Scotland	Male	940973
Hylobates lar	White-handed Gibbon	3508	National Museum of Scotland	Female	939611

interest (in this case bone) out of the surrounding background and tissues where it is embedded. The CT-scans of the different hominoid species were segmented; DICOM files were imported into Seg3D v. 2.1 (CIBC, USA) where each specimen was segmented by applying a combination of case-specific thresholding values and manual painting techniques. Scapulae can be complicated to segment because their blade is extremely thin at certain areas. As a result all the models were dilated one extra voxel, to avoid possible holes in the mesh that could affect the FEA results. After performing this procedure and manually checking the results, the extra voxel layer was removed by using an erode function in the same software. The scapulae were modeled as solid parts composed only by cortical bone. Surfaces were then generated and exported as .STL files into Geomagic Studio v. 12 (Geomagic, USA). Using this software, possible errors in the polygon mesh were detected and corrected in order to remove protruding vertices and localized holes. The models had dissimilar number of elements derived from the differences in the original scan resolution; therefore they were decimated to a number of elements ranging from 20,000 to 25,000 mesh triangles. All the models were globally remeshed to simplify their element geometry, keeping the number of mesh triangles in a similar number range (i.e., 20,000–25,000). The remeshing process was applied to generate a more homogenous mesh in terms of the shape of the triangles, their distribution on the surface, and their connectivity. In addition, one individual was selected as a reference to perform a best-fit alignment using the same software in order to align all the models with respect to a common reference plane. This procedure was carried out prior to FEA to align all the models, so that loads could be applied in the same axis and to allow easier interpretation of stress results. Basically, the procedure consisted in fitting two scapula models at each time by measuring from point to point and adjusting the location of the target model to the stationary reference specimen until the average deviation was as low as possible using an iterative process (sample size: 10,000). The sums of squares of the distances between the sample pairs were minimized over all the rigid motions that could realign the two models

to achieve the best-fit alignment of them. This procedure was repeated for each one of the analyzed specimens. The models were then exported as .OBJ files into Autodesk 3ds Max 2012 (AutoDesk, USA), where they were converted into .SAT files. The models were then imported into Abaqus v. 6.13 (Simulia, USA) as closed manifold solid parts in order to carry out an implicit static FEA. Finite element validation analyses have shown that both four-node and eight-node tetrahedral, and mixed four-node tetrahedral and eight-node hexahedral meshes perform well when compared with experimental data (Panagiotopoulou et al., 2011). Likewise, it has been shown that meshes composed by more than 200,000 elements show negligible stress differences between models with four- or ten-node tetrahedra elements (Brassey et al., 2013). Because ten-node tetrahedra are computationally more expensive than those composed by four nodes, the surfaces were meshed using four-node tetrahedral elements (C3D4) by applying a built-in Delaunay meshing algorithm in Abaqus v. 6.13. FE meshes were verified in the same software to find poor-meshed areas or low quality elements (i.e. aspect ratio >10). When found, those areas were re-meshed to improve mesh quality.

Material properties and boundary conditions. Many researchers are currently trying to produce more accurate finite element models by incorporating more detailed information such as muscle activation data, anisotropic material properties, several different tissues with dissimilar material attributes, etc. (Ross et al., 2005; Strait et al., 2005; Kupczik et al., 2007; Gröning et al., 2011; Rayfield, 2011). These kinds of analyses have shown that when this type of information is included, the correlation between simulations and experimental data is usually increased. Nevertheless, in this work FEA was used in a comparative fashion rather than being used to validate the models. Because of the fact that hominoid scapulae are relatively uncommon (belonging most of the time to museum specimens), destructive experimental mechanical approaches are
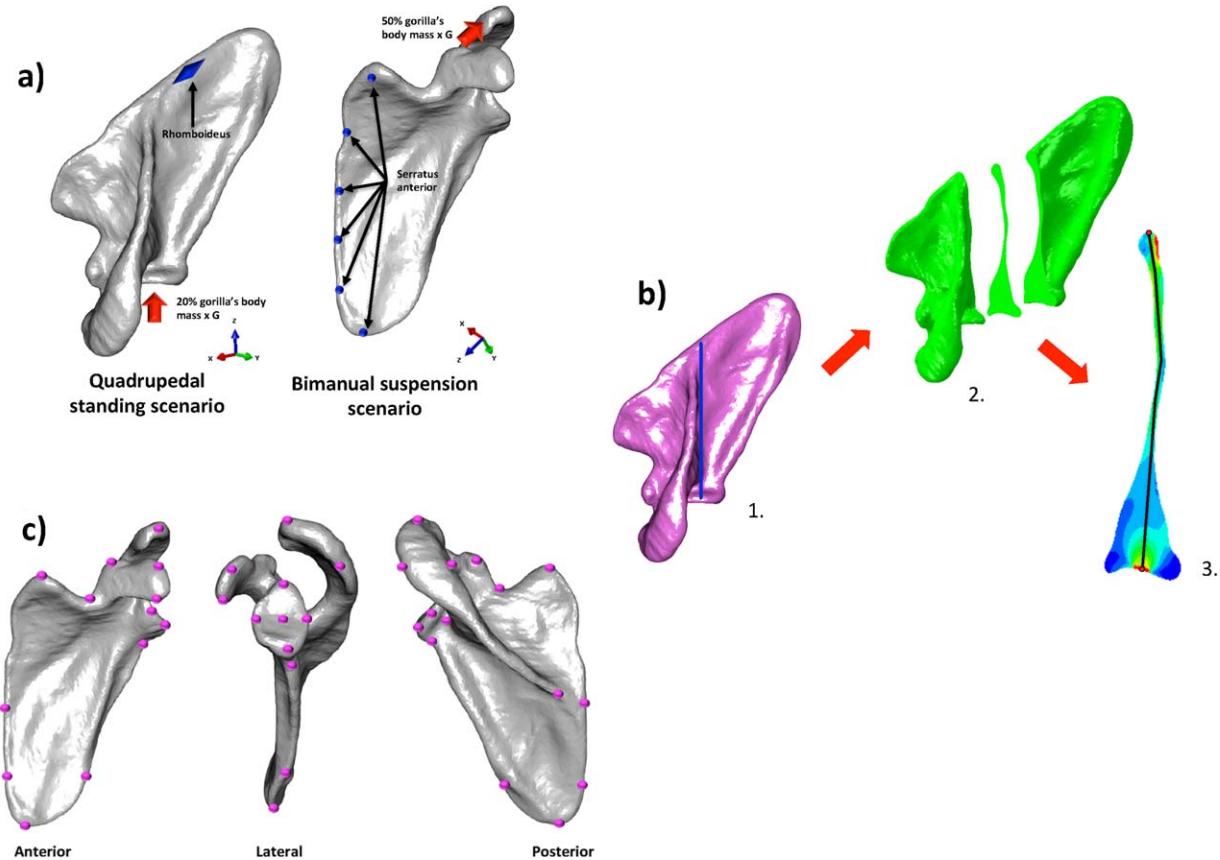
Fig. 1. Three-dimensional volumetric models of the hominoid scapulae considered in this study. [Color figure can be viewed in the online issue, which is available at wileyonlinelibrary.com.]

typically difficult or impossible to perform. The present study therefore applied FEA as a structural comparative technique rather than trying to specifically recreate how the hominoid is loaded during life; the idea was to compare a general measure of mechanical performance taking into account phylogenetic relationships. Furthermore, living specimens would probably withstand the tensile strain and stresses experienced during locomotion mostly on their shoulder soft tissues such as muscles, ligaments, and tendons rather than directly on their scapulae. Even though shoulder muscle origin and insertions for hominoids are known (Diogo et al., 2010,2012,2013a,2013b; Diogo and Wood, 2012) and physiological cross-sectional areas of some the muscles are available for some of the analyzed species (Veeger et al., 1991; Keating et al., 1993; Thorpe et al., 1999; Cheng and Scott, 2000; Carlson, 2006; Oishi et al., 2008, 2009; Michilsens et al., 2009; Peterson and Rayan, 2011; Myatt et al., 2012), the specific activation patterns are unknown for the majority of the species when performing the analyzed postures. These reasons ratified the decision of carrying out simpler comparative structural analyses instead of simulating in detail loading scenarios based on unknown or uncertain information. This means that the current work can be better understood as an analysis of how the mechanical behavior of the hominoid scapula is related to its shape, rather than being a highly-realistic simulation of how the scapula is loaded in vivo.

After the construction of the finite element mesh, it was necessary to specify the mechanical properties of the elements composing the specimens. Even though several material properties for primate cortical and trabecular bone have been published especially for humans (e.g., Currey and Butler, 1975; Williams and Lewis, 1982; Currey, 1988; Dechow et al., 1993; Ding et al., 1998; Zysset et al., 1999; Margulies and Thibault, 2000; Phelps et al., 2000; Dechow and Hylander, 2000; Peterson and Dechow, 2003; Havill et al., 2003; Bayraktar et al., 2004; Kaneko et al., 2004; Wang et al., 2006a,b; van Eijden et al., 2006; Hofmann et al., 2006; Kupczik et al., 2007; Daegling et al., 2009), there is almost a total absence of material property values for the analyzed hominoid scapulae. We used rough average values for mammalian-longitudinal cortical bone samples (Currey, 2002) (Young's modulus: 18 GPa; Poisson's ratio 0.3). The scapulae were modeled as solid models composed only of cortical bone in order to simplify the

analyses, as well as to limit the number of assumptions. In fact, recent evidence has shown that FEA applied to specimens with unknown internal architecture can produce reliable results, even when the internal bone architecture cannot be modeled in detail (Fitton et al., 2015). In addition, scapulae do not exhibit high internal complexity in comparison with other bones, because most of the scapular blade consists of only a thin layer of compact tissue (i.e., cortical bone). Although bone generally behaves anisotropically, it was modeled as a linear elastic and isotropic material due to the same reasons outlined above. Besides, it has been shown that isotropic modeling seems to have little effect compared to anisotropic modeling on the pattern of stress (Chen and Povirk, 1996; Strait et al., 2005). Apart from assigning material properties, it was necessary to define boundary conditions (Bhatti, 2005). Two essential boundary conditions were specified; one recreating the action the rhomboideus, and another simulating the constraint imposed by the serratus anterior, as shown in Figure 2a. It was decided to constrain these areas because in both quadrupedal and suspensory situations the forces applied to the shoulder region seem to be predominantly supported by the muscles attached to the vertebral border of the scapula (Badoux, 1974). In these areas the displacements were only constrained in the z-direction in both cases because the forces were applied only in that direction. These boundary conditions were defined to prevent rigid body motions of the geometry and counteract residual moments (from errors when applying the loadings), but without over-constraining the models.

Loading scenarios. The scapula is one of the most complex bones of the primate skeleton due to its particular shape and because it is subjected to a great variety of forces from attached muscles during its movement (Roberts, 1974; Aiello and Dean, 1990). This bone is subject to a number of muscle, ligament, and joint reaction forces during elevation of the arm, that are difficult to quantify (Bagg and Forrest, 1986; Johnson et al., 1996; Kibler and McMullen, 2003; Fayad et al., 2006; Amadi et al., 2008; Bello-Hellegouarch et al., 2013). Quantitative and qualitative estimates of all the muscles, ligaments, and joint reaction forces acting on the human scapula during humeral abduction have shown that the scapula is relatively loaded all over its structure during abduction (van der Helm,

Fig. 2. *Pan paniscus* scapula used to depict **a**) FEA loading scenarios: the red arrows represent the force vectors and their direction, while the blue shapes represent the applied constraints. The constraints representing the action of serratus anterior and rhomboideus muscles were applied in both the quadrupedal standing and bimanual suspension scenarios by limiting displacement in the z-axis; **b**) Extraction method of the stress values: 1) At the center of the glenoid cavity a slice on the x-axis was defined (blue line), 2) this slice was separated and 3) two coordinates at each extreme of the slice (red dots) were used to define a path (black line) divided in 101 equidistant points used to extract von Mises stress values; **c**) 3D landmarks used to perform GM analyses. [Color figure can be viewed in the online issue, which is available at wileyonlinelibrary.com.]

1994; Gupta and van der Helm, 2004). It is therefore extremely difficult to define realistic loading scenarios and necessary to simplify the load cases in order to avoid excessive assumptions.

One important consideration to take into account when analyzing different individuals using FEA is how to make the obtained results comparable. Strain energy is proportional to the square of the load and to volume (Dumont et al., 2009), hence it is important to account for size differences when performing strain energy comparisons. Several solutions have been proposed to compare total strain between different specimens. Suggestions include scaling the loads to yield similar force:surface area ratio or scaling them to a relevant biological measurement (e.g., bite force, moment arm, animal weight) (Fitton et al., 2012; Parr et al., 2012; Brassey et al., 2013). Another possibility is to scale the models to achieve the same surface area or same volume, or to simply scale the obtained results from the analysis with respect to a sensible measure (Dumont et al., 2009). In the present work, it was decided to normalize scapular size by volume while applying the same forces to all the individuals during the FEA. This decision was based on the fact that this approach seems more suitable to evaluate how scapular shape affects mechanical strength. All the scapulae were scaled to have the same volume as the gorilla specimen (i.e., 387810.84 mm^3) in Geomagic Studio

v. 12 (Geomagic, USA), and depending on the specific loading scenarios, different percentages of the reported body weight of the gorilla specimen (i.e., 176 kg) were applied to simulate the mechanical loadings. The biomechanical performance of different hominoid scapulae was tested in two basic static scenarios (Fig. 2a).

Quadrupedal standing: African apes predominantly use knuckle-walking when travelling. According to Hunt (2004), terrestrial quadrupedalism represents 96% of the locomotor behavior in mountain gorillas, 64.4% in lowland gorillas, and 35.3% in bonobos, but only 9.9% in chimpanzees. African ape scapular morphology is therefore expected to show clearer adaptations to terrestrial quadrupedalism. It is important to take in to account that chimpanzees and other primates support most of their body mass on their hind limbs during quadrupedalism rather than on their forelimbs (Reynolds, 1985; Kimura, 1992; Demes et al., 1994; Li et al., 2004; Raichlen et al., 2009). Nonetheless, due to the greater use of terrestrial locomotion modes in the African apes than in orangutans or gibbons, it is reasonable to expect that their forelimbs would be less specialized for arboreal behaviors. Even though African apes do use suspensory behaviors as a static postural activity, it is likely their scapulae are not as specialized for more recurrent suspensory behaviors such as those observed in gibbons and orangutans.

Although adult humans do not use their forelimbs for quadrupedal locomotion, the same loading scenario was applied for comparative purposes. Hominoid forelimbs support about 40% of the body weight during terrestrial quadrupedalism (Reynolds, 1985; Kimura, 1992; Demes et al., 1994; Li et al., 2004; Raichlen et al., 2009). Hence, the total applied load was calculated as 20% of the gorilla's body mass Mb; kg) multiplied by gravitational acceleration (G: 9.81 m s^{-2}), because only one scapula was analyzed per individual. This yielded a total force vector of 345.31 N., which was directed towards the center of the glenoid cavity in the z-axis, and applied in 24 nodes (total force/24 nodes). In addition, two models (one gibbon and the gorilla) were selected to carry out additional simulations to the test the sensitivity of the results to small differences in the application angle of the load vector, so it was changed in 5°. The results were extracted according to the procedure described in Figure 2b and a correlation was estimated to assess the level of concordance between the original stress values and those obtained after changing the load vector (Gibbon: R^2: 0.981, P value: <0.001; Gorilla: R^2: 0.969, P value: <0.001) . Therefore, the results seem to be robust to at least small changes in load direction.

Bimanual suspension: Arm-hanging is probably the only common ape posture requiring complete abduction of the arm (Hunt, 1991a,b,1992,2004). It has been suggested that the cranially oriented glenoid fossa observed among apes may be adaptive to distribute strains more evenly over the glenohumeral joint capsule during arm-hanging (Hunt, 1991b,). The long and narrow scapular shape exhibited by apes has been hypothesized to increase the mechanical advantage of the trapezius and serratus anterior during the scapular rotation necessary for arm-raising (Ashton and Oxnard, 1963, 1964b; Oxnard, 1967). However some hominoid species probably use this locomotor behavior more often than others. For instance, the highly arboreal gibbons and orangutans are expected to better cope with strains derived from this posture than the more quadrupedal species.

Even though earlier studies (Roberts, 1974; Tuttle and Basmajian, 1978) suggested that no scapulohumeral muscle was activated during bimanual or unimanual hanging assuming that joint integrity was kept solely by osseoligamentous structures, new evidence have proved the contrary. Opposed to the common idea that no muscle activation is required while the body is suspended beneath the hand (likely causing transarticular tensile stress at the glenoid cavity), hominoid electromyography data during bimanual hanging has shown that there is a continuous activity in the infraspinatous, posterior deltoid, and teres minor muscles (Larson and Stern, 1986; Larson and Stern, 2013). It has been pointed out that when climbing or hanging, primates activate the levator scapulae and trapezius muscles to prevent the caudal movement of the scapula (Larson and Stern, 1986). The resulting dorsal rotation of the caudal angle of the scapula is counteracted by the action of the caudal portion of the serratus anterior (Larson and Stern, 2013). This implies that the scapula seems to achieve its equilibrium during suspension by the coordinated action of levator scapulae and cranial trapezius, as well as the caudal serratus (Larson and Stern, 1986). In addition, to avoid the pulling of the scapula in a ventral direction, the activity of the caudal portion of the trapezius is required (Larson et al., 1991). In fact it has been observed that this muscular portion is prominently developed in apes (Aiello and Dean, 1990). It has been also men-

tioned that some of the forces applied to the shoulder region during suspension are supported by the muscles attached to the vertebral border of the scapula (i.e., serratus anterior and rhomboideus) (Badoux, 1974). The models were loaded in a simpler scenario by applying total load estimated as 50% of the gorilla's body mass Mb; kg) multiplied by gravitational acceleration (G: 9.81 m s^{-2}), because the total animal weight was supported by the two shoulders, thus yielding a total force vector of 863.28 N. This tensile force vector was directed away from the acromion in the z axis and it was also applied on 24 nodes (total force/24 nodes).
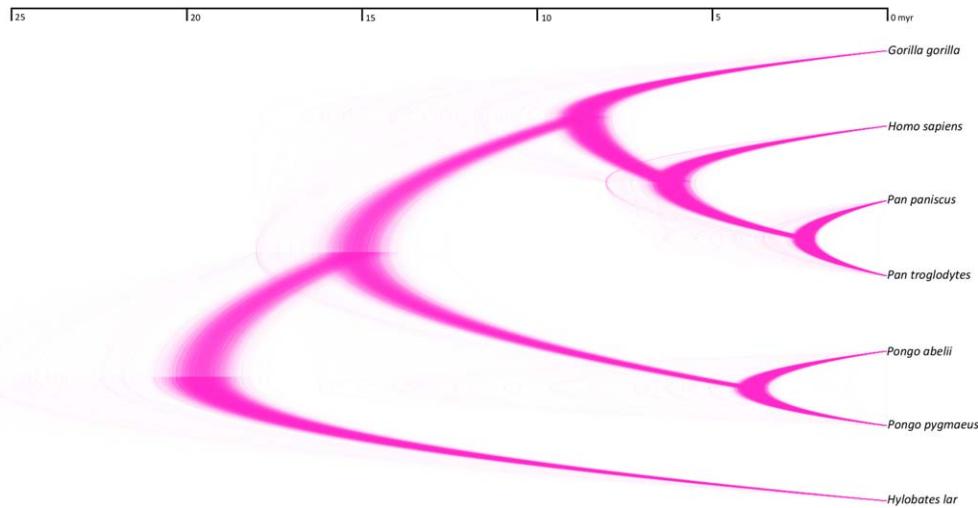
Solution. After defining the material properties and establishing the boundary conditions, the models were submitted into the Abaqus implicit solver. Each specimen was subjected to two different simulations: a) quadrupedal standing and b) bimanual suspension. Stress values were obtained and exported as .CSV files.

Statistical analyses of FEA results. von Mises stress values were obtained from 101 locations extracted along a path as described in Figure 2b. Starting from the center of the glenoid a slice on the x-axis was selected. Two points were defined at each opposite extremes of the slice and between these two coordinates a path was established where 101 equidistant points were positioned to extract stress values. These values were imported into R v.3.1.3 (http://www.R-project.org/) to carry out statistical analyses. The average values per species were calculated for each one of the locations. To visualize these results, a UPGMA clustering was estimated by calculating the Euclidean distances between species using the hclust() function of the package "stats." In addition a Principal Components Analysis (PCA) was performed using the princomp() function of the same package in order to reduce the number variables of this high dimensional dataset, and to subsequently perform the multivariate multiple regressions and the PGLS regressions. Because of the fact that the obtained stress could have values that differ in orders of magnitude between anatomical loci, the PCA was carried out based on the correlation matrix to standardize these possible scale differences. The number of PCs used in the successive analyses was selected to account for ca. 95% of the total variance of the sample.

Geometric morphometrics

The 3D surface models were imported into the R package "geomorph" where 20 homologous landmarks were collected on each one of the analyzed specimens using the digit.fixed() function (Adams and Otárola-Castillo, 2013) (Fig. 2c). All the GM analyses were carried out in the same package. A generalized procrustes analysis was applied to extract the shape variables from the raw landmark data, by removing all the differences due to translation, rotation and scale (Bookstein, 1991). The average shape and biomechanical performance was estimated for each species and used in the subsequent analyses. A PCA of the procrustes coordinates was performed in order to find the orthogonal axes of maximal variation, thus allowing the visualization of scapular shape variation. A consensus phylogeny (described below) was projected onto the space identified by the first two PCs obtained from the covariance matrix of the average shapes of the analyzed taxa. Using this consensus phylogeny, both morphological (i.e., shape variables) and biomechanical (i.e., stress values)

Fig. 3. 10,000 molecular phylogenetic trees plotted to overlap on top of each other in order to represent the evolutionary relationships of the analyzed taxa. The high density of the main branches is indicative of a high consistency between trees. The consensus tree was estimated and used in the subsequent comparative analyses. The plot was generated using DensiTree 2.01 (Bouckaert, 2010) and the phylogenies were obtained from the 10KTrees website (http://10ktrees.fas.harvard.edu/Primates/index.html). [Color figure can be viewed in the online issue, which is available at wileyonlinelibrary.com.]

phylogenetic signal were estimated using a generalization of the Kappa statistic suitable for highly multivariate data using the physignal() function (Blomberg et al., 2003; Adams, 2014). This method, denominated as Kmult, is based on the equivalency between statistical methods based on covariance matrices and those based on distance matrices, thus allowing a convenient way to assess phylogenetic signal in high-dimensional multivariate traits, such as those analyzed here (Adams, 2014). The K-statistic varies between 0 (no phylogenetic signal in the data, for instance with a star phylogeny) to 1 or more (data fit a Brownian motion model of evolution) (Blomberg et al., 2003). To analyze the relationship between shape and function a multiple multivariate regression of shape variables and stress PC scores was performed using the procD.lm() function. Subsequently, in order to examine the relationship between morphology and biomechanical performance taking into account the phylogenetic structure of the data a PGLS regression of shape variables and stress PC scores was performed using the procD.pgls() function. The idea in both cases was to evaluate the amount of shape explained by functional demands (Piras et al., 2013). The PGLS regressions were carried out using the procD.pgls() function. It is important to consider that the phylogenetic covariance matrix is just a 7×7 matrix, which is a limitation. In previous methodological papers (e.g., Blomberg and Garland, 2002; Blomberg et al., 2003), it has been suggested that about 15–20 OTUs are the minimum to have an acceptable statistical power, hence the obtained results have to be cautiously considered. All the aforementioned analyses were carried out in R v. 3.0.3. (http://www.R-project.org/).

Phylogeny

Using the 10kTrees Website (http://10ktrees.fas.harvard.edu/Primates/index.html), 10,000 phylogenies of the analyzed hominoid species were downloaded using the third version of this dataset (Arnold et al., 2010) (Fig. 3). These phylogenies were sampled from a Bayesian phylogenetic analysis of molecular data for eleven mitochondrial and six autosomal genes that were available in GenBank (Arnold et al., 2010). The advantage of using the 10kTrees dataset

that it allows the generation of a set of phylogenetic trees suitable for comparative research that actually reflects uncertainty levels in the understanding of phylogenetic relationships, as well as providing a robust way to test phylogenetic relationships. The consensus tree of these 10,000 phylogenies was estimated and used in the subsequent comparative analyses.
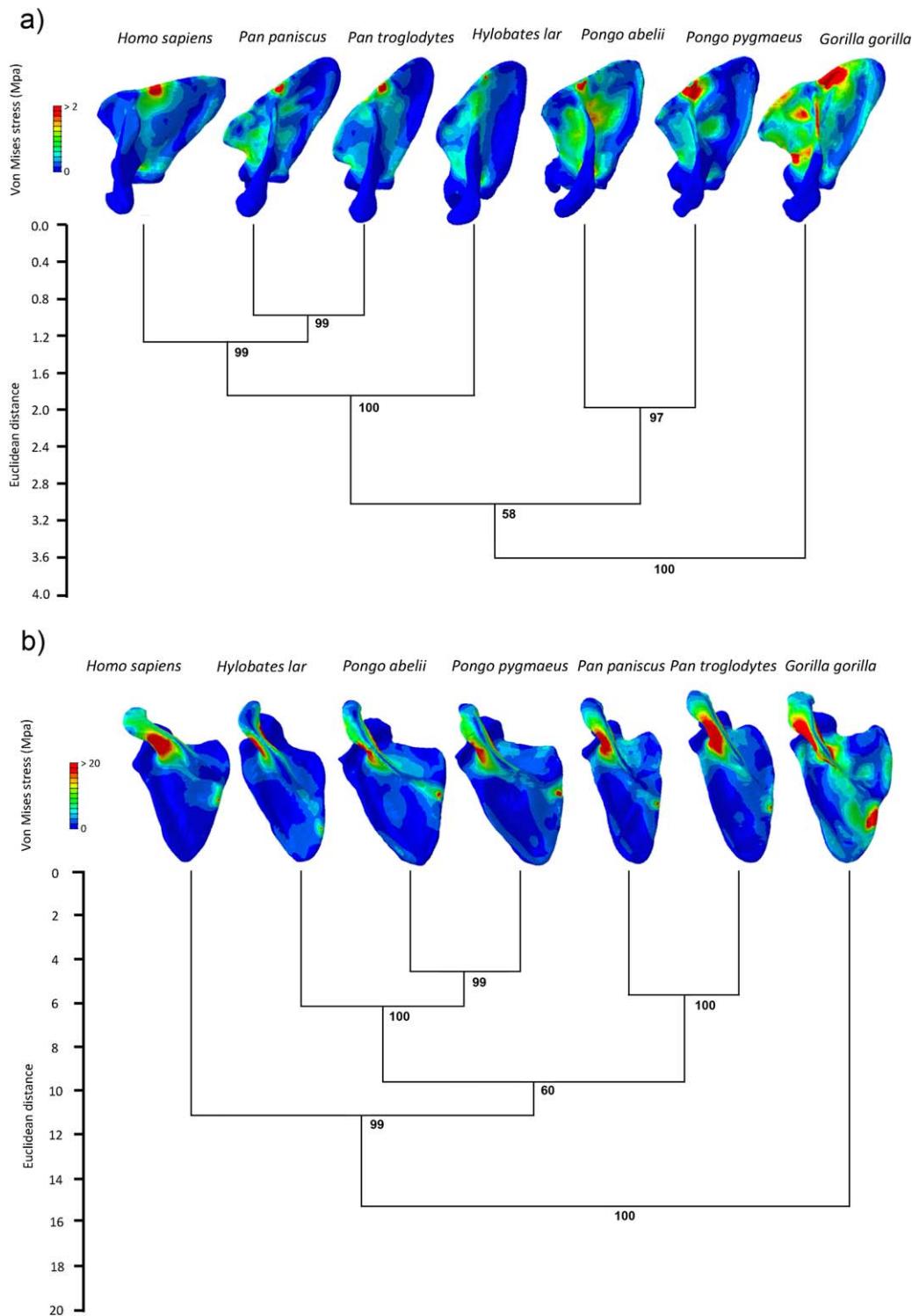
RESULTS
FEA

All the analyzed individuals showed a stress widely distributed on the scapular blade, although it was logically higher in the locations where the constraints were placed (Fig. 4) (the stress values used in the analyses are available in the Supporting Information 2). The suspension scenario logically showed greater stress values (mostly on the acromion) than the quadrupedal standing simulation, due to the fact that higher loads were applied. *Hylobates lar* experienced the lowest stress for both loading scenarios when compared with rest of the hominoids, while the gorilla specimen showed the highest stress values. Interestingly, the pongids showed relatively high stress values for the standing scenario, while exhibiting relatively similar values to the gibbons during the suspension scenario. Biomechanical performance measured as von Mises stress also showed significant phylogenetic signal (quadrupedal standing, Kmult: 0.73; P value: 0.022; 10,000 perm. and bimanual suspension, Kmult: 0.67; P value: 0.042; 10,000 perm.). The UPGMA clustering of the standing scenario partially followed the hominoid phylogeny, although the gibbon and the gorilla were in reverse positions. On the other hand, UPGMA clustering of the suspension scenario showed that the suspensory species grouped together with lower stress values as compared with the rest of specimens.

GM
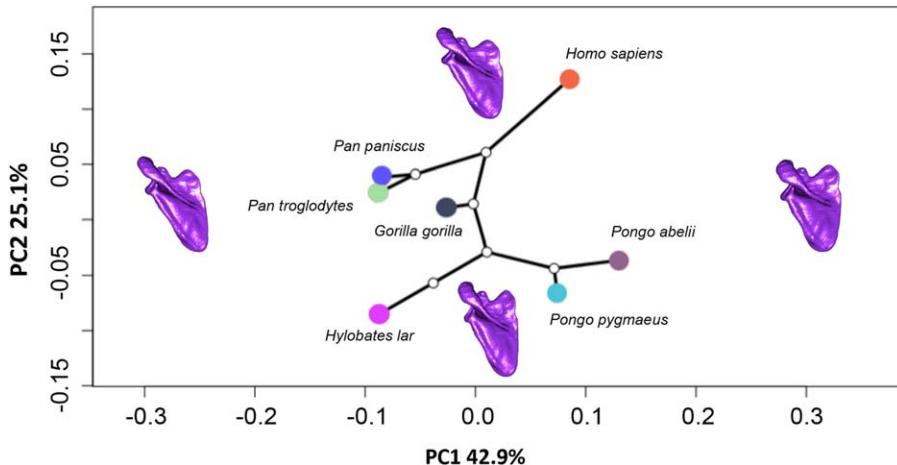
Phylogenetic signal was found for shape (Kmult: 0.74; P value: 0.007; 10,000 perm.) but not for centroid size (Kmult: 1.09; P value: 0.07; 10,000 perm.). Regarding shape

Fig. 4. UPGMA dendrogram of the von Mises stress values extracted from the different scapulae: **a**) quadrupedal standing and **b**) bimanual suspension. Bootstrap values at nodes were calculated after 10,000 permutations. Above each dendrogram the finite element models were drawn to depict the distributions of von Mises stress observed in the different hominoid scapulae. [Color figure can be viewed in the online issue, which is available at wileyonlinelibrary.com.]

(Fig. 5), the lack of overlapping branches of the phylogeny projected onto the shape space seems to imply that there is little evidence to support convergent evolution in the hominoid scapular shape, although further tests are required. The variation along PC1 could be described as more slender shapes at the positive side (e.g., *Hylobates lar*; *Pan troglodytes*) while the scapular morphologies occupying the negative side were relatively wider (e.g., *Homo sapiens*). Interestingly, *Homo* and *Pongo* morphology seem to be the most divergent compared to the other nonhuman

Fig. 5. Phylomorphospace of the hominoid scapular variation. The first two principal components (PCs) were used to display the majority of the morphological variation, while the projected phylogeny shows the evolutionary relationship between the analyzed taxa. The scapulae models were used to depict morphological variation along the PC axes. The model closest to the mean shape was warped to match the multivariate mean using the thin plate spline method (Bookstein, 1991). Then the obtained average model was warped to represent the variation along the two plotted PC axes. [Color figure can be viewed in the online issue, which is available at wileyonlinelibrary.com.]

hominoids. The multiple multivariate regressions of shape variables on the stress PC scores showed that there is significant relationship between scapular morphology and biomechanical performance (quadrupedal standing: adjusted-R^2: 0.79; F: 5.5918; P value: 0.022; bimanual suspension: adjusted-R^2: 0.63; F: 3.5333; P value: 0.006; 10,000 permutation rounds). However, only the PGLS regression of shape variables on the PC scores of the standing scenarios stress values was significant (quadrupedal standing: adjusted-R^2: 0.26; F: 1.4212; P value: 0.044; bimanual suspension: adjusted-R^2: 0.21; F: 1.4066; P value: 0.074; 10,000 permutation rounds). The low adjusted R^2 values are partially explained due to the reduced sample size, hence these results must be cautiously considered.

DISCUSSION

Previous studies have shown that primate scapular morphology is primarily related to positional behavior and/or movement needs (Oxnard, 1998). In fact, scapular morphological variation has been interpreted as being a reflection of the functional demands related to particular locomotion requirements (Inman et al., 1944; Oxnard, 1969; Radinsky, 1987; Larson, 1993; Hildebrand and Goslow, 1998). However, it is still not completely clear what the relationship is between scapular form and function. This question is relevant in order to address whether scapular shape reflects mostly functional or phylogenetic signals, because it has been frequently assumed that the postcranium is the product of stronger functional signals rather than containing phylogenetic information (Pilbeam, 1996, 2004; Ward, 1997; Lockwood, 1999; Collard et al., 2001). This assumption can lead to profoundly biased evolutionary reconstructions, in spite of the cumulative evidence that demonstrates the significant phylogenetic structure in mammalian postcrania (Sánchez-Villagra and Williams, 1998; Young, 2003, 2005). In spite of the widespread idea that the scapular morphology mainly reflects functional demands, our results showed that shape exhibited significant phylogenetic signal. This means that closely-related species tend to show similar trait values due to their common

ancestry. This is consistent with more recent research that proposed within the functional structure of the scapula there is phylogenetic signal as well (Young, 2003, 2008). Although Young (2008) states that this phylogenetic signal is particularly noticeable at infant stages, we were able to clearly identify it in adult scapulae. The FEA results also showed significant phylogenetic signal, thus closest related species tended to show similar stress values in both loading scenarios, as broadly observed in the UPGMA clustering. However, as previously mentioned these results have to be carefully considered due to the reduced number of analyzed OTU's. It is necessary to increase the phylogenetic extent of this analysis including more anthropoid species so that the analysis can be more robust.

The FEA results showed that most species seem to behave relatively similarly under the two loading scenarios, with gibbons exhibiting the lowest stress levels, probably because their scapulae have to cope with the elevated stresses resulting from their highly demanding locomotion mode. Because of the fact that material properties were the same for all the models and that the same load was applied to all the specimens after scaling them to the same volume, it is possible to suggest that the particularly different scapular morphology of the gibbons could be the main factor reducing the experienced stress. Even though the locomotor morphology of gibbons is qualitatively similar to the anatomy of the other hominoids (Swindler and Wood, 1973), the highly suspensory locomotion mode of the gibbons has contributed to certain specialized anatomical features such as an axially elongated scapula (Takahashi, 1990). This could imply that their particular scapular morphology is adjusted to support their highly demanding locomotion habits. Interestingly, orangutans showed relatively higher stress values in the standing scenario but relatively lower values in the suspension case (similar to the gibbon values). Perhaps the slow climbing locomotion mode observed in these animals could explain this observation, because these species are noticeable slower and less acrobatic than the other hominoids. However, it is necessary to

include a broader sample of primate species in order to test this issue in a more comprehensive and robust manner.

The FEA results also showed that for the two analyzed loading scenarios, the stress was relatively distributed all over the scapular blade, although logically the higher localized areas were the locations where the forces were applied and where the constraints were positioned. This result is consistent with quantitative and qualitative studies that have shown that the scapula is relatively loaded all over its structure (van der Helm, 1994; Gupta and van der Helm, 2004). However in the suspension scenario higher loads were observed in the acromion. Epidemiological reports in human populations have shown that scapular fractures are extremely uncommon, showing the lowest incidence among all fractures, normally requiring exceptionally large amounts of energy to be affected (e.g., motor vehicle accidents) (van Staa et al., 2001). Of the different fractures that affect the bony components of the shoulder girdle, clavicle fractures are significant and notoriously more common (Armstrong and Van der Spuy, 1984; Nordqvist and Petersson, 1995). The scapula is wrapped by soft tissue and the clavicle tends to fracture more frequently, suggesting that when the scapula is loaded an important portion of the load is transmitted to the clavicle that seems to behave as a strut. The present FEA models are consistent with this possibility showing higher stress value at the scapular spine when they are "pulled" upwards such as in the suspension scenario.

The phylomorphospace (Fig. 5) showed that scapular shape seems to be consistent with the phylogenetic history of the group, thus morphological variation seems to relatively follow the evolutionary history. The absence of overlapping branches in the phylomorphospace suggests that scapular shape variation does not exhibit evident convergent evolution, however further analyses are required. Humans and orangutans showed the most divergent morphologies when compared to the rest of the hominoids (they were mostly distinguished by PC1, which accounted for 42.9% of the scapular shape variation). The morphological variation along this axis could be described as more slender shapes at the negative side (e.g., *Hylobates lar*; *Pan troglodytes*), while the scapular morphologies occupying the positive side were relatively wider (e.g., *Homo sapiens*, *Pongo abelii*). On the other hand, PC2 seems to separate between more arboreal species (i.e., orangutans and gibbons) and the rest of the hominoids. The morphological variation along this particular axis is associated with a scapular spine that points upwards in the negative portion of the axis, while the upper part exhibits morphologies that tend towards more horizontal spines. Additionally, the shapes occupying the negative side of the axis present different morphologies of the superior angles in comparison with those located on the positive side. This area provides the attachment site for some fibers of the levator scapulae muscle, thus suggesting different loading regimes of this muscle when elevating the scapula between arboreal and non-arboreal hominoid species.

There was a significant relationship between scapular shape and biomechanical performance both for the multiple multivariate regressions and when phylogenetic nonindependence was taken into account by performing the PGLS regression (excepting the suspension scenario, which was almost significant for this latter test). This means that there is relationship between scapular shape and its function, with at least part of the scapular shape variation due to non-phylogenetic factors, probably related to functional demands. This is logical, because the mechanical behavior of a structure depends on the combination of the geometry (i.e., shape) and the material properties that constitute the structure itself. Nonetheless, it is important to interpret all these results with caution, due to the small sample size used here. Further studies should increase the analyzed specimens to generate more robust statistical analyses. Interestingly, the most slender specimens (i.e., hylobatids) showed lower stress levels compared to the rest of the hominoids. In fact, hylobatids are clearly distinguished from other hominoids by a very angled spine and small infraspinous and supraspinous fossae. These specific differences might reflect gibbon adaptations to the highly specialized hylobatid locomotion (i.e., brachiation). Nonetheless, it is intriguing that gibbons and chimpanzees are distinguished along PC2, occupying almost the same position in PC1. Along this axis there is an overall similarity between panids and hylobatids. Both groups posses a narrow scapula from the vertebral border to the glenoid, with short and more acutely angled spine relative to the axillary border. The similarities suggest that these morphological traits could be an ancestral condition of apes, or could have arisen as convergent traits due to common function. Nevertheless, there are few specific locomotor similarities between panids and hylobatids, once the arboreal and suspensory adaptations shared also with *Pongo* and *Gorilla* are excluded. The analyses also revealed that *Homo* exhibit a derived morphology expressed in a relatively broader blade, probably associated with the fact that humans normally do not extensively use their arms during locomotion in comparison with the rest of the hominoids. Perhaps the biggest loads on human shoulders might relate to carrying, then being consequently tensile and complex. Human scapulae occupy the opposite morphological position of gibbons in the morphospace both in PC1 and PC2, suggesting a scapular shape possibly devoted to less demanding biomechanical regimens.

Interestingly, the scapula of *Pongo* seems to be distinct compared to the rest of hominoids (Young, 2003, 2008). The present study has also shown that this genera stands out when compared to the other hominoids due to its outlier position in the different analyses that were carried out. They have a scapular shape unique among the hominoids, which can be described as a combination of suspensory and quadrupedal characteristics. This trait combination is interesting; because orangutans are highly arboreal and suspensory, but these characters seem to suggest a closer morphological affinity to arboreal quadrupeds (Young, 2008). This distinctive morphology seems to combine both traits that have been traditionally associated with quadrupeds (e.g., glenoid greatest width caudally located and a scapular spine that extends to the vertebral border) and others that are typical of non-quadrupedal species (e.g., a cranially oriented glenoid cavity and long scapular shape blade that is also cranially oriented). The pongid scapular spine is comparatively robust, thus suggesting a larger trapezius attachment compared with the other hominoids. Nevertheless, its glenoid cavity seems to be more similar to the quadrupedal condition, although lacking the distinct lip that supposedly limits limb mobility during forelimb extension (Larson, 1993). A possible explanation for this singular morphology is that forelimb-dominated slow

climbing in orangutans could be related to these anatomical features, because they use more cautious pronograde suspensory behaviors compared to the rest of the African apes (Thorpe and Crompton, 2005, 2006). The particular shoulder morphology of orangutans could be related to suspensory postures and locomotion that imply placing the shoulder in orientations requiring special stabilization, especially while slowly moving through the canopy.

It has long been thought that hominoids are best defined by a common set of morpho-functional traits related to the trunk and upper limb, in which the scapula is characterized by being located on the back of the rib-cage, while the glenohumeral joint would be adapted to allow extensive abduction (Keith, 1923; Rose, 1997; Larson, 1998). It has been suggested that these shared characteristics are related to forelimb-suspensory locomotion or brachiation. This idea has led us to consider hominoids as being relatively homogenous postcranially (Ward, 1997), despite evidence indicating that there is more variability than initially believed (Larson, 1998). For instance, locomotor ecology and recent analyses of the available fossil evidence indicate that suspensory locomotion may have been acquired independently by several hominoid lineages. In fact, it has been argued that Miocene apes characteristically lack many of the traits associated with suspensory behaviors that are present in their crown descendants (e.g., *Sivapithecus* and *Pongo*) (Begun and Kivell, 2011). The possible physical attributes of the last common ancestor of all hominoids have been discussed for a long time (Pilbeam, 2002). It has been traditionally thought that the majority of the postcranial resemblances of the crown hominoids correspond to shared-derived features (Schultz, 1930; Larson, 1998), however based on Miocene hominoid postcranial discoveries, this perspective has been recently re-examined (Begun and Kordos, 1997; Larson, 1998). These new fossils exhibit morphologies that differ with what would have been typically expected, thus raising the possibility that some of the extant ape postcranial similarities could be homoplasies (Begun, 1993). Furthermore, the inferences regarding Miocene hominoid positional behavior have shown that most of the fossil taxa seems to differ from the extant apes in that they seem to have been pronograde arboreal quadrupeds, although some exceptions have been proposed as well (Rose, 1997; Ward, 1997; Moyà-Solà et al., 2009). Although this research did not try to address this issue directly, the results show there is no generic and homogenous scapular morphology, but it noticeably varies in the different analyzed taxa. Hominoid scapular shape variation seems to be firstly distinguishing between "broad" versus "slender" scapulae, while secondly between arboreal and non-primarily arboreal hominoids. This morphological arrangement can be useful when discussing if the arboreal specializations observed in some of this species are in fact symplesiomorphies, as usually interpreted, or on the contrary represent evolutionary adaptations to novel environments. Hence it is important to consider this information when testing evolutionary models that explain the appearance of suspensory features gradually accreting in time (Moyà-Solà et al., 2004) or evolving as an integrated array (Pilbeam, 1996).

A limitation of the present study is that in reality shoulder soft tissues would mostly cope with strain and stress experienced by the shoulder (especially during the suspension scenario) but due to simplicity reasons, they were not modeled. In fact one of the main limitations of the proposed loading scenarios is that none of the muscular, ligamentous, capsular, fascia, or tendinous elements were considered, due to the absence of standardized data or because it was not possible to find information about their properties for all the analyzed species. Even though this is an unrealistic assumption, the objective of the present study was mostly comparative. Another limitation is that only relatively few stress values were analyzed (just 101 values in one slice of the models), which merely represents a localized part of the scapular biomechanical performance. Even though it was sufficient to carry out the presented analyses, following studies should include stress values more widely distributed on the scapula.

The present study has showed that the analysis of form and function using GM and FEA was able to cast some light regarding the functional and phylogenetic contributions in hominoid scapular morphology. Future studies should generate an integrative approach to analyze both shape and biomechanical data using more realistic loading scenarios derived from both observational and simulation data (e.g., multibody dynamics).

ACKNOWLEDGMENTS

LITERATURE CITED

Adams DC. 2014. A generalized K statistic for estimating phylogenetic signal from shape and other high-dimensional multivariate data. Syst Biol 63:685–697.

Adams DC, Otárola-Castillo E. 2013. geomorph: an R package for the collection and analysis of geometric morphometric shape data. Methods Ecol E 4:393–399.

Adams DC, Rohlf FJ, Slice DE. 2004. Geometric morphometrics: ten years of progress following the "revolution." Ital J Zool 71:5–16.

Adams DC, Rohlf FJ, Slice DE. 2013. A field comes of age: geometric morphometrics in the 21st century. Hystrix Ital J Mammal 21:7–14.

Aiello L, Dean C. 1990. An introduction to human evolutionary anatomy. London: Academic Press.

Alemseged Z, Spoor F, Kimbel WH, Bobe R, Geraads D, Reed D, Wynn JG. 2006. A juvenile early hominin skeleton from Dikika, Ethiopia. Nature 443:296–301.

Amadi HO, Hansen UN, Wallace AL, Bull AMJ. 2008. A scapular coordinate frame for clinical and kinematic analyses. J Biomech 41:2144–2149.

Armstrong CP, Van der Spuy J. 1984. The fractured scapula: importance and management based on a series of 62 patients. Injury 15:324–329.

Arnold C, Matthews LJ, Nunn CL. 2010. The 10kTrees website: a new online resource for primate phylogeny. Evol Anthropol Issues News Rev 19:114–118.

Ashton EH, Oxnard CE. 1963. The musculature of the primate shoulder. Trans Zool Soc Lond 29:553–650.

Ashton EH, Oxnard CE. 1964a. Functional adaptations in the primate shoulder girdle. Proc Zool Soc Lond 142:49–66.

Ashton EH, Oxnard CE. 1964b. Locomotor patterns in primates. Proc Zool Soc Lond 142:1–28.

Astúa D. 2009. Evolution of scapula size and shape in didelphid marsupials (didelphimorphia: didelphidae). Evolution 63: 2438–2456.

Badoux D. 1974. Structure and function of the primate scapula. In: Jenkins FAJ, editor. Primate locomotion. Elsevier, New York: Academic Press. p 171–200.

Bagg SD, Forrest WJ. 1986. Electromyographic study of the scapular rotators during arm abduction in the scapular plane. Am J Phys Med 65:111–124.

Bayraktar HH, Morgan EF, Niebur GL, Morris GE, Wong EK, Keaveny TM. 2004. Comparison of the elastic and yield properties of human femoral trabecular and cortical bone tissue. J Biomech 37:27–35.

Beaupré GS, Carter DR. 1992. Finite element analysis in biomechanics. In: Biewener AA, editor. Biomechanics-structures and systems: a practical approach. Oxford: RL Press at Oxford University Press.

Begun DR. 1993. New catarrhine phalanges from Rudabánya (Northeastern Hungary) and the problem of parallelism and convergence in hominoid postcranial morphology. J Hum E 24:373–402.

Begun DR, Kivell TL. 2011. Knuckle-walking in Sivapithecus? The combined effects of homology and homoplasy with possible implications for pongine dispersals. J Hum E 60:158–170.

Begun DR, Kordos L. 1997. Phyletic affinities and functional convergence in dryopithecus and other miocene and living hominids. In: Begun DR, Ward CV, Rose MD, editors. Function, phylogeny, and fossils. Advances in primatology. US: Springer. p 291–316.

Bello-Hellegouarch G, Potau JM, Arias-Martorell J, Pastor JF, Pérez-Pérez A. 2013. A comparison of qualitative and quantitative methodological approaches to characterizing the dorsal side of the scapula in hominoidea and its relationship to locomotion. Int J Primatol 34:315–336.

Berger LR, Ruiter DJ, de Churchill SE, Schmid P, Carlson KJ, Dirks PHGM, Kibii JM. 2010. Australopithecus sediba: a new species of *Homo*-like australopith from South Africa. Science 328:195–204.

Bhatti MA. 2005. Fundamental finite element analysis and applications: with mathematica and MatlabComputations, 1st ed. Hoboken, NJ: Wiley.

Blomberg SP, Garland T. 2002. Tempo and mode in evolution: phylogenetic inertia, adaptation and comparative methods. J Evol Biol 15:899–910.

Blomberg SP, Garland T, Ives AR. 2003. Testing for phylogenetic signal in comparative data: behavioral traits are more labile. Evolution 57:717–745.

Bookstein FL. 1991. Morphometric tools for landmark data: geometry and biology. Cambridge: Cambridge University Press.

Bookstein FL. 2013. Allometry for the twenty-first century. Biol Theor 7:10–25.

Bouckaert RR. 2010. DensiTree: making sense of sets of phylogenetic trees. Bioinformatics 26:1372–1373.

Brassey CA, Margetts L, Kitchener AC, Withers PJ, Manning PL, Sellers WI. 2013. Finite element modelling versus classic beam theory: comparing methods for stress estimation in a morphologically diverse sample of vertebrate long bones. J R Soc Interface R Soc 10:20120823.

Campoli G, Bolsterlee B, van der Helm F, Weinans H, Zadpoor AA. 2014. Effects of densitometry, material mapping and load estimation uncertainties on the accuracy of patient-specific finite-element models of the scapula. J R Soc Interface 11: 20131146.

Carlson KJ. 2006. Muscle architecture of the common chimpanzee (*Pan troglodytes*): perspectives for investigating chimpanzee behavior. Primates 47:218–229.

Chan LK. 2007. Scapular position in primates. Folia Primatol (Basel) 78:19–35.

Chen X, Povirk G. 1996. Assessing errors introduced by modeling the anisotropic human mandible isotropically with the finite element method. Am J Phys Anthropol Suppl 22:83.

Cheng EJ, Scott SH. 2000. Morphometry of *Macaca mulatta* forelimb. I. Shoulder and elbow muscles and segment inertial parameters. J Morphol 245:206–224.

Churchill SE, Holliday TW, Carlson KJ, Jashashvili T, Macias ME, Mathews S, Sparling TL, Schmid P, Ruiter DJ, de Berger LR. 2013. The upper limb of australopithecus sediba. Science 340:1233477.

Clabaut C, Bunje PME, Salzburger W, Meyer A. 2007. Geometric morphometric analyses provide evidence for the adaptive character of the tanganyikan cichlid fish radiations. Evolution 61:560–578.

Collard M, Gibbs S, Wood BA. 2001. Phylogenetic utility of higher primate postcranial morphology. Am J Phys Anthropol Suppl 32:52.

Corruccini RS, Ciochon RL. 1976. Morphometric affinities of the human shoulder. Am J Phys Anthropol 45:19–37.

Corruccini RS, Ciochon RL. 1978. Morphoclinal variation in the anthropoid shoulder. Am J Phys Anthropol 48:539–542.

Cox PG, Fagan MJ, Rayfield EJ, Jeffery N. 2011. Finite element modelling of squirrel, guinea pig and rat skulls: using geometric morphometrics to assess sensitivity. J Anat 219:696–709.

Currey JD. 1988. The effect of porosity and mineral content on the Young's modulus of elasticity of compact bone. J Biomech 21:131–139.

Currey JD. 2002. Bones: Structure and Mechanics, 1st ed. Princeton, NJ: Princeton University Press.

Currey JD, Butler G. 1975. The mechanical properties of bone tissue in children. J Bone Joint Surg Am 57:810–814.

Curtis N, Witzel U, Fitton L, O'higgins P, Fagan M. 2011. The mechanical significance of the temporal fasciae in *Macaca fascicularis*: an investigation using finite element analysis. Anat Rec Adv Integr Anat Evol Biol 294:1178–1190.

D'Août K, Vereecke EE. 2011. Primate locomotion linking field and laboratory research. New York: Springer.

Daegling DJ, Hotzman JL, McGraw WS, Rapoff AJ. 2009. Material property variation of mandibular symphyseal bone in colobine monkeys. J Morphol 270:194–204.

Davis D. 1949. The shoulder architecture of bears and other carnivores. Fieldiana: Zoology, Chicago Nat Hist Museum. 31: 285–305.

Dechow PC, Hylander WL. 2000. Elastic properties and masticatory bone stress in the Macaque mandible. Am J Phys Anthropol 112:553–574.

Dechow PC, Nail GA, Schwartz-Dabney CL, Ashman RB. 1993. Elastic properties of human supraorbital and mandibular bone. Am J Phys Anthropol 90:291–306.

Demes B, Larson SG, Stern JJT, Jungers WL, Biknevicius AR, Schmitt D. 1994. The kinetics of primate quadrupedalism: "hindlimb drive" reconsidered. J Hum E 26:353–374.

Ding M, Dalstra M, Linde F, Hvid I. 1998. Mechanical properties of the normal human tibial cartilage-bone complex in relation to age. Clin Biomech 13:351–358.

Diogo R, Potau JM, Pastor JF. 2013a. Photographic and descriptive musculoskeletal atlas of chimpanzees: with notes on the attachments, variations, innervation, function and synonymy and weight of the muscles, 1st ed. Boca Raton, FL: CRC Press.

Diogo R, Potau JM, Pastor JF, dePaz FJ, Ferrero EM, Bello G, Barbosa M, Aziz MA, Burrows AM, Arias-Martorell J, Wood BA. 2012. Photographic and descriptive musculoskeletal atlas of gibbons and siamangs, 1st ed. St. Helier: CRC Press.

Diogo R, Potau JM, Pastor JF, dePaz FJ, Ferrero EM, Bello G, Barbosa M, Wood BA. 2010. Photographic and descriptive musculoskeletal atlas of gorilla: with notes on the attachments, variations, innervation, synonymy and weight of the muscles, 1st ed. Enfield, NH: CRC Press.

Diogo R, Potau JM, Pastor JF, Paz FJ de, Barbosa M, Ferrero EM, Bello G, Aziz MA, Arias-Martorell J, Wood B. 2013b. Photographic and descriptive musculoskeletal atlas of orangutans: with notes on the attachments, variations, innervations, function and synonymy and weight of the muscles. Boca Raton: CRC Press.

Diogo R, Wood BA. 2012. Comparative anatomy and phylogeny of primate muscles and human evolution. Boca Raton, FL: CRC Press.

Dumont ER, Davis JL, Grosse IR, Burrows AM. 2011. Finite element analysis of performance in the skulls of marmosets and tamarins. J Anat 218:151–162.

Dumont ER, Grosse IR, Slater GJ. 2009. Requirements for comparing the performance of finite element models of biological structures. J Theor Biol 256:96–103.

Fayad F, Hoffmann G, Hanneton S, Yazbeck C, Lefevre-colau MM, Poiraudeau S, Revel M, Roby-Brami A. 2006. 3D scapular kinematics during arm elevation: effect of motion velocity. Clin Biomech 21:932–941.

Feldesman MR. 1976. The primate forelimb: a morphometric study of locomotor diversity. Eugene, Oregon: Department of Anthropology, University of Oregon.

Figueirido B, Serrano-Alarcón FJ, Slater GJ, Palmqvist P. 2010. Shape at the cross-roads: homoplasy and history in the evolution of the carnivoran skull towards herbivory. J Evol Biol 23: 2579–2594.

Fitton LC, Prôa M, Rowland C, Toro-Ibacache V, O'Higgins P. 2015. The impact of simplifications on the performance of a finite element model of a *Macaca fascicularis* cranium. Anat Rec Hoboken NJ 298:107–121.

Fitton LC, Shi JF, Fagan MJ, O'Higgins P. 2012. Masticatory loadings and cranial deformation in *Macaca fascicularis*: a finite element analysis sensitivity study. J Anat 221:55–68.

Fleagle JG. 1977. Locomotor behavior and muscular anatomy of sympatric Malaysian leaf-monkeys (*Presbytis obscura* and *Presbytis melalophos*). Am J Phys Anthropol 46:297–307.

Fleagle JG. 1998. Primate adaptation and evolution. London: Academic Press.

Friedman RJ, LaBerge M, Dooley RL, O'Hara AL. 1992. Finite element modeling of the glenoid component: effect of design parameters on stress distribution. J Shoulder Elbow Surg 1: 261–270.

Green DJ, Alemseged Z. 2012. Australopithecus afarensis scapular ontogeny, function, and the role of climbing in human evolution. Science 338:514–517.

Gröning F, Fagan MJ, O'Higgins P. 2011. The effects of the periodontal ligament on mandibular stiffness: a study combining finite element analysis and geometric morphometrics. J Biomech 44:1304–1312.

Gupta S, van der Helm FCT. 2004. Load transfer across the scapula during humeral abduction. J Biomech 37:1001–1009.

Gupta S, van der Helm FCT, Sterk JC, van Keulen F, Kaptein BL. 2004. Development and experimental validation of a three-dimensional finite element model of the human scapula. Proc Inst Mech Eng 218:127–142.

Haile-Selassie Y, Latimer BM, Alene M, Deino AL, Gibert L, Melillo SM, Saylor BZ, Scott GR, Lovejoy CO. 2010. An early Australopithecus afarensis postcranium from Woranso-Mille, Ethiopia. Proc Natl Acad Sci USA 107:12121–12126.

Harmon LJ, Kolbe JJ, Cheverud JM, Losos JB. 2005. Convergence and the multidimensional niche. Evol Int J Org E 59: 409–421.

Havill LM, Mahaney MC, Czerwinski SA, Carey KD, Rice K, Rogers J. 2003. Bone mineral density reference standards in adult baboons (*Papio hamadryas*) by sex and age. Bone 33: 877–888.

Hermida JC, Flores-Hernandez C, Hoenecke HR, D'Lima DD. 2014. Augmented wedge-shaped glenoid component for the correction of glenoid retroversion: a finite element analysis. J Shoulder Elbow Surg 23:347–354.

Hildebrand M, Goslow G. 1998. Analysis of vertebrate structure, 5th ed. New York: Wiley.

Hofmann T, Heyroth F, Meinhard H, Fränzel W, Raum K. 2006. Assessment of composition and anisotropic elastic properties of secondary osteon lamellae. J Biomech 39:2282–2294.

Hunt KD. 1991a. Positional behavior in the Hominoidea. Int J Primatol 12:95–118.

Hunt KD. 1991b. Mechanical implications of chimpanzee positional behavior. Am J Phys Anthropol 86:521–536.

Hunt KD. 1992. Positional behavior of Pan troglodytes in the Mahale Mountains and Gombe Stream National Parks, Tanzania. Am J Phys Anthropol 87:83–105.

Hunt KD. 2004. The special demands of great ape locomotion and posture. In: Russon AE, David RB, editors. The evolution of thought. Cambridge: Cambridge: University Press.

Inman VT, Saunders JB deC. M, Abbott LC. 1944. Observations on the function of the shoulder joint. J Bone Joint Surg Am 26:1–30.

Johnson GR, Spalding D, Nowitzke A, Bogduk N. 1996. Modelling the muscles of the scapula morphometric and coordinate data and functional implications. J Biomech 29:1039–1051.

Kaneko TS, Bell JS, Pejcic MR, Tehranzadeh J, Keyak JH. 2004. Mechanical properties, density and quantitative CT scan data of trabecular bone with and without metastases. J Biomech 37:523–530.

Keating JF, Waterworth P, Shaw-Dunn J, Crossan J. 1993. The relative strengths of the rotator cuff muscles: a cadaver study. J Bone Joint Surg Ser B 75:137–140.

Keith A. 1923. Hunterian Lectures on man's posture: its evolution and disorders. Br Med J 1:669–672.

Kibler WB, McMullen J. 2003. Scapular dyskinesis and its relation to shoulder pain. J Am Acad Orthop Surg 11:142–151.

Kimes KR, Siegel MI, Sadler DL. 1981. Musculoskeletal scapular correlates of plantigrade and acrobatic positional activities in *Papio cynocephalus* anubis and *Macaca fascicularis*. Am J Phys Anthropol 55:463–472.

Kimura T. 1992. Hindlimb dominance during primate high-speed locomotion. Primates 33:465–476.

Klingenberg CP, Ekau W. 1996. A combined morphometric and phylogenetic analysis of an ecomorphological trend: pelagization in Antarctic fishes (Perciformes: Nototheniidae). Biol J Linn Soc 59:143–177.

Kupczik K. 2008. Do it yourself virtual biomechanics: basic concepts and technical aspects of finite element analysis in vertebrate morphology. J Anthropol Sci 86:193–198.

Kupczik K, Dobson CA, Fagan MJ, Crompton RH, Oxnard CE, O'Higgins P. 2007. Assessing mechanical function of the zygomatic region in macaques: validation and sensitivity testing of finite element models. J Anat 210:41–53.

Kupczik K, Lev-Tov Chattah N. 2014. The adaptive significance of enamel loss in the mandibular incisors of cercopithecine primates (Mammalia: Cercopithecidae): a finite element modelling study. PLoS One 9:e97677.

Lacroix D, Murphy LA, Prendergast PJ. 2000. Three-dimensional finite element analysis of glenoid replacement prostheses: a comparison of keeled and pegged anchorage systems. J Biomech Eng 122:430–436.

Larson SG. 1993. Functional morphology of the shoulder in primates. In: Gebo DL, editor. Postcranial adaptations in nonhuman primates. Northern Illinois: University Press, DeKalb.

Larson SG. 1995. New characters for the functional interpretation of primate scapulae and proximal humeri. Am J Phys Anthropol 98:13–35.

Larson SG. 1998. Parallel evolution in the hominoid trunk and forelimb. Evol Anthropol Issues News Rev 6:87–99.

Larson SG. 2007. Evolutionary transformation of the hominin shoulder. Evol Anthropol Issues News Rev 16:172–187.

Larson SG, Stern JT. 1986. EMG of scapulohumeral muscles in the chimpanzee during reaching and "arboreal" locomotion. Am J Anat 176:171–190.

Larson SG, Stern JT Jr. 2013a. Rotator cuff muscle function and its relation to scapular morphology in apes. J Hum E 65: 391–403.

Larson SG, Stern JT, Jungers WL. 1991. EMG of serratus anterior and trapezius in the chimpanzee: scapular rotators revisited. Am J Phys Anthropol 85:71–84.

Li Y, Crompton RH, Wang W, Savage R, Günther MM. 2004. Hind limb drive, hind limb steering? Functional differences between fore and hind limbs in chimpanzee quadrupedalism. In: Shaping Primate Evolution. Cambridge Studies in Biological and Evolutionary Anthropology. Cambridge: Cambridge University Press.

Lockwood CA. 1999. Homoplasy and adaptation in the atelid postcranium. Am J Phys Anthropol 108:459–482.

Margulies SS, Thibault KL. 2000. Infant skull and suture properties: measurements and implications for mechanisms of pediatric brain injury. J Biomech Eng 122:364–371.

Meloro C, Raia P, Piras P, Barbera C, O'higgins P. 2008. The shape of the mandibular corpus in large fissiped carnivores: allometry, function and phylogeny. Zool J Linn Soc 154:832–845.

Michilsens F, Vereecke EE, D'Août K, Aerts P. 2009. Functional anatomy of the gibbon forelimb: adaptations to a brachiating lifestyle. J Anat 215:335–354.

Miller RA. 1932. Evolution of the pectoral girdle and fore limb in the primates. Am J Phys Anthropol 17:1–56.

Milne N, O'Higgins P. 2012. Scaling of form and function in the xenarthran femur: a 100-fold increase in body mass is mitigated by repositioning of the third trochanter. Proc R Soc B Biol Sci 279:3449–3456.

Monteiro LR, Nogueira MR. 2010. Adaptive radiations, ecological specialization, and the evolutionary integration of complex morphological structures. Evolution 64:724–744.

Moyà-Solà S, Köhler M, Alba DM, Casanovas-Vilar I, Galindo J. 2004. Pierolapithecus catalaunicus, a new middle miocene great ape from Spain. Science 306:1339–1344.

Moyà-Solà S, Alba DM, Almécija S, Casanovas-Vilar I, Köhler M, Esteban-Trivigno SD, Robles JM, Galindo J, Fortuny J. 2009. A unique middle miocene European hominoid and the origins of the great ape and human clade. Proc Natl Acad Sci USA 106:9601–9606.

Müller HJ. 1967. Form und Funktion der Scapula. Z Für Anat Entwicklungsgeschichte 126:205–263.

Myatt JP, Crompton RH, Payne-Davis RC, Vereecke EE, Isler K, Savage R, D'Août K, Günther MM, Thorpe SKS. 2012. Functional adaptations in the forelimb muscles of non-human great apes. J Anat 220:13–28.

Nogueira MR, Peracchi AL, Monteiro LR. 2009. Morphological correlates of bite force and diet in the skull and mandible of phyllostomid bats. Funct Ecol 23:715–723.

Nordqvist A, Petersson CJ. 1995. Incidence and causes of shoulder girdle injuries in an urban population. J Shoulder Elbow Surg 4:107–112.

Ogihara N, Aoi S, Sugimoto Y, Tsuchiya K, Nakatsukasa M. 2011. Forward dynamic simulation of bipedal walking in the Japanese macaque: investigation of causal relationships among limb kinematics, speed, and energetics of bipedal locomotion in a nonhuman primate. Am J Phys Anthropol 145:568–580.

Ogihara N, Yamanaka A, Ishida MNH. 2003. Functional morphology of primate scapula based on finite element analysis. Primate Res 19:203–215.

O'Higgins P. 2000. The study of morphological variation in the hominid fossil record: biology, landmarks and geometry. J Anat 197:103–120.

O'Higgins P, Cobb SN, Fitton LC, Gröning F, Phillips R, Liu J, Fagan MJ. 2011. Combining geometric morphometrics and functional simulation: an emerging toolkit for virtual functional analyses. J Anat 218:3–15.

O'Higgins P, Fitton LC, Phillips R, Shi J, Liu J, Gröning F, Cobb SN, Fagan MJ. 2012. Virtual functional morphology: novel approaches to the study of craniofacial form and function. Evol Biol 39:521–535.

O'Higgins P, Milne N. 2013. Applying geometric morphometrics to compare changes in size and shape arising from finite elements analyses. Hystrix Ital J Mammal 24:126–132.

Oishi M, Ogihara N, Endo H, Asari M. 2008. Muscle architecture of the upper limb in the orangutan. Primates 49:204–209.

Oishi M, Ogihara N, Endo H, Ichihara N, Asari M. 2009. Dimensions of forelimb muscles in orangutans and chimpanzees. J Anat 215:373–382.

Oxnard CE. 1967. The functional morphology of the primate shoulder as revealed by comparative anatomical, osteometric and discriminant function techniques. Am J Phys Anthropol 26:219–240.

Oxnard CE. 1968. The architecture of the shoulder in some mammals. J Morphol 126:249–290.

Oxnard CE. 1969. The descriptive use of neighborhood limited classification in functional morphology: an analysis of the shoulder in primates. J Morphol 129:127–148.

Oxnard CE. 1973. Functional inferences from morphometrics: problems posed by uniqueness and diversity among the primates. Syst Biol 22:409–424.

Oxnard CE. 1998. The information content of morphometric data in primates: function, development, and evolution. In: Strasser E, Fleagle JG, Rosenberger AL, McHenry H, editors.

Primate locomotion: recent advances. Vol. Symposium on Primate Locomotion. New York: Plenum Press. p 255–275.

Oxnard CE, Ashton EH. 1962. Structure and function in bones and associated soft parts in primates. Birmingham: University of Birmingham.

Panagiotopoulou O, Kupczik K, Cobb SN. 2011. The mechanical function of the periodontal ligament in the macaque mandible: a validation and sensitivity study using finite element analysis. J Anat 218:75–86.

Parr WCH, Wroe S, Chamoli U, Richards HS, McCurry MR, Clausen PD, McHenry C. 2012. Toward integration of geometric morphometrics and computational biomechanics: new methods for 3D virtual reconstruction and quantitative analysis of finite element models. J Theor Biol 301:1–14.

Pearson OM, Lieberman DE. 2004. The aging of Wolff's "law": ontogeny and responses to mechanical loading in cortical bone. Am J Phys Anthropol 125:63–99.

Peres-Neto PR, Jackson DA. 2001. How well do multivariate data sets match? The advantages of a Procrustean superimposition approach over the Mantel test. Oecologia 129:169–178.

Peterson J, Dechow PC. 2003. Material properties of the human cranial vault and zygoma. Anat Rec Discov Mol Cell Evol Biol 274A:785–797.

Peterson SL, Rayan GM. 2011. Shoulder and upper arm muscle architecture. J Hand Surg 36:881–889.

Phelps JB, Hubbard GB, Wang X, Agrawal CM. 2000. Microstructural heterogeneity and the fracture toughness of bone. J Biomed Mater Res 51:735–741.

Pierce SE, Angielczyk KD, Rayfield EJ. 2008. Patterns of morphospace occupation and mechanical performance in extant crocodilian skulls: a combined geometric morphometric and finite element modeling approach. J Morphol 269:840–864.

Pilbeam D. 1996. Genetic and morphological records of the hominoidea and hominid origins: a synthesis. Mol Phylogenet E 5:155–168.

Pilbeam D. 2002. Perspectives on the miocene hominoidea. In: Hartwig WC, editor. The primate fossil record. Cambridge: Cambridge University Press. p 303–310.

Pilbeam D. 2004. The anthropoid postcranial axial skeleton: comments on development, variation, and evolution. J Exp Zoolog B Mol Dev E 302:241–267.

Piras P, Maiorino L, Teresi L, Meloro C, Lucci F, Kotsakis T, Raia P. 2013. Bite of the cats: relationships between functional integration and mechanical performance as revealed by mandible geometry. Syst Biol 62:878–900.

Piras P, Sansalone G, Teresi L, Kotsakis T, Colangelo P, Loy A. 2012. Testing convergent and parallel adaptations in talpids humeral mechanical performance by means of geometric morphometrics and finite element analysis. J Morphol 273:696–711.

Preuschoft H. 1973. Functional anatomy of the upper extremity. In: Bourne G, editor. The chimpanzee, Vol. 6. Basel: Karger.

Preuschoft H. 2004. Mechanisms for the acquisition of habitual bipedality: are there biomechanical reasons for the acquisition of upright bipedal posture? J Anat 204:363–384.

Preuschoft H, Hohn B, Scherf H, Schmidt M, Krause C, Witzel U. 2010. Functional analysis of the primate shoulder. Int J Primatol 31:301–320.

Radinsky LB. 1987. The evolution of vertebrate design, 1st ed. Chicago: University of Chicago Press.

Raia P, Carotenuto F, Meloro C, Piras P, Pushkina D. 2010. The shape of contention: adaptation, history, and contingency in ungulate mandibles. Evolution 64:1489–1503.

Raichlen DA, Pontzer H, Shapiro LJ, Sockol MD. 2009. Understanding hind limb weight support in chimpanzees with implications for the evolution of primate locomotion. Am J Phys Anthropol 138:395–402.

Rayfield EJ. 2007. Finite element analysis and understanding the biomechanics and evolution of living and fossil organisms. Annu Rev Earth Planet Sci 35:541–576.

Rayfield EJ. 2011. Strain in the ostrich mandible during simulated pecking and validation of specimen-specific finite element models. J Anat 218:47–58.

Reynolds TR. 1985. Stresses on the limbs of quadrupedal primates. Am J Phys Anthropol 67:351–362.

Roberts D. 1974. Structure and function of the primate scapula. In: Jenkins FAJ, editor. Primate locomotion. Elsevier, New York: Academic Press. p 171–200.

Rodman P. 1984. Foraging and social systems of orangutans and chimpanzees. In: Rodman P, Cant JG, editors. Adaptations for foraging in nonhuman primates. New York: Columbia University Press. p 134–160.

Rose MD. 1974. Postural adaptations in new and old world monkeys. In: Jenkins FAJ, editor. Primate locomotion. New York: Academic Press. p 201–222.

Rose MD. 1979. Positional behaviour of natural populations: some quantitative results of a field study on *Colobus guereza* and *Cercopithecus aethiops*. In: Morbeck M, Preuschoft H, Gomberg N, editors. Environment, behavior and morphology: dynamic interactions in primates. New York: G. Fischer. p 75–94.

Rose MD. 1993. Functional anatomy of the elbow and forearm in primates. In: Gebo D, editor. Postcranial adaptation in nonhuman primates. DeKalb: Northern Illinois University Press. p 70–95.

Rose MD. 1997. Functional and phylogenetic features of the forelimb in miocene hominoids. In: Begun DR, Ward CV, Rose MD, editors. Function, phylogeny, and fossils. Advances in primatology. US: Springer. p 79–100.

Ross CF. 2005. Finite element analysis in vertebrate biomechanics. Anat Rec Discov Mol Cell Evol Biol 283A:253–258.

Ross CF, Patel BA, Slice DE, Strait DS, Dechow PC, Richmond BG, Spencer MA. 2005. Modeling masticatory muscle force in finite element analysis: sensitivity analysis using principal coordinates analysis. Anat Rec Discov Mol Cell Evol Biol 283A:288–299.

Rüber L, Adams DC. 2001. Evolutionary convergence of body shape and trophic morphology in cichlids from Lake Tanganyika. J Evol Biol 14:325–332.

Sánchez-Villagra MR, Williams BA. 1998. Levels of homoplasy in the evolution of the mammalian skeleton. J Mamm E 5: 113–126.

Schmidt M. 2005. Quadrupedal locomotion in squirrel monkeys (Cebidae: *Saimiri sciureus*): a cineradiographic study of limb kinematics and related substrate reaction forces. Am J Phys Anthropol 128:359–370.

Schmidt M. 2008. Forelimb proportions and kinematics: how are small primates different from other small mammals? J Exp Biol 211:3775–3789.

Schmidt M, Fischer MS. 2000. Cineradiographic study of forelimb movements during quadrupedal walking in the brown lemur (Eulemur fulvus, primates: Lemuridae). Am J Phys Anthropol 111:245–262.

Schmidt M, Krause C. 2011. Scapula movements and their contribution to three-dimensional forelimb excursions in quadrupedal primates. In: D'Août K, Vereecke EE, editors. Primate locomotion. Developments in primatology: progress and prospects. New York: Springer. p 83–108.

Schultz AH. 1930. The skeleton of the trunk of and limbs of the higher primates. Hum Biol 2:303–438.

Schultz AH. 1961. Vertebral column and thorax. Basel: S Karger Pub.

Sellers WI, Crompton RH. 2004. Using sensitivity analysis to validate the predictions of a biomechanical model of bite forces. Ann Anat Anat Anz 186:89–95.

Sellers WI, Pataky TC, Caravaggi P, Crompton RH. 2010. Evolutionary robotic approaches in primate gait analysis. Int J Primatol 31:321–338.

Shea BT. 1986. Scapula form and locomotion in chimpanzee evolution. Am J Phys Anthropol 70:475–488.

Slice DE. 2007. Geometric morphometrics. Annu Rev Anthropol 36:261–281.

Smith JM, Savage RJG. 1956. Some locomotory adaptations in mammals. J Linn Soc Lond Zool 42:603–622.

Stern JT, Oxnard CE. 1973. Primate locomotion: Some links with evolution and morphology. In: Hofer H, Schultz AH, editors. Primatologia 4. Basel: Karger.

Strait DS, Wang Q, Dechow PC, Ross CF, Richmond BG, Spencer MA, Patel BA. 2005. Modeling elastic properties in finite-element analysis: how much precision is needed to produce an accurate model? Anat Rec Discov Mol Cell Evol Biol 283A:275–287.

Strait DS, Weber GW, Neubauer S, Chalk J, Richmond BG, Lucas PW, Spencer MA, Schrein C, Dechow PC, Ross CF, Grosse IR, Wright BW, Constantino P, Wood BA, Lawn B, Hylander WL, Wang Q, Byron C, Slice DE, Smith AL. 2009. The feeding biomechanics and dietary ecology of *Australopithecus africanus*. Proc Natl Acad Sci 106:2124–2129.

Swindler DR, Wood B. 1973. An atlas of primate gross anatomy. Seattle: University of Washington Press.

Takahashi LK. 1990. Morphological basis of arm-swinging: multivariate analyses of the forelimbs of hylobates and ateles. Folia Primatol (Basel) 54:70–85.

Taylor AB. 1997. Scapula form and biomechanics in gorillas. J Hum E 33:529–553.

Thorpe SKS, Crompton RH. 2005. Locomotor ecology of wild orangutans (*Pongo pygmaeus* abelii) in the Gunung Leuser Ecosystem, Sumatra, Indonesia: a multivariate analysis using log-linear modelling. Am J Phys Anthropol 127:58–78.

Thorpe SKS, Crompton RH. 2006. Orangutan positional behavior and the nature of arboreal locomotion in Hominoidea. Am J Phys Anthropol 131:384–401.

Thorpe SKS, Crompton RH, Günther MM, Ker RF, McNeill Alexander R. 1999. Dimensions and moment arms of the hind- and forelimb muscles of common chimpanzees (*Pan troglodytes*). Am J Phys Anthropol 110:179–199.

Tseng ZJ. 2013. Testing adaptive hypotheses of convergence with functional landscapes: a case study of bone-cracking hypercarnivores. PLoS One 8:e65305.

Tuttle RH, Basmajian JV. 1978. Electromyography of pongid shoulder muscles. II. Deltoid, rhomboid and "rotator cuff." Am J Phys Anthropol 49:47–56.

van der Helm FCT. 1994. Analysis of the kinematic and dynamic behavior of the shoulder mechanism. J Biomech 27: 527–550.

van Eijden TMGJ, van der Helm PN, van Ruijven LJ, Mulder L. 2006. Structural and mechanical properties of mandibular condylar bone. J Dent Res 85:33–37.

van Staa TP, Dennison EM, Leufkens HGM, Cooper C. 2001. Epidemiology of fractures in England and Wales. Bone 29: 517–522.

Veeger HEJ, Van Der Helm FCT, Van Der Woude LHV, Pronk GM, Rozendal RH. 1991. Inertia and muscle contraction parameters for musculoskeletal modelling of the shoulder mechanism. J Biomech 24:615–629.

Wang Q, Strait DS, Dechow PC. 2006a. A comparison of cortical elastic properties in the craniofacial skeletons of three primate species and its relevance to the study of human evolution. J Hum E 51:375–382.

Wang Q, Strait DS, Dechow PC. 2006b. Fusion patterns of craniofacial sutures in rhesus monkey skulls of known age and sex from Cayo Santiago. Am J Phys Anthropol 131:469–485.

Ward CV. 1997. Functional anatomy and phyletic implications of the hominoid trunk and hindlimb. In: Begun DR, Ward CV, Rose MD, editors. Function, phylogeny, and fossils. Advances in primatology. US: Springer. p 101–130.

Weber GW, Bookstein F. 2011. Virtual anthropology: a guide to a new interdisciplinary field. Wien: Springer.

Whitehead PF, Larson SG. 1994. Shoulder motion during quadrupedal walking in *Cercopithecus aethiops*: integration of cineradiographic and electromyographic data. J Hum E 26:525–544.

Williams JL, Lewis JL. 1982. Properties and an anisotropic model of cancellous bone from the proximal tibial epiphysis. J Biomech Eng 104:50–56.

Wolff J. 1892. Das Gesetz der Transformation der Knochen. Berlin: Hirschwald.

Wroe S, Ferrara TL, McHenry CR, Curnoe D, Chamoli U. 2010. The craniomandibular mechanics of being human. Proc R Soc B Biol Sci 277:3579–3586.

Wroe S, Moreno K, Clausen P, Mchenry C, Curnoe D. 2007. High-resolution three-dimensional computer simulation of

hominid cranial mechanics. Anat Rec Adv Integr Anat Evol Biol 290:1248–1255.

Yongpravat C, Kim HM, Gardner TR, Bigliani LU, Levine WN, Ahmad CS. 2013. Glenoid implant orientation and cement failure in total shoulder arthroplasty: a finite element analysis. J Shoulder Elbow Surg 22:940–947.

Young NM. 2003. A reassessment of living hominoid postcranial variability: implications for ape evolution. J Hum E 45:441–464.

Young NM. 2004. Modularity and integration in the hominoid scapula. J Exp Zoolog B Mol Dev E 302B:226–240.

Young NM. 2005. Estimating hominoid phylogeny from morphological data: character choice, phylogenetic signal and postcranial data. In: Lieberman DE, Smith R, Kelley J, editors. Interpreting the Past: essays on human, primate and mammal evolution in honor of David Pilbeam. Interpret past Brill Acad Boston 19–31.

Young NM. 2006. Function, ontogeny and canalization of shape variance in the primate scapula. J Anat 209:623–636.

Young NM. 2008. A comparison of the ontogeny of shape variation in the anthropoid scapula: Functional and phylogenetic signal. Am J Phys Anthropol 136:247–264.

Young RL, Haselkorn TS, Badyaev AV. 2007. Functional equivalence of morphologies enables morphological and ecological diversity. Evol Int J Org E 61:2480–2492.

Zollikofer CP, Leon MPD. 2005. Virtual reconstruction: a primer in computer-assisted paleontology and biomedicine, 1st ed. Hoboken, NJ: Wiley-Liss.

Zysset PK, Edward Guo X, Edward Hoffler C, Moore KE, Goldstein SA. 1999. Elastic modulus and hardness of cortical and trabecular bone lamellae measured by nanoindentation in the human femur. J Biomech 32:1005–1012.

2.7 Supporting information

(S1) Further details about the sample

(S2) Stress values used in the analyses: a) Standing scenario; b) Suspension scenario.

These supplementary materials can also be found in a slightly different format at:
http://onlinelibrary.wiley.com/doi/10.1002/ajpa.22882/abstract

2.7.1 Supporting Information 1. Table 2.2 Further details about the analysed sample

Species	Common name	Accesion Number	Number of elements	Average aspect ratio	Aspect ratio % > 10	Voxel size	Original volume (mm3)
Pan paniscus	Bonobo	Desmond	953156	1.60	0.000000	0.56x0.56x1.00 mm	100802.34
Pongo abelii	Sumatran Orangutan	9653	935358	1.60	0.000011	0.625x0.625x0.3 mm	114133.66
Pongo pygmaeus	Bornean Orangutan	Satsuki (GAIN 37)	996480	1.60	0.000000	0.624x0.624x0.5mm	118083.86
Homo sapiens	Human	Visible Human Female	985562	1.59	0.000006	1x1x1 mm	105571.26
Homo sapiens	Human	Visible Human Male	962225	1.60	0.000000	1x1x1 mm	162169.66
Gorilla gorilla	Gorilla	Willie (GAIN 23)	931087	1.60	0.000008	0.71x0.71x0.50 mm	387810.84
Hylobates lar	White-handed Gibbon	3308	939611	1.61	0.000000	0.75x0.75x1mm	18812.69
Hylobates lar	White-handed Gibbon	3508	940973	1.61	0.000000	0.55x0.55x1.20mm	19071.00
Pan troglodytes	Chimpanzee	10048	950295	1.61	0.000000	0.361x0.361x1.0 mm	120347.76
Pan troglodytes	Chimpanzee	9783	952156	1.60	0.000011	0.20x0.20x0.20 mm	75133.91
Pan troglodytes	Chimpanzee	9266	936693	1.61	0.000002	0.50x0.50x0.50 mm	94149.51

Stress point	Gorilla gorilla	Homo sapiens	Hylobates lar	Pan paniscus	Pan troglodytes	Pongo abelii	Pongo pygmaeus

2.7.2 Supporting information 2. Table 2.3 a) von Mises stress values were obtained from 101 locations extracted along a path as described in Figure 2b for the standing scenario.

Stress point	*Gorilla gorilla*	*Homo sapiens*	*Hylobates lar*	*Pan paniscus*	*Pan troglodytes*	*Pongo abelii*	*Pongo pygmaeus*
1	1.06	1.06	0.28	0.62	0.45	0.70	0.19
2	0.78	0.67	0.27	0.50	0.38	0.76	0.20
3	0.65	0.45	0.33	0.48	0.46	0.87	0.24
4	0.66	0.46	0.37	0.53	0.48	0.98	0.30
5	0.69	0.60	0.39	0.56	0.54	1.12	0.37
6	0.72	0.57	0.40	0.58	0.55	1.05	0.45
7	0.73	0.60	0.40	0.60	0.57	1.02	0.53
8	0.79	0.69	0.39	0.59	0.56	0.95	0.59
9	0.83	0.73	0.39	0.58	0.55	0.90	0.66
10	0.88	0.72	0.39	0.55	0.53	0.81	0.72
11	0.91	0.76	0.38	0.53	0.51	0.80	0.77
12	0.93	0.76	0.37	0.50	0.49	0.80	0.82
13	0.98	0.75	0.37	0.49	0.49	0.81	0.84
14	1.04	0.76	0.36	0.48	0.48	0.82	0.86
15	1.09	0.75	0.35	0.49	0.49	0.85	0.87
16	1.10	0.75	0.35	0.50	0.50	0.88	0.88
17	1.14	0.76	0.35	0.50	0.51	0.95	0.92
18	1.12	0.71	0.34	0.51	0.53	0.97	0.99
19	1.13	0.71	0.35	0.51	0.54	1.04	1.01
20	1.24	0.69	0.36	0.52	0.56	1.12	1.06
21	1.14	0.66	0.37	0.54	0.57	1.18	1.05
22	0.94	0.63	0.37	0.54	0.61	1.16	1.07
23	0.90	0.61	0.38	0.53	0.65	1.21	1.06
24	0.89	0.58	0.39	0.53	0.66	1.24	1.00
25	0.96	0.56	0.39	0.51	0.69	1.26	0.99
26	1.03	0.54	0.40	0.51	0.69	1.22	0.95
27	1.07	0.53	0.40	0.47	0.69	1.26	0.96
28	1.02	0.51	0.40	0.46	0.70	1.21	0.93

29	0.98	0.50	0.40	0.48	0.71	1.17	0.94
30	0.94	0.52	0.40	0.48	0.73	1.07	0.92
31	0.87	0.54	0.40	0.47	0.72	1.01	0.91
32	0.88	0.56	0.40	0.48	0.73	1.03	0.89
33	0.84	0.56	0.40	0.49	0.68	0.96	0.86
34	0.82	0.56	0.39	0.49	0.65	0.93	0.83
35	0.80	0.58	0.39	0.48	0.62	0.89	0.79
36	0.78	0.58	0.38	0.47	0.61	0.87	0.78
37	0.74	0.58	0.38	0.46	0.60	0.81	0.76
38	0.75	0.56	0.37	0.44	0.60	0.77	0.77
39	0.75	0.55	0.37	0.44	0.58	0.73	0.77
40	0.73	0.56	0.36	0.42	0.58	0.70	0.77
41	0.70	0.54	0.36	0.39	0.54	0.65	0.78
42	0.72	0.52	0.36	0.39	0.51	0.65	0.81
43	0.72	0.53	0.36	0.37	0.49	0.66	0.83
44	0.69	0.53	0.35	0.38	0.47	0.66	0.84
45	0.64	0.53	0.35	0.41	0.47	0.67	0.83
46	0.59	0.51	0.35	0.41	0.48	0.67	0.81
47	0.58	0.48	0.35	0.41	0.47	0.67	0.77
48	0.60	0.46	0.35	0.42	0.48	0.63	0.75
49	0.61	0.45	0.35	0.42	0.48	0.64	0.72
50	0.61	0.40	0.35	0.42	0.48	0.62	0.69
51	0.58	0.36	0.35	0.43	0.48	0.58	0.65
52	0.56	0.33	0.35	0.43	0.47	0.58	0.63
53	0.50	0.34	0.34	0.43	0.46	0.54	0.61
54	0.47	0.34	0.34	0.44	0.44	0.53	0.57
55	0.44	0.35	0.34	0.43	0.44	0.51	0.56
56	0.42	0.34	0.33	0.42	0.44	0.50	0.57
57	0.42	0.34	0.33	0.42	0.43	0.50	0.53
58	0.42	0.35	0.32	0.41	0.42	0.50	0.50
59	0.46	0.35	0.32	0.40	0.41	0.49	0.50
60	0.47	0.35	0.32	0.39	0.40	0.49	0.47
61	0.48	0.35	0.32	0.39	0.38	0.49	0.46

62	0.52	0.36	0.32	0.37	0.37	0.48	0.44
63	0.55	0.37	0.32	0.36	0.36	0.46	0.42
64	0.58	0.37	0.32	0.36	0.35	0.45	0.41
65	0.62	0.38	0.32	0.34	0.33	0.44	0.39
66	0.64	0.38	0.32	0.33	0.32	0.42	0.37
67	0.65	0.38	0.33	0.32	0.31	0.40	0.36
68	0.66	0.38	0.33	0.31	0.30	0.39	0.36
69	0.62	0.39	0.34	0.30	0.29	0.38	0.35
70	0.59	0.37	0.35	0.30	0.28	0.38	0.35
71	0.56	0.36	0.35	0.29	0.27	0.37	0.35
72	0.53	0.35	0.36	0.29	0.27	0.36	0.34
73	0.51	0.34	0.37	0.29	0.27	0.36	0.34
74	0.49	0.33	0.37	0.29	0.26	0.35	0.34
75	0.48	0.32	0.38	0.29	0.26	0.35	0.34
76	0.47	0.31	0.39	0.29	0.26	0.34	0.33
77	0.48	0.31	0.39	0.29	0.26	0.34	0.34
78	0.51	0.31	0.39	0.30	0.26	0.34	0.34
79	0.54	0.31	0.39	0.30	0.27	0.34	0.34
80	0.58	0.31	0.39	0.31	0.27	0.34	0.34
81	0.64	0.32	0.39	0.32	0.28	0.34	0.35
82	0.69	0.32	0.39	0.32	0.29	0.35	0.36
83	0.77	0.33	0.40	0.33	0.30	0.35	0.36
84	0.89	0.34	0.40	0.34	0.31	0.36	0.38
85	0.98	0.35	0.42	0.36	0.32	0.38	0.39
86	1.08	0.37	0.45	0.37	0.34	0.40	0.41
87	1.06	0.39	0.47	0.39	0.36	0.42	0.43
88	0.80	0.42	0.52	0.41	0.39	0.44	0.45
89	0.53	0.45	0.56	0.45	0.42	0.48	0.48
90	0.58	0.50	0.60	0.49	0.46	0.51	0.51
91	0.66	0.55	0.66	0.54	0.51	0.56	0.54
92	0.73	0.60	0.73	0.60	0.56	0.62	0.58
93	0.82	0.68	0.81	0.67	0.62	0.70	0.64
94	0.92	0.76	0.91	0.76	0.68	0.79	0.72

95	1.10	0.86	1.02	0.86	0.79	0.91	0.81
96	1.30	0.97	1.17	0.98	0.89	1.05	0.93
97	1.56	1.14	1.37	1.12	1.02	1.21	1.11
98	1.72	1.29	1.56	1.23	1.15	1.38	1.27
99	1.73	1.50	1.78	1.35	1.28	1.50	1.45
100	0.58	1.69	1.84	1.30	1.39	1.57	1.52
101	0.36	1.76	2.24	1.76	1.42	2.59	2.06

Stress point	Gorilla gorilla	Homo sapiens	Hylobates lar	Pan paniscus	Pan troglodytes	Pongo abelii	Pongo pygmaeus

2.7.2 Supporting information 2. Table 2.3 b) von Mises stress values were obtained from 101 locations extracted along a path as described in Figure 2b for the suspension scenario.

Stress point	Gorilla gorilla	Homo sapiens	Hylobates lar	Pan paniscus	Pan troglodytes	Pongo abelii	Pongo pygmaeus
1	1.67	5.16	2.63	2.14	2.32	1.77	2.81
2	2.36	4.76	2.11	1.92	2.02	1.83	2.75
3	2.97	4.24	1.52	1.87	2.38	1.77	2.83
4	3.09	3.55	1.01	2.17	2.26	1.73	3.00
5	2.66	3.49	1.13	3.48	2.35	1.88	2.53
6	2.41	3.61	1.30	4.44	2.45	2.02	2.27
7	2.24	3.51	1.57	4.65	2.55	1.94	2.08
8	2.15	3.24	1.69	4.61	2.60	1.88	2.06
9	2.03	2.96	1.79	4.59	2.62	1.82	2.13
10	2.15	2.81	1.86	4.34	2.62	2.00	2.01
11	2.07	2.89	1.82	4.03	2.52	2.20	2.12
12	1.95	2.93	1.81	3.69	2.60	2.33	2.07
13	1.99	3.12	1.78	3.42	2.63	2.43	1.94
14	1.83	3.34	1.75	3.33	2.66	2.71	1.94
15	1.69	3.66	1.71	3.26	2.75	2.91	1.72
16	1.65	3.78	1.68	3.18	2.83	2.79	1.64
17	1.64	3.67	1.65	3.28	2.92	2.80	1.68
18	1.68	3.41	1.63	3.29	2.95	2.77	1.75
19	1.92	3.06	1.61	3.33	2.99	2.58	1.78
20	1.97	2.71	1.61	3.35	3.13	2.64	1.75
21	2.15	2.49	1.60	3.39	3.15	2.29	2.07
22	2.33	2.34	1.60	3.44	3.21	2.53	2.25
23	2.34	2.18	1.60	3.44	3.37	2.35	2.51
24	2.60	2.08	1.60	3.46	3.37	2.24	2.69
25	2.47	2.00	1.60	3.50	3.36	2.31	2.75
26	2.67	2.01	1.59	3.54	3.31	2.09	2.68
27	2.81	2.08	1.59	3.35	3.26	2.13	2.59
28	3.00	2.15	1.57	3.31	3.27	1.96	2.31

29	3.62	2.19	1.57	3.25	3.25	1.82	2.11
30	3.48	2.18	1.57	3.24	3.31	1.74	1.88
31	4.04	2.22	1.58	3.24	3.28	1.63	1.84
32	4.89	2.13	1.57	3.08	3.19	1.61	1.70
33	4.84	2.10	1.58	2.95	3.09	1.53	1.50
34	4.64	2.02	1.58	2.85	3.03	1.57	1.46
35	4.38	2.01	1.59	2.68	2.93	1.61	1.37
36	4.25	1.91	1.61	2.61	2.86	1.72	1.30
37	4.45	1.89	1.58	2.46	2.78	1.74	1.19
38	4.67	1.86	1.59	2.50	2.73	1.71	1.08
39	4.93	1.84	1.59	2.43	2.66	1.63	0.99
40	4.96	1.83	1.61	2.49	2.58	1.65	0.91
41	4.70	1.81	1.64	2.34	2.53	1.65	0.95
42	4.46	1.76	1.65	2.38	2.42	1.74	1.15
43	4.28	1.74	1.65	2.51	2.40	1.74	1.38
44	4.20	1.69	1.66	2.61	2.32	1.91	1.64
45	4.10	1.62	1.70	2.69	2.26	1.98	2.05
46	3.99	1.56	1.68	2.74	2.24	2.14	2.35
47	3.97	1.50	1.70	2.73	2.17	2.24	2.45
48	3.80	1.45	1.70	2.70	2.17	2.46	2.59
49	3.65	1.41	1.73	2.72	2.12	2.50	2.73
50	3.58	1.37	1.71	2.72	2.06	2.50	2.69
51	3.33	1.27	1.73	2.80	2.04	2.61	2.67
52	3.03	1.21	1.72	2.75	1.98	2.73	2.72
53	2.59	1.15	1.71	2.61	1.97	2.85	2.83
54	2.33	1.11	1.72	2.52	1.84	3.01	2.81
55	1.91	1.07	1.72	2.40	1.79	2.96	2.63
56	1.84	1.03	1.70	2.24	1.72	3.15	2.43
57	1.99	0.96	1.66	2.08	1.68	2.98	2.20
58	2.09	0.95	1.65	1.93	1.60	2.79	2.11
59	2.20	0.91	1.63	1.88	1.59	2.56	2.01
60	2.32	0.91	1.66	1.72	1.61	2.37	1.96
61	2.47	0.87	1.75	1.76	1.57	2.20	1.82

62	2.79	0.83	1.70	1.75	1.59	2.24	1.74
63	2.72	0.82	1.75	1.69	1.58	2.22	1.72
64	2.91	0.79	1.78	1.64	1.60	2.28	1.68
65	3.17	0.76	1.83	1.62	1.60	2.38	1.71
66	3.43	0.74	1.85	1.68	1.61	2.33	1.84
67	3.92	0.74	1.85	1.71	1.58	2.37	1.95
68	4.26	0.73	1.87	1.71	1.59	2.38	2.09
69	4.73	0.74	1.91	1.71	1.60	2.43	2.18
70	5.21	0.74	1.85	1.72	1.57	2.45	2.27
71	4.85	0.74	1.97	1.80	1.57	2.52	2.26
72	4.44	0.74	1.92	1.85	1.59	2.57	2.37
73	4.13	0.74	1.95	1.79	1.60	2.60	2.48
74	3.83	0.74	2.06	1.82	1.59	2.74	2.57
75	3.49	0.72	2.16	1.81	1.58	2.76	2.58
76	3.06	0.70	2.30	1.77	1.55	2.73	2.61
77	2.73	0.67	2.42	1.72	1.56	2.63	2.54
78	2.33	0.64	2.47	1.71	1.59	2.53	2.42
79	2.30	0.60	2.57	1.64	1.54	2.42	2.37
80	2.27	0.57	2.62	1.54	1.56	2.30	2.18
81	2.92	0.51	2.64	1.42	1.45	2.11	2.07
82	2.38	0.47	2.68	1.37	1.45	1.92	1.91
83	1.80	0.42	2.64	1.21	1.40	1.74	1.73
84	1.38	0.37	2.49	1.10	1.33	1.54	1.54
85	1.15	0.32	2.21	1.05	1.27	1.36	1.37
86	0.99	0.26	1.96	0.84	1.16	1.21	1.21
87	1.00	0.23	1.68	0.85	1.04	1.05	1.06
88	0.84	0.19	1.40	0.72	0.92	0.91	0.92
89	0.75	0.16	1.13	0.67	0.83	0.80	0.82
90	0.61	0.14	0.91	0.60	0.72	0.68	0.70
91	0.51	0.11	0.72	0.57	0.64	0.58	0.61
92	0.42	0.10	0.58	0.52	0.56	0.49	0.52
93	0.36	0.08	0.48	0.45	0.49	0.42	0.46
94	0.33	0.07	0.39	0.40	0.43	0.37	0.41

95	0.32	0.06	0.33	0.36	0.38	0.34	0.38
96	0.34	0.06	0.29	0.35	0.34	0.34	0.36
97	0.38	0.06	0.26	0.37	0.31	0.36	0.36
98	0.47	0.07	0.24	0.42	0.31	0.41	0.38
99	0.66	0.08	0.24	0.50	0.32	0.49	0.41
100	0.75	0.08	0.25	0.60	0.35	0.61	0.47
101	0.91	0.10	0.27	0.72	0.41	0.73	0.54

CHAPTER 3

Analyzing the Sclerocarpy Adaptations of the Pitheciidae Mandible using Finite Element Analysis and Geometric Morphometrics

Analyzing the Sclerocarpy Adaptations of the Pitheciidae Mandible using Finite Element Analysis and Geometric Morphometrics

Thomas A. Püschel[1]*, Jordi Marcé-Nogué[2], Thomas M. Kaiser[2], Robert J. Brocklehurst[1], William I. Sellers[1].

1) School of Earth and Environmental Sciences, University of Manchester, Michael Smith Building, Oxford Road, Manchester, M13 9PT, United Kingdom.
2) Center of Natural History (CeNak), Universität Hamburg, Martin-Luther-King-Platz 3, Hamburg, 20146, Germany.

Short Title: Sclerocarpy and the pitheciid jaw

*Corresponding author: Thomas A. Püschel
E-mail: thomas.puschel@postgrad.manchester.ac.uk
Phone: +44 (0) 7476608464
Postal address: School of Earth and Environmental Sciences, University of Manchester, Michael Smith Building, Oxford Road, Manchester, M13 9PT, United Kingdom.

Abstract

Primates are interpreted to be ancestrally adapted to frugivory, although some modern groups show clear adaptations to other diets. Among them, pitheciids stand out for specifically predating seeds. This dietary specialization is known as sclerocarpy and refers to the extraction of seeds from surrounding hard tissues using the anterior dentition followed by the mastication of seeds by the molars. It has been proposed that *Callicebus–Pithecia–Chiropotes-Cacajao* represent a morphocline of increasingly specialized anatomical traits for sclerocarpic foraging, although this has not been biomechanically tested. This study addresses whether there is a sclerocarpic specialization gradient in the mandibular morphology of pitheciids, and also tests whether mandibular shape is associated with mandibular strength. Finite element analysis (FEA) was used to simulate two biting scenarios and the obtained stress values were compared between different pitheciids. Geometric morphometrics (GM) were used to test the association between mandibular shape and stress values. The obtained results show that there is indeed a relative specialization continuum in the pitheciid mandible for some aspects of shape as expected for the morphocline hypothesis, although from a biomechanical perspective *Cacajao* and *Chiropotes* showed a similar performance, thus not exhibiting the expected gradient. Additionally, it was found that there is a significant association between mandibular shape and stress values. The present results are expected to contribute to a better insight regarding the ecomorphological relationship between mandibular morphology and mechanical performance among pitheciids.

Keywords: Pitheciidae; Sclerocarpy; Mandible; Finite Element Analysis; Geometric Morphometrics

3.1 Introduction

Primates are often interpreted as morphologically and behaviorally adapted to frugivory, this trait being regarded as the ancestral condition of this order (Kay, 1984; Fleagle and McGraw, 1999). Nearly all primates will eat fruit when available: however it has been argued that it is almost always an ephemeral resource in natural environments (Steege and Persaud, 1991; Chapman et al., 1999) and fruits provide a variable amount of essential nutrients (Oftedal et al., 1991; Conklin-Brittain et al., 1998; Milton, 1998; Norconk and Conklin-Brittain, 2004; Norconk et al., 2009). Many frugivorous primates also add insects and/or leaves to their diets in order to both balance their nutritional intake as well as to supply possible deficiencies in their food (Fleagle, 2013). Besides the main dietary groups of fruit, leaves and insects, there are also several other incidental food items that can contribute important nutrients or serve as fallback items when required, such as flowers, gum, bark, fungus, lichen, pith and seeds (Conklin-Brittain et al., 1998; Lambert, 1998; Lambert et al., 2004; Sayers and Norconk, 2008; Grueter et al., 2009; Marshall et al., 2009; Norconk et al., 2009). Among these different dietary items, seeds are relevant nutritional items for at least 31 primate species that consume seeds either seasonally or regularly (Norconk et al., 2013). Seed predation has been defined as the action of masticating and ingesting seeds or whole fruits that include seeds (Norconk et al., 2013). Due to the fact that seeds are often well protected against predation, seed predators show a broad variety of adaptations to extract them from protecting tissues and later consume them. Primates typically tend to prefer the soft, outer layers of the fruit (i.e. the pericarp). The soft parts are obtained by swallowing the fruit whole, or by removing the edible portions with teeth and/or hands and then dropping the seeds (Kay et al., 2013). Whole seeds ingested together with the soft outer layers can germinate if passed intact through the gastrointestinal tract (Norconk et al., 2013). However, among primates, pitheciines (i.e. *Pithecia*, *Chiropotes*, *Cacajao*) follow a different pattern. They actively extract seeds from the fruit, chewing them before swallowing, and are consequently recognized as seed predators (Rosenberger, 1992). Some other primates from South America are sporadic seed predators, but pitheciines appear to be specialized to varying degrees in seed predation or sclerocarpic foraging (van Roosmalen et al., 1988). Even though this specific dietary strategy is rare among primates, it might have arisen as

way to reduce dietary stresses and competition with sympatric taxa during periods of scarcity of other preferred food (Davis, 1996; Norconk et al., 2009). The seeds of unripe fruit seem to represent a particularly unique means of acquiring fundamental nutrients, especially when considering that young seeds are an exceptionally good source of lipids, proteins, and carbohydrates (Kinzey and Norconk, 1993; Norconk and Conklin-Brittain, 2004).

Sclerocarpy refers to the extraction of seeds using the anterior dentition (i.e. incisors, canines and/or the first premolar in the tooth row) and hands, followed by the mastication of seed by the molars (Kinzey and Norconk, 1990). Interestingly, within the Pitheciidae the pitheciines are the quintessential example of this type of seed predation; in fact the pitheciin fossil record (e.g. *Proteropithecia neuquensis*, *Nuciruptor rubicae*) suggests that the lineage began to fill their hard-object feeding niche around the middle Miocene, thus scleorcarpic foraging is a relatively old trait in this lineage (Meldrum and Kay, 1997; Kay et al., 1998, 2013). Pitheciids comprise two distinctive platyrrhine sub-families: the Callicebinae consisting of the genus *Callicebus* (titi monkeys) and the Pitheciinae comprising *Pithecia* (sakis), *Chiropotes* (bearded sakis) and *Cacajao* (uakaris). All these genera predate hard unripe seeds to a varying degree, although only the Pitheciinae exhibit most marked specializations to this particular diet, showing noticeable modifications of the cranium, mandible, dentition, cranial musculature and viscera (Kinzey, 1992; Norconk and Veres, 2011; Kay et al., 2013; Ledogar et al., 2013; Norconk et al., 2013). These features are particularly evident and developed in *Cacajao* (Kinzey, 1992); nonetheless, in all three pitheciin genera the most significant food element consumed is seeds. Furthermore, it is been shown that when resources are scarce, *Pithecia*, *Chiropotes* and *Cacajao* further increase their seed consumption (Norconk et al., 2009). Pitheciins are pre-dispersal seed predators (Janzen, 1971), therefore they eat fruit primarily covered with a hard pericarp that is subsequently opened with their canines and/or incisors (Kinzey and Norconk, 1990). *Callicebus* also share the seed-eating habits of pitheciines but to a lesser degree, although it has been reported that almost a quarter of the diet of *Callicebus personatus* (Müller, 1996), and almost half of that of *Callicebus lugens* may correspond to immature seeds (Palacios et al., 1997). Some authors have actually proposed that *Callicebus–Pithecia–Chiropotes-Cacajao* represent a morphocline of increasingly specialized anatomical traits for sclerocarpic foraging (Kay, 1990;

Kinzey, 1992; Rosenberger, 1992; Meldrum and Kay, 1997). A pattern of derived traits related to this feeding behavior distinguish the living pitheciids from any other extant platyrrhine (Kay, 1990; Rosenberger, 1992).

In this sclerocarpy specialization gradient, *Callicebus* would represent the least specialized genus for seed predation among the pitheciids, because it lacks some of the dental and mandibular associated with sclerocarpy, such as enlarged canines, molarized premolars and flatter molars with poorly developed crests (Kinzey, 1992). Nonetheless, *Callicebus* does show some seed predation features, like a posterior deepening of the mandible, as well as narrow and elongated incisors (Kinzey, 1992). On the other hand, *Pithecia*, *Chiropotes* and *Cacajao* would exhibit adaptations for sclerocarpy in an increasing manner (Kay et al., 2013). All of these genera exhibit an incisor–canine complex that enables a specialized puncturing and prying mechanism (Kay et al., 2013). The lower incisors are narrow, styliform and particularly procumbent, which creates a gouge (Kay et al., 2013). The canines are enlarged, laterally splayed, and have a sharp lingual crest (i.e. entocristid), producing a triangular cross-section (Rosenberger and Tejedor, 2013). This specialized large-seed scraping and splitting mechanism is powered by extremely hypertrophied mastication musculature with associated posterior jaw deepening (Rosenberger and Tejedor, 2013). The first lower molars are also enlarged (Kinzey, 1992; Norconk et al., 2013), and they show molarized last premolars with high complexity and low relief, shear, and curvature of molar occlusal surfaces (Ledogar et al., 2013; Winchester et al., 2014). Interestingly, it has been shown that the molar enamel of pitheciins is relatively thin and often crenulated, although it exhibits extremely well-defined Hunter-Schreger bands, a trait that seems to strengthen the enamel and prevent cracks from propagating through the tooth (Koenigswald and Pfretzschner, 1987; Rensberger, 1993). On the other hand, *Callicebus* exhibits relatively thin and radial enamel with no evident Hunter-Schreger bands, indicative of a softer diet (Martin et al., 2003). This relatively thin molar enamel exhibited by the pitheciins could be related to the fact that although they are sclerocarpic foragers that open hard husks with their canines and/or anterior incisors, the seeds that they then chew are relatively soft and pliable when compared to the ones consumed by other primates. For instance, the other platyrrhine that often consumes hard objects (i.e. *Cebus*) has probably the thickest molar enamel of all primates (Dumont, 1995;

Martin et al., 2003). This is possibly an adaptation that slows wear, thus prolonging the life of the tooth, in particular their relief and cusps. Taking into account the extreme hardness of the items ingested by *Cebus*, such adaptation might be of crucial benefit. However, it is important to keep in mind that even though the seeds consumed by the pitheciines are soft, the sclerotized pericarp that protects them is still extremely hard. For example, the maximum hardness of the pericarp ingested by *Pithecia pithecia* is approximately five times that of fruits ingested by *Ateles,* while the maximum hardness recorded for fruits ingested by *Chiropotes satanas* was 27 times that of the hardest fruit opened by *Ateles* (Kinzey and Norconk, 1990).

Even though several studies report on some specific phenotypic aspects related to the sclerocarpic behavior of the pitheciids, there are only few quantitative analyses focusing on the sclerocarpy adaptations of the mandibular morphology. For instance, Wright (2005) compared the mechanical advantage (MA) of the jaw-closing muscles at different biting positions across ten platyrrhine species, focusing especially on *Cebus* spp. due to their known durophagic behavior. He found that *Cebus* showed the highest MA for the jaw-closing muscles (excepting the medial pterygoid), while *Chiropotes satanas* exhibited the next highest MA followed by *Pithecia pithecia, Lagothrix lagotricha* and *Ateles paniscus* (Wright, 2005). On the other hand *Alouatta seniculus*, *Callicebus* spp. and *Aotus trivirgatus* exhibited the least MA among the analyzed species (Wright, 2005). In another study, Anapol & Lee (1994) estimated the temporalis and masseter lever arms for eight platyrrhine species, focusing mostly on variation among lever arm lengths. They noticed that the temporalis lever arm showed relatively more variation than the masseter lever arm (Norconk et al., 2009). They measured moment arms for the temporalis, masseter and medial pterygoid in 22 platyrrhine species, in a similar fashion to Wright (2005). Subsequently, Anapol & Lee (1994) scaled these measurements by the proportion of the total jaw-adductor muscle weight each muscle represents based on the few platyrrhine data provided by Turnbull (1970). It was found that individual moment arms and average moment arm scale close to or slightly below isometry relative to incisor, canine and molar biting moment arms (Norconk et al., 2009). They also found that relative MA among platyrrhines seemed to trend toward a size-related decrease in biting leverage, especially for biting along the post-canine dentition (i.e. smaller platyrrhines seemed to have greater MA on average than larger species for

biting at M1) (Norconk et al., 2009). They also found that among the non-callitrichines, *Cebus apella* exhibited the highest leverage for biting, while *Chiropotes satanas* and *Cacajao melanocephalus* have the next highest advantage followed by *Pithecia pithecia* and *Cebus albifrons*. Consequently, they proposed that these results support previous observations suggesting that "hard-object" feeders have relatively greater MAs, predominantly during anterior tooth use (Anapol and Lee, 1994; Wright, 2005). In addition to these MA estimations, Norconk et al. (2009) also attempted to summarize morphological variation in load bearing ability across platyrrhine species by carrying out a principal component analysis (PCA) of various ratios calculated from a set of mandibular measurements. They interpreted their PC1 as a general jaw robusticity factor, where *Chiropotes satanas* and *Cacajao melanocephalus* had the largest scores followed by *Cebus*, thus suggesting these taxa must have relatively robust mandibles, likely due to their ingestion of mechanically challenging seeds (Bouvier, 1986; Kinzey, 1992; Anapol and Lee, 1994).

In spite of all these valuable studies, most of these investigations have been restricted to morphological comparisons and simple biomechanical comparisons (i.e. comparing lever arms and MA), with fewer studies using modern virtual functional morphology techniques or experimental approaches applied to analyze platyrrhine mandibles (Ross et al., 2013, 2016). In the present study we chose to focus on the mandible rather than the whole cranium, because this latter structure exhibits a morphology associated with multiple and diverse functions, while the lower jaw is primarily involved in food acquisition and consumption, and consequently it would be expected that its morphology better reflects dietary adaptations (Hiiemae and Kay, 1972; Hiiemae, 1978; Hylander et al., 1987; Chew et al., 1988; Agrawal et al., 1998; Vinyard et al., 2003; Gröning et al., 2012; O'Higgins et al., 2012). In fact it has been stated that understanding the biomechanical behavior of the primate mandible seems to be essential to gain insight about primate dietary adaptations, and thus about their evolution (Wroe et al., 2010; Perry et al., 2011). This study investigates the biomechanical performance of four different pitheciid species representing the seed predation specialization gradient using finite element analysis (FEA). FEA is a technique that reconstructs stress, strain, and deformation in material structures that has become a standard part of the biomechanical toolkit (Rayfield, 2007). The application of FEA to analyze primate

mandibular morphology is particularly relevant, due to the limited number of studies where ecological data on primate diet is used to explicitly test biomechanical hypotheses. It was expected that those species that rely more on seed consumption should exhibit stronger jaws (i.e. lower stress values) due to morphological adaptations to this particular diet, when compared to those species that eat fewer seeds. In addition, we examined the relationship between mandibular shape and mandibular strength (i.e. stress values) by using geometric morphometrics (GM). GM refers to the quantitative analysis of Cartesian coordinates representing form (i.e., shape and size) and how it covaries with respect to other factors (e.g., biomechanics, development, ecology, genetics, etc.) (O'Higgins, 2000; Adams et al., 2013). Based on the evidence that has shown that skeletal morphology reflects to a certain extent the mechanical pressures exerted during life (Pearson and Lieberman, 2004; Ruff et al., 2006; Barak et al., 2011), it was expected that mandibular shape would be significantly associated with stress values. The two following hypotheses were tested:

H1: The strength of the mandible obtained from the FEA simulations reflect the sclerocarpy specialization gradient described for pitheciids. Consequently, the results observed in the mandible should show a gradient from weaker to stronger mandibles following the seed predation specialization observed in this group (i.e. *Callicebus–Pithecia–Chiropotes-Cacajao*).

H2: Mandibular shape is significantly associated with mandibular strength (measured as stress values).

3.2 Methods
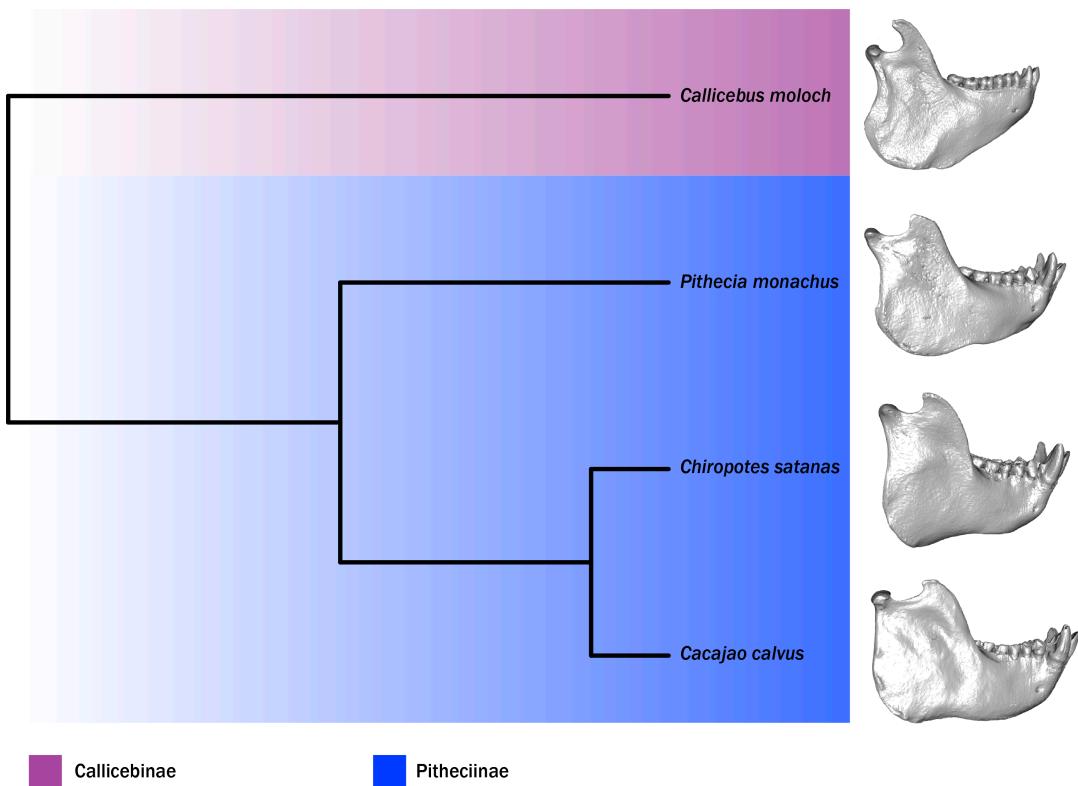
This research met the animal research requirements of the UK, and adhered to the American Society of Primatologists principles for the ethical treatment of non-human primates.

3.2.1 Sample

The CT-scan data of four pitheciid species housed at the Museum of Comparative Zoology - Harvard University (Cambridge, MA, USA) were obtained from the Morphosource database (http://morphosource.org/) (Table 3.1; Fig. 3.1) (Copes et al., 2016). The species under study are *Cacajao calvus, Callicebus moloch, Chiropotes satanas* and *Pithecia monachus.* This sample was selected to consider one member of every genus within Pitheciidae, in order to represent the proposed sclerocarpy specialization gradient exhibited by this group. All specimens were adult with no reported or evident pathologies associated with their mandibular anatomy. The *Callicebus moloch* and *Cacajao calvus* individuals were male according to the information available from the museum records. Unfortunately, there was no information regarding the sex of the two other analyzed specimens. Nonetheless, it is well known that black-bearded sakis (i.e. *Chiropotes satanas*) are only slightly sexually dimorphic (Hershkovitz, 1985; Smith & Jungers, 1997), and that *Pithecia monachus* also shows minor sexual dimorphism in their skull morphology, the males being on average only slightly larger (in all measurements) when compared to females (Hershkovitz, 1987). Therefore, this uncertainty should not affect our results, particularly when considering that the FEA represents simplified loading scenarios. Further details regarding the scanning process can be found in http://morphosource.org/ or in the Harvard Museum of Comparative Zoology database http://mczbase.mcz.harvard.edu/SpecimenSearch.cfm

Table 3.1 Sample

Species	Accession number	Scan resolution [mm]
Cacajao calvus	MCZ-27870	0.08
Callicebus moloch	MCZ-20186	0.05
Chiropotes satanas	MCZ-BOM-6028	0.053
Pithecia monachus	MCZ-27124	0.05

Figure 3.1 Analyzed pitheciid mandibles plotted next to a consensus phylogenetic tree computed from 10,000 phylogenies downloaded from the 10kTrees dataset (http://10ktrees.fas.harvard.edu/Primates/index.html) (Arnold et al., 2010).

Image segmentation

The CT-scans of the different pitheciid species were segmented in the following manner. DICOM files were imported into AVIZO v. 9.1 (VSG, USA) where each specimen was segmented by applying a combination of manual painting techniques and case-specific thresholding. The segmented models were then converted to CAD models (Marcé-Nogué et al., 2015). During this step, surface irregularities from model generation were repaired using the refinement and smoothing tools from Rhinoceros v. 5.0 (McNeel & associates). The models were all oriented with respect to the same occlusal plane to facilitate the comparison between them. This occlusal plane was defined as an imaginary surface that 'touched' the incisal edges of the incisors and the tips of the occluding surfaces of the posterior teeth.

115

3.2.2 Finite element analysis

Model properties
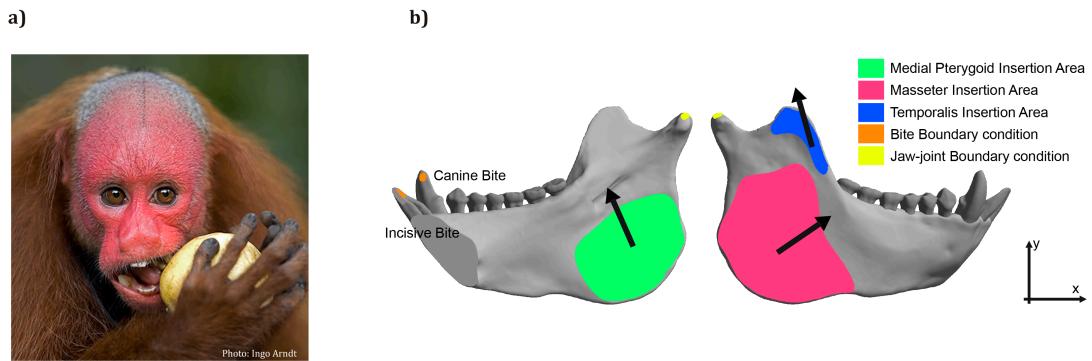
A structural static analysis to evaluate the biomechanical behavior of the four different jaws during biting was performed using the Finite Element Package ANSYS 17.1 on a Dell Precision™ Workstation T5500. It is important to bear in mind that the objective of this study was to develop a FEA structural comparative analysis; therefore we were not interested in the *in vivo* value of load forces or resulting stresses. The aim was to analyze mandibular strength under equivalent loads and comparable loading scenarios. Consequently in this work FEA was used in a comparative fashion rather than being used to validate the models against experimental data. FEA was applied as a structural comparative technique, the idea being to compare a general measure of mechanical performance. This means that any simplification performed in our models is present in all the four jaws and is therefore not affecting our macroscopic comparisons because the same simplifications were applied to all the models.

In this study, we obtained the von Mises stress distribution in the jaw under the chosen loading conditions, which reflect different feeding scenarios. Von Mises criterion is the most accurate value for predicting fracture location when isotropic material properties are used in cortical bone (Doblaré et al., 2004). Elastic, linear and homogeneous material properties were assumed for the bone using the following values from *Macaca*: Young Modulus E=21 GPa and Poisson´s ratio v=0.3 for the mandible (Strait et al., 2005), while for the teeth the values for the enamel were E=99.4 GPa and v=0.3 (Constantino et al., 2012). Strait et al. (2005) have shown that the Young's Modulus of bone in the primate skull varies depending on the analyzed anatomical locations, ranging from 12.5 GPa (posterior portion of the zygomatic arch) to 20.8 GPa (anterior zygomatic). However, the use of these values is not crucial for the development of the analyses proposed here because these values do not affect the results when a relative comparison of stress results between models is performed (Gil et al., 2015). The models were segmented as a solid models without including trabecular bone properties because it has been shown that the exclusion of trabecular bone does not affect the overall results of a

FEA (Fitton et al., 2015). Additionally, we decided not to segment the periodontal ligament (PDL) because there is a considerable debate in the literature regarding the importance or not of modeling the PDL in FEA (Bright, 2014). Some modeling studies of the primate mandible have suggested that the presence or absence of the PDL might affect the obtained results substantially throughout the whole structure (e.g. Marinescu et al., 2005; Gröning et al., 2011), while other researchers found that it is only important in the areas immediately adjacent to the teeth (e.g. Panagiotopoulou et al., 2011). Likewise, models of the crania of *Cebus* (Wood et al., 2011) found that the PDL had exclusively local effects when performing FEA. Therefore, we decided not to include this extra variable in our models until its role is better understood, because it can introduce further uncertainties in our models that might confuse our result interpretation. Finally, the jaws were meshed using an adaptive mesh of hexahedral elements also using ANSYS v. 17.1 (Marcé-Nogué et al., 2015). The model meshes ranged between 200,000-500,000 elements depending on the particular specimen and biting case.

Boundary conditions and applied loadings

The available literature on sclerocarpic foraging was reviewed in order to define sensible loading conditions (van Roosmalen et al., 1988; Norconk et al., 2013). Based on the available descriptions of sclerocarpic foraging behavior, it was possible to establish commonalities regarding the way in which the pitheciines extract seeds. They basically apply two different bites, either using their procumbent incisors or their wedge-shaped canines (Fig. 3.2a), seemingly depending on the hardness of the fruit (Norconk et al., 2013). For instance, it has been reported that *Chiropotes* bites a hole into the fruit at the edge of the operculum when dealing with *Eschweilera* fruits from the Brazil nut family (Lecythidaceae) (van Roosmalen et al., 1988). Then it uses its incisors like a can opener to pop the operculum off and gain access to the seeds inside. When feeding on the very hard seedpods of larger Lecythidaceae such as *Lecythis davisii*, sakis use their powerful wedge-shaped canines rather than their incisors (van Roosmalen et al., 1988).

Figure 3.2 a) *Cacajao calvus* individual biting a hole into a fruit using its wedge-shaped canines; b) Free-body diagram of the applied biomechanical scenarios showing boundary conditions, muscular forces and insertion areas, as well as dental positions used to simulate Incisive Bite and Canine Bite.

Boundary conditions were defined to represent the loads and fixed displacements that the mandibles experience during two biting scenarios (Fig. 3.2b). The first boundary condition restrained the condyle at the level of the contact points with the mandibular fossa of the cranium in order to represent the immobilization of the mandible constraining the translation of the jaw in all the directions. The analysis simulated an instantaneous event at static equilibrium, in order to examine overall patterns of stress distribution in the mandible. In order to simulate biting, a fixed displacement boundary condition in the y-axis was applied in two different dental positions: 1) Incisive bite: at the occlusal edge of the central incisive and 2) Canine bite: at the tip of the canine (Fig 3.2b).

The muscular insertion areas of the masseter, medial pterygoid and temporalis were defined in the model in order to apply the forces of muscular contraction during the bite in the jaw. The directions of the forces were defined by lines joining the centroid of the insertion area on the skull with the centroid of the insertion areas on the mandible (Supporting information 1 of this chapter). The reduced Physiological Cross-Section Areas (PCSA) of *P. monachus* were obtained from (Anapol et al., 2008) for the temporalis (163 mm^2), masseter (133 mm^2) and the medial pterygoid (84 mm^2). Assuming a value of 0.3MPa as muscular contraction pressure (Alexander, 1992)], the muscle force was obtained for *P. monachus*, which was used again as a reference model (Table 3.2).

Table 3.2 Muscle forces and volumes of the models

Model	Volume of the jaw [mm³]	Pterigoid Force [N]	Masseter Force [N]	Temporalis Force [N]
Callicebus moloch	3288.3	22.92	36.28	44.47
Pithecia monachus	3792	25.2	39.9	48.9
Chiropotes satanas	6923.9	37.65	59.61	73.05
Cacajao calvus	11554	52.96	83.86	102.77

Scaling

One relevant concern to be considered when analyzing different individuals using FEA is how to compare models that differ in shape and size (Dumont et al., 2009). In this study, the values of muscular forces applied in the models were calculated according to the methodology developed by Marcé-Nogué et al. (2013) and rearranged for 3D models by Fortuny et al. (2015) based on scaling the forces via the volume ratio (Equation 1). V_B is the volume of the reference model and V_A is the volume of the scaled model. The muscular force (F) of both models A and B were related with the variation of the volume (V) of the skull as stated in equation 1 (Table 3.2). *P. monachus* was used as the reference model B in Equation 1, scaling the values of these forces in the other models to enable an appropriate comparison.

Equation 1.

$$F_A = \left(\sqrt[3]{\frac{V_A}{V_B}} \right)^2 F_B$$

Analysis of the FEA results
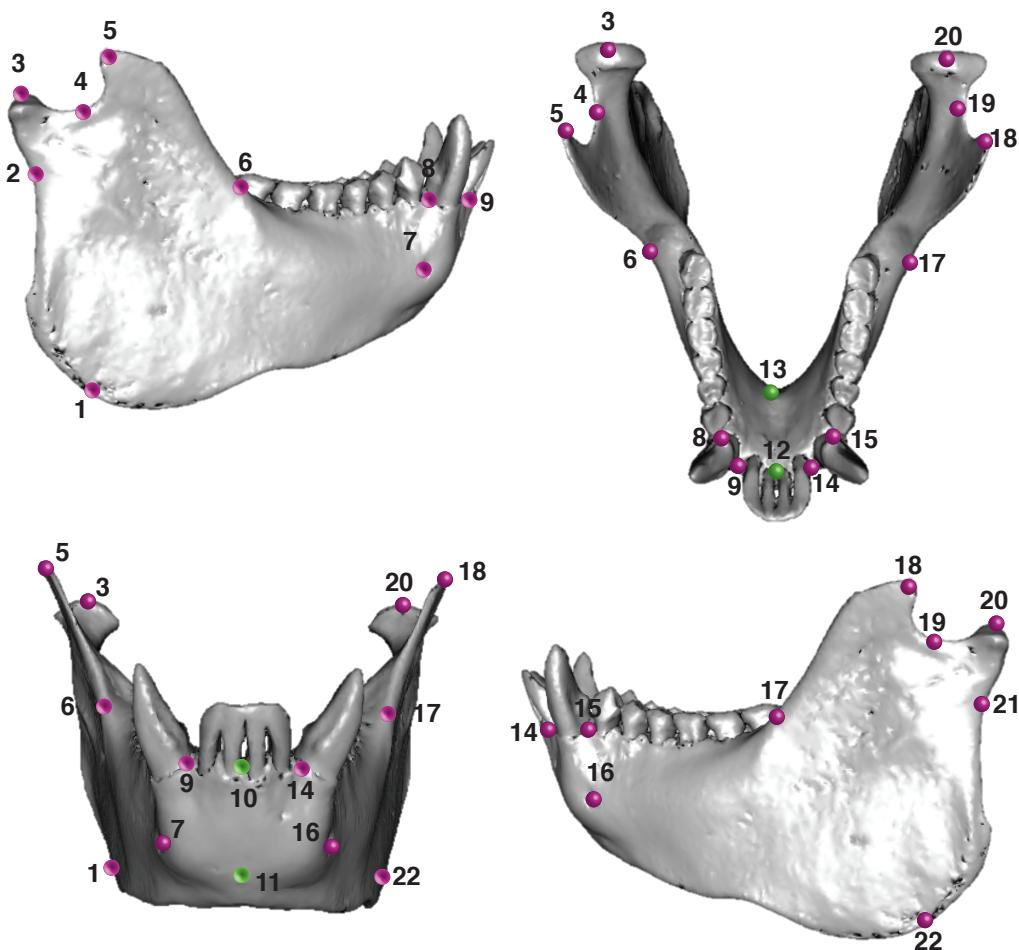
In order to facilitate the comparison between models, quantitative measurements of the relative strength of the different jaws were used to summarize the FEA results.

The von Mises stress distributions of the different mandibles were evaluated using their average values and presented using box-plots to display their stress distributions following the proposal by Farke (2008), who recommends plotting stress distributions as quantitative data. However, the use of box-plots for the stress and statistics derived from them (e.g. percentiles or whiskers) requires the use of a quasi-ideal mesh (QIM), thus involving corrections for mesh non-uniformity. In the present paper we used QIM for our models -a mesh where all the elements have practically the same size- thus allowing the display the obtained stress values as boxplots (Marcé-Nogué et al., 2016). Due to the fact that a QIM is a non-uniform mesh (i.e. different elements have dissimilar sizes, although nearly identical in a QIM), new statistics that take into account this non-uniformity were estimated, such as the mesh-weighted arithmetic mean (MWAM) and the mesh-weighted median (MWM). For the MWAM some data points contribute more than others depending on the size of the element (i.e. the sum of the value of the von Mises stress for each element multiplied by its own volume and divided by the total volume), while the MWM is defined as the division of the median of the product of stress and volume by the median of the volume (Marcé-Nogué et al., 2016). These values (i.e. MWAM and MWM), are required to estimate the percentage error of the arithmetic mean (PEofAM) and percentage error of the median (PEofM), which are statistics used to ensure that our models were good QIMs as described in (Marcé-Nogué et al., 2016).

3.2.3 Association between mandibular shape and stress values

Shape variables were obtained using GM methods (Slice, 2007; Zelditch et al., 2012). Landmark acquisition was carried out by TP in Landmark Editor v.3.6 (IDAV) (Wiley et al., 2005) by collecting 22 homologous and well-defined 3D points (Fig. 3.3). GM and statistical analysis were carried out in R using the 'geomorph' package (Adams and Otárola-Castillo, 2013). A generalized Procrustes analysis was applied to extract the shape variables from the raw landmark data, by removing all the differences due to translation, rotation and scale (Bookstein, 1991). This generalized Procrustes analysis took into account object symmetry; therefore two separate matrices were generated, representing the symmetric and asymmetric components of shape variation respectively (Klingenberg et al., 2002). The

symmetric component represents shape variation among individuals in what could be regarded as a left-right average, while the asymmetric component represents the differences between the original and mirrored configurations (Klingenberg et al., 2002). For the following analyses only the symmetric component was analyzed. We did not find a significant result from a regression of shape on centroid size (R^2:0.59; F: 2.9128; p-value: 0.1028); therefore we thought it unnecessary to correct for allometric effects by for instance estimating size-adjusted shape coordinates.

Figure 3.3 3D landmarks used to perform GM analyses. Green spheres represent the median landmarks, while the purple ones correspond to bilateral coordinates.

A PCA of the symmetric component was carried out to visualize the main axes of variation in mandibular shape. The associations between mandibular shape (i.e. Procrustes coordinates), and mandibular strength (i.e. stress percentile values: M25, M50, M75, M95) for the two biting scenarios was assessed by carrying out two
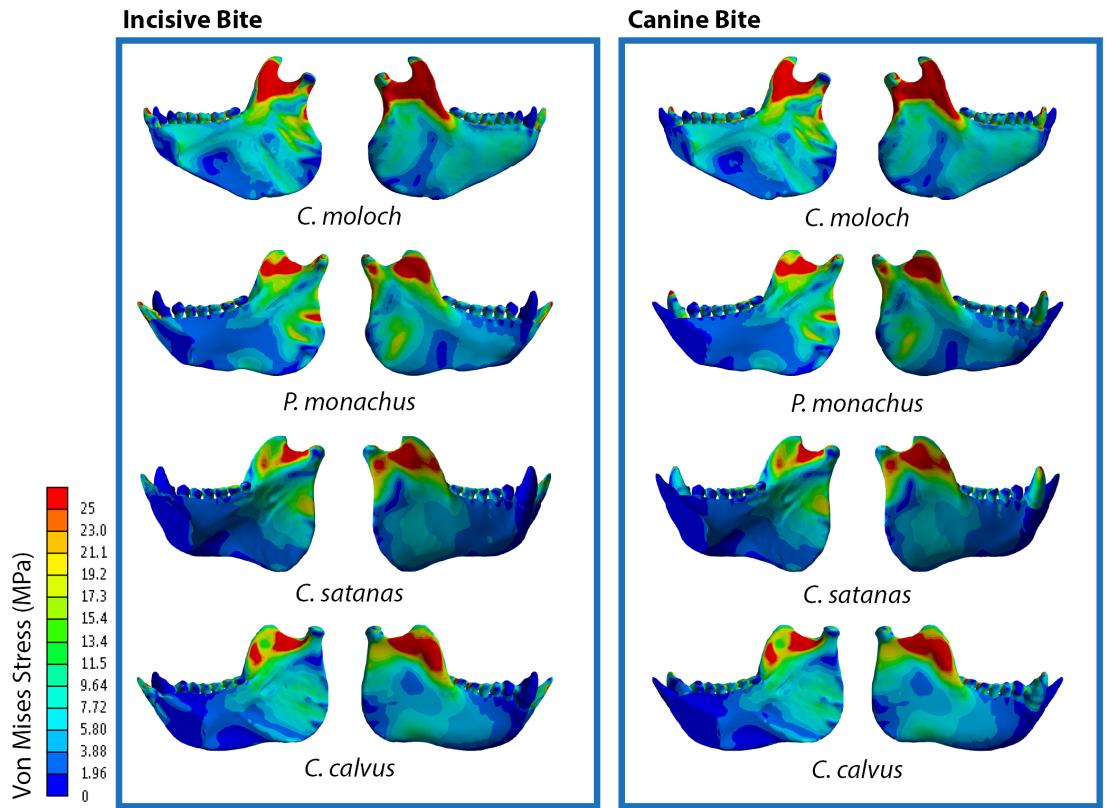
partial least squares (PLS) analyses (Corti and Rohlf, 2001). PLS computes the degree of covariation between the two datasets, and it has the advantage that it does not assume that one block of variables is dependent on the other (Rohlf and Corti, 2000). In order to visualize shape changes, the model closest to the mean shape was warped to match the multivariate mean using the thin plate spline method (Bookstein, 1991). Then the obtained average model was warped to represent the shape changes along the first PLS.

3.3 Results
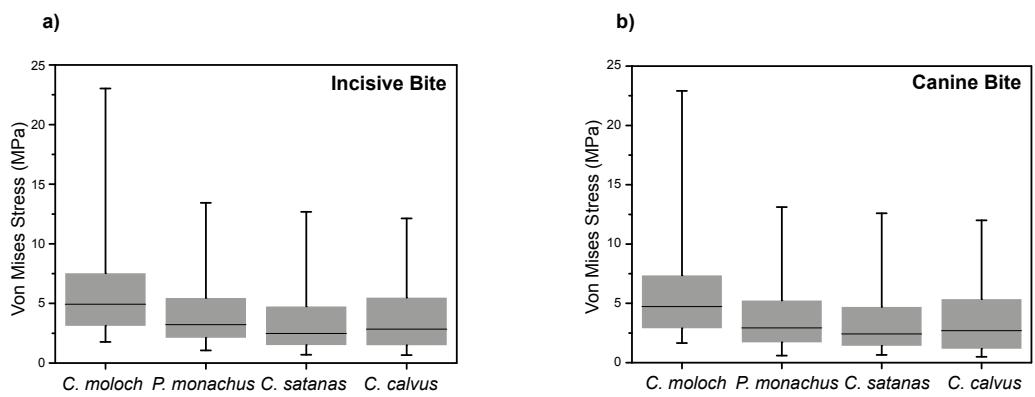
3.3.1 Finite element analysis

The visual representation of the von Mises stress distributions for each mandible is a useful proxy for qualitative comparisons regarding their biomechanical behavior because these stress patterns can be interpreted as a sign of relative strength independent of orientation (e.g. specimens exhibiting higher stress would be weaker) (Fig. 3.4). All the models in Figure 4 showed higher stresses in the ramus than in the corpus of the mandible. When comparing the different models, *Callicebus moloch* showed a greater area of higher stress, whereas *Chiropotes satanas* and *Cacajao calvus* showed lower stress, with the corpus being the area exhibiting more noticeable higher stresses.

Figure 3.5. shows the stress distribution of the QIM in boxplots. These boxplots show that the stress values in the mandible of *Callicebus moloch* exhibit a wider range, including higher stresses than the other models. The boxplots also show that *Chiropotes satanas* and *Cacajao calvus* have a more restricted range of stress values. Peak stresses were lowest in *Cacajo calvus*, although on average *Chiropotes satanas* exhibited a lower value than *Cacajao calvus*. The MWAM, the stress quartile values of the boxplots, the estimated bite forces and the MA (measured as bite force/total muscle force) can be found in Table 3. All the values were calculated for the two loading cases. MWM, the percentage error of the arithmetic mean (PEofAM) and the percentage error of the median (PEofM) used to ensure QIM are provided in the Supporting information 2 of this chapter.

Figure 3.4 von Mises stress distribution for the analyzed species under the boundary conditions defined for Incisive Bite and Canine Bite.

Figure 3.5. Box-plots of the von Mises stress values for the analyzed species for the two loading scenarios: a) Incisive Bite and b) Canine Bite.

Table 3.3 FEA results
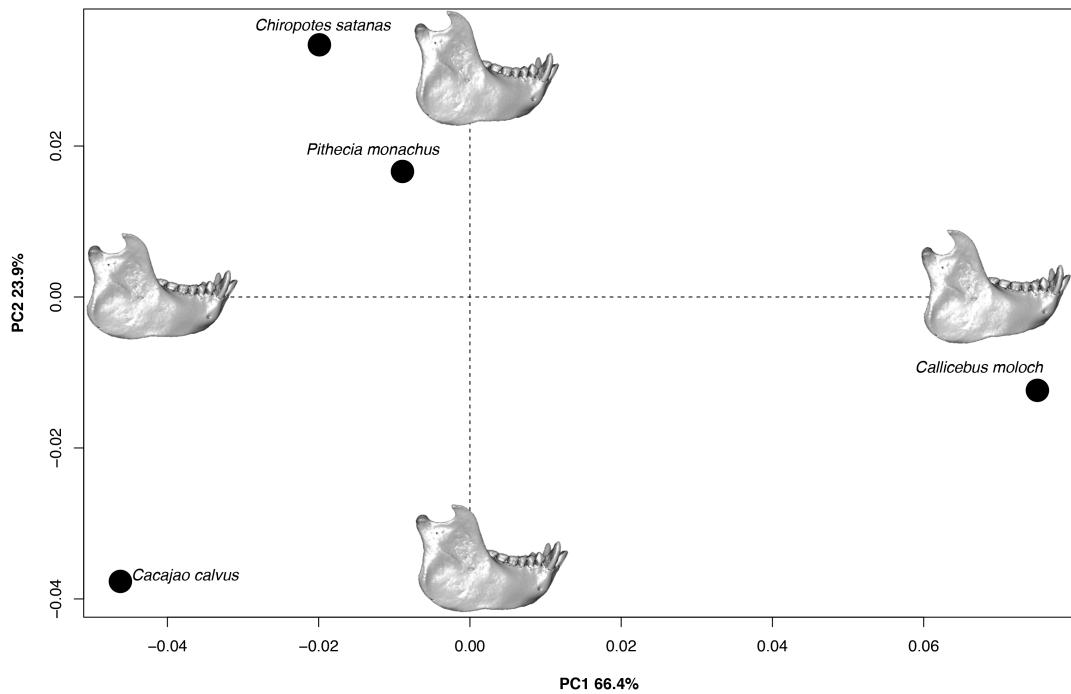
CASE 1: INCISIBE BITE

SPECIES	Elements	MWAM	M(25%)	M(50%)	M(75%)	M(95%)	Bite Force [N]	MA
Callicebus moloch	423408	7.3543	3.1165	4.9367	7.5291	23.0320	43.70	0.42
Pithecia monachus	424951	4.6569	2.1194	3.2242	5.4614	13.4340	52.17	0.46
Chiropotes satanas	200860	3.9060	1.5034	2.4837	4.7484	12.6745	65.82	0.39
Cacajao calvus	414016	4.1775	1.4877	2.8424	5.4829	12.1230	99.27	0.41

CASE 2: CANINE BITE

SPECIES	Elements	MWAM	M(25%)	M(50%)	M(75%)	M(95%)	Bite Force [N]	MA
Callicebus moloch	423375	7.1881	2.9043	4.7315	7.3541	22.9088	77.14	0.44
Pithecia monachus	424957	4.3300	1.7180	2.9363	5.2324	13.1210	103.89	0.50
Chiropotes satanas	200687	3.8387	1.4213	2.4214	4.6992	12.5952	104.62	0.40
Cacajao calvus	336121	3.9948	1.1794	2.6936	5.3559	11.9980	164.5	0.44

Key: MWAM: mesh-weighted average mean; M(25%): 25% percentile; M(50%): 50% percentile; M(75%):75% percentile;

M(95%): 95% percentile; MA: mechanical advantage.

3.3.2 Geometric morphometrics
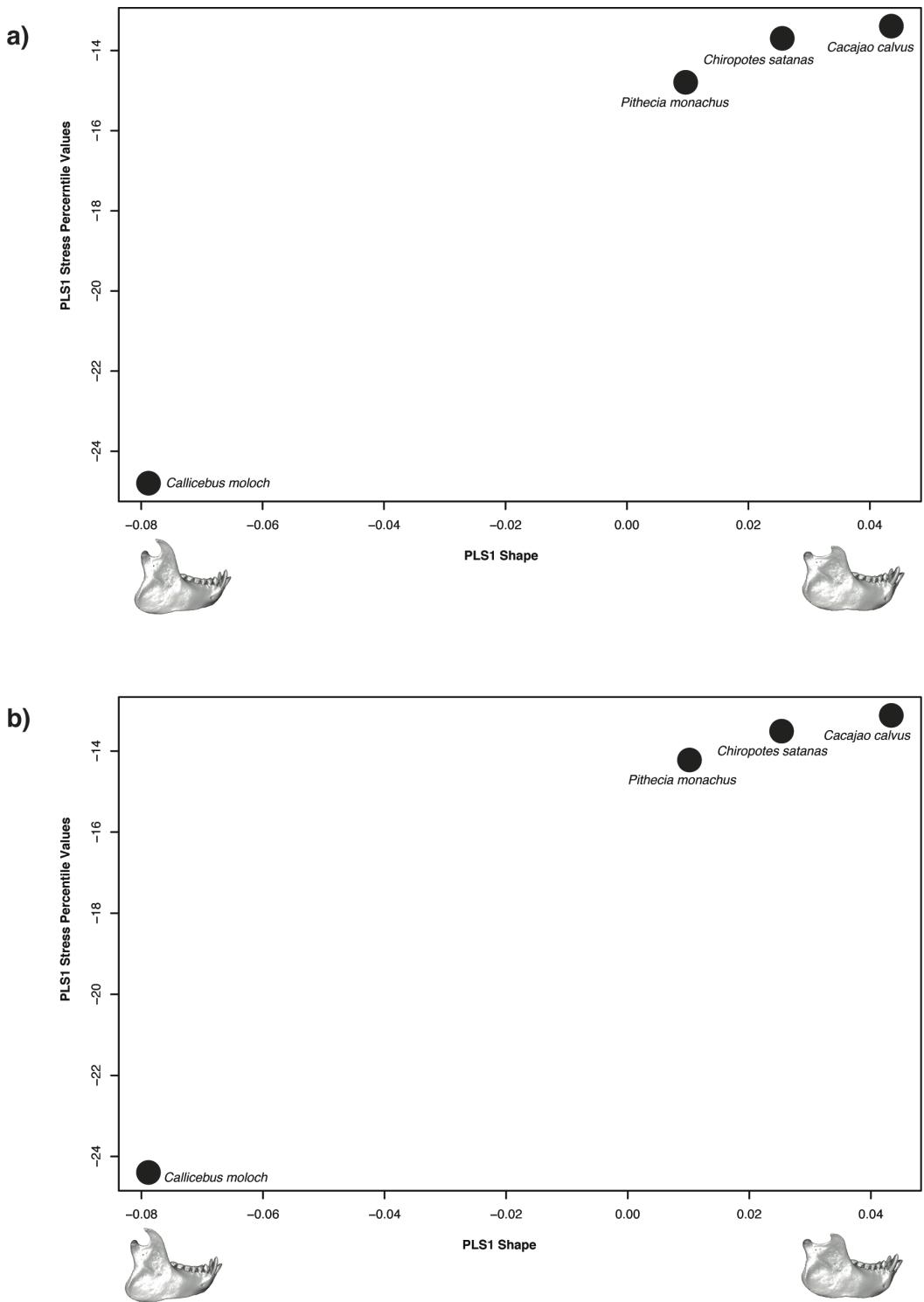
The PCA of the symmetric component shows the morphological differences between the analyzed species (Fig. 3.6). The first two PCs accounted for 90.3% of the total shape variation, thus providing a reasonable approximation of the total amount of shape variation. PC1 seems to represent the robusticty morphocline described for this platyrrhine family. The warped model on the left of the plot is characterized by less pronounced coronoid processes and a more 'robust' ramus, while on the right of the graph the warped lower jaw exhibited a more 'gracile' mandibular body and higher coronoid processes. In other words, the positive side of the axis describes more 'gracile' mandibles showing elongated mandibular corpus along with a narrower gonial angle, while the negative side shows more 'robust' mandibles exhibiting a shorten mandibular ramus and less projecting coronoid process. On the other hand, PC2 distinguishes between *Chiropotes-Pithecia* and *Callicebus-Cacajao*. The warped model on the top of the plot shows a relatively antero-posteriorly thinner mandibular ramus when compared to the model at the bottom of the graph, which is more 'robust' with a shorter and broader ramus.

Figure 3.6. Morphospace of the pitheciid mandibular variation. The first two principal components (PCs) were used to display most of the morphological variation. The mandible models were used to depict the morphological variation along the first two PC axes that accounted for ca. 90.3% of the total shape variation. The model closest to the mean shape was warped to match the multivariate mean using the thin plate spline method (Bookstein, 1991). Then the obtained average model was warped to represent the variation along the two plotted PC axes.

3.3.3 Association between mandibular shape and stress values

We found a strong and significant association between mandibular shape and percentile stress values for the incisive (r-PLS: 0.988; p-value: 0.02; RV-coefficient: 0.81; p-value: 0.043; 9,999 perm. rounds; Fig. 3.7a) and canine bite scenarios (r-PLS: 0.986; p-value: 0.026; RV-coefficient: 0.807; p-value: 0.042; 9,999 perm. rounds; Fig. 3.7b). In both analyses the first PLS axes accounted for almost all the observed covariation. Warped models are provided in Figure 3.7 to visualize the covariation between shape and stress values.

126

Figure 3.7 PLS analyses of shape and stress percentile values (M25, M50, M75, M95) for the two loading scenarios: a) Incisive Bite and b) Canine Bite. The consensus model was warped to represent the variation along PLS1.

3.4 Discussion

Regarding H1, we found that there is a gradient of relative morphological 'robusticity' represented by PC1, which accounts for 66.4% of the variance in the sample. As expected more gracile shapes (i.e. *Callicebus moloch*) are located opposite to more robust morphologies (i.e. *Cacajao calvus*). Nonetheless, PC2 distinguishes these two opposite morphologies from the other analyzed taxa (i.e. *Pithecia monachus* and *Chiropotes satanas*), which seem to be characterized by vertically elongated condyles and symphyses. In addition, we found a coherent trend with the sclerocarpy specialization gradient for the estimated bite force, increasing from *Callicebus* towards *Cacajao*. This result is consistent with H1 due to the fact that the analyzed species exhibit high dietary demands on their anterior dentition in an incremental fashion (i.e. *Callicebus–Pithecia–Chiropotes-Cacajao*). Nonetheless, bite force is associated with size; therefore caution is required when interpreting this result because *Cacajao* corresponds to the larger analyzed species. In addition, our results do not demonstrate the expected trend in mandibular strength for the analyzed species. Even though *Chiropotes* and *Cacajao* showed similar stress values, the former exhibited on average the lowest values for both loading scenarios, but not lower peak stress. The third pitheciine, *Pithecia monachus* also showed similar values, although occupying an intermediate position between these robust forms and *Callicebus moloch*, hence supporting the argument that among the analyzed taxa, this species represents the less robust member of this seed-eating clade (Kinzey, 1992; Anapol and Lee, 1994).

Although this result could be regarded as intriguing, previous studies have found similar results applying different techniques. For instance, when analyzing robusticity using shape ratios of mandibular condyle, corpus and symphysis by using a PCA, they also found that *Chiropotes* followed by *Cacajao* and then *Cebus* have the largest scores along PC1, thus suggesting these taxa have relatively robust mandibles probably due to their consumption of mechanically challenging seeds (e.g. Bouvier, 1986; Kinzey, 1992; Anapol & Lee, 1994). Additionally, they also devised a biomechanical robusticity index for platyrrhines by combining several measures of the masticatory apparatus (Norconk et al., 2009). They averaged z-scores for 10 relative measures of the masticatory apparatus associated with load bearing, dental

function and bite force production and found again that *Chiropotes* followed by *Cacajao* and then by *Cebus* exhibit the largest average scores for this masticatory apparatus index. The present results are consistent with these previous findings, showing that the strongest pitheciid mandible corresponds to *Chiropotes*, despite the fact that apparently this genus consumes fewer seeds than *Cacajao* (although some studies have reported higher seed consumption percentages for *Chiropotes*; see for instance Kinzey, 1992; Kinzey & Norconk, 1990). We found that *Chiropotes* exhibits the strongest mandible closely followed by *Cacajao*. One possible explanation about the slightly higher stresses found in *Cacajao* can be advanced by considering the results from the upper part of the boxplots. Although *Chiropotes* presents on averaged a stronger lower jaw than *Cacajao*, it is the latter which exhibits higher values of stress in the peak areas of the jaw (see for instance the 95% percentile). It must be noted that an unusually high stress appears where the boundary conditions are set as a simple support. These stresses are artificially inflated by the constraints imposed on the model due to a numerical singularity (Marcé-Nogué et al., 2015). This numerical singularity is a consequence of the applied mathematical approach, and consequently it is not related to any biological process. In those areas, stresses have the tendency to increase in value towards infinity; therefore, results of these areas should not be considered in the qualitative analysis of the mandible. To avoid this problem with the highest stresses and following the suggestions of Walmsley et al. (2013) and Marcé-Nogué et al. (2016), the analysis of the 95% percentile of the boxplot was used as the peak stress value in the jaw. If we assume the same bone properties for all the models as done here, the obtained results suggest that, in spite of being stronger on average, the application of extremely high forces during biting in *Chiropotes* would more likely result in a fracture or generate a non-comfortable stress state in some areas of the mandible, than if equivalent forces are applied in *Cacajao*.. Therefore there is some evidence for a mandibular strength trend, at least for this biomechanical aspect. Nonetheless, it is important to also notice that the differences between these two taxa are really small, so both would represent two mandibular phenotypes adjusted for sclerocarpy.

Regarding MA, our results showed an intriguing pattern that has not been previously observed, where the most sclerocarpic species show the lowest MA (i.e. Incisive bite: Callicebus moloch: 0.42, Pithecia monachus: 0.46, Chiropotes satanas:

0.39, Cacajao calvus: 0.41; Canine bite: Callicebus moloch: 0.44, Pithecia monachus: 0.50, Chiropotes satanas: 0.40, Cacajao calvus: 0.44). When comparing the MA of the platyrrhine masticatory apparatus, Norconk et al. (2009) found that among the non-callitrichines, the durophagus *Cebus* possesses the highest leverage for biting at the canines and incisors followed by *Chiropotes* and then by *Cacajao*, supporting previous observations that predominant seed feeders seem to exhibit relatively greater mechanical advantage, especially during anterior tooth use (Anapol and Lee, 1994; Wright, 2005). One possible explanation for the observed disagreement might be related to the fact that Norconk et al. (2009) used a simplified approach assuming one vertical vector for all the jaw closing muscles, while our estimation differs because it considered three separate muscles and their respective vector orientations. In addition, it is important to consider that the present paper has a reduced sample size, so future studies addressing MA should consider more individuals.

It is also important to consider that *Cacajao* might not be such a hard-fruit feeder after all (Barnett et al., 2016). A recent study has shown that *Cacajao ouakary* is not randomly biting on the surface of fruits, but that on the contrary they focused on those areas needing less force to penetrate in order to gain access to the seeds (Barnett et al., 2016). This behavior was interpreted as being an energy saving mechanism, and/or be performed to reduce the risk of damaging the teeth used in food acquisition (Barnett et al., 2016). This probably also implies that related species might show a similar behavior and that consequently pitheciine should not be simply regarded as nut-cracking primates exclusively applying brute force to break fruit's pericarps (Barnett et al., 2016). Nonetheless, it is relevant to also notice that even though they are selecting the weakest areas of the pericarp, getting access to the seeds still requires substantial force and that this behavior could be repeated several hundred times per day (Ayres, 1989).

The platyrrhine masticatory apparatus experiences significant internal loads in the mandibular condyles, corpora and symphyses during biting and mastication (e.g. Hylander, 1979a; b, 1984, 1985; Hylander et al., 1987). One possible solution to bear these loadings is to either increase in size as observed in the pitheciid lineage and/or change in shape in a certain direction that could improve load bearing ability, which

could to explain why *Chiropotes* is on average stronger in the two tested biting scenarios than the other analyzed genera. Nonetheless its position in the PCA near *Pithecia*, seems to imply that actually *Cacajao* modified its morphology towards a different region of the morphospace. *Cacajao* shows a slightly more restricted stress distribution (Fig. 4) than *Chiropotes*, thus showing more evenness in its stress distribution (i.e. both the box and the whiskers in Fig 4. are smaller). This means that the stress is more uniformly distributed in *Cacajao* as compared to *Chiropotes*, which exhibits some areas of particularly higher stress (e.g. in the ramus).

The ecological implications of these morphological differences are the subject of some speculation. The geographic ranges of *Chiropotes* and *Cacajao* are completely allopatric, excepting a possible zone of sympatry in the northern Amazon basin (Boubli, 2002). This geographic distribution might explain the broad ecomorphological similarities between these two genera, which could perhaps imply that they are too competitive to coexist in the same habitat (Ayres and Prance, 2013). As previously discussed, both uakaris and bearded sakis are highly specialized morphologically for the consumption of immature seeds (Kinzey, 1992; Rosenberger, 1992). These similarities are even more striking when considering that some studies have shown that seed consumption in bearded sakis can reach levels similar to uakaris in some observation sites. *Cacajao*'s seed consumption is about 66.9% (Norconk et al., 2009), while *Chiropotes satanas* has reported percentages of 63% (Port-Carvalho and Ferrari, 2004) or even a striking 91% (Kinzey and Norconk, 1990; Kinzey, 1992), while other species such as *Chiropotes sagulatus* have reported values of 86% (Kinzey and Norconk, 1990). This information might imply that instead of having a linear transition in sclerocarpy specialization from *Callicebus* to *Cacajao,* both *Chiropotes* and *Cacajao* might represent to two different phenotypes specialized in sclerocarpy. In brief terms, it seems that there is a relative specialization gradient in the pitheciid mandible as expected for the morphocline hypothesis but only for some aspects of shape (i.e. PC1). In addition, the support for the morphocline hypothesis regarding stress values is ambiguous depending on whether peak or mean stress is analyzed. It conclusion it seems that the proposed *Callicebus–Pithecia–Chiropotes-Cacajao* morphocline of increasingly specialized anatomical traits for sclerocarpic foraging would be rather better described as

Callicebus–Pithecia–Chiropotes/Cacajao at least for some of the traits analyzed in the present paper.

Regarding H2, we found that that mandibular shape and mandibular strength are strongly associated in spite of the reduced sample size, thus indicating the high strength of this association. This is reasonable, since the mechanical behavior of a structure depends on the combination of the geometry (i.e. shape) and the material properties of the structure itself. Other studies have found an association between cranial and mandibular shape and stress values in other groups (Pierce et al., 2008, 2009; Piras et al., 2013), which has been explained since skeletal morphology reflects to a certain degree the mechanical demands exerted during life (Barak et al., 2011; Pearson & Lieberman, 2004; Ruff et al., 2006). In the case of the mandible these demands can be interpreted as being mostly associated with food acquisition and consumption (Agrawal et al., 1998; Chew et al., 1988; Gröning et al., 2012; Hiiemae & Kay, 1972; Hiiemae, 1978; Hylander et al., 1987; O'Higgins et al., 2012; Vinyard et al., 2003). Previous studies focused on the proposed connection between mandibular form and diet in mammals have not found a straightforward link between them (e.g. Turnbull, 1970; Raia et al., 2010; Meloro & O'Higgins, 2011). A recent study that applied morphometric techniques found that in primates there is a significant but weak influence of diet on mandibular shape variation when the order Primates is analyzed altogether, but not in anthropoids and catarrhines when tested separately (Meloro et al., 2015). Nonetheless, they found that diet is an important factor in the diversification of platyrrhines, showing some of the highest values of variance explained by feeding habits. This association between morphology and diet has been also identified for the shape of the temporomandibular joint in Platyrrhini (Terhune, 2011, 2013). Although our results are limited to only one of the platyrrhine families, they can complement the evidence described above by relating mandibular morphology and the stress derived from a food acquisition behavior (i.e. sclerocarpy). In addition, the present results were not based solely on morphology, but obtained from hypothesis-driven biomechanical analyses, thus providing much clearer evidence for the mechanical interpretation of the observed shape differences. The present results are expected to contribute to a better insight regarding the ecomorphological relationship between mandibular morphology and mechanical performance among pitheciids, and platyrrhines more generally.

3.5 Acknowledgements

3.6 References

Adams, D.C., Otárola-Castillo, E., 2013. geomorph: an r package for the collection and analysis of geometric morphometric shape data. Methods in Ecology and Evolution. 4, 393–399.

Adams, D.C., Rohlf, F.J., Slice, D.E., 2013. A field comes of age: geometric morphometrics in the 21st century. Hystrix the Italian Journal of Mammalogy. 21, 7–14.

Agrawal, K.R., Lucas, P.W., Bruce, I.C., Prinz, J.F., 1998. Food properties that influence neuromuscular activity during human mastication. Journal of Dental Research. 77, 1931–1938.

Alexander, R.M., 1992. Exploring biomechanics animals in motion. New York Scientific American Library Distributed by W.H. Freeman.

Anapol, F., Lee, S., 1994. Morphological adaptation to diet in platyrrhine primates. American Journal of Physical Anthropology. 94, 239–261.

Anapol, F., Shahnoor, N., Ross, C.F., 2008. Scaling of Reduced Physiologic Cross-Sectional Area in Primate Muscles of Mastication. In: Vinyard, C., Ravosa, M.J., Wall, C. (Eds.), Primate Craniofacial Function and Biology, Developments In Primatology: Progress and Prospects. Springer US, pp. 201–216.

Arnold, C., Matthews, L.J., Nunn, C.L., 2010. The 10kTrees website: A new online resource for primate phylogeny. Evolutionary Anthropology: Issues, News, and Reviews. 19, 114–118.

Ayres, J.M., 1989. Comparative feeding ecology of the Uakari and Bearded Saki, Cacajao and Chiropotes. Journal of Human Evolution. 18, 697–716.

Ayres, J.M., Prance, G.T., 2013. On the distribution of Pitheciine monkeys and Lecythidaceae trees in Amazonia. In: Veiga, L.M., Barnett, A.A., Ferrari, S.F., Norconk, M.A. (Eds.), Evolutionary Biology and Conservation of Titis,Sakis and Uacaris, Cambridge Studies in Biological and Evolutionary Anthropology. Cambridge University Press, pp. 127-140.

Barak, M.M., Lieberman, D.E., Hublin, J.-J., 2011. A Wolff in sheep's clothing: Trabecular bone adaptation in response to changes in joint loading orientation. Bone. 49, 1141–1151.

Barnett, A.A., Bezerra, B.M., Santos, P.J.P., Spironello, W.R., Shaw, P.J.A., MacLarnon, A., Ross, C., 2016. Foraging with finesse: A hard-fruit-eating primate selects the weakest areas as bite sites. American Journal of Physical Anthropology. 160, 113–125.

Bookstein, F.L., 1991. Morphometric Tools for Landmark Data: Geometry and Biology. Cambridge University Press, Cambridge.

Boubli, J.P., 2002. Western extension of the range of bearded sakis: a possible new taxon of Chiropotes sympatric with Cacajao in the Pico da Neblina National Park, Brazil. Neotropical Primates. 10, 1–4.

Bouvier, M., 1986. Biomechanical scaling of mandibular dimensions in New World Monkeys. International Journal of Primatology. 7, 551–567.

Bright, J.A., 2014. A review of paleontological finite element models and their validity. Journal of Paleontology. 88, 760–769.

Chapman, C.A., Wrangham, R.W., Chapman, L.J., Kennard, D.K., Zanne, A.E., 1999. Fruit and flower phenology at two sites in Kibale National Park, Uganda. Journal of Tropical Ecology. 15, 189–211.

Chew, C.L., Lucas, P.W., Tay, D.K.L., Keng, S.B., Ow, R.K.K., 1988. The effect of food texture on the replication of jaw movements in mastication. Journal of Dentistry. 16, 210–214.

Conklin-Brittain, N.L., Wrangham, R.W., Hunt, K.D., 1998. Dietary Response of Chimpanzees and Cercopithecines to Seasonal Variation in Fruit

Abundance. II. Macronutrients. International Journal of Primatology. 19, 971–998.

Constantino, P.J., Lee, J.J.-W., Gerbig, Y., Hartstone-Rose, A., Talebi, M., Lawn, B.R., Lucas, P.W., 2012. The role of tooth enamel mechanical properties in primate dietary adaptation. American Journal of Physical Anthropology. 148, 171–177.

Copes, L.E., Lucas, L.M., Thostenson, J.O., Hoekstra, H.E., Boyer, D.M., 2016. A collection of non-human primate computed tomography scans housed in MorphoSource, a repository for 3D data. Scientific Data. 3.

Corti, M., Rohlf, F.J., 2001. Chromosomal speciation and phenotypic evolution in the house mouse. Biological Journal of the Linnean Society. 73, 99–112.

Davis, L.C., 1996. Functional and Phylogenetic Implications of Ankle Morphology in Goeldi's Monkey (Callimico goeldii). In: Norconk, M.A., Rosenberger, A.L., Garber, P.A. (Eds.), Adaptive Radiations of Neotropical Primates. Springer US, pp. 133–156.

Doblaré, M., García, J.M., Gómez, M.J., 2004. Modelling bone tissue fracture and healing: a review. Engineering Fracture Mechanics. 71, 1809–1840.

Dumont, E.R., 1995. Enamel Thickness and Dietary Adaptation among Extant Primates and Chiropterans. Journal of Mammalogy. 76, 1127–1136.

Dumont, E.R., Grosse, I.R., Slater, G.J., 2009. Requirements for comparing the performance of finite element models of biological structures. Journal of Theoretical Biology. 256, 96–103.

Farke, A.A., 2008. Frontal sinuses and head-butting in goats: a finite element analysis. Journal of Experimental Biology. 211, 3085–3094.

Fitton, L.C., Prôa, M., Rowland, C., Toro-Ibacache, V., O'higgins, P., 2015. The impact of simplifications on the performance of a finite element model of a Macaca fascicularis cranium. The Anatomical Record. 298, 107–121.

Fleagle, J.G., 2013. Primate Adaptation and Evolution, 3rd Revised edition edition. ed. Academic Press, Amsterdam ; Boston.

Fleagle, J.G., McGraw, W.S., 1999. Skeletal and dental morphology supports diphyletic origin of baboons and mandrills. Proceedings of the National Academy of Sciences. 96, 1157–1161.

Fortuny, J., Marcé-Nogué, J., Heiss, E., Sanchez, M., Gil, L., Galobart, À., 2015. 3D Bite Modeling and Feeding Mechanics of the Largest Living Amphibian, the Chinese Giant Salamander Andrias davidianus (Amphibia:Urodela). PLOS ONE. 10, e0121885.

Gil, L., Marcé-Nogué, J., Sánchez, M., 2015. Insights into the controversy over materials data for the comparison of biomechanical performance in vertebrates. Palaeontologia Electronica. 18.1.12A, 1–24.

Gröning, F., Fagan, M., O'higgins, P., 2012. Modeling the Human Mandible Under Masticatory Loads: Which Input Variables are Important? The Anatomical Record: Advances in Integrative Anatomy and Evolutionary Biology. 295, 853–863.

Gröning, F., Fagan, M.J., O'Higgins, P., 2011. The effects of the periodontal ligament on mandibular stiffness: a study combining finite element analysis and geometric morphometrics. Journal of Biomechanics. 44, 1304–1312.

Grueter, C.C., Li, D., Ren, B., Wei, F., Xiang, Z., van Schaik, C.P., 2009. Fallback foods of temperate-living primates: A case study on snub-nosed monkeys. American Journal of Physical Anthropology. 140, 700–715.

Hershkovitz, P., 1987. The taxonomy of south American sakis, genus Pithecia (Cebidae, Platyrrhini): A preliminary report and critical review with the description of a new species and a new subspecies. American Journal of Primatology. 12, 387–468.

Hershkovitz, P., Hershkovitz, P., 1985. A preliminary taxonomic review of the South American bearded saki monkeys genus Chiropotes (Cebidae, Platyrrhini), with the description of a new subspecies .Field Museum of Natural History, Chicago.

Hiiemae, K., Kay, R.F., 1972. Trends in the Evolution of Primate Mastication. Nature. 240, 486–487.

Hiiemae, K.M., 1978. Mammalian mastication: a review of the activity of the jaw muscles and the movements they produce in chewing. In: Butler, P.M., Joysey K.A.(Eds.). Development, function and evolution of teeth. Academic press, London. pp. 359–398.

Hylander, W.L., 1979. The functional significance of primate mandibular form. Journal of Morphology. 160, 223–239.

Hylander, W.L., 1979. Mandibular function in Galago crassicaudatus and Macaca fascicularis: an in vivo approach to stress analysis of the mandible. Journal of Morphology. 159, 253–296.

Hylander, W.L., 1984. Stress and strain in the mandibular symphysis of primates: a test of competing hypotheses. American Journal of Physical Anthropology. 64, 1–46.

Hylander, W.L., 1985. Mandibular Function and Biomechanical Stress and Scaling. American Zoologist. 25, 315–330.

Hylander, W.L., Johnson, K.R., Crompton, A.W., 1987. Loading patterns and jaw movements during mastication in Macaca fascicularis: a bone-strain, electromyographic, and cineradiographic analysis. American Journal of Physical Anthropology. 72, 287–314.

Janzen, D.H., 1971. Seed Predation by Animals. Annual Review of Ecology and Systematics. 2, 465–492.

Kay, R.F., 1984. On the use of anatomical features to infer foraging behavior in extinct primates. In: Rodman, P.S., Cant, J.G.H. (Eds.), Adaptations for Foraging in Nonhuman Primates. Columbia University Press: New York, New York, pp. 21–53.

Kay, R.F., 1990. The Platyrrhine Fossil RecordThe phyletic relationships of extant and fossil Pitheciinae (Platyrrhini, Anthropoidea). Journal of Human Evolution. 19, 175–208.

Kay, R.F., Johnson, D., Meldrum, D.J., 1998. A new pitheciin primate from the middle Miocene of Argentina. American Journal of Primatology. 45, 317–336.

Kay, R.F., Meldrum, D.J., Takai, M., 2013. Pitheciidae and other platyrrhine seed predators. In: Veiga, L.M., Barnett, A.A., Ferrari, S.F., Norconk, M.A. (Eds.), Evolutionary Biology and Conservation of Titis, Sakis and Uacaris, Cambridge Studies in Biological and Evolutionary Anthropology. Cambridge University Press, Cambridge, pp. 3-12.

Kinzey, W.G., 1992. Dietary and dental adaptations in the Pitheciinae. American Journal of Physical Anthropology. 88, 499–514.

Kinzey, W.G., Norconk, M.A., 1990. Hardness as a basis of fruit choice in two sympatric primates. American Journal of Physical Anthropology. 81, 5–15.

Kinzey, W.G., Norconk, M.A., 1993. Physical and chemical properties of fruit and seeds eaten by Pithecia and Chiropotes in Surinam and Venezuela. International Journal of Primatology. 14, 207–227.

Klingenberg, C.P., Barluenga, M., Meyer, A., 2002. Shape Analysis of Symmetric Structures: Quantifying Variation Among Individuals and Asymmetry. Evolution. 56, 1909–1920.

Koenigswald, W. v, Pfretzschner, H.U., 1987. Hunter-Schreger-Bänder im Zahnschmelz von Säugetieren (Mammalia). Zoomorphology. 106, 329–338.

Lambert, J.E., 1998. Primate digestion: Interactions among anatomy, physiology, and feeding ecology. Evolutionary Anthropology: Issues, News, and Reviews. 7, 8–20.

Lambert, J.E., Chapman, C.A., Wrangham, R.W., Conklin-Brittain, N.L., 2004. Hardness of cercopithecine foods: implications for the critical function of enamel thickness in exploiting fallback foods. American Journal of Physical Anthropology. 125, 363–368.

Ledogar, J.A., Winchester, J.M., St. Clair, E.M., Boyer, D.M., 2013. Diet and dental topography in pitheciine seed predators. American Journal of Physical Anthropology. 150, 107–121.

Marcé Nogué, J., DeMiguel, D., Fortuny Terricabras, J., Trivigno, E., Gil Espert, L., others, 2013. Quasi-homothetic transformation for comparing the mechanical performance of planar models in biological research. Palaeontologia electronica. 16, 1–15.

Marcé-Nogué, J., De Esteban-Trivigno, S., Escrig, C., Gil, L., 2016. Accounting for differences in element size and homogeneity when comparing Finite Element models: Armadillos as a case study. Palaeontologia Electronica. 19, 1–22.

Marcé-Nogué, J., Fortuny, J., Gil, L., Sánchez, M., 2015. Improving mesh generation in Finite Element Analysis for functional morphology approaches. Spanish Journal of Palaeontology. 31, 117–132.

Marinescu, R., Daegling, D.J., Rapoff, A.J., 2005. Finite-element modeling of the anthropoid mandible: the effects of altered boundary conditions. The Anatomical Record. Part A, Discoveries in Molecular, Cellular, and Evolutionary Biology. 283, 300–309.

Marshall, A.J., Boyko, C.M., Feilen, K.L., Boyko, R.H., Leighton, M., 2009. Defining fallback foods and assessing their importance in primate ecology and evolution. American Journal of Physical Anthropology. 140, 603–614.

Martin, L.B., Olejniczak, A.J., Maas, M.C., 2003. Enamel thickness and microstructure in pitheciin primates, with comments on dietary adaptations of the middle Miocene hominoid Kenyapithecus. Journal of Human Evolution. 45, 351–367.

Meldrum, D.J., Kay, R.F., 1997. Nuciruptor rubricae, a new Pitheciin seed predator from the Miocene of Colombia. American Journal of Physical Anthropology. 102, 407–427.

Meloro, C., Cáceres, N.C., Carotenuto, F., Sponchiado, J., Melo, G.L., Passaro, F., Raia, P., 2015. Chewing on the trees: Constraints and adaptation in the evolution of the primate mandible. Evolution. 69, 1690–1700.

Meloro, C., O'Higgins, P., 2011. Ecological Adaptations of Mandibular Form in Fissiped Carnivora. Journal of Mammalian Evolution. 18, 185–200.

Milton, K., 1998. Physiological Ecology of Howlers (Alouatta): Energetic and Digestive Considerations and Comparison with the Colobinae. International Journal of Primatology. 19, 513–548.

Müller, K.-H., 1996. Diet and Feeding Ecology of Masked Titis (Callicebus personatus). In: Norconk, M.A., Rosenberger, A.L., Garber, P.A. (Eds.), Adaptive Radiations of Neotropical Primates. Springer US, pp. 383–401.

Norconk, M.A., Conklin-Brittain, N.L., 2004. Variation on Frugivory: The Diet of Venezuelan White-Faced Sakis. International Journal of Primatology. 25, 1–26.

Norconk, M.A., Grafton, B.W., McGraw, W.S., 2013. Morphological and ecological adaptations to seed predation - a primate-wide perspective. In: Veiga, L.M., Barnett, A.A., Ferrari, S.F., Norconk, M.A. (Eds.), Evolutionary Biology and Conservation of Titis, Sakis and Uacaris, Cambridge Studies in Biological and Evolutionary Anthropology. Cambridge University Press, Cambridge, pp. 55-71.

Norconk, M.A., Veres, M., 2011. Physical Properties of Fruit and Seeds Ingested by Primate Seed Predators with Emphasis on Sakis and Bearded Sakis. The Anatomical Record: Advances in Integrative Anatomy and Evolutionary Biology. 294, 2092–2111.

Norconk, M.A., Wright, B.W., Conklin-Brittain, N.L., Vinyard, C.J., 2009. Mechanical and Nutritional Properties of Food as Factors in Platyrrhine Dietary Adaptations. In: Garber, P.A., Estrada, A., Bicca-Marques, J.C., Heymann, E.W., Strier, K.B. (Eds.), South American Primates, Developments in Primatology: Progress and Prospects. Springer New York, pp. 279–319.

Oftedal, O.T., Whiten, A., Southgate, D.A.T., Van Soest, P., 1991. The Nutritional Consequences of Foraging in Primates: The Relationship of Nutrient Intakes to Nutrient Requirements. Philosophical Transactions: Biological Sciences. 334, 161–170.

O'Higgins, P., 2000. The study of morphological variation in the hominid fossil record: biology, landmarks and geometry. Journal of Anatomy. 197, 103–120.

O'Higgins, P., Fitton, L.C., Phillips, R., Shi, J., Liu, J., Gröning, F., Cobb, S.N., Fagan, M.J., 2012. Virtual Functional Morphology: Novel Approaches to the Study of Craniofacial Form and Function. Evolutionary Biology. 39, 521–535.

Palacios, E., Rodríguez, A., Defler, T.R., 1997. Diet of a Group of Callicebus torquatus lugens (Humboldt, 1812) During the Annual Resource Bottleneck in Amazonian Colombia. International Journal of Primatology. 18, 503–522.

Panagiotopoulou, O., Kupczik, K., Cobb, S.N., 2011. The mechanical function of the periodontal ligament in the macaque mandible: a validation and sensitivity study using finite element analysis. Journal of Anatomy. 218, 75–86.

Pearson, O.M., Lieberman, D.E., 2004. The aging of Wolff's "law": Ontogeny and responses to mechanical loading in cortical bone. American Journal of Physical Anthropology. 125, 63–99.

Perry, J.M.G., Hartstone-Rose, A., Logan, R.L., 2011. The Jaw Adductor Resultant and Estimated Bite Force in Primates. Anatomy Research International. 2011, e929848.

Pierce, S.E., Angielczyk, K.D., Rayfield, E.J., 2008. Patterns of morphospace occupation and mechanical performance in extant crocodilian skulls: A combined geometric morphometric and finite element modeling approach. Journal of Morphology. 269, 840–864.

Pierce, S.E., Angielczyk, K.D., Rayfield, E.J., 2009. Shape and mechanics in thalattosuchian (Crocodylomorpha) skulls: implications for feeding behaviour and niche partitioning. Journal of Anatomy. 215, 555–576.

Piras, P., Maiorino, L., Teresi, L., Meloro, C., Lucci, F., Kotsakis, T., Raia, P., 2013. Bite of the Cats: Relationships between Functional Integration and Mechanical Performance as Revealed by Mandible Geometry. Systematic Biology. 62, 878–900.

Port-Carvalho, M., Ferrari, S.F., 2004. Occurrence and diet of the black bearded saki (Chiropotes satanas satanas) in the fragmented landscape of western Maranhão, Brazil. Neotropical Primates. 12, 17–21.

Raia, P., Carotenuto, F., Meloro, C., Piras, P., Pushkina, D., 2010. The Shape of Contention: Adaptation, History, and Contingency in Ungulate Mandibles. Evolution. 64, 1489–1503.

Rayfield, E.J., 2007. Finite Element Analysis and Understanding the Biomechanics and Evolution of Living and Fossil Organisms. Annual Review of Earth and Planetary Sciences. 35, 541–576.

Rensberger, J., 1993. Adaptation of enamel microstructure to differences in stress intensity in the eocene Perissodactyl hyracotherium. In: Kobayashi, I., Mutvei, H., Sahni, A. (Eds.), Structure, Formation and Evolution of Fossil Hard Tissues. Tokai University Press, Tokyo, pp. 131–145.

Rosenberger, A.L., 1992. Evolution of feeding niches in new world monkeys. American Journal of Physical Anthropology. 88, 525–562.

Rosenberger, A. L., & Tejedor, M. F. (2013). The misbegotten: long lineages, long branches and the interrelationships of Aotus, Callicebus and the saki-uacaris. In: Veiga, L.M., Barnett, A.A., Ferrari, S.F., Norconk, M.A. (Eds.), Evolutionary Biology and Conservation of Titis, Sakis and Uacaris, Cambridge Studies in Biological and Evolutionary Anthropology. Cambridge University Press, Cambridge, pp. 13-22.

Ross, C.F., Iriarte-Diaz, J., Reed, D.A., Stewart, T.A., Taylor, A.B., 2016. In vivo bone strain in the mandibular corpus of Sapajus during a range of oral food processing behaviors. Journal of Human Evolution. 98, 36–65.
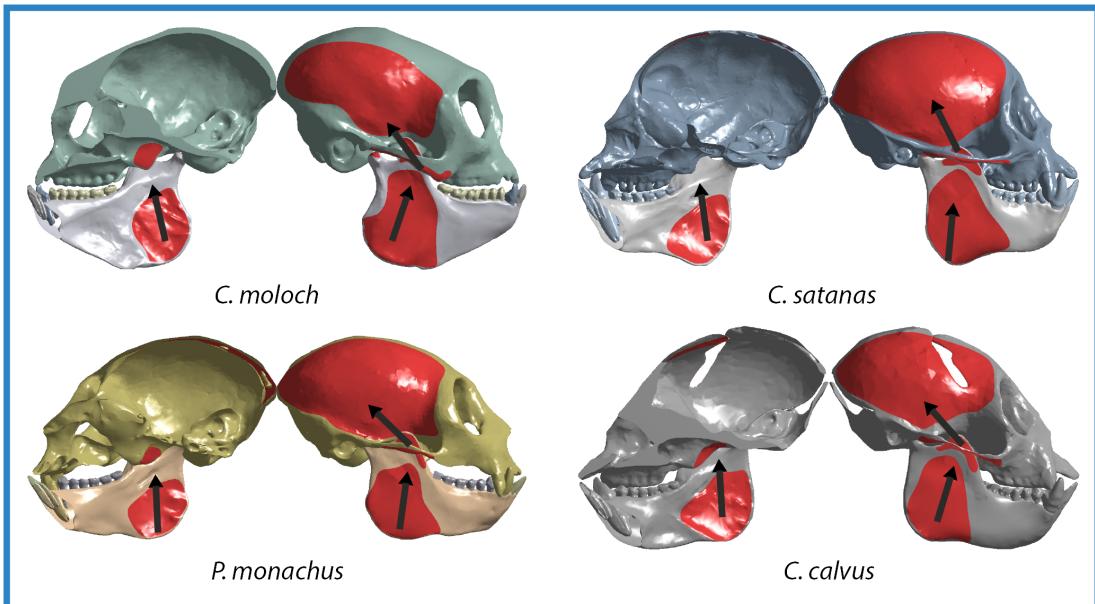
Ross, C. F., Porro, L. B., Orsbon, C., Stewart, T., Taylor, A. B., & Iriarte-Diaz, J. (2013). Finite element model of the Cebus mandible under different loading conditions. American Journal of Physical Anthropology. 150(s56.)

Ruff, C., Holt, B., Trinkaus, E., 2006. Who's afraid of the big bad Wolff?: "Wolff's law" and bone functional adaptation. American Journal of Physical Anthropology. 129, 484–498.

Sayers, K., Norconk, M.A., 2008. Himalayan Semnopithecus entellus at Langtang National Park, Nepal: Diet, Activity Patterns, and Resources. International Journal of Primatology. 29, 509–530.

Slice, D.E., 2007. Geometric Morphometrics. Annual Review of Anthropology. 36, 261–281.

Smith, R.J., Jungers, W.L., 1997. Body mass in comparative primatology. Journal of Human Evolution. 32, 523–559.

Steege, H. ter, Persaud, C.A., 1991. The phenology of Guyanese timber species: a compilation of a century of observations. Vegetatio. 95, 177–198.

Strait, D.S., Wang, Q., Dechow, P.C., Ross, C.F., Richmond, B.G., Spencer, M.A., Patel, B.A., 2005. Modeling elastic properties in finite-element analysis: How much precision is needed to produce an accurate model? The Anatomical Record Part A: Discoveries in Molecular, Cellular, and Evolutionary Biology. 283A, 275–287.

Terhune, C.E., 2011. Modeling the biomechanics of articular eminence function in anthropoid primates. Journal of Anatomy. 219, 551–564.

Terhune, C.E., 2013. Dietary correlates of temporomandibular joint morphology in the great apes. American Journal of Physical Anthropology. 150, 260–272.

Turnbull, W.D., 1970. Mammalian masticatory apparatus. Field Museum Press, Chicago.

Van Roosmalen, M.G.M., Mittermeier, R.A., Fleagle, J.G., 1988. Diet of the northern bearded saki (Chiropotes satanas chiropotes): A neotropical seed predator. American Journal of Primatology. 14, 11–35.

Vinyard, C.J., Wall, C.E., Williams, S.H., Hylander, W.L., 2003. Comparative functional analysis of skull morphology of tree-gouging primates. American Journal of Physical Anthropology. 120, 153–170.

Walmsley, C.W., Smits, P.D., Quayle, M.R., McCurry, M.R., Richards, H.S., Oldfield, C.C., Wroe, S., Clausen, P.D., McHenry, C.R., 2013. Why the Long

Face? The Mechanics of Mandibular Symphysis Proportions in Crocodiles. PLoS ONE. 8, e53873.

Wiley, D.F., Amenta, N., Alcantara, D.A., Ghost, D., Kil, Y.J., Delson, E., Harcourt-Smith, W., Rohlf, F.J., St John, K., Hamann, B., 2005. Evolutionary morphing. In: EEE Visualization, 2005. VIS 05.

Winchester, J.M., Boyer, D.M., St. Clair, E.M., Gosselin-Ildari, A.D., Cooke, S.B., Ledogar, J.A., 2014. Dental topography of platyrrhines and prosimians: Convergence and contrasts. American Journal of Physical Anthropology. 153, 29–44.

Wood, S.A., Strait, D.S., Dumont, E.R., Ross, C.F., Grosse, I.R., 2011. The effects of modeling simplifications on craniofacial finite element models: The alveoli (tooth sockets) and periodontal ligaments. Journal of Biomechanics. 44, 1831–1838.

Wright, B.W., 2005. Craniodental biomechanics and dietary toughness in the genus Cebus. Journal of Human Evolution. 48, 473–492.

Wroe, S., Ferrara, T.L., McHenry, C.R., Curnoe, D., Chamoli, U., 2010. The craniomandibular mechanics of being human. Proceedings of the Royal Society B: Biological Sciences. 277, 3579–3586.

Zelditch, M.L., Swiderski, D.L., Sheets, H.D., 2012. Geometric Morphometrics for Biologists: A Primer. Academic Press.

3.7 Supporting information

(S1) Forces directions and muscle insertion areas

(S2) Statistics used to ensure a Quasi-ideal Mesh (QIM)

Figure 3.8 The muscle insertion areas are painted in red for the masseter, temporalis and medial pterygoid muscles on the mandibles and crania of the species under analysis. The black arrows represents the muscle vector orientations used in the finite element analysis (FEA). Please notice that even though the *C. calvus* individual is missing a portion of the skull that area was also considered for all practical purposes.

3.7.2 Supporting information 2. Table 3.4 Statistics used to ensure a Quasi-ideal Mesh (QIM)

CASE 1: INCISIBE BITE			
SPECIES	MWM	PEofAM	PEofM
Callicebus moloch	4.7463	0.8217	4.0120
Pithecia monachus	3.1779	0.7572	1.4557
Chiropotes satanas	2.4395	0.8045	1.8103
Cacajao calvus	2.7807	0.6106	2.2193
CASE 2: CANINE BITE			
SPECIES	MWM	PeofAM	PeofM
Callicebus moloch	4.5570	0.8296	3.8302
Pithecia monachus	2.8832	0.8206	1.8406
Chiropotes satanas	2.3625	0.8959	2.4931
Cacajao calvus	2.6305	0.6034	2.4007

Key: MWM:mesh-weighted mean ;PEofAM: Percentage Error of the Arithmetic Mean; PEofM: Percentage Error of the Median.

CHAPTER 4

The evolution of the platyrrhine talus: A comparative analysis of the phenetic affinities of the Miocene platyrrhines with their modern relatives

The evolution of the platyrrhine talus: A comparative analysis of the phenetic affinities of the Miocene platyrrhines with their modern relatives

Thomas A. Püschel [a, *], Justin T. Gladman [b, c], René Bobe [d, e], William I. Sellers [a]

[a] School of Earth and Environmental Sciences, University of Manchester, M13 9PL, United Kingdom
[b] Department of Anthropology, The Graduate Center, CUNY, New York, NY, USA
[c] NYCEP, New York Consortium in Evolutionary Primatology, New York, NY, USA
[d] Departamento de Antropología, Universidad de Chile, Santiago, Chile
[e] Institute of Cognitive and Evolutionary Anthropology, School of Anthropology, University of Oxford, United Kingdom

A B S T R A C T

Platyrrhines are a diverse group of primates that presently occupy a broad range of tropical-equatorial environments in the Americas. However, most of the fossil platyrrhine species of the early Miocene have been found at middle and high latitudes. Although the fossil record of New World monkeys has improved considerably over the past several years, it is still difficult to trace the origin of major modern clades. One of the most commonly preserved anatomical structures of early platyrrhines is the talus. This work provides an analysis of the phenetic affinities of extant platyrrhine tali and their Miocene counterparts through geometric morphometrics and a series of phylogenetic comparative analyses. Geometric morphometrics was used to quantify talar shape affinities, while locomotor mode percentages (LMPs) were used to test if talar shape is associated with locomotion. Comparative analyses were used to test if there was convergence in talar morphology, as well as different models that could explain the evolution of talar shape and size in platyrrhines. Body mass predictions for the fossil sample were also computed using the available articular surfaces. The results showed that most analyzed fossils exhibit a generalized morphology that is similar to some 'generalist' modern species. It was found that talar shape covaries with LMPs, thus allowing the inference of locomotion from talar morphology. The results further suggest that talar shape diversification can be explained by invoking a model of shifts in adaptive peak to three optima representing a phylogenetic hypothesis in which each platyrrhine family occupied a separate adaptive peak. The analyses indicate that platyrrhine talar centroid size diversification was characterized by an early differentiation related to a multidimensional niche model. Finally, the ancestral platyrrhine condition was reconstructed as a medium-sized, generalized, arboreal, quadruped.

1. Introduction

Modern New World monkeys (NWM) occupy a diverse array of habitats, ranging from the Amazonian Basin, the semi-deciduous Atlantic Forest, to the fringes of great forests such as in the Venezuelan plains (Rylands and Mittermeier, 2009; Fleagle, 2013). The occupation of these diverse environments has been accompanied by distinct behavioral, morphological and ecological adaptations, which are broadly correlated with specific phylogenetic groups (Ford and Davis, 1992; Rosenberger, 1992; Fleagle and Reed, 1996; Fleagle et al., 1999; Rosenberger, 2002; Youlatos, 2004; Rosenberger et al., 2009). Whilst the modern day success of the group is clear, the evolutionary history of these lineages is still highly debated (Youlatos and Meldrum, 2011). Currently one of the main difficulties in platyrrhine paleontology is the scarcity of data available from the Eocene and Oligocene, because most platyrrhine fossils have been dated to the Miocene or the Pleistocene of South America and the Caribbean (Rímoli, 1977; MacPhee and Woods, 1982; MacPhee et al., 2003; Kay and Cozzuol, 2006; Tejedor et al., 2006; Fleagle et al., 2012; Perkins et al., 2012), although there are

* Corresponding author.
  E-mail address: thomas.puschel@postgrad.manchester.ac.uk (T.A. Püschel).

notable exceptions from Bolivia and Peru (Hoffstetter, 1969; Rosenberger, 1981; Wolff, 1984; Rosenberger et al., 1991; Takai and Anaya, 1996; Takai et al., 2000; Kay et al., 2002; Bond et al., 2015). Most of these fossils are composed of fragmentary dental remains, with several species, such as *Branisella boliviana* (Hoffstetter, 1969), *Mohanimico hershkovitzi* (Luchterhand et al., 1986), *Szalatavus attricuspis* (Rosenberger et al., 1991), *Solimoea acrensis* (Kay and Cozzuol, 2006), *Insulacebus toussaintiana* (Cooke et al., 2011), *Perupithecus ucayaliensis* (Bond et al., 2015), *Panamacebus transitus* (Bloch et al., 2016) and *Canaanimico amazonensis* (Marivaux et al., 2016a), being classified based on limited dental traits.

Interestingly, most of the fossil platyrrhine species of the early Miocene have been found at middle and high latitudes (i.e., central Chile and Patagonia), which are areas that are nowadays uninhabited by non-human primates (Bordas, 1942; Fleagle and Bown, 1983; Fleagle et al., 1987; Fleagle and Kay, 1989; Fleagle, 1990; Meldrum, 1990; Flynn et al., 1995; Tejedor, 2002, 2003, 2005a,b), as well as one from a tropical-equatorial area (i.e., Peruvian Amazonia) (Marivaux et al., 2012) and one from Panama (Bloch et al., 2016). Even though the NWM fossil record has improved considerably over the past several years (Tejedor, 2008; Bond et al., 2015; Kay, 2015a; Bloch et al., 2016; Marivaux et al., 2016a,b), it is still difficult to trace the origin of major modern clades (i.e., Atelidae, Pitheciidae and Cebidae), especially considering that some of the earliest fossil taxa may fall outside the crown radiation (Kay et al., 2008; Hodgson et al., 2009; Kay and Fleagle, 2010; Youlatos and Meldrum, 2011; but for a different opinion see Schrago, 2007; Rosenberger, 2010). There are two diverging positions regarding the relationship between the early platyrrhine fossils and the modern species that have been proposed: the long lineage hypothesis (LLH) and the stem platyrrhine hypothesis (SPH) (Kay et al., 2008). The LLH states that modern platyrrhines are defined by a number of long-lived clades and that most of the known fossil taxa belong to these lineages (Rosenberger et al., 2009). This position is supported by some divergence date estimates based on molecular clock data (Schneider et al., 2001; Opazo et al., 2006; Schrago, 2007). The SPH proposes that most of the early Patagonian fossil taxa are not ancestral to the modern clades (Kay et al., 2008; Kay and Fleagle, 2010). Instead they represent a sister group of all living platyrrhines that occupied niches analogous to those filled by modern NWM (Kay et al., 2008; Hodgson et al., 2009; Kay and Fleagle, 2010). Kay and Fleagle (2010) indicate that dissimilar methods can produce varying results starting from the same data and that alternate divergence times lend support to the SPH. Nonetheless, it is important to consider that a phylogenetic meta-analysis carried out by Perez and Rosenberger (2014) comparing the topologies of the 31 major neontological phylogenies concluded that major disparities are rather common among the hypotheses concerning higher level relationships of platyrrhines (e.g., the position of *Aotus*). Additionally, they also found that the correspondence among phylogenetic trees seems to depend on the type of dataset analyzed (i.e., nuclear DNA, mtDNA, Alu sequences, morphology or mixed data), which implies that the biological characteristics emphasized in different datasets intrinsically influence the likelihood of producing similar reconstructions (Perez and Rosenberger, 2014).

One of the most commonly preserved anatomical elements in the platyrrhine fossil record is the talus (Tejedor, 2008). Many Argentinian platyrrhine taxa exhibit at least one preserved talus (i.e., *Carlocebus carmenensis*, *Soriacebus ameghinorum*, *Dolichocebus gaimanensis*, *Proteropithecia neuquenensis*), while in Chile (Río Cisnes) and Peru (Madre de Dios) the post-cranial fossil record is represented by tali (Bordas, 1942; Fleagle and Bown, 1983; Fleagle et al., 1987; Fleagle and Kay, 1989; Fleagle, 1990; Meldrum, 1990; Flynn et al., 1995; Tejedor, 2002, 2003, 2005a,b; Marivaux et al., 2012). Many of the Colombian fossils from La Venta also have preserved tali (i.e., *Neosamiri fieldsi*, *Aotus dindensis*, *Cebupithecia sarmientoi*) and the Miocene Caribbean fossil of *Paralouatta marianae* is represented only by one talus (MacPhee et al., 2003). Furthermore, the talus is important because it has been suggested that its morphology could reflect postural adaptations, based on its central position in the foot as well as its functional relationship with other foot bones (Lisowski et al., 1974; Boyer et al., 2010, 2015; Yapuncich and Boyer, 2014; Yapuncich et al., 2015). The talus is the principal mechanical link between the leg and the foot, hence it is responsible for transmitting forces derived from an animal's body mass, as well as allowing mobility and providing stability during most postural and locomotor behaviors (Boyer et al., 2015). Consequently, it has been argued that the talus is a useful element for both functional and phylogenetic analyses based on its high prevalence and good preservation in the fossil record, and also because its intricate morphology coupled with a relatively straightforward functional role in the ankle joint allow postural and locomotor inferences (Gebo, 1986, 1988, 2011; Boyer and Seiffert, 2013). Even though some platyrrhine fossil tali have been analyzed using linear morphometrics (Meldrum, 1990), there is an absence of current morphometric and comparative analyses that could provide important information regarding the evolution of this anatomical structure.

In this study we analyze Miocene fossil platyrrhine talar shape and size in the context of a broad comparative sample representing all extant platyrrhine families. Modern NWM are represented by three families that are well-defined based on congruent morphological and molecular data (Aristide et al., 2015; Kay, 2015b), except for the still debated position of *Aotus*, which has been classified either as a member of the cebines, as a sister group of the callitrichines or as a pithecid (Kay, 1990; Rosenberger et al., 1990; Rosenberger, 2002; Wildman et al., 2009). These clades show remarkable adaptions to different environments, occupying very distinct habitats and climates. Consequently their ecomorphological adaptations and body sizes are variable, ranging in the modern platyrrhine clade from 100 g to more than 10,000 g (Ford and Davis, 1992). Thus, this research has four objectives. First, to examine morphological affinities, and identify the phenetic affinities between fossil and living NWM tali. Second, to analyze locomotor mode percentages to understand the relationship between locomotion and talar shape and reconstruct the ancestral locomotor condition of the NWM. Third, to undertake evolutionary modeling to test if there is morphological convergence among NWMs and model the possible evolutionary processes explaining observed diversity in talar shape and size. Fourth, to predict body mass for the fossil sample.

2. Material and methods

2.1. Sample

The comparative sample included platyrrhines from nearly every extant genus in order to capture the full morphological diversity of the extant crown group ($n = 203$; 40 species; Table 1). The fossil sample included most of the available Miocene platyrrhine tali ($n = 15$; eight species plus two specimens that have not been taxonomically assigned; Table 2). A total of 34 three-dimensional (3D) tali scans were downloaded from Morphosource (http://morphosource.org/) — an online repository of 3D scan data (Copes et al., 2016) — as ply surface models, while the rest were

Table 1
Extant sample.

Species	n	Postural behavior
Alouatta caraya	16	Clamber/suspensory
Alouatta seniculus	15	Clamber/suspensory
Aotus azarae	19	Arboreal quadrupedalism
Aotus infulatus	1	Arboreal quadrupedalism
Aotus nancymaae	2	Arboreal quadrupedalism
Aotus trivirgatus	3	Arboreal quadrupedalism
Ateles belzebul	6	Clamber/suspensory
Ateles fusciceps	3	Clamber/suspensory
Ateles geoffroyi	4	Clamber/suspensory
Ateles marginatus	2	Clamber/suspensory
Cacajao calvus	8	Arboreal quadrupedalism
Callicebus cupreus	3	Arboreal quadrupedalism
Callicebus donacophilus	5	Arboreal quadrupedalism
Callicebus moloch	4	Arboreal quadrupedalism
Callicebus personatus	1	Arboreal quadrupedalism
Callicebus torquatus	1	Arboreal quadrupedalism
Callimico goeldii	7	Leaper/clawed
Callithrix geoffroyi	2	Leaper/clawed
Callithrix jacchus	8	Leaper/clawed
Callithrix penicillata	1	Leaper/clawed
Cebuella pygmaea	5	Leaper/clawed
Cebus albifrons	10	Arboreal quadrupedalism
Cebus apella	14	Arboreal quadrupedalism
Cebus nigritus	1	Arboreal quadrupedalism
Cebus olivaceus	5	Arboreal quadrupedalism
Chiropotes satanas	4	Arboreal quadrupedalism
Lagothrix lagotricha	5	Clamber/suspensory
Leontopithecus rosalia	5	Leaper/clawed
Mico argentatus	1	Leaper/clawed
Mico humeralifer	1	Leaper/clawed
Mico melanurus	1	Leaper/clawed
Pithecia monachus	1	Arboreal quadrupedalism
Pithecia pithecia	2	Arboreal quadrupedalism
Saguinus fuscicollis	1	Leaper/clawed
Saguinus leucopus	1	Leaper/clawed
Saguinus midas	6	Leaper/clawed
Saguinus mystax	6	Leaper/clawed
Saguinus oedipus	1	Leaper/clawed
Saimiri boliviensis	16	Arboreal quadrupedalism
Saimiri sciureus	6	Arboreal quadrupedalism
Total	203	

scanned for this study (details of the sample are provided in the Supplementary Online Material [SOM] S1).

2.2. 3D surface rendering

Surface models were imported into Geomagic Studio v. 12 (Geomagic, USA). Using this software, possible errors in the polygon mesh were identified and adjusted to remove localized holes and protruding vertices. When the 3D models where particularly large, they were globally re-meshed to simplify their element geometry.

2.3. Morphological affinities
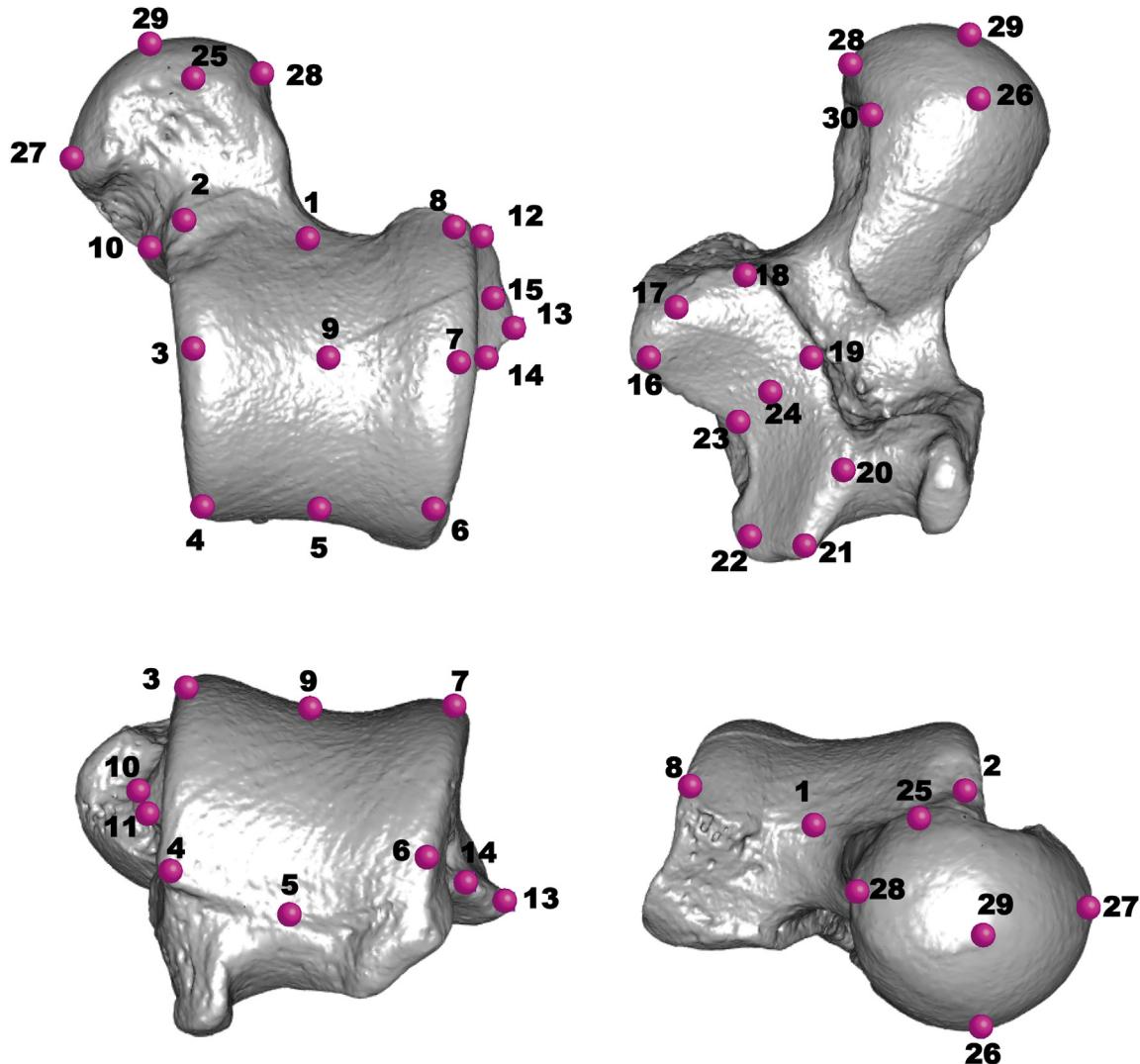
The 3D models of platyrrhine fossils and extant individuals were used to carry out geometric morphometric (GM) analyses. Most of the specimens were right tali, but some of them were reflected when necessary to provide a uniformly right-sided dataset. First, a series of 30 Cartesian coordinates were collected on the surface of the models following the homologous landmark map proposed by Turley and Frost (2013) (Fig. 1). These coordinates were collected using Landmark editor v. 3.6 (Wiley et al., 2005) and then imported into R 3.4.0 (http://www.R-project.org/) to carry out the GM analyses using the 'geomorph' package (Adams and Otárola-Castillo, 2013). A Procrustes superimposition was performed on these coordinates, to remove differences due to scale, translation and rotation, thus obtaining shape variables (Bookstein, 1997). Because some of the fossils had missing landmarks due to postdepositional damage (SOM S2), a missing data imputation procedure was performed (Gunz et al., 2009). By using the complete cases from the extant comparative sample, multivariate regression was used to estimate the location of the missing landmarks using the estimate.missing() function in 'geomorph' (Adams and Otárola-Castillo, 2013). Here each landmark with missing values was regressed on all other landmarks for the set of complete extant specimens, and the missing landmark values were then predicted by this linear regression model (Gunz et al., 2009). This procedure was carried out to avoid the problem of having different specimens with different missing landmarks. Then, the obtained shape variables were used in a principal component analysis (PCA) to establish initial morphological affinities between all extinct and extant species using the prcomp() function from the 'stats' package (R Core Team, 2017).

A canonical variates analysis (CVA) of the extant species was carried out using the shape variables and taxonomic family as a priori category to test whether talar morphology could be used to distinguish between these different taxonomical levels (Tallman and Cooke, 2016). This analysis was carried out using the CVA() function from the R package 'Morpho' (Schlager, 2017). Then, using the obtained canonical coefficients, the different fossils were defined within the taxonomical levels to establish possible similarities. Based on the work of Youlatos and Meldrum (2011), the platyrrhine species were classified according to their main locomotion mode in three categories (i.e., clamber/suspensory, leaper/clawed and arboreal quadrupedalism) (Table 1) and another CVA was performed using these categories. This CVA was initially carried out with the extant comparative sample and then, using the obtained canonical coefficients, the different fossils were defined within the proposed locomotion categories. In this way it was possible to have an initial approximation of the possible locomotor repertoires of the fossil specimens, as well as to test if talar shape could be used to distinguish different locomotor habits. The

Table 2
Fossil sample.

Fossil	Age (Ma)	Locality	Previous body mass estimates (g)	Accession number
Dolichocebus gaimanensis	~20.0	Sarmiento, Chubut, Argentina	1500	MACN 362
Carlocebus carmenensis ($n = 4$)	17.5–16.5	Pinturas, Santa Cruz, Argentina	2500	MACN 271, 304, 368, 396
Soriacebus ameghinorum	17.5–16.5	Pinturas, Santa Cruz, Argentina	1800	MACN 397
Madre de Dios	~18.75–16.5	Atalaya, Cusco, Upper Madre de Dios Basin, Peru	250–500	MUSM 2024
Río Cisnes	16.5	Alto Río Cisnes, Chile	?	SGO.PV 974
Proteropithecia neuquenensis	15.8	Collón Curá, Neuquén, Argentina	1500	MLP 91-IX-1-119
Aotus dindensis[a]	13.0–13.2	La Venta, Magdalena Valley, Colombia	1000	IGMKU 8802
Cebupithecia sarmientoi	13.5–11.8	La Venta, Magdalena Valley, Colombia	1602	UCMP 38762
Neosaimiri fieldsi ($n = 3$)[a]	12.0–13.2	La Venta, Magdalena Valley, Colombia	725	IGMKU 89030, 89031, 89199
Paralouatta marianae[a]	~17.5–18.5	Domo de Zaza, Lagunitas Formation, Cuba	?	MNHNCu 76.3059

[a] Scans obtained from casts.

Figure 1. Thirty landmarks in situ illustrated using a talus of *Chiropotes satanas* (AMNH 95760). The talus is visualized in a dorsal, plantar, anterior, and posterior view.

percentage of correct classification of the two performed CVAs was assessed via a jackknife resampling procedure.

Additionally, to visualize morphological affinities between the extant species and the fossils, a morphological affinity dendogram was generated by applying Ward's method for agglomerative-hierarchical cluster analysis, since this algorithm has been recommended for morphometric data (Hammer and Harper, 2008). Euclidean distances were used as the similarity index, and the dendrogram was computed using all the principal components (PCs) from the PCA considering the extant species and the fossils.

Additionally, all the shape changes associated with the proposed analyses were visualized, when necessary, using 3D warpings of the surface models. First one of the surface models closest to the consensus configuration was warped to match the multivariate mean using the thin plate spline method (Bookstein, 1997), then the obtained average model was warped to represent the morphological variation depending on the different analyses performed.
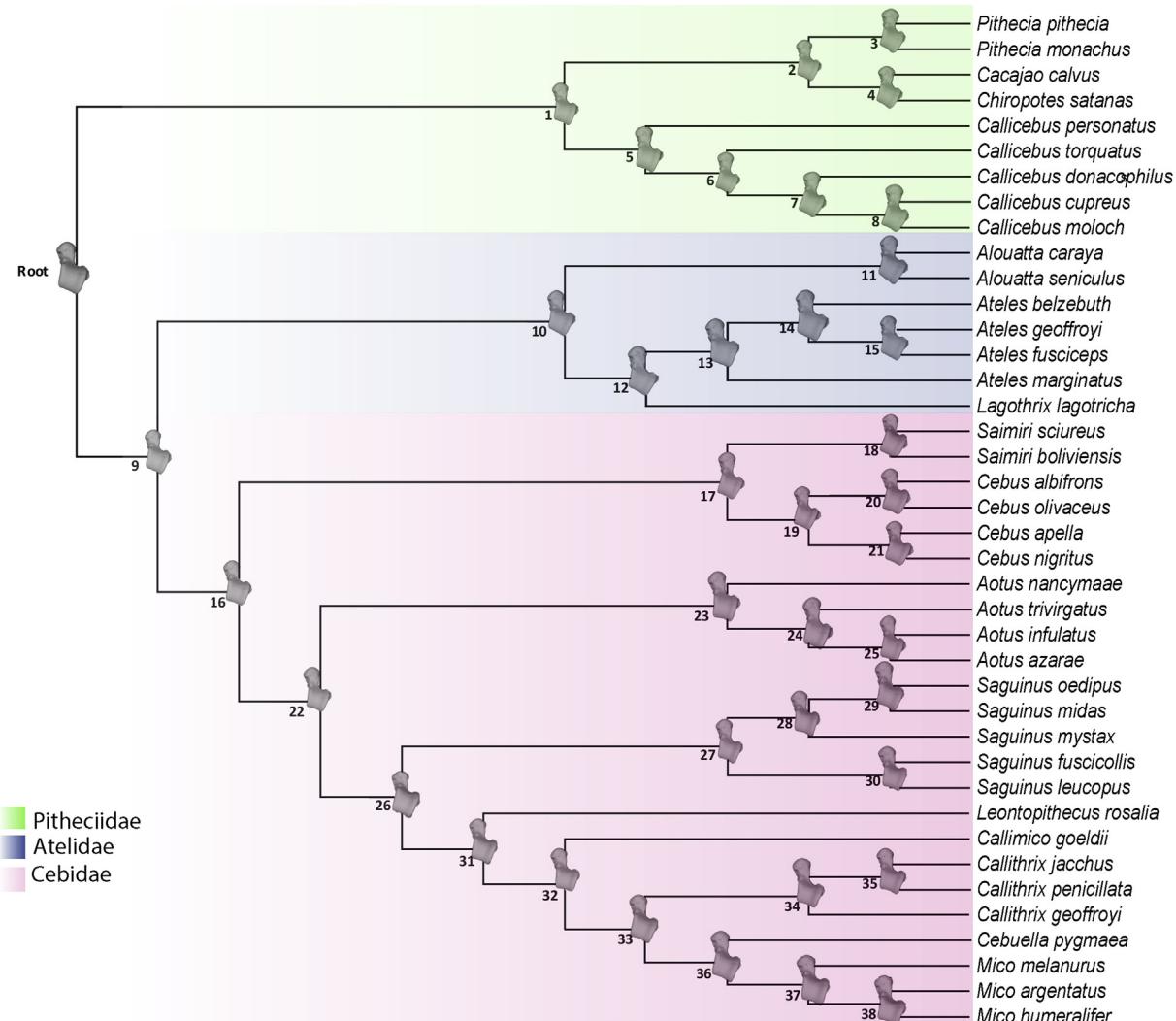
2.4. Phylogeny

An up-to-date platyrrhine phylogeny (Aristide et al., 2015) was modified slightly in Mesquite v. 3.04 (Maddison and Maddison,

2017), adjusting some species names to match those in the morphological dataset, adding some species (*Ateles marginatus*, *Aotus infulatus*, *Chiropotes satanas*, *Mico melanurus*, and *Saguinus leucopus*; Sena et al., 2002; Bonvicino et al., 2003; Araripe et al., 2008; Menezes et al., 2010; Morales-Jimenez et al., 2015) by hand and removing species for which there were no talar data. The resulting phylogeny (Fig. 2; SOM S3) was used to perform all the described comparative analyses.

2.5. Locomotor mode percentages

It was necessary to establish if there was a significant association between talar morphology and locomotion to test whether talar morphology is a good proxy for locomotion. First the locomotor mode percentages (LMPs) (i.e., the percentage time a species spends performing a certain locomotor behavior) of 31 platyrrhine species were obtained from Youlatos and Meldrum (2011). This dataset compiled several sources from different publications, and considered five different locomotor behaviors: bridge/suspensory locomotion, arboreal quadrupedal walk, clamber/vertical climb, leap/drop/hop, and clawed locomotion. A PCA of the correlation matrix of the LMPs of the species used in the present study ($n = 23$) was carried out to see if main locomotion modes could be

Figure 2. Extant platyrrhine phylogeny used in the present study. Node numbers are displayed. In the nodes, the ancestral shape reconstructions are shown, using the squared-change parsimony approach of Maddison (1991).

distinguished. The phylogenetic signal of the LMPs was estimated using a mathematical generalization of the K-statistic (Blomberg et al., 2003) appropriate for multivariate data (i.e., Kmult) (Adams, 2014). The K-statistic varies between 0 (no phylogenetic signal in the data as in a star phylogeny) to 1 (data fit a Brownian motion (BM) model of evolution) or significantly more (species are more similar than expected under BM) (Blomberg et al., 2003). Subsequently, both a standard partial least squares (PLS) and a phylogenetic PLS analysis were performed to examine the association between the LMPs and the shape variables of the species that were present in both datasets (Rohlf and Corti, 2000). The standard PLS calculates the degree of covariation between the two datasets, while the phylogenetic PLS also accounts for phylogeny under a BM model of evolution (Adams and Felice, 2014). Partial least squares has the advantage that it does not assume that one set of variables is dependent on the other, thus being a useful tool for assessing the relationship between sets of variables that might covary but for which there is no a priori directional relationship (Rohlf and Corti, 2000). These results were expected to contribute to the understanding of the relationship between talar morphology and locomotion. In addition, the first two PCs of the PCA of the LMPs were used to estimate the ancestral states for internal nodes, first using

maximum likelihood and then by interpolating the states along the branches of the tree according to Felsenstein (1985) in the R package 'phytools' (Revell, 2012, 2013). In this way, we tried to reconstruct the ancestral locomotor condition of the NWM using published locomotion data.

2.6. Evolutionary modeling

Phylogenetic signal was estimated for talar shape, centroid size and body mass using the Kmult statistic (Adams, 2014). To visualize the phylogenetic relationships in the morphospace, the phylogeny was projected onto the space identified by the first two PCs obtained from the covariance matrix of the average shapes of the analyzed taxa (Klingenberg and Gidaszewski, 2010). In addition, by using the squared-change parsimony approach of Maddison (1991) the ancestral body masses, centroid sizes and shapes (Fig. 2) for the different nodes of the phylogeny were estimated. This approach was preferred because the squared-change parsimony reconstruction has maximum posterior probability under a BM evolutionary model (Maddison, 1991). Therefore, the ancestral reconstructions represent conservative hypotheses about the possible trait values of the actual ancestors.

A multivariate phylogenetic generalized least square regression (PGLS) was used to evaluate the association between shape and some size measures (i.e., body mass and centroid size) to analyze the influence of allometry on talar shape. Even though talar centroid size and body size are highly correlated ($R^2 = 0.94$; p-value < 0.001), two separate regressions were performed using these two size measures to provide a full picture. By modeling residual variation assuming a BM evolution mode, PGLS takes into account the expected absence of independence across taxa due to phylogenetic structuration, which is expected to affect the covariance in trait values (Adams, 2014). The body mass data were gathered from the available literature (Smith and Jungers, 1997; Aristide et al., 2015). As male and female body mass are highly correlated among the living platyrrhine species, average body mass was used in the analyses (Aristide et al., 2015).

The first five PCs of the extant dataset (63.57% of explained variance) were used in the following comparative analyses based on the results obtained from a broken-stick model used to assess significance of variance (Jackson, 1993). This procedure was performed to reduce the number of variables, given that 40 taxa, each one represented by 30 3D landmarks, were analyzed.

It was tested whether talar morphology exhibited shape convergence between some of the platyrrhine groups by using the SURFACE method implemented as the runSurface() function from the R package 'surface' (Ingram and Mahler, 2013). This method fits a model of adaptive radiation in which lineages might experience shifts to adaptive peaks on a macro-evolutionary landscape without reference to a priori hypotheses specifying which lineages correspond to particular peaks (Mahler et al., 2013). Starting with an Ornstein-Uhlenbeck (OU) model in which all species are attracted to a single adaptive peak in trait space (Butler and King, 2004), SURFACE uses a stepwise model selection process based on the finite-samples Akaike information criterion (AICc) to fit increasingly complex multi-peak models (Mahler et al., 2013). In the 'forward phase' a new peak shift is added to the branch of the phylogeny that most improves model fit across all traits, and shifts are added until none results in further improvement (i.e., ΔAICc < 2) (Ingram and Mahler, 2013). Then in the 'backward phase' the method assesses whether the AICc score is improved further by collapsing regimes in different branches to shift toward shared adaptive peaks rather than requiring each to occupy a unique peak, to identify possible convergence (Mahler et al., 2013). This 'backward phase' proceeds step by step until no further improvement is achieved. The SURFACE method can thus survey several hundred OU models, obtaining a model with the highest absolute statistical support among those explored. Importantly, convergence is understood here as described by Ingram and Mahler (2013) as evolution towards the same adaptive peak, therefore distinguishing between convergence occurring as a result of deterministic adaptation to specific ecological conditions and convergence occurring by chance under simple random-walk processes (Stayton, 2015). SURFACE does not consider the evolutionary correlations among variables, thus being unable to fit data in a multivariate way, therefore the model found by SURFACE was translated into the 'mvMORPH' package and tested along diverse alternative hypotheses in order to test if the SURFACE model was also the best adaptive explanation for the evolution of talar shape.

It has been suggested that the talus has been shaped through habitat utilization within specific contexts − both locomotor and ecological − therefore being associated with the adaptive radiation suggested for platyrrhine evolution (Youlatos and Meldrum, 2011). Using the platyrrhine phylogeny and talar shape and size data a series of evolutionary models were tested for congruence with the actual morphological data (Freckleton et al., 2003). Model selection

analyses were performed with the 'mvMORPH' package for R (Clavel et al., 2015), which allowed fitting several evolutionary models to trait data and a phylogeny in a multivariate framework. For each model, the relative fit was assessed using the AICc (Burnham and Anderson, 2013). Several models were assessed, with BM as the simplest, while more complex models included early burst (EB) (Harmon et al., 2010) as well as several adaptive OU models (Butler and King, 2004). Under BM, trait evolution is simulated as a random walk through trait space, and phenotypic difference between sister taxa is expected to grow proportional to the sum of branch lengths between them (Wilson et al., 2015). Support for a BM model suggests that morphological disparity is uniformly increasing over time. In the EB model, the rates of Brownian evolution decays exponentially with time, thus representing niche-filling scenarios (Harmon et al., 2010). Support for the EB model suggests that most of the morphological disparity present in extant NWM was partitioned early in their evolutionary history and therefore provides weight to the LLH (Harmon et al., 2010). The OU model describes trait evolution under stabilizing selection, whereby there is attraction to a selective optimum; the strength of attraction to this selective optimum (i.e., the strength of selection) is measured using the α parameter (Butler and King, 2004). Several OU models were constructed (SOM S4) to test if adaptive evolution could explain talar shape diversification. Each one of the proposed models represents an alternative biological hypothesis regarding the possible factors that might have influenced the adaptive landscape for platyrrhines. These models were based on different adaptive evolution hypotheses and ecological niches suggested for platyrrhine species (Rosenberger, 1992; Norconk et al., 2009; Youlatos and Meldrum, 2011; Allen and Kay, 2012; Aristide et al., 2015, 2016). Many of the analyzed models were derived and adapted from the work of Aristide et al. (2015, 2016), however due to the fact that these models were generated to analyze different traits (i.e., brain shape and body mass), only those that were more general were applied, while others were not considered. In addition, other models specifically designed for talar morphology were generated.

The first multi-peak model contained three separate optima that corresponded to the three platyrrhine families (OU-Clade), while the second was based on data concerning diet composition (OU-Diet Composition) and also had three optima (i.e., average annual percentages of plant parts and insects in the diets of platyrrhine genera) (Norconk et al., 2009). This diet model was considered because access to different diets requires differences in both locomotion and postural repertoire (Rosenberger, 1992). The third (OU-Locomotion A) was defined according to main locomotion categories and had three optima (clamber/suspensory, leaper/clawed and arboreal-quadrupedalism) (Youlatos and Meldrum, 2011). Another locomotor model (OU-Locomotion B) similar to the previous one was tested, however in this one, only *Callimico, Callithrix* and *Cebuella* were considered within the leaper/clawed category, while the rest of the callitrichines were classified as arboreal quadrupeds based on the fact that they exhibited higher percentages of arboreal quadrupedal walking (Youlatos and Meldrum, 2011). Additionally a third locomotor model (OU-Locomotion C) was designed by combining the OU-Locomotion A and the convergence result obtained from the SURFACE method; this model had four optima representing the three locomotor categories already mentioned, as well as one adaptive peak representing the convergence result found by SURFACE.

Following Aristide et al. (2015, 2016) a multidimensional niche model was defined (OU-Multidimensional Niche) with five optima that combined diet and locomotion information (Rosenberger, 1992). Two other models were generated based on the main

canopy level occupied by the different species analyzed. The first one (OU-Canopy A) had three different optima (understory, middle and upper), while the second (OU-Canopy B) had four optima, which were the same as the three previous ones, but included an additional optimum for *Aotus*, which has been observed occupying all canopy levels with relative frequency (Fleagle, 2013). The canopy level classifications were performed using the data available in the Animal Diversity Web (ADW) of the University of Michigan (http://animaldiversity.org/) and Fleagle (2013). Different canopy levels are differentially structured, thus requiring different locomotor behaviors, therefore it was expected that these differences might impact on talar morphology.

It is relevant to bear in mind that these different evolutionary models are generated to help in the understanding of possible underlying evolutionary processes, but they do not necessarily represent complete explanations (i.e., model selection is not an end in itself but a helpful approach in contributing to reasoning about the evolutionary mechanisms that might explain the observed variation in the analyzed traits) (Cressler et al., 2015). The different OU models based on different biological criteria were tested and their relative fit was assessed using AICc scores. In this manner, a measure of the relative explanatory power of each hypothesis (ΔAICc) was obtained. In addition to the OU models based on biological criteria, a single-peak OU model was also tested (if supported, that would suggest that there is a single, optimal talar shape for all of the platyrrhines), as well as a model representing the result obtained from the SURFACE method.
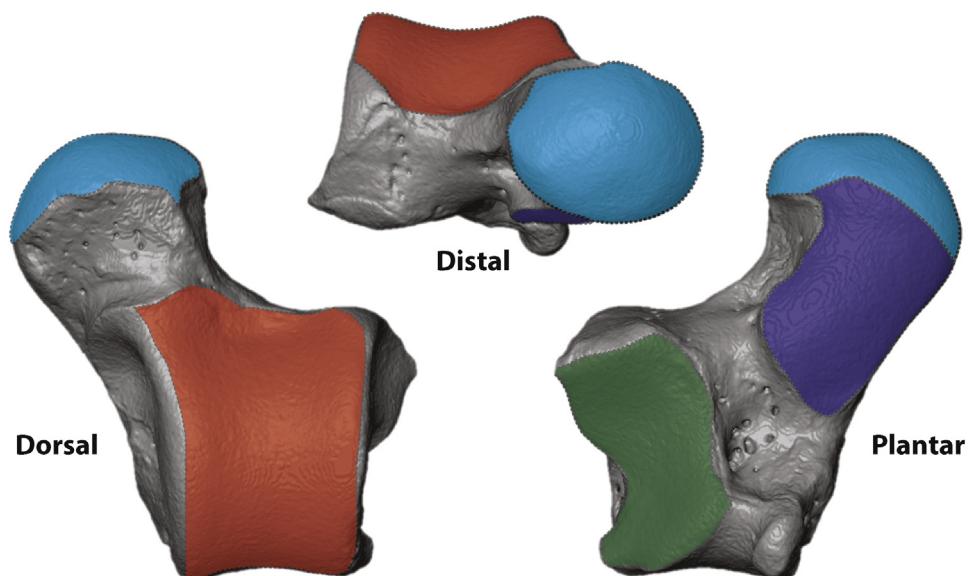
A mean relative disparity-through-time (DTT) plot of the temporal pattern of change in relative talar shape disparity along the platyrrhine phylogeny was calculated using the first five PCs obtained from the shape PCA and also for centroid size (Harmon et al., 2003). Disparity was measured as $D = \sum (d_i)/n - 1$ where d_i is the pairwise Euclidean distance between species and n is the number of species. First, disparity was calculated for the entire platyrrhine clade, and then for each sub-clade. Disparity of each sub-clade was standardized by dividing it by the disparity of the entire clade (relative disparity sensu Harmon et al., 2003). Such analyses allow comparison of the observed pattern of intra-clade versus among-clade disparity through time with a BM expectation. Therefore,

high relative disparity values are a sign of extensive within-clade diversification and among-clade overlap, whereas values near 0 might imply that variation is mostly partitioned among clades (Harmon et al., 2003). The 'geiger' package for R (Harmon et al., 2008) was used to generate DTT plots.

2.7. Body mass

Due to the lack of body mass predictions for the Río Cisnes talus and for *P. marianae*, as well as the absence of robust mass predictions for some of the other fossils, it was decided to include calculation of this relevant biological information for the fossil sample under study. The predicted masses of the fossil taxa were derived from surface area measurements of the talar articular facets taken directly from 3D digital models. Articular surfaces of the talus have proven to be reliable and accurate predictors of body mass across primates, and using 3D surface areas taken directly from digitized models of the fossil has yielded precise and accurate results (Lieberman et al., 2001; Yapuncich et al., 2015). Mass regressions were based on a sample of 123 individual platyrrhine tali from across 15 genera (SOM S5) that were MicroCT scanned at the Shared Materials Instrumentation Facility (SMIF) at Duke University or the Microscopy and Imaging Facility (MIF) at the American Museum of Natural History. The creation of 3D surface models, the measurement of facet surface areas, and the construction of new mass predictive equations follows methods set out in Yapuncich et al. (2015).

Facet measurements from all 123 individuals were reduced to 40 species-dimorphic average data points; male and female individuals of the same species were all averaged into a single data point unless reported dimorphism levels were above 20%. Taxa with dimorphism levels above this threshold were treated as separate male and female data points for that species. All published body mass data for the dimorphism cutoffs and for the creation of the mass regressions was taken from Smith and Jungers (1997). Body mass data from the literature were regressed onto the averaged facet surface area data to generate four independent body mass estimates from articular surfaces of the talus: the ectal (or posterior calcaneal) facet, navicular facet, sustentacular facet,

Figure 3. Facet measurements for the talus in dorsal, distal, and plantar orientations. Articular surface areas were measured for the ectal (green), trochlear (red), navicular (light blue) and sustentacular facets (dark blue). Talus measurements shown on *Callimico goeldii* (USNM 395455). (For interpretation of the references to color in this figure legend, the reader is referred to the web version of this article.)

and trochlear (lateral tibial) facet (Fig. 3). Unlike in the sample of extant tali, the fossil sample did not consistently have all four facets pristinely represented for every individual so an average mass derived from estimates of all intact facets was used for the body mass prediction.

3. Results
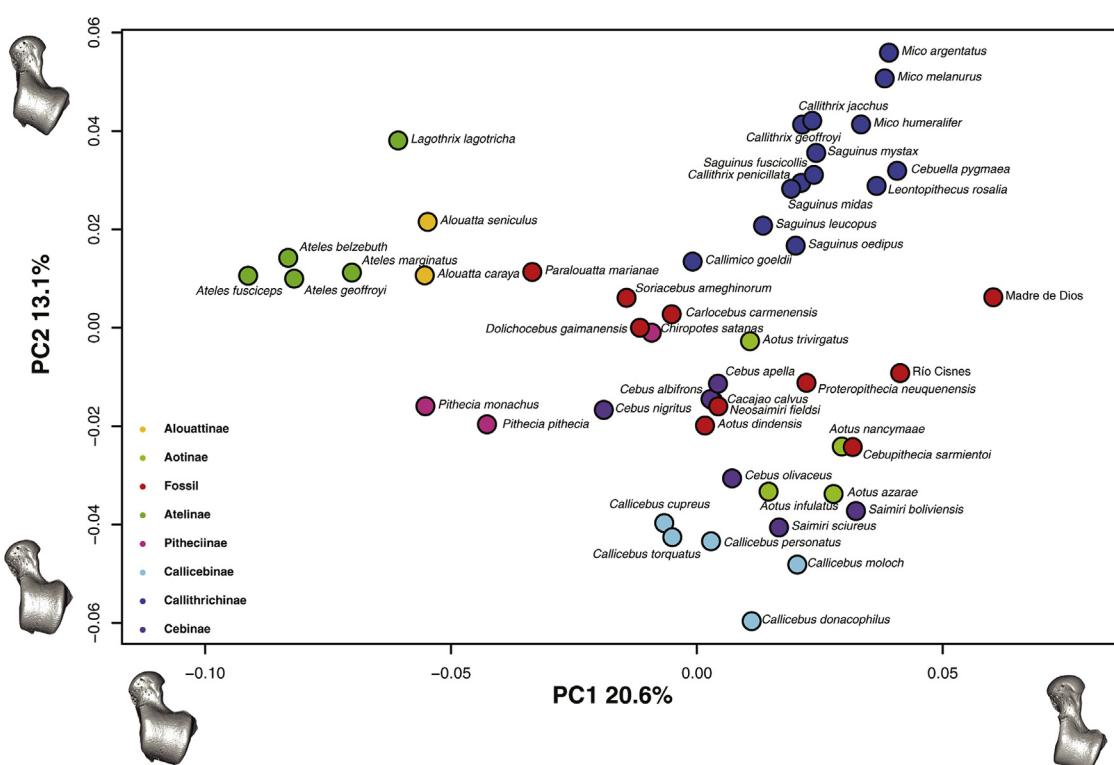
3.1. Morphological affinities

The PCA shows three major regions of occupied shape space (Fig. 4), which tend to correspond to the previously described locomotor categories. Principal component 1 mostly distinguished between the small-bodied Callitrichinae, exhibiting claw-assisted scansorial and clinging positional behaviors towards one extreme of the axis, and the large-bodied Atelidae, exhibiting climbing/clambering and suspensory behaviors with tail-assisted suspension toward the other extreme (Youlatos and Meldrum, 2011). The more derived locomotor behaviors described above were separated from increasingly quadrupedal species on PC2. There was a central cluster of more 'generalist' species, which are predominately quadrupedal although they engage in other locomotor behaviors, such as *Chiropotes* and *Cebus*, while the negative extreme of PC2 was occupied by the most quadrupedal species (i.e., *Saimiri* and *Callicebus*). The Pitheciinae, which are located at the center of the plot, are divided between the most quadrupedal species (i.e., *Cacajao* and *Chiropotes*) from those that exhibit more suspensory behaviors (i.e., *Pithecia*), which are located almost at the same position as *Alouatta* along PC1. Interestingly, some *Cebus* species and the Pitheciinae subfamily exhibit the most 'generalist' talar morphology. The variation on the negative side of PC1 can be associated with a longer posterior and shorter anterior calcaneal facet, a broader talar head, a lower trochlea, and increased trochlear wedging. These traits have been linked with greater mobility of the subtalar and transverse talar joints, along with a greater range of flexion-extension at the upper ankle joint (Meldrum, 1990). The morphological variation on the positive side of PC1 is related to a relatively increased anterior calcaneal facet and relatively shorter trochlea antero-posteriorly with more parallel lateral and medial rims. These features have been associated with frequent leaping as observed in some callitrichines (Meldrum, 1990). In contrast, PC2 mostly differentiates between decreased dorso-lateral articular surfaces on the positive side of the axis and those showing increased dorso-lateral articular surfaces on the negative side.

Most of the fossil sample is located at the center of the PCA, in an area of the morphospace mostly occupied by locomotor 'generalist' species. Only one fossil specimen, the Madre de Dios talus, occupies an area on an extreme of the plot. The oldest Patagonian fossils (*Dolichocebus, Soriacebus* and *Carlocebus*) are located near the center of the PCA, while *A. dindensis* and *N. fieldsi* are located among *Cebus* and *Cacajao*. Río Cisnes and Madre de Dios are located in zones of the morphospace that are not shared with any extant species under analysis. Although on PC2 these specimens are located in the 'generalist' area of the morphospace, on PC1 they are unique. *Proteropithecia* occupies a position between the cebids and Río Cisnes, whilst *Paralouatta* occupies a position near *Alouatta*.

The two CVAs showed clear and significant differentiation both among the platyrrhine families and according to locomotion (Table 3 and Fig. 5a and 5b). Consequently, it seems that talar morphology is a good descriptor of taxonomic affiliation at least at the family level, and that its shape reflects different locomotor behaviors. When classified according to the extant platyrrhine families, most of the fossils were classified as members of Cebidae or in some cases as belonging to Pitheciidae. These results are

Figure 4. Principal component analysis (PCA) of the talar shape variables (only the two first PCs are shown) including both the extant and fossil samples. One of the models closest to the mean shape was warped to match the multivariate mean using the thin plate spline method. The obtained average model was then warped to represent the variation along the two plotted PC axes in both analyses. Note that *Cacajao calvus* is not miscolored, but *Cebus albifrons* exactly overlays it.

Table 3
Canonical variate analyses results.

a) Extant sample

Extant sample classification:	% Correctly classified (jacknifed)		
	Family	Locomotion	
	95.57%	98.03%	

Mahalanobis distances among taxonomic families and *p*-values (above the diagonal)	Atelidae	Cebidae	Pitheciidae
Atelidae	0	*p* < 0.0001	*p* < 0.0001
Cebidae	11.4336	0	*p* < 0.0001
Pitheciidae	11.1636	5.9898	0

Mahalanobis distances among locomotor categories and *p*-values (above the diagonal)	Leaper/clawed	Clamber/suspensory	Arboreal quadrupedalism
Leaper/clawed	0	*p* < 0.0001	*p* < 0.0001
Clamber/suspensory	12.3204	0	*p* < 0.0001
Arboreal quadrupedalism	7.9371	11.1666	0

b) Fossil sample

	Obtained classification	Posterior probabilities		
	Family	Atelidae	Cebidae	Pitheciidae
Dolichocebus gaimanensis	Cebidae	0.00000006	0.99999994	0.00000000
Madre de Dios	Cebidae	0.00000000	0.99999999	0.00000001
Río Cisnes	Cebidae	0.00000000	0.99994768	0.00005232
Cebupithecia sarmientoi	Cebidae	0.00000000	0.99999257	0.00000743
Carlocebus carmenensis	Cebidae	0.00000000	0.99999257	0.00000000
Soriacebus ameghinorum	Pitheciidae	0.00000000	0.03667571	0.96332429
Proteropithecia neuquenensis	Cebidae	0.00000000	0.72229885	0.27770115
Neosaimiri fieldsi	Cebidae	0.00000000	0.99999257	0.00000000
Aotus dindensis	Pitheciidae	0.00000000	0.03768954	0.96231046
Paralouatta marianae	Cebidae	0.00000000	0.99999999	0.00000001

	Locomotion	Leaper/clawed	Clamber/suspensory	Arboreal quadrupedalism
Dolichocebus gaimanensis	Arboreal quadrupedalism	0.062085723	0.024260237	0.913654040
Madre de Dios	Leaper/clawed	0.999883487	0.000000000	0.000116513
Río Cisnes	Arboreal quadrupedalism	0.000000003	0.000000000	0.999999997
Cebupithecia sarmientoi	Arboreal quadrupedalism	0.000000034	0.000000000	0.999999966
Carlocebus carmenensis	Arboreal quadrupedalism	0.000000010	0.000000000	0.999999990
Soriacebus ameghinorum	Arboreal quadrupedalism	0.000000013	0.000000000	0.999999987
Proteropithecia neuquenensis	Arboreal quadrupedalism	0.000000084	0.000000000	0.999999916
Neosaimiri fieldsi	Arboreal quadrupedalism	0.002491686	0.000002963	0.997505351
Aotus dindensis	Arboreal quadrupedalism	0.000000153	0.000000000	0.999999847
Paralouatta marianae	Arboreal quadrupedalism	0.004193355	0.000000000	0.995806645
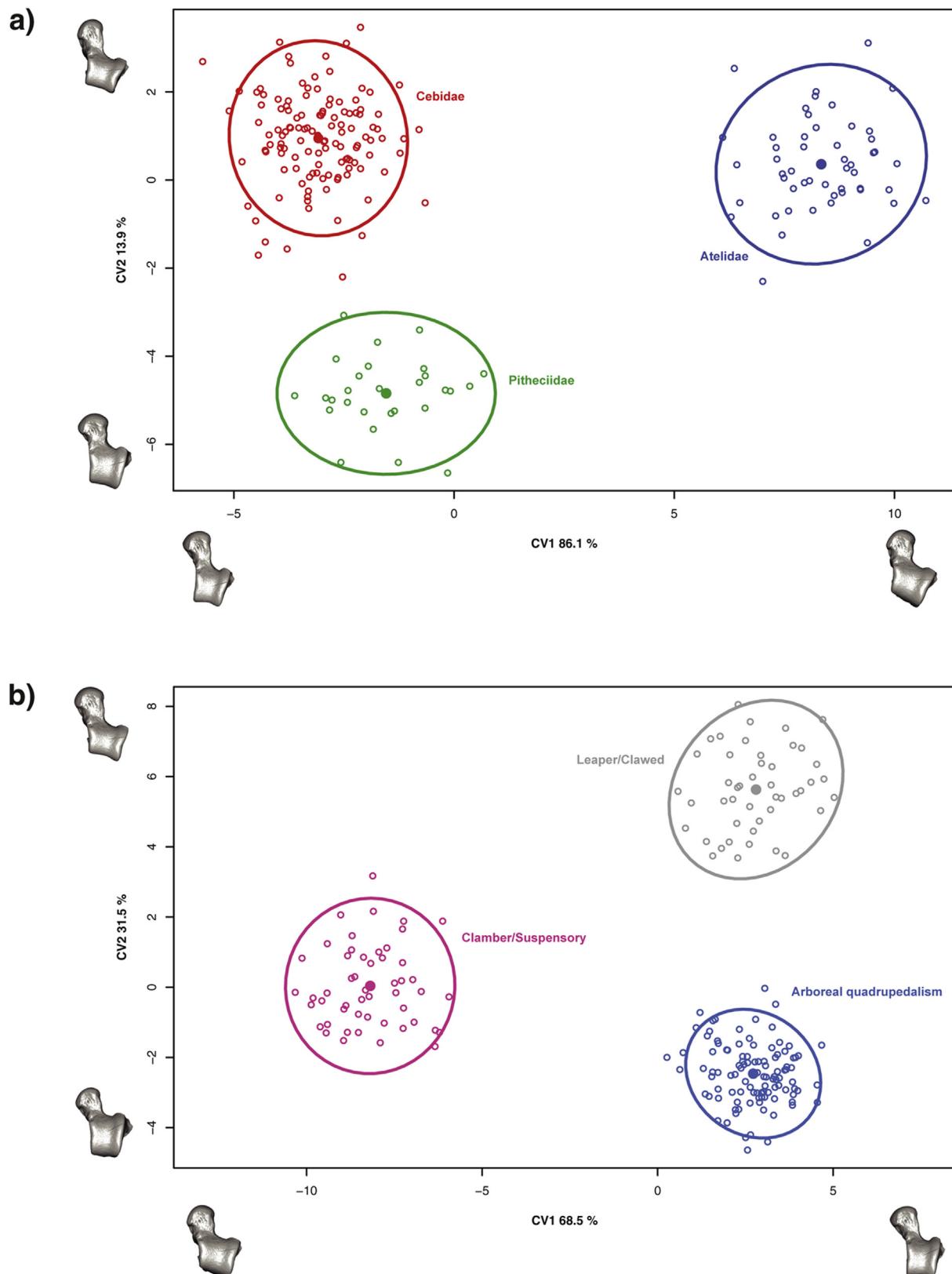
consistent with the PCA that indicated most fossils tend to show an intermediate morphology, most similar to the Pitheciinae and Cebinae subfamilies. This morphology could be interpreted as potentially primitive for platyrrhines. In morphological terms, the shape changes associated with CV1 are a broader and lower trochlear surface with a shorter talar neck on the positive side of the axis, while the negative side is related to a narrower, higher and saddle-shaped trochlea, along with a longer talar neck. A more wedge shaped trochlea lies on the positive side of CV2, while the negative side shows a narrower and higher trochlear surface. The CVA using locomotor categories classified most fossils as arboreal quadrupeds, with only Madre de Dios being classified differently, as leaper/clawed. The morphological changes are broadly similar to the ones described above for the family CVA, especially for CV1, but with the axes inverted.

The agglomerative-hierarchical cluster analysis of the PCs using Ward's method showed the morphological affinities between extant species and the fossils (Fig. 6). Three main clusters are easily noticeable, one comprising the most suspensory species (i.e., the Atelidae and *Pithecia*), another consisting of most of the Callithrichinae (excepting *Callimico* and *S. leucopus*), and another one containing all the fossil specimens and mostly arboreal quadrupedal and locomotor 'generalist' species (e.g., *Saimiri*, *Callicebus*, *Aotus* and *Cebus*). This analysis revealed that most fossils are relatively similar, clustering in certain groups within this locomotor 'generalist' and arboreal quadrupedal cluster. For instance,
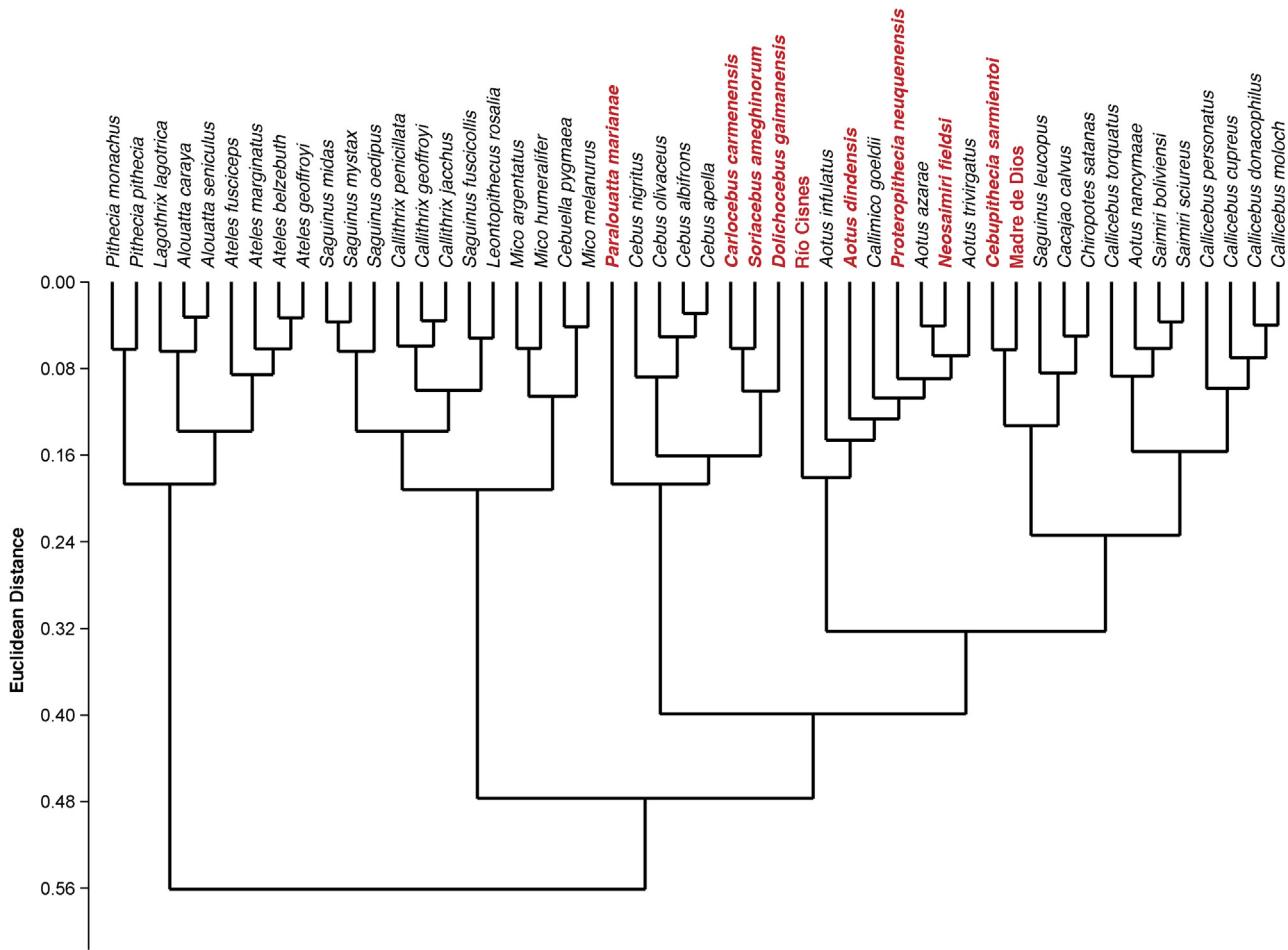
C. carmenensis, *Soriacebus* and *Dolichocebus* clustered together with *Cebus* and *Paralouatta*. *N. fieldsi*, *A. dindensis*, *P. neuquenensis* and Río Cisnes clustered within a group comprising *Callimico* and most of *Aotus*, whilst *Cebupithecia* clustered together with Madre de Dios in a group consisting of *S. leucopus*, *Cacajao*, *Chiropotes*, *Callicebus* and *Saimiri*.

3.2. Locomotor mode percentages

Locomotor mode percentages showed a significant phylogenetic signal (Kmult: 0.54; *p*-value: 1e-04; 10,000 permutations). In a similar fashion to the shape PCA, the PCA of the LMPs showed a clear distinction along PC1 between the suspensory species (i.e., atelids) and those exhibiting leaping and vertical clinging (i.e., callitrichines). Principal component 2 distinguished mainly the most quadrupedal species (i.e., *Callicebus* and *Saimiri*) from species with other locomotor behaviors (Fig. 7a). At the center of the plot there is an overlap of 'generalist' quadrupedal species that also exhibit other locomotor behaviors, although less frequently. Interestingly, *Pithecia pithecia* is located next to Callitrichinae due to its frequent leaping behaviors (Walker, 2005), in contrast to the talar shape PCA where it is located relatively near suspensory species on PC1. The LMPs also showed a strong and significant covariation with talar shape (r-PLS: 0.84; *p*-value: 0.0022; 10,000 permutations), as well as when accounting for the phylogenetic structure of the data (phylogenetic r-PLS: 0.87; *p*-value: 0.0014; 10,000

Figure 5. Canonical variate analyses (CVA) of talar shape using a) taxonomic family categories and b) locomotor classifications. The circles represent 90% confidence intervals, while the filled dots correspond to the group means. One of the models closest to the mean shape was warped to match the multivariate mean using the thin plate spline method, then the obtained average model was warped to represent the variation along the two plotted CV axes in both analyses.

Figure 6. Hierarchical clustering analysis of shape PCs using Ward's method. Fossils are in bold and red, while extant species are in black. (For interpretation of the references to color in this figure legend, the reader is referred to the web version of this article.)
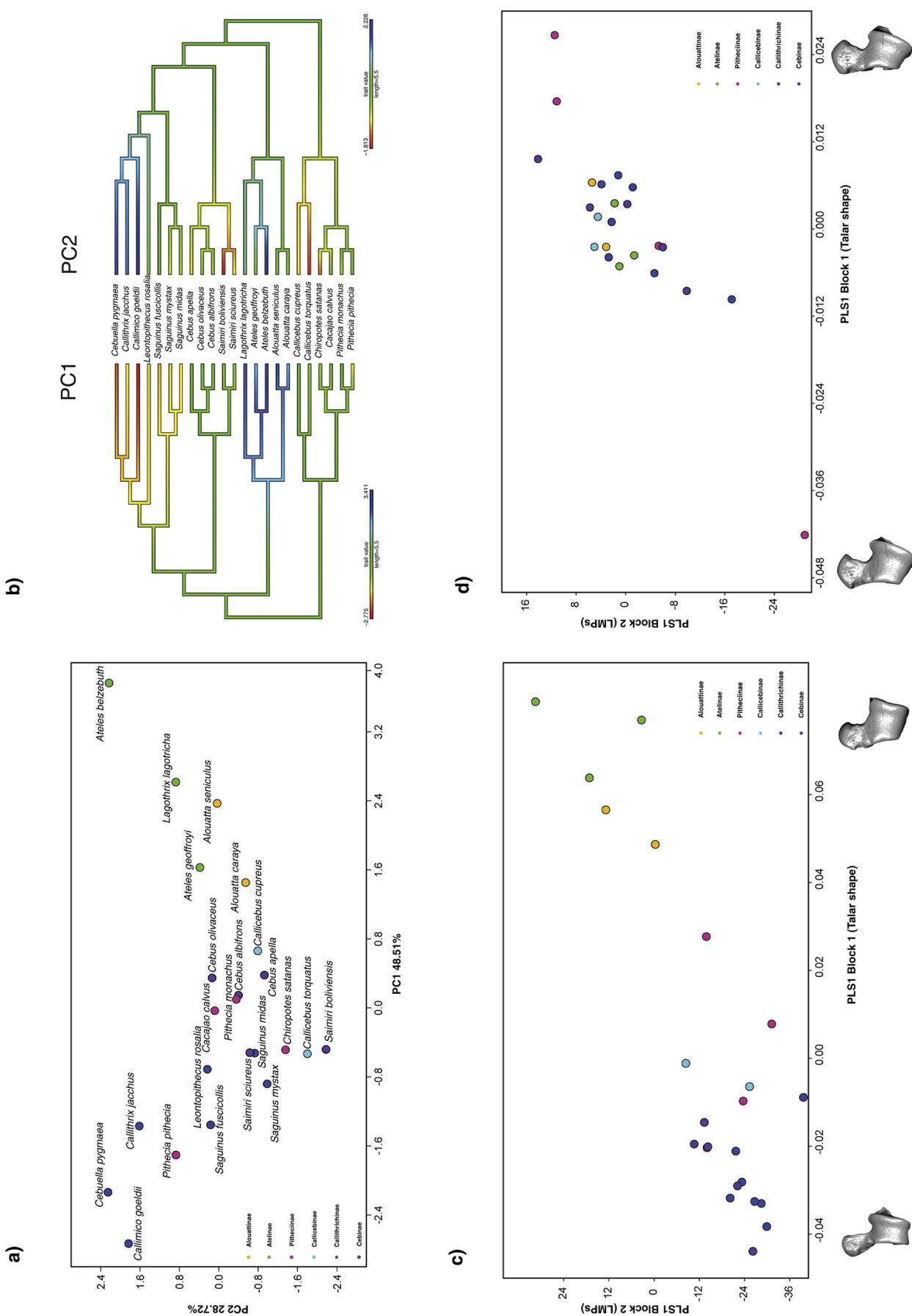
permutations) (Fig. 7c and 7d, respectively), thus establishing that there is a robust association between talar shape and locomotor behavior. The PC loadings and PLS singular vectors for the loco-motor mode percentages are provided in SOM S6. The PC1 of the LMP values for each species, mapped on the phylogeny using a maximum-likelihood ancestral character estimation method based on a BM model of evolution, showed results consistent with the previously mentioned analyses. The ancestral state was recon-structed as arboreal quadrupedalism, while both suspension and leaping/clawed locomotion are derived locomotor behaviors (Fig. 7b). The ancestral state reconstruction for the PC2 of the LMPs showed a distinction between the most quadrupedal species and the other locomotor behaviors (Fig. 7b).

3.3. Evolutionary modeling
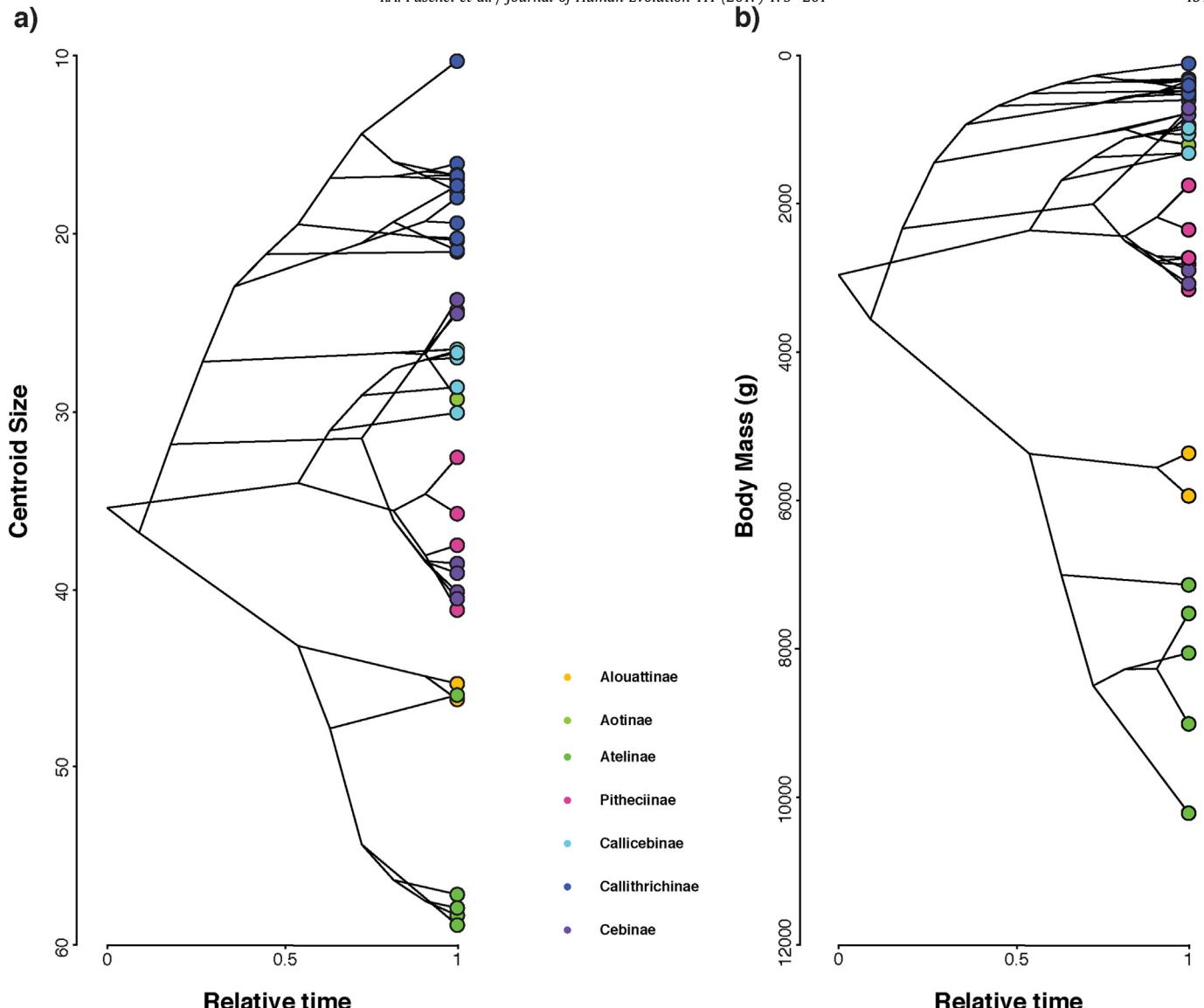
Phylogenetic signal was found for shape (Kmult: 0.46; *p*-value: 1e-04; 10,000 permutations), centroid size (K: 3.03; p-value: 1e-04; 10,000 permutations), and body mass (K: 3.09; p-value: 1e-04; 10,000 permutations). The obtained traitgrams showed that early on during platyrrhine evolution there is a strong divergence in size, particularly for the large-bodied Atelidae (i.e., talar centroid size and body mass) (Fig. 8a and 8b). The ancestral platyrrhine at the root of the phylogeny was reconstructed as a medium-sized mon-key (body mass: 2966 g; 95% LCI: 1623 g; UCI: 4309 g), with a talar centroid size similar to *Pithecia monachus* (centroid size: 35 mm; 95% LCI: 29 mm; UCI: 41 mm). The phylomorphospace (Fig. 9.)

shows an almost total absence of overlap between major phylo-genetic branches, thus suggesting that there is no evident conver-gence in talar shape among the main platyrrhine clades. Nonetheless, there is some overlap in the negative side of PC2 be-tween mostly arboreal quadrupedal species. Interestingly, the best model found by the SURFACE method exhibited six different adaptive regimes, with one of them convergent between *Callicebus* and *Saimiri*, thus suggesting a possible convergent scenario for talar shape for these genera (SOM S7). These same genera showed the most negative values in Figure 7b, thus also suggesting possible convergence. In addition these two genera are closely located in the phylomorphospace (Fig. 9), which could indicate a possible convergence, although further analyses are required. It is also important to consider that the SURFACE method used five PCs, while the phylomorphospace displays only the first two axes, so it is possible that convergent features between *Saimiri* and *Callicebus* are more evident when considering more aspects of variation. The phylomorphospace also shows that the main platyrrhine lineages occupy the three major locomotor regions already mentioned for the PCA.

The broken stick model applied to assess the significance of variance of the PCA of the extant sample showed that only the first five PCs had eigenvalues larger than the values randomly generated by the model. These five PCs accounted for 63.57% of the total variance of the sample, thus providing a reasonable approximation of the total amount of talar shape variation. The PGLSs showed that there was a weak but significant association between the first five

Figure 7. a) Principal component analysis (PCA) of the LMPs (i.e., bridge/suspensory locomotion, arboreal quadrupedal walk, clamber/vertical climb, leap/drop/hop, and clawed locomotion); b) PC1 (left) and PC2 (right) values of the LMPs for each species mapped on the phylogeny, the values at nodes and branches were reconstructed using a maximum-likelihood ancestral character estimation method based on a Brownian motion model of evolution; c) depicts the standard partial least squares (PLS) and d) the phylogenetic PLS analysis of the LMPs and the shape variables. One of the models closest to the mean shape was warped to match the multivariate mean using the thin plate spline method, then the obtained average model was warped to represent the covariation between the two blocks of data for PLS1.
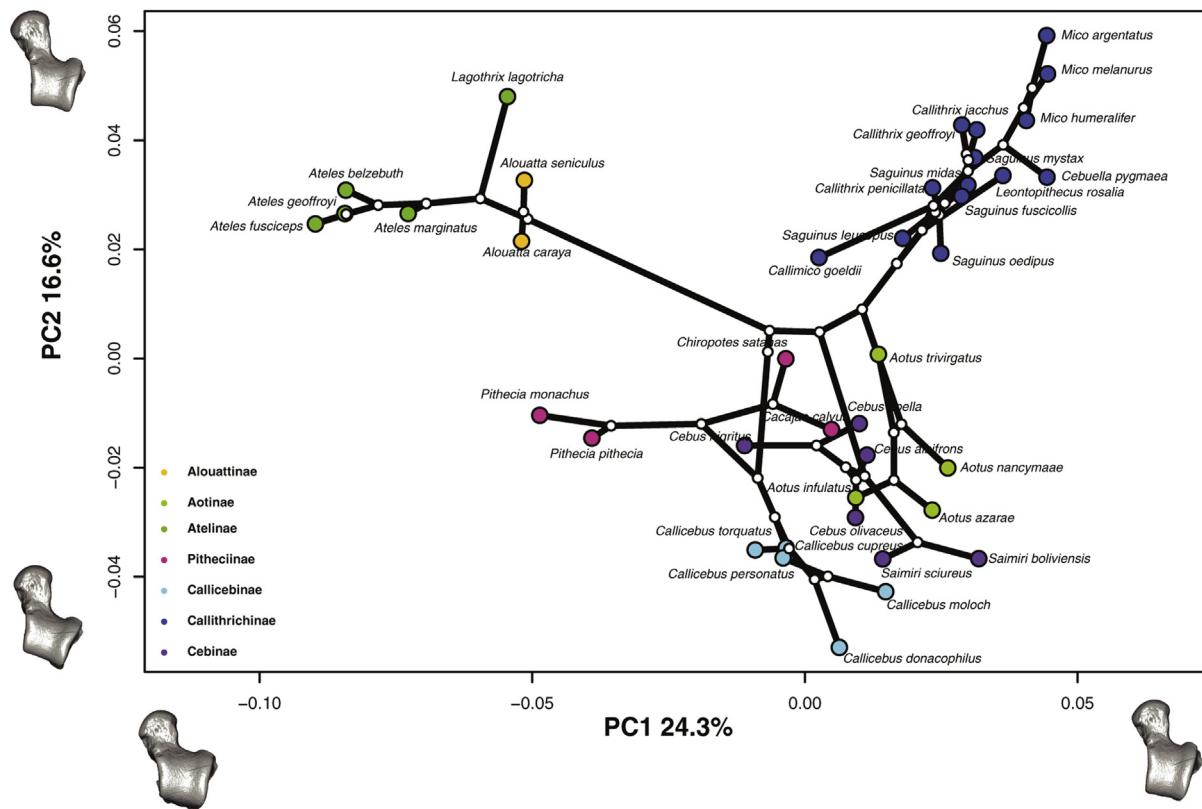
Figure 8. Traitgram of a) talar centroid size and b) body mass of the 40 extant platyrrhine species considered here. Both body mass (K: 3.09; *p*-value: 1e-04; 10,000 permutations) and centroid size (K: 3.03; *p*-value: 1e-04; 10,000 permutations) showed significant phylogenetic signals.

PCs and centroid size (R^2: 0.058; F: 2.35; *p*-value: 0.002; 10,000 permutations) and body mass (R^2: 0.064; F: 2.61; *p*-value: 0.001; 10,000 permutations). Nonetheless, the association is extremely weak; therefore talar shape variation cannot be merely attributed to evolutionary allometric effects.

Several evolutionary models were tested to understand the evolutionary history of both talar shape and centroid size. The overall fit of these evolutionary models is shown in Table 4. For the shape data, the OU-Clade model was the best supported, showing an Akaike weight much higher than any of the other alternative models. This model has three adaptive peaks for each of the three platyrrhine families. For the centroid size data the best supported model was the OU multidimensional-niche hypothesis (Rosenberger, 1992). It is important to bear in mind that one limitation regarding the applied approach is the possible lack of power to detect complex OU models in a multivariate fashion when using many variables (e.g., five PCs) and a relatively small sample (e.g., 40 species). Different evolutionary processes determined the number of species in a particular clade of interest (in the present case 40) therefore there is an intrinsic natural limit to the complexity of the

models that can be fit to these systems (i.e., ratio between parameters and sample size). Consequently caution is required when interpreting this analysis because some of the most complex OU models might have performed poorly due to the above limitation and not because they are biologically irrelevant.

Figure 10 shows the DTT plots for a) shape and b) centroid size. The morphological disparity index (MDI) was used to assess the obtained results and it is defined as the area between the observed DTT curve and the median of the simulated DTT curves (Harmon et al., 2003). The shape data seem to follow what is expected under a BM model of evolution (MDI: 0.005), thus suggesting that variation is mainly partitioned according to Brownian expectation (i.e., as expected given platyrrhine phylogeny). On the other hand, centroid size (MDI: −0.181) indicates that the average sub-clade disparity along platyrrhine evolution is lower than expected under a BM. Values drop almost to zero from the early divergence of the platyrrhines, exhibiting minimal variation over time, thus suggesting that most size variation appears among the main NWM sub-clades. The observed pattern is suggestive of an early adaptive radiation due to a niche-filling scenario.

Figure 9. Phylomorphospace of the extant platyrrhine sample (only the first two PCs are shown). One of the models closest to the mean shape was warped to match the multivariate mean using the thin plate spline method, then the obtained average model was warped to represent the variation along the two plotted PC axes in both analyses.

3.4. Body mass prediction

All relevant statistics for each of the body mass regressions are reported in Table 5. As previously explained, the fossil sample did not consistently have all four facets represented for every individual so an average body mass estimate was computed (Table 6). All fossils had at least two, and as many as four, facets from which to derive an average mass estimate. Estimates for each individual facet with 95% confidence intervals are also provided in Table 6.

The final average estimates are, on the whole, consistent with previously published mass estimates for these fossils based on a variety of different regression methods (Conroy, 1987; Kay et al.,

1998, 2008; MacPhee and Meldrum, 2006; Cooke et al., 2011; Youlatos and Meldrum, 2011; Marivaux et al., 2012).

4. Discussion
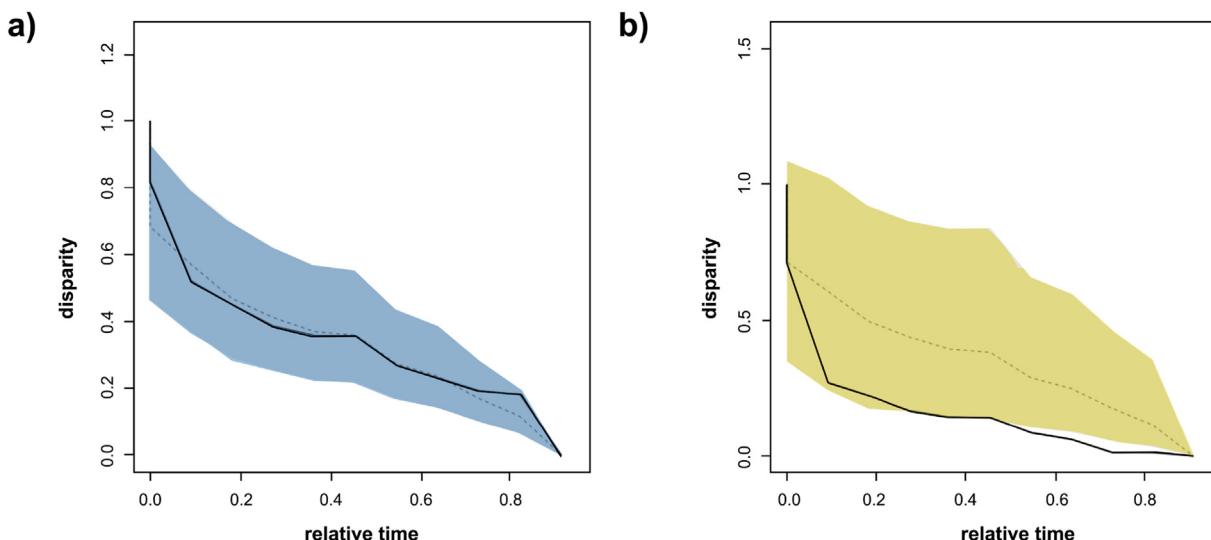
Understanding the evolution of the platyrrhine talus is relevant not only because its morphology has been associated with locomotor behaviors (as confirmed here with the PLS analyses) but also because it is one of the few anatomical structures available in many of the oldest platyrrhine fossils (Youlatos and Meldrum, 2011). The present study contributes to a better understanding of the evolution of this structure. Talar shape shows a significant phylogenetic

Table 4
Results of macroevolutionary models fit to shape (five PCs) and centroid size data.

Variable	Shape					Centroid Size				
Model[a]	LogL	Number of parameters	AICc	ΔAICc	Akaike weight	LogL	Number of parameters	AICc	ΔAICc	Akaike weight
BM	446.4964	20	−848.3	12.693077	0.00	−156.5986	2	317.5215	13.214472	0.00
OU1	170.3437	35	−322.6593	538.333781	0.00	−153.0637	3	312.7942	8.487174	0.01
EB	446.2441	21	−845.2973	15.695827	0.00	−156.5986	3	319.8638	15.556814	0.00
OU Clade	488.9381	45	−860.9931	0	0.87	−151.0611	5	313.8869	9.579939	0.01
OU Diet Composition	486.1226	45	−855.362	5.631088	0.05	−149.0932	5	309.951	5.644053	0.05
OU Locomotion A	483.4993	45	−850.1156	10.877499	0.00	−151.8403	5	315.4453	11.138277	0.00
OU Locomotion B	480.5911	45	−844.2991	16.693992	0.00	−152.3345	5	316.4337	12.126677	0.00
OU Locomotion C	483.62	50	−833.0119	27.98118	0.00	−151.8807	6	318.3068	13.999845	0.00
OU Multidimensional Niche	491.7533	55	−830.7289	30.264228	0.00	−143.4035	7	304.307	0	0.91
OU SURFACE	499.674	60	−826.6861	34.306953	0.00	−148.6272	8	317.8995	13.592512	0.00
OU Canopy A	494.7928	45	−855.3575	5.63561	0.05	−149.9652	5	314.4759	10.168915	0.01
OU Canopy B	485.1215	50	−853.3599	7.633165	0.02	−152.0587	6	315.8821	11.575105	0.00

[a] BM = Brownian motion; OU = Ornstein-Uhlenbeck; EB = Early Burst; models and other abbreviations described in text.

Figure 10. Disparity-through-time (DTT) plots for a) talar shape (i.e., first five PCs) and b) centroid size. Relative disparity at each point indicates the average extant disparity of the sub-clades that had an ancestor at that time with respect to the whole clade disparity. The dashed line represents the expectation under a BM model of evolution (estimated through simulations), while the colored shadow depicts its 95% confidence interval.

Table 5
Relevant statistics for body mass regressions.[a]

Regression statistics ($n = 40$)							
Facet	R^2	% SEE	Slope (m)	Slope 95% CI	Intercept (b)	Int. 95% CI	QMLE
Ectal	0.958	26.32	1.223	(1.139, 1.307)	3.308	(3.014, 3.601)	1.028
Trochlear	0.961	25.11	1.243	(1.161, 1.325)	2.189	(1.836, 2.541)	1.025
Navicular	0.964	24.28	1.274	(1.193, 1.356)	2.643	(2.329, 2.956)	1.024
Sustentacular	0.950	29.13	1.299	(1.201, 1.397)	2.997	(2.652, 3.343)	1.033

[a] SEE = standard error of estimate; CI = confidence interval; QMLE = Quasi-Maximum Likelihood Estimator.

signal, which indicates that closely related species tend to show similar trait values due to common ancestry. However, at the same time it was found that talar shape significantly covaries with locomotor behavior as measured in LMPs, and thus its morphology can be used to infer some aspects of locomotor repertoire. The modeling analyses found that the phylogenetic hypothesis was the best model to explain talar shape evolution in platyrrhines, while talar centroid size diversification was characterized by an early differentiation related to a multidimensional niche model, in a similar fashion as found for body mass (Aristide et al., 2015). It might seem intriguing that in spite of the high covariation between talar shape and locomotion, the different locomotor models were not the best explanation of talar shape evolution.

One possible reason for this disagreement could be the lack of power to detect complex OU models in a multivariate fashion when using many variables (e.g., five PCs) and a relatively small sample (e.g., 40 species). At least applying current approaches, there is an intrinsic natural limit to the complexity of the models that can be fit to this kind of systems, which is determined by the number of species under analysis. In the present study the most complex models for talar shape (e.g., OU-SURFACE) far exceed the sample size under the study, thus having less power to detect a possibly significant pattern, as compared to simpler models, due to the high number of parameters involved. In spite of this limitation, the simpler analyzed locomotion models (i.e., OU-Locomotion A and B) have the same number of parameters as the model with the highest support (i.e., OU-Clade), therefore at least for the simpler OU models, parameter number does not account for the observed disagreement. It is important to keep in mind that in spite of the inherent limitations of these different evolutionary models, they

allow to test different possible evolutionary processes that could explain the observed trait variation. Even though they represent simplified scenarios, by testing them it is possible to quantitatively assess different proposed hypotheses that could explain the diversity of the traits under analysis. In addition, it is also important to consider that the PLS analyses maximize the covariation between two blocks of data, without providing the underlying cause for the observed covariance, while the model-fitting approach tested a series of evolutionary models for congruence with the actual morphological data in order to provide a possible explanation about the underlying causes explaining the observed talar shape and size diversity. Therefore, it is possible that the phylogenetic model might be combining locomotion and other factors that could account for shape differentiation because it is well-known that the distinct behavioral, morphological and ecological adaptations seen in NWM are broadly correlated to specific phylogenetic groups (Ford and Davis, 1992; Rosenberger, 1992; Fleagle and Reed, 1996; Fleagle et al., 1999; Rosenberger, 2002; Youlatos, 2004; Rosenberger et al., 2009). Interestingly, it was found that even though there is a significant association between shape and size, it is quite weak when accounting for phylogeny. Finally, the ancestral NWM was reconstructed as a medium-sized (~3000 g) arboreal quadruped with generalized talar morphology, consistent with the primitive talar morphology observed in most fossils.

4.1. Morphological affinities

Principal component 1 clearly distinguished between species with adaptations for suspensory/climbing behavior from species

Table 6
Estimates for each individual facet with 95% confidence intervals (CI) and body mass average estimates.

Genus	Species	Specimen ID	Facet[a]	Mass (g)	Mass (g) 95% CI
Neosaimiri	*fieldsi*	IGMKU 89030	Ectal	—	—
			Trochlea	—	—
			Sust.	823	(448, 1510)
			Nav.	694	(413, 1165)
			Average	**759**	
Neosaimiri	*fieldsi*	IGMKU 89031	Ectal	717	(410, 1250)
			Trochlea	838	(492, 1427)
			Sust.	816	(444, 1498)
			Nav.	755	(450, 1266)
			Average	**781**	
Neosaimiri	*fieldsi*	IGMKU 89199	Ectal	—	—
			Trochlea	—	—
			Sust.	667	(362, 1226)
			Nav.	1077	(643, 1801)
			Average	**872**	
Aotus	*dindensis*	IGM 8802	Ectal	651	(373, 1137)
			Trochlea	933	(548, 1586)
			Sust.	881	(480, 1616)
			Nav.	1029	(614, 1721)
			Average	**874**	
Carlocebus	*carmenensis*	MACN304	Ectal	2667	(1533, 4635)
			Trochlea	2903	(1707, 4934)
			Sust.	2988	(1630, 5476)
			Nav.	3096	(1849, 5183)
			Average	**2914**	
Carlocebus	*carmenensis*	MACN271	Ectal	—	—
			Trochlea	—	—
			Sust.	2655	(1449, 4862)
			Nav.	2364	(1413, 3952)
			Average	**2509**	
Carlocebus	*carmenensis*	MACN368	Ectal	1543	(888, 2680)
			Trochlea	—	—
			Sust.	2211	(1208, 4046)
			Nav.	—	—
			Average	**1877**	
Carlocebus	*carmenensis*	MACN396	Ectal	—	—
			Trochlea	2579	(1517, 4381)
			Sust.	3080	(1680, 5644)
			Nav.	2752	(1644, 4603)
			Average	**2803**	
Soriacebus	*ameghinorum*	MACN397	Ectal	1429	(822, 2482)
			Trochlea	1981	(1167, 3363)
			Sust.	1687	(921, 3085)
			Nav.	1787	(1069, 2986)
			Average	**1721**	
Dolichocebus	*gaimenensis*	MACN362	Ectal	1520	(874, 2639)
			Trochlea	—	—
			Sust.	1681	(919, 3076)
			Nav.	—	—
			Average	**1601**	
Madre de dios	—	MUSM 2204	Ectal	298	(168, 527)
			Trochlea	—	—
			Sust.	375	(201, 695)
			Nav.	384	(226, 648)
			Average	**352**	
Paralouatta	*marianae*	MNHNCu 76.3059	Ectal	5029	(2877, 8788)
			Trochlea	5071	(2969, 8662)
			Sust.	4026	(2191, 7397)
			Nav.	—	—
			Average	**4709**	
Proteropithecia	*neuquenensis*	MLP91lX1	Ectal	1647	(948, 2861)
			Trochlea	2038	(1200, 3459)
			Sust.	2291	(1251, 4192)
			Nav.	2050	(1226, 3425)
			Average	**2006**	
Rio Cisnes	—	SGO.PV_974	Ectal	1020	(586, 1773)
			Trochlea	1573	(926, 2670)
			Sust.	2122	(1159, 3882)
			Nav.	1325	(792, 2215)
			Average	**1510**	

Table 6 (*continued*)

Genus	Species	Specimen ID	Facet[a]	Mass (g)	Mass (g) 95% CI
Cebupithecia	*sarmientoi*	UCMP_38762	Ectal	1438	(827, 2497)
			Trochlea	1533	(903, 2603)
			Sust.	2961	(1615, 5426)
			Nav.	1368	(818, 2287)
			Average	**1825**	

[a] Nav. = navicular; Sust. = sustentacular.

exhibiting frequent leaping/vertical clinging. The mixture of traits observed for the most suspensory species (i.e., broader head, greater trochlear wedging, a lower trochlea and a shorter anterior and longer posterior calcaneal facet) has been associated with greater mobility of the subtalar and transverse tarsal joints, along with conjoint rotation of the upper ankle joint and a greater range of flexion-extension, which has been related to the flexibility necessary during climbing (Meldrum, 1990). The talar morphology at the other extreme of PC1 can be described by an anteroposteriorly shorter trochlea with more parallel medial and lateral rims and a longer anterior calcaneal facet. These features have been associated with the frequent leaping behavior observed in callitrichines (Youlatos and Meldrum, 2011). In contrast PC2 mainly distinguished between the combination of atelids and callitrichines (i.e., most derived locomotor behaviors) and the more arboreal quadrupedal forms, which can themselves be separated between more 'generalist' shapes (i.e., more similar to the fossils such as *Cebus* and the Pitheciinae) and morphologies showing increased dorso-lateral surfaces such as those observed in *Callicebus* and *Saimiri*. Most fossils occupied central positions in the morphospace, exhibiting principally generalized morphologies. These generalized talar shapes could be perhaps related to lower frequencies engaging in more specialized locomotor behaviors, which were probably not common among most Miocene specimens. Interestingly, the Madre de Dios specimen exhibited the most distinct morphology, occupying a region of the morphospace, which is not occupied by any extant species. This unique morphology could perhaps represent a distinctive locomotor repertoire not observed in any extant species, however further analyses are required to test this hypothesis.

4.2. Morphological affinities of the analyzed NWM fossils

The oldest platyrrhine fossil with well-described postcranial elements is *D. gaimanensis* from the Sarmiento Formation, Chubut Province, Argentina (Kay et al., 2008). There is still disagreement regarding the phyletic position of this species, and different interpretations have been proposed (Kay et al., 2008; Kay and Fleagle, 2010; Rosenberger, 2010). Based on a series of apparent cranial and postcranial synapomorphies, the LLH perspective states that these fossils are an early member of the lineage leading to modern *Saimiri* (Reeser, 1984; Gebo and Simons, 1987; Tejedor, 2008; Rosenberger et al., 2009; Rosenberger, 2010). The SPH view characterizes this fossil and others as stem platyrrhines, relying mostly on a large cranio-dental parsimony analysis (Meldrum, 1993; Kay et al., 2008; Hodgson et al., 2009; Kay and Fleagle, 2010). The only postcranial element that has been ascribed to *D. gaimanensis* is the well-preserved talus analyzed here, which has been traditionally described as morphologically similar to *Saimiri*, *Cebus*, and *Callicebus*. However, it has also been described as lacking some of the most conspicuous platyrrhine features (Reeser, 1984; Gebo and Simons, 1987; Ford, 1988, 1990; Meldrum, 1990). The present analyses showed that the talar morphology of *D. gaimanensis* is quite

generalized in the morphospace illustrated in Figure 4, which may suggest a combination of characters that are primitive amongst Platyrrhini; according to the CV scores it would be classified as a member of Cebidae. As previously pointed out, some species of *Cebus*, as well as some pitheciids, show a 'generalist' talar shape, so this resemblance might be attributed to a conserved morphology. The clustering analysis located this specimen next to *Soriacebus*, *Carlocebus*, *Cebus* and *Paralouatta* suggesting again that the oldest fossil individuals exhibit a similar primitive morphology. It is interesting that *Cebus* clustered with the oldest analyzed fossils, which could be due to the already mentioned 'generalist' morphology. Based on semicircular canal data, *D. gaimanensis* has been described as being relatively agile with medium scores similar to the one observed in cebids (Ryan et al., 2012). The present analyses are consistent with these data, indicating that *D. gaimanensis* was most likely an arboreal quadruped based on the results obtained in the CVA. Its morphology indicates a generalized function with a preponderance of frequent arboreal quadrupedal activities (Meldrum, 1993). The body mass estimate is 1600 g, which is similar to previous estimates based on dentition (i.e., 1500 g; Kay et al., 2008) and to extant platyrrhines such as *Pithecia pithecia*.

Carlocebus is the other NWM from Pinturas, although it is evidently larger than *Soriacebus* (Tejedor, 2005b). Its teeth exhibit a more generalized morphology that is thought to be most similar to the Callicebinae (Fleagle and Tejedor, 2002), although some have interpreted this resemblance as homoplasic or primitive. Proponents of the SPH relate *C. carmenensis* to an earlier platyrrhine radiation more closely related to *D. gaimanensis* (Kay et al., 2008). Luckily, there are four well-preserved tali ascribed to *Carlocebus,* thus allowing some degree of intra-specific variability (Meldrum, 1990). These tali have been described as similar to *Saimiri* or Callitrichinae, due to their moderately low and broad trochlea, a very broad, slightly medially directed talar neck, and a broad shallow posterior calcaneal facet (Meldrum, 1990). The present analyses suggest that *Carlocebus* also shows a generalized talar morphology (Fig. 4), similar to *Dolichocebus* and *Soriacebus*. The CVA analysis indicates a morphological affinity with Cebidae. In terms of locomotion, *Carlocebus* is believed to have used a combination of quadrupedal activities with some moderate leaping and/or clambering (Ford, 1990; Meldrum, 1990). The present analyses generally support this view, suggesting mostly arboreal quadrupedal activities. This positional behavioral profile is congruent with its reconstructed paleo-environment and proposed frugivorous diet (Youlatos and Meldrum, 2011). The obtained body mass predictions for the four *Carlocebus* tali range between 1877 and 2913 g, which is consistent with previously published estimates (i.e., 2500 g; Fleagle and Tejedor, 2002) and is similar to extant genera such as *Cebus* or *Chiropotes*.

Soriacebus ameghinorum was found in the Pinturas formation and was initially described as having resemblances to Callitrichinae and Pitheciinae (Luchterhand et al., 1986), later being classified as an early member of the latter group (Rosenberger et al., 1990; Rosenberger, 1992; Tejedor, 2008). Nonetheless, as with the rest of the older platyrrhine fossils, it has also been defined as a stem NWM (Kay, 1990; Kay et al., 2008; Kay and Fleagle, 2010). The single available talus analyzed here has been portrayed as resembling those of *Alouatta* and *Pithecia* (Meldrum, 1990). The present analysis indicates that *S. ameghinorum* exhibits an ancestral talar morphology similar to *Dolichocebus* and *Carlocebus,* which are among the oldest Miocene fossils. The analyses carried out to reconstruct its locomotor behavior indicate that it was most likely an arboreal quadruped. It is still debated if the relative talar morphology affinities between *S. ameghinorum* and the pitheciines indicate phylogenetic affinity or homoplasy (Youlatos and Meldrum, 2011). Another possibility is that *S. ameghinorum*

exhibits an ancestral morphology that was conserved in the pitheciine lineage. The average body mass estimate for this fossil was 1720 g, thus being similar to previous dental estimates (i.e., 1800 g; Fleagle and Tejedor, 2002) and comparable to the body mass of extant NWM such as *P. pithecia.*

The Madre de Dios talus found in Peruvian Amazonia represents the first early Miocene platyrrhine from northern South America (Marivaux et al., 2012), although recent findings have provided more specimens from the late Miocene of the Peruvian Amazonia belonging to two distinct Cebidae (Marivaux et al., 2016b). In addition to these discoveries, the Peruvian Amazonia has recently provided interesting new findings that contribute to the understanding of early platyrrhine evolution (Bond et al., 2015; Marivaux et al., 2016a,b). The discovery of *P. ucayaliensis* from the latest Eocene or Early Oligocene (Bond et al., 2015) and *C. amazonensis* (Marivaux et al., 2016a) from the Late Oligocene, clearly indicates that platyrrhines were well-established in the Amazonian Basin early, thus confirming the expected distribution of NWM in the Neotropics (Marivaux et al., 2016a,b). Given that the Madre de Dios talus is a rare example of the NWM postcranial fossil record in Peruvian Amazonia, analyzing it is highly relevant. The talus has not been taxonomically assigned, but has been described as displaying a mixture of talar characteristics mainly found among the Cebidae, and more specifically in the Cebinae (Marivaux et al., 2012). Nonetheless, what is remarkable about this specimen is its reduced size that is most similar to that of the marmosets and tamarins (Cebidae, Callitrichinae). The Madre de Dios talus has been described as being a tiny *Saimiri*-like cebine that was primarily an arboreal quadruped, but also engaged in frequent horizontal leaping and vertical clinging (Marivaux et al., 2012). The analyses performed in this paper showed that the Madre de Dios talus exhibits a particularly distinct morphology. The PCA showed Madre de Dios occupying a region of the morphospace not occupied by any other specimen, which could be related to its particular combination of traits. Interestingly, Madre de Dios clusters with *Cebupithecia* and within a group also comprising *Cacajao*, *Chiropotes* and *S. leucopus*. The CVA using platyrrhine families as categories classified Madre de Dios within the Cebidae, while the locomotion CVA categorized it as the only fossil classified as leaper/clawed. Madre de Dios seems to combine in its morphology some more primitive aspects common to all the analyzed fossils, with some derived characters similar to some members of the Callitrichinae. The evidence thus suggests that Madre de Dios seems to be a small-sized cebid that engaged in leaping and vertical clinging as part of its locomotor repertoire as suggested by its morphological similarities with the callitrichines. The obtained body mass estimate is 352 g, which is within previously proposed ranges (i.e., 250—500 g; Marivaux et al., 2012), and similar to some of the extant callitrichines.

The Río Cisnes talus from the Chilean site of Alto Río Cisnes is currently taxonomically unassigned and dates to the Friasian South American Land Mammal Ages (SALMA) ~16 Ma (Tejedor, 2003). This talus is about the size of that of *Pithecia*, and has been described as being morphologically similar to that of *Callicebus* or a smaller version of a *Carlocebus* talus (Tejedor, 2003, 2008). The analyses performed here suggest that the Río Cisnes talus shows a similar morphology to that observed in *Aotus*, *Proteropithecia* and *Neosaimiri*. The CVA classified this talus as similar to the Cebidae. It has been suggested that the moderately high talar body with the parallel-sided rims and the relatively long neck could be associated with increased leaping in what otherwise looks to be a generalized arboreal quadruped (Gebo and Simons, 1987; Meldrum, 1990). The locomotion CVA is in agreement with this proposal. Finally, the first body mass estimate of 1509 g for this fossil was provided, which is similar to other fossils and to the largest *Callicebus* species and the smallest *P. pithecia*.

Proteropithecia neuquenensis, a medium-sized platyrrhine known from a single talus and isolated teeth, was found in the Collón Curá formation in Neuquén, Argentina and based on dental traits has been classified as a pitheciin ancestor (Kay et al., 1998). The *P. neuquenensis* talus has been described as exhibiting a general similarity to *Callicebus* or *Aotus* (Ford, 1988; Meldrum, 1990). The PCA showed that *P. neuquenensis* occupies a position between the Patagonian and La Venta fossils, suggesting a potentially good representative for primitive talar morphology in some crown fossil taxa. The cluster analysis located it in a group with *Aotus*, Río Cisnes, *Proteropithecia* and *Callimico.* The CVA classified *P. neuquenensis* as belonging to Cebidae, however it also has a posterior probability of 0.278 of being classified as Pitheciidae. The talus has been described as having an oval head, moderate neck length, a wedged trochlea and an extended anterior proximal calcaneal facet, all of which have been interpreted as associated with the required ankle stability to perform arboreal quadrupedal activities and moderate leaping (Kay et al., 1998). That *P. neuquenensis* was classified as an arboreal quadrupedalist in the present study is consistent with these interpretations. The body mass prediction for this fossil was 2006 g, which is similar to some *Pithecia* species.

Cebupithecia sarmientoi is well represented in La Venta, Colombia. *Cebupithecia* was a medium-sized monkey with associated cranial, mandibular, and dental remains along with a partial skeleton; together the relatively complete *Cebupithecia* fossils suggest a phylogenetic position within Pitheciinae (Hartwig and Meldrum, 2002). However, *Cebupithecia* lacks many Pitheciinae apomorphic postcranial characters (Fleagle and Meldrum, 1988; Ford, 1990; Hartwig and Meldrum, 2002). The PCA showed that *C. sarmientoi* is located on the morphospace near most owl monkeys, exhibiting a morphology similar to *Aotus nancymaae*. As was the case for *Proteropithecia*, the CVA classified *Cebupithecia* within Cebidae. The clustering analysis located it next to Madre de Dios, which is intriguing. *Cebupithecia* has been traditionally reconstructed as exhibiting mainly quadrupedal behaviors with moderate amounts of leaping, in a similar fashion to the cebines and *Callicebus* (Meldrum and Lemelin, 1991). Consistently, the CVA analysis using locomotor categories classified *C. sarmientoi* as an arboreal quadruped. The obtained body mass prediction is 1825 g, which is similar to previous predictions (i.e., 1602 g; Cooke et al., 2011) and to *P. pithecia.*

The analyzed specimen of *A. dindensis* was discovered within the Monkey Unit in the site of La Venta, Colombia (Setoguchi and Rosenberger, 1987; Gebo et al., 1990), and it was classified as a member of *Aotus,* due to its particular morphological characteristics, although it differs from the extant members of this genus in being smaller and having a slightly more square-shaped talar body (Gebo et al., 1990). This specimen exhibits a robust talar body, with parallel trochlear rims and only a slight proximal wedging (Gebo et al., 1990). Its trochlear surface is relatively flat, while the talar head and neck are very wide (Gebo et al., 1990). This combination of morphological features has been interpreted as being associated with an extensive use of arboreal quadrupedalism (Gebo, 1988, 1989), with no indication of frequent climbing or leaping (Gebo et al., 1990). It is debated whether *A. dindensis* is an actual species or if it is conspecific with *Monhanamico hershkovitzi* (for further details see Kay, 1990; Rosenberger et al., 1990). Nonetheless, in the present study we subscribe to the classification of Gebo et al. (1990). *Aotus dindensis* is located near *N. fieldsi* in the morphospace, occupying a position within the locomotor 'generalist' area. The cluster analysis located this fossil within a group with most *Aotus*, Río Cisnes, *Proteropithecia* and *Neosaimiri*. In the family CVA, this specimen was classified as a member of the Pitheciidae, while the locomotor analysis categorized it as an arboreal quadrupedal

species, as previously suggested by Gebo et al. (1990). The average body mass prediction for *A. dindensis* is 873 g, thus being only slightly smaller than previous predictions (i.e., 1000 g; Cooke et al., 2011).

A number of postcranial specimens belonging to *N. fieldsi* have been discovered at La Venta, Colombia, and interpreted as ancestral to the extant genus *Saimiri* (Stirton, 1951; Szalay and Delson, 1979; Rosenberger et al., 1990; Takai, 1994). The talar morphology of *Neosaimiri* has been described as exhibiting parallel trochlear lips, a narrow trochlear surface, a relatively small and flattened talar head and moderately long talar neck (Nakatsukasa et al., 1997). Similarities in postcranial morphology between *Neosaimiri* and *Saimiri* suggest arboreal quadrupedalism to be its predominant locomotor behavior, although it probably engaged in leaping with relative frequency (Gebo et al., 1990; Meldrum et al., 1990). The PCA showed that *Neosamiri* is similar to some *Cebus* species, *Cacajao* and *A. dindensis* based on the two first PC axes. The family CVA classified *Neosaimiri* as Cebidae, while its inferred main locomotor behavior was arboreal quadrupedalism. The average body mass predictions for multiple individuals range between 758 and 871 g, which is only slightly larger than published dental predictions (i.e., 725 g; Cooke et al., 2011).

Paralouatta marianae was designated on the basis of a single talus from the Early Miocene locality of Domo de Zaza, Cuba (MacPhee et al., 2003). This talus has been described as being only subtly different from that of *Paralouatta varonai* even though 17–18 Ma allegedly separate them (MacPhee and Meldrum, 2006) and *P. marianae* is significantly smaller. There is no good morphological comparison for the talus of *Paralouatta* among extant NWM (MacPhee and Iturralde-Vinent, 1995). MacPhee and Iturralde-Vinent (1995) particularly noted that the Atelidae differ from *Paralouatta* in having a 'wedged' trochlea with a low trochlear relief, which would be related to maximizing mobility at the talocrural joint, whilst *Paralouatta* exhibits a talus more suited for stability rather than mobility. The talus of *Paralouatta* has a clearly noticeable cotylar fossa facing an extended medial malleolus articular surface, thus offering a stable seating for the medial malleolus (MacPhee and Iturralde-Vinent, 1995). The cotylar fossa, which is typically absent in large-bodied platyrrhines, is present in Old World monkeys such as *Theropithecus*, hence the suggestion of semiterrestriality in *Paralouatta* (MacPhee and Meldrum, 2006). The PCA showed that *Paralouatta* occupied a position close to *Alouatta*, as well as to some of the oldest Patagonian fossils (i.e., *Soriacebus, Dolichocebus* and *Carlocebus*). The hierarchical clustering analysis located this fossil close to *Cebus* and *Dolichocebus, Carlocebus* and *Soriacebus*. The family CVA classified *Paraloutta* within the Cebidae, while the locomotion CVA categorized it as an arboreal quadruped. In terms of locomotion, the results suggest arboreal quadrupedalism, however the analyses lacked terrestrial or semiterrestrial categories so it is not possible to rule out these potential specializations. Further analyses considering terrestrial Old World monkeys would be required to test this possibility. The body mass prediction carried out in this study for *P. marianae* employed highly accurate postcranial surface area regressions to compute the first body mass data for this specimen, which predicts 4708 g for this taxon. This value is similar to previous body mass predictions for *Antillothrix bernensis* based on craniodental measurements (i.e., 4.7 kg; Rosenberger et al., 2011), thus being slightly smaller than the extant Alouattinae species.

4.3. Locomotor mode percentages

The PLS analyses provide strong evidence for the association between talar shape and locomotion (measured as LMP); therefore talar shape can be used to infer locomotion. The talus is primarily

stiffened by trabecular networks (unlike the diaphysis in long bones) and is the principal mechanical connection between the leg and the foot (Parr et al., 2013); it not only transmits the forces derived from the body mass, but also provides stability and/or mobility for the hind limbs during diverse postural and locomotor behaviors (Boyer et al., 2015). Many authors have proposed that mechanical loading regulates trabecular remodeling (e.g., Carter et al., 1987; Turner, 1998; Zadpoor et al., 2012), therefore different locomotor repertoires would have exerted differential loading regimes on the talus, thus gradually shaping it during NWM evolution.

In terms of locomotion reconstruction, all of the present analyses are consistent with the suggestion that the ancestral condition for the platyrrhines was predominantly arboreal quadrupedal. The PCA of the LMPs (Fig. 7a) showed that there is a good separation of groups. The groups cluster according to locomotor categories, principally distinguishing between the more specialized or derived forms along the respective axes. Large-bodied taxa using climbing/suspension (i.e., atelids) were distinguished from small-bodied species using claw-climbing, clinging and vertical leaping (i.e., callitrichines) along PC1, while PC2 separated between medium-sized NWM characterized by different levels of quadrupedalism, with some taxa occupying a central more 'generalist' position. The mapping of the PC1 of the LMPs on the platyrrhine phylogeny showed that the ancestral condition exhibited values similar to those expected for predominantly quadrupedal taxa, and that both the suspensory/clamber and leaper/vertical clinging locomotor repertoires evolved posteriorly in two different groups of NWM (i.e., atelids and callitrichines, respectively). The same procedure was repeated for PC2, which showed a distinction between the less quadrupedal genera (e.g., *Ateles, Callithrix, Callimico*), and those that exhibited higher levels of quadrupedalism. Interestingly, *Saimiri* and *Callicebus* showed the highest level of quadrupedalism (i.e., lowest PC2 score), thus repeating the convergence scenario found by the SURFACE method. For this variable, the ancestral state reconstruction was also found to be a quadrupedal condition, although not as specialized as in *Saimiri* or *Callicebus*, but more 'generalist' such as the Pitheciinae *Chiropotes* and *Cacajao*, the Callitrichinae *Saguinus* and *Leontopithecus* or even *Alouatta*.

4.4. Evolutionary modeling

The present model selection results show that it is possible to explain talar shape diversification by invoking an OU model of adaptive peak shifts to three optima, defined by the different platyrrhine families. The OU-Clade model — a fully phylogenetic hypothesis where each platyrrhine family occupied a separate adaptive peak — was the best supported among all the tested hypotheses. This is consistent with the structuring of the data in the shape phylomorphospace (Fig. 9) where the platyrrhine families occupy mainly three distinct areas. This result means that each platyrrhine family has its own talar shape optimum, which could be associated with the previously described locomotor categories (climbing/suspension in Atelidae, arboreal quadrupedalism in Pitheciidae, and leaping in Cebidae), but also to other ecological differences such as canopy levels or diet. Nonetheless, some members of the Cebidae are more quadrupedal; hence this result is intriguing. One possibility is that *Cebus*, *Saimiri* and *Aotus* exhibit an ancestral talar morphology on its way towards the optimum nearer the callitrichines, or simply that the first five PCs do not totally represent the subtleties of shape variation in the platyrrhine family. In any case, the obtained results in combination with the DTT plot suggest that talar morphological diversification gradually differentiated into three distinct areas of the morphospace that are related mainly to phylogenetic clades (with some slight convergence between *Callicebus* and *Saimiri* as observed in the phylomorphospace and the SURFACE model). Some species seem to retain the primitive morphology similar to the one observed across the fossil sample (e.g., *Cebus* and *Cacajao*). In contrast, the least supported model was the OU1 model, suggesting that there is not a single unique adaptive optimum for talar shape in the NWM.

Talar centroid size followed the pattern observed in previous research regarding platyrrhine body mass (Aristide et al., 2015) and brain shape (Aristide et al., 2016), where there were several unique and shared optima, mainly defined by the multidimensional ecological niche hypothesis (i.e., OU-Multidimensional niche), which combined both diet and locomotion information (Rosenberger, 1992). As found by these previous studies (Aristide et al., 2015, 2016), it seems that talar centroid size — a generally good proxy for body mass (Halenar, 2011) — evolved in the platyrrhine radiation initially by a rapid diversification, as observed in the DTT plot of centroid size. This is similar to the trend observed for body mass by Aristide et al. (2015), likely because both are scale measurements that are highly correlated. This relationship was likely associated with a differentiation among NWM families within an ecological adaptive landscape mostly defined by locomotion and diet (Rosenberger, 1992; Aristide et al., 2015). It has been previously proposed that size diversification in platyrrhines was mostly related to diet variation (Marroig and Cheverud, 2001; Perez et al., 2011), however the present results align with other findings that support a more complex scenario where platyrrhine evolution among the main lineages is linked to size changes related to a multidimensional niche (Rosenberger, 1980, 1992, Aristide et al., 2015, 2016). Nonetheless, it is important to note that even though the diet ecological dimension alone is not enough to explain platyrrhine centroid size and body mass diversification, the other best supported models for centroid size is related to diet (i.e., OU-Diet Composition). The locomotion model alone was poorly supported. Perhaps this indicates the relative contribution of these different factors to the OU-Multiple Niche model, although further investigations are required. The DTT plot shows how centroid size disparity is high during the early branching of the phylogeny, possibly related to changes in ecological opportunity (Harmon et al., 2003). The magnitude of the centroid size disparity is strikingly high during the early branching processes (Figs. 8a and 10b), similar to that found by Aristide et al. (2015) for body mass, thus supporting again the distinctiveness of the platyrrhine radiation (Delson and Rosenberger, 1984). Interestingly it seems that this early differentiation in size was not coupled with immediate changes in talar shape, but that these structural changes occurred gradually following the different NWM family differentiations. The fossil evidence supports these results since the different morphological analyses showed that most fossils exhibit a generalist and possibly primitive morphology, while showing significant size variation according to the obtained predictions ranging from 352 g (Madre de Dios) to 4708 g (*P. marianae*). This is consistent with previous results that have suggested that body size partitioning in platyrrhines is already evident in ancient lineages (Aristide et al., 2015).

One of the main predictions of an adaptive radiation hypothesis is that phenotypes diversify early in the branching process of the phylogeny in relation to certain ecological factors (Schluter, 2000; Losos, 2011). Previous eco-functional studies have indicated that there are natural size thresholds structuring platyrrhine locomotor-dietary niches (Rosenberger, 1992; Youlatos and Meldrum, 2011; Fleagle, 2013). The ecological opportunity that existed during the early evolutionary history of platyrrhines was most likely a significant factor influencing body size changes among the main clades as observed in both the centroid size and body mass traitgrams and DTT plots (Figs. 8 and 10) (Aristide et al., 2015). The present results support that along with this initial diversification in body size, likely due to ecological opportunity, there was probably a

subsequent gradual differentiation in talar shape (as observed in Figs. 9 and 10a). These shape changes in talar morphology were more marked in the two lineages that evolved notably different locomotion repertoires compared to the ancestral condition (i.e., atelids and callitrichines), while other groups still exhibit a talar shape relatively similar to the one observed in most of the analyzed fossils (e.g., *Chiropotes*, *Cacajao*, *Cebus*).

4.5. Implications for platyrrhine evolution

The placement of the fossil species on the PCA (Fig. 4) showed that most extinct taxa occupy the central area defined by quadrupedal 'generalist' species (an area occupied by some extant species exhibiting different frequencies of additional climbing or leaping behavior). This is consistent with the CVA and the ancestral trait reconstruction for the LMPs that indicated that the ancestral platyrrhine condition was probably predominantly quadrupedal with only minor contributions from other more specialized locomotor behaviors. Nonetheless, until the recovery of postcranial elements for the earliest platyrrhine fossils (e.g., *Branisella* and *Perupithecus*), not much can be said with certainty about the ancestral locomotor condition of the very first platyrrhines, especially if these fossils are considered to belong to an ancient radiation of stem platyrrhines that did not lead to crown NWM (Rosenberger et al., 1991; Takai et al., 2000; Kay et al., 2008). This would imply that studying the locomotor diversity observed in the extant NWM would point to the ancestral condition of the last common ancestor of modern platyrrhine species, rather than the earliest ancestor of all platyrrhines (i.e., extinct and extant) (Ford, 1988; Youlatos and Meldrum, 2011).

Due to the absence of post-cranial material belonging to the oldest found platyrrhines, it is perhaps relevant to discuss the obtained results in relation to other primate fossils that have known tali. Platyrrhines are considered to be a monophyletic group that emerged during the African Eocene (Ciochon and Chiarelli, 1980; Houle, 1999; Oliveira et al., 2009), and most of the primate fossil evidence for that time period comes from three groups from the Fayum of Egypt (i.e., the propliopithecids, the oligopithecids and the parapithecoids) (Fleagle and Simons, 1982, 1983; Seiffert et al., 2000; Simons, 2004). Among these fossils, it has been proposed that *Apidium* (Hoffstetter, 1980; Ford, 1990; Fleagle and Kay, 1994; Takai et al., 2000) or *Proteopithecus* (Simons, 1989, 1997; Simons and Seiffert, 1999; Gladman et al., 2013) might represent the ancestral NWM morphotype better. *Apidium* is usually interpreted as being a frequent leaper (Fleagle and Simons, 1983, 1995; Gebo et al., 2000, 2012; although for a different opinion see Ryan et al., 2012), while *Proteopithecus* has been described as relying on agile quadrupedal locomotion, probably also involving some pronograde leaping (Gebo et al., 1994; Simons and Seiffert, 1999; Seiffert et al., 2000; Ryan et al., 2012), therefore it might be speculated that the ancestral platyrrhine was a leaper. Nonetheless, the shape of the oldest Miocene talus analyzed here (i.e., *Dolichocebus*) has been described as distinctively different from the Fayum fossils (Gebo and Simons, 1987) and the present results indicate that all the oldest materials are more similar to the 'generalized' shape of *Cebus* rather than to specialized leapers such as the Callitrichinae (Figs. 4 and 6). In addition, leaping behavior is notoriously associated with size. Thus, the smaller the body size of the ancestral platyrrhine, the more likely leaping may be a factor. From the traitgrams in Figure 8 it is notable that the ancestral centroid size and body mass reconstruction for the ancestral platyrrhine condition (i.e., root of the phylogeny) corresponds to the body mass of *Cebus* (~3000 g), while its talar size is similar to *Pithecia monachus*. However, this analysis estimates the ancestral size condition using the data from only the modern NWM, which represent only a subset of all Platyrrhini

through time. Furthermore, the ancestral state reconstructions have the known limitation that the probability of computing the correct ancestral condition decreases as the temporal depth increases (Martins and Cunningham, 1999). Therefore caution is required when extrapolating this result. Furthermore, when reconstructing locomotor behaviors, it is mostly the dominant locomotor modes that are reconstructed and not the entire repertoire of positional behaviors (MacPhee and Meldrum, 2006). For instance, saying that the ancestral locomotor condition of the platyrrhines was most likely arboreal quadrupedalism does not imply that this specimen was incapable of a wide variety of behaviors (such as leaping, climbing, running, suspension, and clambering), but rather that arboreal quadrupedalism was its predominant locomotor mode (MacPhee and Meldrum, 2006). In summary, the present results point to an ancestral morphological pattern that can be described as a generalized, medium-sized, arboreal quadruped as has been previously suggested (Ford, 1988; Gebo et al., 1990; Tallman and Cooke, 2016).

Even though the present research did not attempt to resolve the debate regarding the LLH and SPH, the results do provide some interesting insights to trigger further research. The early Miocene fossils analyzed here from Patagonia have been hypothesized to represent either a distinct ancient radiation or the early ancestors of the modern clades (Rosenberger et al., 2009). The results show that all these fossils (i.e., *Dolichocebus*, *Soriacebus* and *Carlocebus*) clustered together along with *Paralouatta* and some generalized species (i.e., *Cebus*) (Fig. 6). This can be interpreted according to the two existing competing hypotheses in the following manner. Under the SPH perspective, both the basal fossil platyrrhines and the ancestors of the living NWM would have exhibited a primitive morphology associated with a more 'generalist' arboreal quadrupedalist locomotor behavior. This implies that the fossil forms were adapted to niches in the early Miocene southern forests analogous to those of the ancestral forms of the extant NWM (i.e., a convergence scenario). Another possible interpretation under the SPH perspective is that rather than convergent evolution, the observed morphological pattern could just be the retention of characteristics from an older ancestor. Therefore, even if there was a stem radiation followed by the modern crown radiation, the modern radiation had to come from one of the stem taxa, thus the observed similarity in talar morphology could be merely the retention of ancestral traits. On the other hand, under the LLH, the fact that most fossils exhibit a primitive morphology is explained by noting that these fossils might represent the ancestral forms leading to the extant lineages or members of the same long-lived lineages. It is important to bear in mind that the present study focused on only one anatomical structure, the talus, hence these results are limited and caution is required when extrapolating these results to reconstruct the evolutionary history of platyrrhines.

5. Conclusion

In spite of the numerous studies and decades of research, a comprehensive understanding of the evolutionary history of platyrrhines is still lacking. This is highlighted by the continued debates on the proto-platyrrhine immigration to South America (Houle, 1999; Oliveira et al., 2009; Cachel, 2015), on the issue regarding the SPH and LLH hypotheses (Kay et al., 2008; Kay and Fleagle, 2010; Rosenberger, 2010; Perez and Rosenberger, 2014; Kay, 2015b) and on the phylogenetic position of the genus *Aotus* (Menezes et al., 2010; Rosenberger and Tejedor, 2013; Aristide et al., 2015). Whilst this study does not provide definitive answers to any of these major questions, it does provide additional context. In particular it shows that locomotor behavior has a strong influence on talus morphology and it indicates that the earliest NWM had a

generalized quadrupedal lifestyle as has been previously proposed (e.g., Ford, 1988; Tallman and Cooke, 2016) and that the ancestral platyrrhine was probably medium-sized (reconstructed body mass: 2966 g; 95% LCI: 1623 g; UCI: 4309 g). Platyrrhines subsequently seemed to evolve towards three different selective optima, represented by the three main locomotion habits observed in extant NWM. In addition, new body mass predictions for all the analyzed Miocene platyrrhines were provided, which show that during the Miocene there was already a noticeable size variation. The present work represents a contribution to the understanding of platyrrhine evolution by applying a combination of GM and comparative techniques in order to understand the evolution of one of the best-represented structures in the platyrrhine fossil record, the talus. This allowed not only to reconstruct aspects of the locomotor behavior of fossil individuals, but also provided information about the evolution of the locomotor diversity observed in extant platyrrhines, its relationship with talar size and shape, and its relation with the adaptive radiation that platyrrhines experienced.

Acknowledgments

Supplementary Online Material

Supplementary online material related to this article can be found at http://dx.doi.org/10.1016/j.jhevol.2017.07.015.

References

Adams, D.C., 2014. A method for assessing phylogenetic least squares models for shape and other high-dimensional multivariate data. Evolution 68, 2675—2688.

Adams, D.C., Felice, R.N., 2014. Assessing trait covariation and morphological integration on phylogenies using evolutionary covariance matrices. PLOS ONE 9, 1—8.

Adams, D.C., Otárola-Castillo, E., 2013. Geomorph: an r package for the collection and analysis of geometric morphometric shape data. Methods Ecol. Evol. 4, 393—399.

Allen, K.L., Kay, R.F., 2012. Dietary quality and encephalization in platyrrhine primates. Proc. R. Soc. B 279, 715—721.

Araripe, J., Tagliaro, C.H., Rêgo, P.S., Sampaio, I., Ferrari, S.F., Schneider, H., 2008. Molecular phylogenetics of large-bodied tamarins, Saguinus spp. (Primates, Platyrrhini). Zool. Scr. 37, 461—467.

Aristide, L., Rosenberger, A.L., Tejedor, M.F., Perez, S.I., 2015. Modeling lineage and phenotypic diversification in the New World monkey (Platyrrhini, Primates) radiation. Mol. Phylogenet. Evol. 82, 375—385.

Aristide, L., dos Reis, S.F., Machado, A.C., Lima, I., Lopes, R.T., Perez, S.I., 2016. Brain shape convergence in the adaptive radiation of New World monkeys. Proc. Natl. Acad. Sci. 113, 2158—2163.

Bloch, J.I., Woodruff, E.D., Wood, A.R., Rincon, A.F., Harrington, A.R., Morgan, G.S., Foster, D.A., Montes, C., Jaramillo, C.A., Jud, N.A., Jones, D.S., MacFadden, B.J.,

2016. First North American fossil monkey and early Miocene tropical biotic interchange. Nature 533, 243—246.

Blomberg, S.P., Garland, T., Ives, A.R., 2003. Testing for phylogenetic signal in comparative data: behavioral traits are more labile. Evolution 57, 717—745.

Bond, M., Tejedor, M.F., Campbell Jr., K.E., Chornogubsky, L., Novo, N., Goin, F., 2015. Eocene primates of South America and the African origins of New World monkeys. Nature 520, 538—541.

Bookstein, F.L., 1997. Morphometric Tools for Landmark Data: Geometry and Biology. Cambridge University Press, Cambridge.

Bordas, A., 1942. Anotaciones sobre un "Cebidae" fósil de Patagonia. Physis 19, 265—269.

Bonvicino, C.R., Boubli, J.P., Otazú, I.B., Almeida, F.C., Nascimento, F.F., Coura, J.R., Seuánez, H.N., 2003. Morphologic, karyotypic, and molecular evidence of a new form of Chiropotes (Primates, Pitheciinae). Am. J. Primatol. 61, 123—133.

Boyer, D.M., Seiffert, E.R., 2013. Patterns of astragalar fibular facet orientation in extant and fossil primates and their evolutionary implications. Am. J. Phys. Anthropol. 151, 420—447.

Boyer, D.M., Seiffert, E.R., Simons, E.L., 2010. Astragalar morphology of Afradapis, a large adapiform primate from the earliest late Eocene of Egypt. Am. J. Phys. Anthropol. 143, 383—402.

Boyer, D.M., Yapuncich, G.S., Butler, J.E., Dunn, R.H., Seiffert, E.R., 2015. Evolution of postural diversity in primates as reflected by the size and shape of the medial tibial facet of the talus. Am. J. Phys. Anthropol. 157, 134—177.

Burnham, K.P., Anderson, D.R., 2013. Model Selection and Multimodel Inference: A Practical Information-Theoretic Approach. Springer, New York.

Butler, M.A., King, A.A., 2004. Phylogenetic comparative analysis: a modeling approach for adaptive evolution. Am. Nat. 164, 683—695.

Cachel, S., 2015. Fossil Primates. Cambridge University Press, Cambridge.

Carter, D.R., Fyhrie, D.P., Whalen, R.T., 1987. Trabecular bone density and loading history: regulation of connective tissue biology by mechanical energy. J. Biomech. 20, 785—794.

Ciochon, R.L., Chiarelli, A.B. (Eds.), 1980. Evolutionary Biology of the New World Monkeys and Continental Drift. Springer, New York.

Clavel, J., Escarguel, G., Merceron, G., 2015. mvmorph: an r package for fitting multivariate evolutionary models to morphometric data. Methods Ecol. Evol. 6, 1311—1319.

Conroy, G.C., 1987. Problems of body-weight estimation in fossil primates. Int. J. Primatol. 8, 115—137.

Cooke, S.B., Rosenberger, A.L., Turvey, S., 2011. An extinct monkey from Haiti and the origins of the Greater Antillean primates. Proc. Natl. Acad. Sci. 108, 2699—2704.

Copes, L.E., Lucas, L.M., Thostenson, J.O., Hoekstra, H.E., Boyer, D.M., 2016. A collection of non-human primate computed tomography scans housed in MorphoSource, a repository for 3D data. Sci. Data 3, 160001.

Cressler, C.E., Butler, M.A., King, A.A., 2015. Detecting adaptive evolution in phylogenetic comparative analysis using the Ornstein-Uhlenbeck model. Syst. Biol. 64, 953—968.

Delson, E., Rosenberger, A.L., 1984. Are there any anthropoid primate living fossils? In: Eldredge, N., Stanley, S.M. (Eds.), Living Fossils, Casebooks in Earth Sciences. Springer, New York, pp. 50—61.

de Oliveira, F.B., Molina, E.C., Marroig, G., 2009. Paleogeography of the South Atlantic: a route for primates and rodents into the New World? In: Garber, P.A., Estrada, A., Bicca-Marques, J.C., Heymann, E.W., Strier, K.B. (Eds.), South American Primates, Developments in Primatology: Progress and Prospects. Springer, New York, pp. 55—68.

Felsenstein, J., 1985. Phylogenies and the comparative method. Am. Nat. 125, 1—15.

Fleagle, J.G., 1990. New fossil platyrrhines from the Pinturas Formation, southern Argentina. J. Hum. Evol. 19, 61—85.

Fleagle, J.G., 2013. Primate Adaptation and Evolution, 3rd edition. Academic Press, Amsterdam.

Fleagle, J.G., Bown, T.M., 1983. New primate fossils from late Oligocene (Colhuehuapian) localities of Chubut Province, Argentina. Folia Primatol. 41, 240—266.

Fleagle, J.G., Kay, R.F., 1989. The dental morphology of Dolichocebus-gaimanensis, a fossil monkey from Argentina. Am. J. Phys. Anthropol. 78, 221.

Fleagle, J.G., Kay, R.F., 1994. Anthropoid origins. In: Fleagle, J.G., Kay, R.F. (Eds.), Anthropoid Origins, Advances in Primatology. Springer, New York, pp. 675—698.

Fleagle, J.G., Meldrum, D.J., 1988. Locomotor behavior and skeletal morphology of two sympatric pitheciine monkeys, Pithecia pithecia and Chiropotes satanas. Am. J. Primatol. 16, 227—249.

Fleagle, J.G., Reed, K.E., 1996. Comparing primate communities: a multivariate approach. J. Hum. Evol. 30, 489—510.

Fleagle, J.G., Simons, E.L., 1982. Skeletal remains of Propliopithecus chirobates from the Egyptian Oligocene. Folia Primatol. 39, 161—177.

Fleagle, J.G., Simons, E.L., 1983. The tibio-fibular articulation in Apidium phiomense, an Oligocene anthropoid. Nature 301, 238—239.

Fleagle, J.G., Simons, E.L., 1995. Limb skeleton and locomotor adaptations of Apidium phiomense, an Oligocene anthropoid from Egypt. Am. J. Phys. Anthropol. 97, 235—289.

Fleagle, J.G., Tejedor, M.F., 2002. Early platyrrhines of southern South America. In: Hartwig, W.C. (Ed.), The Primate Fossil Record. Cambridge University Press, Cambridge, pp. 161—174.

Fleagle, J.G., Powers, D.W., Conroy, G.C., Watters, J.P., 1987. New fossil platyrrhines from Santa Cruz province, Argentina. Folia Primatol. 48, 65—77.

Fleagle, J.G., Janson, C., Reed, K., 1999. Primate Communities. Cambridge University Press, Cambridge.

Fleagle, J.G., Perkins, M.E., Heizler, M.T., Nash, B., Bown, T.M., Tauber, A.A., Dozo, M.T., Tejedor, M.F., 2012. Absolute and relative ages of fossil localities in the Santa Cruz and Pinturas Formations. In: Vizcaíno, S.F., Kay, R.F., Bargo, M.S. (Eds.), Early Miocene Paleobiology in Patagonia. Cambridge University Press, New York, pp. 41—58.

Flynn, J.J., Wyss, A.R., Charrier, R., Swisher, C.C., 1995. An Early Miocene anthropoid skull from the Chilean Andes. Nature 373, 603—607.

Ford, S.M., 1988. Postcranial adaptations of the earliest platyrrhine. J. Hum. Evol. 17, 155—192.

Ford, S.M., 1990. Locomotor adaptations of fossil platyrrhines. J. Hum. Evol. 19, 141—173.

Ford, S.M., Davis, L.C., 1992. Systematics and body size: Implications for feeding adaptations in New World monkeys. Am. J. Phys. Anthropol. 88, 415—468.

Freckleton, R.P., Pagel, M., Harvey, P.H., 2003. Comparative methods for adaptive radiations. In: Gaston, K.J., Blackburn, T.M. (Eds.), Macroecology: Concepts and Consequences. Blackwell, Oxford, pp. 391—407.

Gebo, D.L., 1986. Anthropoid origins—the foot evidence. J. Hum. Evol. 15, 421—430.

Gebo, D.L., 1988. Foot morphology and locomotor adaptation in Eocene primates. Folia Primatol. 50, 3—41.

Gebo, D.L., 1989. Postcranial adaptation and evolution in lorisidae. Primates 30, 347—367.

Gebo, D.L., 2011. Vertical clinging and leaping revisited: vertical support use as the ancestral condition of strepsirrhine primates. Am. J. Phys. Anthropol. 146, 323—335.

Gebo, D.L., Simons, E.L., 1987. Morphology and locomotor adaptations of the foot in early Oligocene anthropoids. Am. J. Phys. Anthropol. 74, 83—101.

Gebo, D.L., Dagosto, M., Rosenberger, A.L., Setoguchi, T., 1990. New platyrrhine tali from La Venta, Colombia. J. Hum. Evol. 19, 737—746.

Gebo, D.L., Simons, E.L., Rasmussen, D.T., Dagosto, M., 1994. Eocene anthropoid postcrania from the Eayum, Egypt. In: Fleagle, J.G., Kay, R.F. (Eds.), Anthropoid Origins. Springer, New York, pp. 203—233.

Gebo, D.L., Dagosto, M., Beard, K.C., Qi, T., Wang, J., 2000. The oldest known anthropoid postcranial fossils and the early evolution of higher primates. Nature 404, 276—278.

Gebo, D.L., Dagosto, M., Ni, X., Beard, K.C., 2012. Species diversity and postcranial anatomy of Eocene primates from Shanghuang, China. Evol. Anthropol. 21, 224—238.

Gladman, J.T., Boyer, D.M., Simons, E.L., Seiffert, E.R., 2013. A calcaneus attributable to the primitive late Eocene anthropoid *Proteopithecus sylviae*: Phenetic affinities and phylogenetic implications. Am. J. Phys. Anthropol. 151, 372—397.

Gunz, P., Mitteroecker, P., Neubauer, S., Weber, G.W., Bookstein, F.L., 2009. Principles for the virtual reconstruction of hominin crania. J. Hum. Evol. 57, 48—62.

Halenar, L.B., 2011. Reconstructing the locomotor repertoire of *Protopithecus brasiliensis*. I. Body size. Anat. Rec. 294, 2024—2047.

Hammer, Ø., Harper, D.A.T., 2008. Paleontological Data Analysis. Blackwell, Oxford.

Harmon, L.J., Schulte, J.A., Larson, A., Losos, J.B., 2003. Tempo and mode of evolutionary radiation in iguanian lizards. Science 301, 961—964.

Harmon, L.J., Weir, J.T., Brock, C.D., Glor, R.E., Challenger, W., 2008. GEIGER: investigating evolutionary radiations. Bioinformatics 24, 129—131.

Harmon, L.J., Losos, J.B., Jonathan Davies, T., Gillespie, R.G., Gittleman, J.L., Bryan Jennings, W., Kozak, K.H., McPeek, M.A., Moreno-Roark, F., Near, T.J., Purvis, A., Ricklefs, R.E., Schluter, D., Schulte II, J.A., Seehausen, O., Sidlauskas, B.L., Torres-Carvajal, O., Weir, J.T., Mooers, A.Ø., 2010. Early bursts of body size and shape evolution are rare in comparative data. Evolution 64, 2385—2396.

Hartwig, W.C., Meldrum, D.J., 2002. Miocene platyrrhines of the northern Neotropics. In: Hartwig, W.C. (Ed.), The Primate Fossil Record. Cambridge University Press, Cambridge, pp. 175—188.

Hodgson, J.A., Sterner, K.N., Matthews, L.J., Burrell, A.S., Jani, R.A., Raaum, R.L., Stewart, C.B., Disotell, T.R., 2009. Successive radiations, not stasis, in the South American primate fauna. Proc. Natl. Acad. Sci. 106, 5534—5539.

Hoffstetter, R., 1969. Un primate de l'Oligocene inférieur sudamericain: *Branisella boliviana* gen. et sp. nov. C. R. Acad. Sci. 269, 434—437.

Hoffstetter, R., 1980. Origin and deployment of New World monkeys emphasizing the southern continents route. In: Ciochon, R.L., Chiarelli, A.B. (Eds.), Evolutionary Biology of the New World Monkeys and Continental Drift, Advances in Primatology. Springer, New York, pp. 103—122.

Houle, A., 1999. The origin of platyrrhines: an evaluation of the Antarctic Scenario and the Floating Island Model. Am. J. Phys. Anthropol. 109, 541—559.

Ingram, T., Mahler, D.L., 2013. SURFACE: detecting convergent evolution from comparative data by fitting Ornstein-Uhlenbeck models with stepwise Akaike Information Criterion. Methods Ecol. Evol. 4, 416—425.

Jackson, D.A., 1993. Stopping rules in principal components analysis: a comparison of heuristical and statistical approaches. Ecology 74, 2204—2214.

Kay, R.F., 1990. The phyletic relationships of extant and fossil Pitheciinae (Platyrrhini, Anthropoidea). J. Hum. Evol. 19, 175—208.

Kay, R.F., 2015a. New World monkey origins. Science 347, 1068—1069.

Kay, R.F., 2015b. Biogeography in deep time — What do phylogenetics, geology, and paleoclimate tell us about early platyrrhine evolution? Mol. Phylogenet. Evol. 82, 358—374.

Kay, R.F., Cozzuol, M.A., 2006. New platyrrhine monkeys from the Solimões Formation (late Miocene, Acre State, Brazil). J. Hum. Evol. 50, 673—686.

Kay, R.F., Fleagle, J.G., 2010. Stem taxa, homoplasy, long lineages, and the phylogenetic position of *Dolichocebus*. J. Hum. Evol. 59, 218—222.

Kay, R.F., Johnson, D., Meldrum, D.J., 1998. A new pitheciin primate from the middle Miocene of Argentina. Am. J. Primatol. 45, 317—336.

Kay, R.F., Williams, B.A., Anaya, F., 2002. The adaptations of *Branisella boliviana*, the earliest South American monkey. In: Plavcan, J.M., Kay, R.F., Jungers, W.L., van Schaik, C.P. (Eds.), Reconstructing Behavior in the Primate Fossil Record, Advances in Primatology. Springer, New York, pp. 339—370.

Kay, R.F., Fleagle, J.G., Mitchell, T.R.T., Colbert, M., Bown, T., Powers, D.W., 2008. The anatomy of *Dolichocebus gaimanensis*, a stem platyrrhine monkey from Argentina. J. Hum. Evol. 54, 323—382.

Klingenberg, C.P., Gidaszewski, N.A., 2010. Testing and quantifying phylogenetic signals and homoplasy in morphometric data. Syst. Biol. 59, 245—261.

Lieberman, D.E., Devlin, M.J., Pearson, O.M., 2001. Articular area responses to mechanical loading: effects of exercise, age, and skeletal location. Am. J. Phys. Anthropol. 116, 266—277.

Lisowski, F.P., Albrecht, G.H., Oxnard, C.E., 1974. The form of the talus in some higher primates: A multivariate study. Am. J. Phys. Anthropol. 41, 191—215.

Losos, J., 2011. Lizards in an Evolutionary Tree: Ecology and Adaptive Radiation of Anoles. University of California Press, Berkeley.

Luchterhand, K., Kay, R.F., Madden, R.H., 1986. *Mohanamico hershkovitzi*, gen. et sp. nov., un primate du Miocène moyen d'Amérique du Sud. C. R. Acad. Sci. 303, 1753—1758.

MacPhee, R.D.E., Iturralde-Vinent, M.A., 1995. Earliest monkey from Greater Antilles. J. Hum. Evol. 28, 197—200.

MacPhee, R.D.E., Meldrum, J., 2006. Postcranial remains of the extinct monkeys of the Greater Antilles, with evidence for semiterrestriality in *Paralouatta*. Am. Mus. Novit. 3516, 1—65.

MacPhee, R.D.E., Woods, C.A., 1982. A new fossil cebine from Hispaniola. Am. J. Phys. Anthropol. 58, 419—436.

MacPhee, R.D.E., Iturralde-Vinent, M., Gaffney, E.S., 2003. Domo de Zaza, an Early Miocene vertebrate locality in South-Central Cuba: with notes on the tectonic evolution of Puerto Rico and the Mona passage. Am. Mus. Novit. 3394, 1—42.

Maddison, W.P., 1991. Squared-change parsimony reconstructions of ancestral states for continuous-valued characters on a phylogenetic tree. Syst. Zool. 40, 304—314.

Maddison, W.P., Maddison, D.R., 2017. Mesquite: a modular system for evolutionary analysis. Version 3.2. http://mesquiteproject.org.

Mahler, D.L., Ingram, T., Revell, L.J., Losos, J.B., 2013. Exceptional convergence on the macroevolutionary landscape in island lizard radiations. Science 341, 292—295.

Marivaux, L., Salas-Gismondi, R., Tejada, J., Billet, G., Louterbach, M., Vink, J., Bailleul, J., Roddaz, M., Antoine, P.-O., 2012. A platyrrhine talus from the early Miocene of Peru (Amazonian Madre de Dios Sub-Andean Zone). J. Hum. Evol. 63, 696—703.

Marivaux, L., Adnet, S., Altamirano-Sierra, A.J., Boivin, M., Pujos, F., Ramdarshan, A., Salas-Gismondi, R., Tejada-Lara, J.V., Antoine, P.-O., 2016a. Neotropics provide insights into the emergence of New World monkeys: New dental evidence from the late Oligocene of Peruvian Amazonia. J. Hum. Evol. 97, 159—175.

Marivaux, L., Adnet, S., Altamirano-Sierra, A.J., Pujos, F., Ramdarshan, A., Salas-Gismondi, R., Tejada-Lara, J.V., Antoine, P.-O., 2016b. Dental remains of cebid platyrrhines from the earliest late Miocene of Western Amazonia, Peru: Macroevolutionary implications on the extant capuchin and marmoset lineages. Am. J. Phys. Anthropol. 161, 478—493.

Marroig, G., Cheverud, J.M., 2001. A comparison of phenotypic variation and covariation patterns and the role of phylogeny, ecology, and ontogeny during cranial evolution of New World monkeys. Evolution 55, 2576—2600.

Martins, E.P., Cunningham, C., 1999. Estimation of ancestral states of continuous characters: a computer simulation study. Syst. Biol. 48, 642—650.

Meldrum, D.J., 1990. New fossil platyrrhine tali from the early Miocene of Argentina. Am. J. Phys. Anthropol. 83, 403—418.

Meldrum, D.J., 1993. Postcranial adaptations and positional behavior in fossil platyrrhines. In: Gebo, D.L. (Ed.), Postcranial Adaptations in Nonhuman Primates. Northern Illinois University, DeKalb, pp. 235—251.

Meldrum, D.J., Fleagle, J.G., Kay, R.F., 1990. Partial humeri of two Miocene Colombian primates. Am. J. Phys. Anthropol. 81, 413—422.

Meldrum, D.J., Lemelin, P., 1991. Axial skeleton of *Cebupithecia sarmientoi* (Pitheciinae, Platyrrhini) from the middle Miocene of La Venta, Colombia. Am. J. Primatol. 25, 69—89.

Menezes, A.N., Bonvicino, C.R., Seuánez, H.N., 2010. Identification, classification and evolution of Owl Monkeys (*Aotus*, Illiger 1811). BMC Evol. Biol. 10, 248.

Morales-Jimenez, A.L., Cortés-Ortiz, L., Di Fiore, A., 2015. Phylogenetic relationships of Mesoamerican spider monkeys (*Ateles geoffroyi*): Molecular evidence suggests the need for a revised taxonomy. Mol. Phylogenet. Evol. 82, 484—494.

Nakatsukasa, M., Takai, M., Setoguchi, T., 1997. Functional morphology of the postcranium and locomotor behavior of *Neosaimiri fieldsi*, a *Saimiri*-like Middle Miocene platyrrhine. Am. J. Phys. Anthropol. 102, 515—544.

Norconk, M.A., Wright, B.W., Conklin-Brittain, N.L., Vinyard, C.J., 2009. Mechanical and nutritional properties of food as factors in platyrrhine dietary adaptations. In: Garber, P.A., Estrada, A., Bicca-Marques, J.C., Heymann, E.W., Strier, K.B. (Eds.), South American Primates, Developments in Primatology: Progress and Prospects. Springer, New York, pp. 279—319.

Opazo, J.C., Wildman, D.E., Prychitko, T., Johnson, R.M., Goodman, M., 2006. Phylogenetic relationships and divergence times among New World monkeys (Platyrrhini, Primates). Mol. Phylogenet. Evol. 40, 274—280.

Parr, W.C.H., Chamoli, U., Jones, A., Walsh, W.R., Wroe, S., 2013. Finite element micro-modelling of a human ankle bone reveals the importance of the

trabecular network to mechanical performance: New methods for the generation and comparison of 3D models. J. Biomech. 46, 200—205.

Perez, S.I., Rosenberger, A.L., 2014. The status of platyrrhine phylogeny: A meta-analysis and quantitative appraisal of topological hypotheses. J. Hum. Evol. 76, 177—187.

Perez, S.I., Klaczko, J., Rocatti, G., Dos Reis, S.F., 2011. Patterns of cranial shape diversification during the phylogenetic branching process of New World monkeys (Primates: Platyrrhini). J. Evol. Biol. 24, 1826—1835.

Perkins, M.E., Fleagle, J.G., Heizler, M.T., Nash, B., Bown, T.M., Tauber, A.A., Dozo, M.T., 2012. Tephrochronology of the Miocene Santa Cruz and Pinturas Formations, Argentina. In: Vizcaíno, S.F., Kay, R.F., Bargo, M.S. (Eds.), Early Miocene Paleobiology in Patagonia. Cambridge University Press, New York, pp. 23—40.

R Core Team, 2017. R: A language and environment for statistical computing. R Foundation for Statistical Computing, Vienna.

Reeser, L.A., 1984. Morphological affinities of new fossil talus of *Dolichocebus gaimanensis*. Am. J. Phys. Anthropol. 63, 206—207.

Revell, L.J., 2012. phytools: an R package for phylogenetic comparative biology (and other things). Methods Ecol. Evol. 3, 217—223.

Revell, L.J., 2013. Two new graphical methods for mapping trait evolution on phylogenies. Methods Ecol. Evol. 4, 754—759.

Rímoli, R.O., 1977. Una nueva especie de monos (Cebidae: Saimirinae: Saimiri) de la Hispaniola. Cuadernos del Centro Dominicano de investigaciones antropológicas (CENDIA). Univ. Autón. St. Domingo 242, 1—14.

Rohlf, F.J., Corti, M., 2000. Use of two-block partial least-squares to study covariation in shape. Syst. Biol. 49, 740—753.

Rosenberger, A.L., 1980. Gradistic views and adaptive radiation of platyrrhine primates. Z. Morphol. Anthropol. 71, 157—163.

Rosenberger, A.L., 1981. Systematics: the higher taxa. In: Coimbra-Filho, A.F., Mittermeier, R. (Eds.), Ecology and Behavior of Neotropical Primates, Vol. 1. Academia Brasileira de Ciencias, Rio de Janeiro, pp. 9—27.

Rosenberger, A.L., 1992. Evolution of feeding niches in New World monkeys. Am. J. Phys. Anthropol. 88, 525—562.

Rosenberger, A.L., 2002. Platyrrhine paleontology and systematics: the paradigm shifts. In: Hartwig, W.C. (Ed.), The Primate Fossil Record. Cambridge University Press, pp. 151—159.

Rosenberger, A.L., 2010. Platyrrhines, PAUP, parallelism, and the Long Lineage Hypothesis: A reply to Kay et al. (2008). J. Hum. Evol. 59, 214—217.

Rosenberger, A.L., Tejedor, M.F., 2013. The misbegotten: long lineages, long branches and the interrelationships of *Aotus, Callicebus* and the saki-uacaris. In: Barnett, A., Viega, L., Ferrari, S., Norconk, M. (Eds.), Evolutionary Biology and Conservation of Titis, Sakis and Uacaris. Cambridge University Press, Cambridge, pp. 13—22.

Rosenberger, A.L., Setoguchi, T., Shigehara, N., 1990. The fossil record of callitrichine primates. J. Hum. Evol. 19, 209—236.

Rosenberger, A.L., Hartwig, W.C., Wolff, R.G., 1991. *Szalatavus attricuspis*, an early platyrrhine primate. Folia Primatol. 56, 225—233.

Rosenberger, A.L., Tejedor, M.F., Cooke, S.B., Pekar, S., 2009. Platyrrhine ecophylogenetics in space and time. In: Garber, P.A., Estrada, A., Bicca-Marques, J.C., Heymann, E.W., Strier, K.B. (Eds.), South American Primates, Developments in Primatology: Progress and Prospects. Springer, New York, pp. 69—113.

Rosenberger, A.L., Cooke, S.B., Rímoli, R., Ni, X., Cardoso, L., 2011. First skull of *Antillothrix bernensis*, an extinct relict monkey from the Dominican Republic. Proc. R. Soc. B 278, 67—74.

Ryan, T.M., Silcox, M.T., Walker, A., Mao, X., Begun, D.R., Benefit, B.R., Gingerich, P.D., Köhler, M., Kordos, L., McCrossin, M.L., Moyà-Solà, S., Sanders, W.J., Seiffert, E.R., Simons, E., Zalmout, I.S., Spoor, F., 2012. Evolution of locomotion in Anthropoidea: the semicircular canal evidence. Proc. R. Soc. B 279, 3467—3475.

Rylands, A.B., Mittermeier, R.A., 2009. The diversity of the New World primates (Platyrrhini): an annotated taxonomy. In: Garber, P.A., Estrada, A., Bicca-Marques, J.C., Heymann, E.W., Strier, K.B. (Eds.), South American Primates, Developments in Primatology: Progress and Prospects. Springer, New York, pp. 23—54.

Schluter, D., 2000. The Ecology of Adaptive Radiation. Oxford University Press, Oxford.

Schneider, H., Canavez, F.C., Sampaio, I., Moreira, M.Â.M., Tagliaro, C.H., Seuánez, H.N., 2001. Can molecular data place each neotropical monkey in its own branch? Chromosoma 109, 515—523.

Schrago, C.G., 2007. On the time scale of new world primate diversification. Am. J. Phys. Anthropol. 132, 344—354.

Seiffert, E.R., Simons, E.L., Fleagle, J.G., 2000. Anthropoid humeri from the late Eocene of Egypt. Proc. Natl. Acad. Sci. 97, 10062—10067.

Sena, L., Vallinoto, M., Sampaio, I., Schneider, H., Ferrari, S.F., Cruz Schneider, M.P., 2002. Mitochondrial COII gene sequences provide new insights into the phylogeny of marmoset species groups (Callitrichidae, Primates). Folia Primatol. 73, 240—251.

Setoguchi, T., Rosenberger, A.L., 1987. A fossil owl monkey from La Venta, Colombia. Nature 326, 692—694.

Simons, E.L., 1989. Description of two genera and species of late Eocene Anthropoidea from Egypt. Proc. Natl. Acad. Sci. 86, 9956—9960.

Simons, E.L., 1997. Preliminary description of the cranium of *Proteopithecus sylviae*, an Egyptian late Eocene anthropoidean primate. Proc. Natl. Acad. Sci. 94, 14970—14975.

Simons, E.L., 2004. The cranium and adaptations of *Parapithecus grangeri*, a stem anthropoid from the Fayum Oligocene of Egypt. In: Ross, C.F., Kay, R.F. (Eds.), Anthropoid Origins, Developments in Primatology: Progress and Prospects. Springer, New York, pp. 183—204.

Simons, E.L., Seiffert, E.R., 1999. A partial skeleton of *Proteopithecus sylviae* (Primates, Anthropoidea): first associated dental and postcranial remains of an Eocene anthropoidean. C. R. Acad. Sci. 329, 921—927.

Schlager, S., 2017. Morpho and Rvcg — Shape Analysis in R. In: Zheng, G., Li, S., Szekely, G. (Eds.), Statistical Shape and Deformation Analysis. Academic Press, Cambridge, pp. 217—256.

Smith, R.J., Jungers, W.L., 1997. Body mass in comparative primatology. J. Hum. Evol. 32, 523—559.

Stayton, C.T., 2015. The definition, recognition, and interpretation of convergent evolution, and two new measures for quantifying and assessing the significance of convergence. Evolution 69, 2140—2153.

Stirton, R.A., 1951. Ceboid Monkeys from the Miocene of Colombia. University of California Press, Berkeley.

Szalay, F.S., Delson, E., 1979. Evolutionary History of the Primates. Academic Press, New York.

Takai, M., 1994. New specimens of *Neosaimiri fieldsi* from La Venta, Colombia: a middle Miocene ancestor of the living squirrel monkeys. J. Hum. Evol. 27, 329—360.

Takai, M., Anaya, F., 1996. New specimens of the oldest fossil platyrrhine, *Branisella boliviana*, from Salla, Bolivia. Am. J. Phys. Anthropol. 99, 301—317.

Takai, M., Anaya, F., Shigehara, N., Setoguchi, T., 2000. New fossil materials of the earliest new world monkey, *Branisella boliviana*, and the problem of platyrrhine origins. Am. J. Phys. Anthropol. 111, 263—281.

Tallman, M., Cooke, S.B., 2016. New endemic platyrrhine humerus from Haiti and the evolution of the Greater Antillean platyrrhines. J. Hum. Evol. 91, 144—166.

Tejedor, M.F., 2002. Primate canines from the early Miocene Pinturas Formation, Southern Argentina. J. Hum. Evol. 43, 127—141.

Tejedor, M.F., 2003. New fossil primate from Chile. J. Hum. Evol. 44, 515—520.

Tejedor, M.F., 2005a. New fossil platyrrhine from Argentina. Folia Primatol. 76, 146—150.

Tejedor, M.F., 2005b. New specimens of *Soriacebus adrianae* Fleagle, 1990, with comments on pitheciin primates from the Miocene of Patagonia. Ameghiniana 42, 249—251.

Tejedor, M.F., 2008. The origin and evolution of Neotropical Primates. Arq. Mus. Nac. 66, 251—269.

Tejedor, M.F., Tauber, A.A., Rosenberger, A.L., Swisher, C.C., Palacios, M.E., 2006. New primate genus from the Miocene of Argentina. Proc. Natl. Acad. Sci. 103, 5437—5441.

Turley, K., Frost, S.R., 2013. The shape and presentation of the catarrhine talus: a geometric morphometric analysis. Anat. Rec. 296, 877—890.

Turner, C.H., 1998. Three rules for bone adaptation to mechanical stimuli. Bone 23, 399—407.

Walker, S.E., 2005. Leaping behavior of *Pithecia pithecia* and *Chiropotes satanas* in eastern Venezuela. Am. J. Primatol. 66, 369—387.

Wildman, D.E., Jameson, N.M., Opazo, J.C., Yi, S.V., 2009. A fully resolved genus level phylogeny of neotropical primates (Platyrrhini). Mol. Phylogenet. Evol. 53, 694—702.

Wiley, D.F., Amenta, N., Alcantara, D.A., Ghost, D., Kil, Y.J., Delson, E., Harcourt-Smith, W., Rohlf, F.J., St John, K., Hamann, B., 2005. Evolutionary morphing. Proc. IEEE Vis. 2005, 431—438.

Wilson, L.A.B., Colombo, M., Sánchez-Villagra, M.R., Salzburger, W., 2015. Evolution of opercle shape in cichlid fishes from Lake Tanganyika — adaptive trait interactions in extant and extinct species flocks. Sci. Rep. 5, 16909.

Wolff, R.G., 1984. New specimens of the primate *Branisella boliviana* from the early Oligocene of Salla, Bolivia. J. Vertebr. Paleontol. 4, 570—574.

Yapuncich, G.S., Boyer, D.M., 2014. Interspecific scaling patterns of talar articular surfaces within primates and their closest living relatives. J. Anat. 224, 150—172.

Yapuncich, G.S., Gladman, J.T., Boyer, D.M., 2015. Predicting euarchontan body mass: A comparison of tarsal and dental variables. Am. J. Phys. Anthropol. 157, 472—506.

Youlatos, D., 2004. Multivariate analysis of organismal and habitat parameters in two neotropical primate communities. Am. J. Phys. Anthropol. 123, 181—194.

Youlatos, D., Meldrum, J., 2011. Locomotor diversification in New World monkeys: running, climbing, or clawing along evolutionary branches. Anat. Rec. 294, 1991—2012.

Zadpoor, A.A., Campoli, G., Weinans, H., 2012. Neural network prediction of load from the morphology of trabecular bone. Appl. Math. Model. 37, 5260—5276.

4.8 Supporting information

(S1) Further details about the sample

(S2) Fossil missing landmarks

(S3) Phylogeny used in the comparative analyses

(S4) Alternative OU models tested in the evolutionary modeling section

(S5) Sample used in the mass regressions

(S6) PC loadings and PLS singular vectors for the locomotor mode percentages (LMPs)

(S7) SURFACE method result

These supplementary materials can also be found in a slightly different format at: http://dx.doi.org/10.1016/j.jhevol.2017.07.015.

4.8.1 Supporting information 1. Table 4.7 Sample details

Id	Species	Genus	Status	Family	Subfamily	Sex	Museum
Dolichocebus_gaimanensis_MACN-362_M4567-4160	*Dolichocebus gaimanensis*	*Dolichocebus*	Extinct	?	?	?	Museo Argentino de Ciencias Naturales, Buenos Aires
Madre_de_Dios_MUSM_2024	?	?	Extinct	?	?	?	Museo de Historia Natural, Lima, Peru
Rio_Cisnes_SGO.PV_974	?	?	Extinct	?	?	?	Museo de Nacional de Historia Natural,Santiago, Chile
Cebupithecia_sarmientoi_UCMP-38762_M17135-1560	*Cebupithecia sarmientoi*	*Cebupithecia*	Extinct	?	?	?	University of California, Berkeley Museum of Paleontology, Berkeley, USA
Alouatta_caraya_AMNH211510	*Alouatta caraya*	*Alouatta*	Extant	Atelidae	Alouattinae	Male	American Museum of Natural History
Alouatta_caraya_AMNH211512	*Alouatta caraya*	*Alouatta*	Extant	Atelidae	Alouattinae	Female	American Museum of Natural History
Alouatta_caraya_AMNH211512	*Alouatta caraya*	*Alouatta*	Extant	Atelidae	Alouattinae	Female	American Museum of Natural History
Alouatta_caraya_AMNH211517	*Alouatta caraya*	*Alouatta*	Extant	Atelidae	Alouattinae	Male	American Museum of Natural History
Alouatta_caraya_AMNH211519	*Alouatta caraya*	*Alouatta*	Extant	Atelidae	Alouattinae	Male	American Museum of Natural History
Alouatta_caraya_AMNH211520	*Alouatta caraya*	*Alouatta*	Extant	Atelidae	Alouattinae	Female	American Museum of Natural History

150

Specimen	Species	Genus	Status	Family	Subfamily	Sex	Institution
Alouatta_caraya_AMNH211521	Alouatta caraya	Alouatta	Extant	Atelidae	Alouattinae	Male	American Museum of Natural History
Alouatta_caraya_AMNH211522	Alouatta caraya	Alouatta	Extant	Atelidae	Alouattinae	Female	American Museum of Natural History
Alouatta_caraya_AMNH211523	Alouatta caraya	Alouatta	Extant	Atelidae	Alouattinae	Male	American Museum of Natural History
Alouatta_caraya_AMNH211524	Alouatta caraya	Alouatta	Extant	Atelidae	Alouattinae	Female	American Museum of Natural History
Alouatta_caraya_AMNH215060	Alouatta caraya	Alouatta	Extant	Atelidae	Alouattinae	Female	American Museum of Natural History
Alouatta_seniculus_AMNH23351	Alouatta seniculus	Alouatta	Extant	Atelidae	Alouattinae	?	American Museum of Natural History
Alouatta_seniculus_AMNH23549	Alouatta seniculus	Alouatta	Extant	Atelidae	Alouattinae	Male	American Museum of Natural History
Alouatta_seniculus_AMNH42316	Alouatta seniculus	Alouatta	Extant	Atelidae	Alouattinae	Female	American Museum of Natural History
Alouatta_seniculus_AMNH132790	Alouatta seniculus	Alouatta	Extant	Atelidae	Alouattinae	Male	American Museum of Natural History
Alouatta_seniculus_AMNH187994	Alouatta seniculus	Alouatta	Extant	Atelidae	Alouattinae	?	American Museum of Natural History
Alouatta_seniculus_AMNH188006	Alouatta seniculus	Alouatta	Extant	Atelidae	Alouattinae	Female	American Museum of Natural History
Alouatta_seniculus_AMNH211531	Alouatta seniculus	Alouatta	Extant	Atelidae	Alouattinae	Female	American Museum of Natural History
Alouatta_seniculus_AMNH211535	Alouatta seniculus	Alouatta	Extant	Atelidae	Alouattinae	Female	American Museum of Natural History

Specimen	Species	Genus	Status	Family	Subfamily	Sex	Institution
Alouatta_seniculus_AMNH211538	*Alouatta seniculus*	*Alouatta*	Extant	Atelidae	Alouattinae	Female	American Museum of Natural History
Alouatta_seniculus_AMNH211542	*Alouatta seniculus*	*Alouatta*	Extant	Atelidae	Alouattinae	Male	American Museum of Natural History
Ateles_belzebul_AMNH95040	*Ateles belzebul*	*Ateles*	Extant	Atelidae	Atelinae	Male	American Museum of Natural History
Ateles_belzebul_AMNH95042	*Ateles belzebul*	*Ateles*	Extant	Atelidae	Atelinae	Male	American Museum of Natural History
Ateles_belzebul_AMNH30192	*Ateles belzebul*	*Ateles*	Extant	Atelidae	Atelinae	Male	American Museum of Natural History
Ateles_belzebul_AMNH188126	*Ateles belzebul*	*Ateles*	Extant	Atelidae	Atelinae	Female	American Museum of Natural History
Ateles_belzebul_AMNH201294	*Ateles belzebul*	*Ateles*	Extant	Atelidae	Atelinae	Female	American Museum of Natural History
Ateles_geoffroyi_AMNH28420	*Ateles geoffroyi*	*Ateles*	Extant	Atelidae	Atelinae	Male	American Museum of Natural History
Ateles_geoffroyi_AMNH172985	*Ateles geoffroyi*	*Ateles*	Extant	Atelidae	Atelinae	?	American Museum of Natural History
Ateles_marginatus_AMNH95041	*Ateles marginatus*	*Ateles*	Extant	Atelidae	Atelinae	Female	American Museum of Natural History
Lagothrix_lagotricha_AMNH188162	*Lagothrix lagotricha*	*Lagothrix*	Extant	Atelidae	Atelinae	Female	American Museum of Natural History
Lagothrix_lagotricha_USNM397392	*Lagothrix lagotricha*	*Lagothrix*	Extant	Atelidae	Atelinae	?	National Museum of Natural History; Smithsonian Institution

Specimen	Species	Genus	Status	Family	Subfamily	Sex	Institution
Lagothrix_lagotricha_USNM538105	*Lagothrix lagotricha*	*Lagothrix*	Extant	Atelidae	Atelinae	Female	National Museum of Natural History; Smithsonian Institution
Lagothrix_sp_AMNH201554	*Lagothrix sp.*	*Lagothrix*	Extant	Atelidae	Atelinae	?	National Museum of Natural History; Smithsonian Institution
Lagothrix_sp_AMNH238487	*Lagothrix sp.*	*Lagothrix*	Extant	Atelidae	Atelinae	Male	American Museum of Natural History
Aotus_azarae_AMNH211458	*Aotus azarae*	*Aotus*	Extant	Cebidae	Cebinae	Male	American Museum of Natural History
Aotus_azarae_AMNH211459	*Aotus azarae*	*Aotus*	Extant	Cebidae	Cebinae	Male	American Museum of Natural History
Aotus_azarae_AMNH211476	*Aotus azarae*	*Aotus*	Extant	Cebidae	Cebinae	Female	American Museum of Natural History
Aotus_azarae_AMNH211478	*Aotus azarae*	*Aotus*	Extant	Cebidae	Cebinae	Female	American Museum of Natural History
Aotus_azarae_AMNH211479	*Aotus azarae*	*Aotus*	Extant	Cebidae	Cebinae	Female	American Museum of Natural History
Aotus_azarae_AMNH211480	*Aotus azarae*	*Aotus*	Extant	Cebidae	Cebinae	Female	American Museum of Natural History
Aotus_azarae_AMNH211481	*Aotus azarae*	*Aotus*	Extant	Cebidae	Cebinae	Female	American Museum of Natural History
Aotus_azarae_AMNH211486	*Aotus azarae*	*Aotus*	Extant	Cebidae	Cebinae	Male	American Museum of Natural History
Aotus_azarae_AMNH215051	*Aotus azarae*	*Aotus*	Extant	Cebidae	Cebinae	Male	American Museum of Natural History

Specimen	Species	Genus	Status	Family	Subfamily	Sex	Institution
Aotus_azarae_AMNH215052	*Aotus azarae*	*Aotus*	Extant	Cebidae	Cebinae	Male	American Museum of Natural History
Aotus_azarae_AMNH215053	*Aotus azarae*	*Aotus*	Extant	Cebidae	Cebinae	Female	American Museum of Natural History
Aotus_azarae_AMNH215054	*Aotus azarae*	*Aotus*	Extant	Cebidae	Cebinae	Male	American Museum of Natural History
Aotus_azarae_AMNH215056	*Aotus azarae*	*Aotus*	Extant	Cebidae	Cebinae	Female	American Museum of Natural History
Aotus_azarae_AMNH215057	*Aotus azarae*	*Aotus*	Extant	Cebidae	Cebinae	Male	American Museum of Natural History
Aotus_azarae_AMNH215059	*Aotus azarae*	*Aotus*	Extant	Cebidae	Cebinae	Male	American Museum of Natural History
Aotus_nancymaae_AMNH239852	*Aotus nancymaae*	*Aotus*	Extant	Cebidae	Cebinae	Female	American Museum of Natural History
Aotus_spNig_AMNH209916	*Aotus sp.*	*Aotus*	Extant	Cebidae	Cebinae	Female	American Museum of Natural History
Aotus_trivirgatus_AMNH187963	*Aotus trivirgatus*	*Aotus*	Extant	Cebidae	Cebinae	Female	American Museum of Natural History
Aotus_trivirgatus_AMNH187967	*Aotus trivirgatus*	*Aotus*	Extant	Cebidae	Cebinae	Male	American Museum of Natural History
Cebus_albifrons_AMNH188018	*Cebus albifrons*	*Cebus*	Extant	Cebidae	Cebinae	Female	American Museum of Natural History
Cebus_albifrons_AMNH209923	*Cebus albifrons*	*Cebus*	Extant	Cebidae	Cebinae	Female	American Museum of Natural History
Cebus_albifrons_AMNH209924	*Cebus albifrons*	*Cebus*	Extant	Cebidae	Cebinae	Male	American Museum of Natural History

Specimen	Species	Genus	Status	Family	Subfamily	Sex	Institution
Cebus_albifrons_AMNH211547	*Cebus albifrons*	*Cebus*	Extant	Cebidae	Cebinae	Male	American Museum of Natural History
Cebus_albifrons_AMNH211567	*Cebus albifrons*	*Cebus*	Extant	Cebidae	Cebinae	Male	American Museum of Natural History
Cebus_albifrons_AMNH211582	*Cebus albifrons*	*Cebus*	Extant	Cebidae	Cebinae	Female	American Museum of Natural History
Cebus_albifrons_AMNH211589	*Cebus albifrons*	*Cebus*	Extant	Cebidae	Cebinae	Female	American Museum of Natural History
Cebus_apella_AMNH133607	*Cebus apella*	*Cebus*	Extant	Cebidae	Cebinae	Male	American Museum of Natural History
Cebus_apella_AMNH133607	*Cebus apella*	*Cebus*	Extant	Cebidae	Cebinae	Male	American Museum of Natural History
Cebus_apella_AMNH133608	*Cebus apella*	*Cebus*	Extant	Cebidae	Cebinae	Female	American Museum of Natural History
Cebus_apella_AMNH133647	*Cebus apella*	*Cebus*	Extant	Cebidae	Cebinae	Female	American Museum of Natural History
Cebus_apella_AMNH133656	*Cebus apella*	*Cebus*	Extant	Cebidae	Cebinae	Male	American Museum of Natural History
Cebus_apella_AMNH133660	*Cebus apella*	*Cebus*	Extant	Cebidae	Cebinae	Female	American Museum of Natural History
Cebus_apella_AMNH133671	*Cebus apella*	*Cebus*	Extant	Cebidae	Cebinae	Female	American Museum of Natural History
Cebus_apella_AMNH133681	*Cebus apella*	*Cebus*	Extant	Cebidae	Cebinae	Female	American Museum of Natural History
Cebus_apella_AMNH133764	*Cebus apella*	*Cebus*	Extant	Cebidae	Cebinae	Female	American Museum of Natural History

Specimen	Species	Genus	Status	Family	Subfamily	Sex	Institution
Cebus_apella_AMNH133815	*Cebus apella*	*Cebus*	Extant	Cebidae	Cebinae	Male	American Museum of Natural History
Cebus_apella_AMNH133851	*Cebus apella*	*Cebus*	Extant	Cebidae	Cebinae	Male	American Museum of Natural History
Cebus_olivaceus_AMNH30196	*Cebus olivaceus*	*Cebus*	Extant	Cebidae	Cebinae	Female	American Museum of Natural History
Cebus_olivaceus_AMNH30200	*Cebus olivaceus*	*Cebus*	Extant	Cebidae	Cebinae	?	American Museum of Natural History
Cebus_olivaceus_AMNH42873	*Cebus olivaceus*	*Cebus*	Extant	Cebidae	Cebinae	Female	American Museum of Natural History
Saimiri_boliviensis_AMNH211596	*Saimiri boliviensis*	*Saimiri*	Extant	Cebidae	Cebinae	Male	American Museum of Natural History
Saimiri_boliviensis_AMNH211597	*Saimiri boliviensis*	*Saimiri*	Extant	Cebidae	Cebinae	Male	American Museum of Natural History
Saimiri_boliviensis_AMNH211598	*Saimiri boliviensis*	*Saimiri*	Extant	Cebidae	Cebinae	Male	American Museum of Natural History
Saimiri_boliviensis_AMNH211600	*Saimiri boliviensis*	*Saimiri*	Extant	Cebidae	Cebinae	Male	American Museum of Natural History
Saimiri_boliviensis_AMNH211609	*Saimiri boliviensis*	*Saimiri*	Extant	Cebidae	Cebinae	Female	American Museum of Natural History
Saimiri_boliviensis_AMNH211623	*Saimiri boliviensis*	*Saimiri*	Extant	Cebidae	Cebinae	Male	American Museum of Natural History
Saimiri_boliviensis_AMNH211633	*Saimiri boliviensis*	*Saimiri*	Extant	Cebidae	Cebinae	Male	American Museum of Natural History
Saimiri_boliviensis_AMNH255858	*Saimiri boliviensis*	*Saimiri*	Extant	Cebidae	Cebinae	Male	American Museum of Natural History

Specimen	Species	Genus	Status	Family	Subfamily	Sex	Institution
Saimiri_boliviensis_AMNH255858	*Saimiri boliviensis*	*Saimiri*	Extant	Cebidae	Cebinae	Male	American Museum of Natural History
Saimiri_sciureus_AMNH136214	*Saimiri sciureus*	*Saimiri*	Extant	Cebidae	Cebinae	Female	American Museum of Natural History
Saimiri_sciureus_AMNH188080	*Saimiri sciureus*	*Saimiri*	Extant	Cebidae	Cebinae	Female	American Museum of Natural History
Saimiri_sciureus_AMNH188086	*Saimiri sciureus*	*Saimiri*	Extant	Cebidae	Cebinae	Female	American Museum of Natural History
Saimiri_sciureus_AMNH188089	*Saimiri sciureus*	*Saimiri*	Extant	Cebidae	Cebinae	Female	American Museum of Natural History
Saimiri_sciureus_AMNH188091	*Saimiri sciureus*	*Saimiri*	Extant	Cebidae	Cebinae	Female	American Museum of Natural History
Saimiri_sp_AMNH188097	*Saimiri sp.*	*Saimiri*	Extant	Cebidae	Cebinae	Male	American Museum of Natural History
Saimiri_sp_AMNH188109	*Saimiri sp.*	*Saimiri*	Extant	Cebidae	Cebinae	Female	American Museum of Natural History
Callimico_goeldii_USNM303323	*Callimico goeldii*	*Callimico*	Extant	Cebidae	Callithrichinae	Male	American Museum of Natural History
Callimico_goeldii_USNM395455	*Callimico goeldii*	*Callimico*	Extant	Cebidae	Callithrichinae	Male	National Museum of Natural History; Smithsonian Institution
Callimico_goeldii_USNM463933	*Callimico goeldii*	*Callimico*	Extant	Cebidae	Callithrichinae	Female	National Museum of Natural History; Smithsonian Institution

Specimen	Species	Genus	Status	Family	Subfamily	Sex	Institution
Callimico_goeldii_USNM464991	*Callimico goeldii*	*Callimico*	Extant	Cebidae	Callithrichinae	Female	National Museum of Natural History; Smithsonian Institution
Callimico_goeldii_USNM575153	*Callimico goeldii*	*Callimico*	Extant	Cebidae	Callithrichinae	Female	National Museum of Natural History; Smithsonian Institution
Callithrix_argentata_USNM399069	*Mico argentatus*	*Callithrix*	Extant	Cebidae	Callithrichinae	Male	National Museum of Natural History; Smithsonian Institution
Callithrix_geoffroyi_USNM518553	*Callithrix geoffroyi*	*Callithrix*	Extant	Cebidae	Callithrichinae	Female	National Museum of Natural History; Smithsonian Institution
Callithrix_geoffroyi_USNM582900	*Callithrix geoffroyi*	*Callithrix*	Extant	Cebidae	Callithrichinae	Male	National Museum of Natural History; Smithsonian Institution
Callithrix_jacchus_AMNH14011	*Callithrix jacchus*	*Callithrix*	Extant	Cebidae	Callithrichinae	Male	National Museum of Natural History; Smithsonian Institution
Callithrix_jacchus_AMNH133688	*Callithrix jacchus*	*Callithrix*	Extant	Cebidae	Callithrichinae	Female	National Museum of Natural History; Smithsonian Institution
Callithrix_jacchus_USNM398848	*Callithrix jacchus*	*Callithrix*	Extant	Cebidae	Callithrichinae	Female	National Museum of Natural History; Smithsonian Institution

Specimen	Species	Genus	Status	Family	Subfamily	Sex	Institution
Callithrix_jacchus_USNM399034	*Callithrix jacchus*	*Callithrix*	Extant	Cebidae	Callithrichinae	Male	National Museum of Natural History; Smithsonian Institution
Callithrix_jacchus_USNM399036	*Callithrix jacchus*	*Callithrix*	Extant	Cebidae	Callithrichinae	Female	National Museum of Natural History; Smithsonian Institution
Callithrix_jacchus_USNM399037	*Callithrix jacchus*	*Callithrix*	Extant	Cebidae	Callithrichinae	Male	National Museum of Natural History; Smithsonian Institution
Callithrix_melanura_USNM574137	*Mico melanurus*	*Callithrix*	Extant	Cebidae	Callithrichinae	Female	National Museum of Natural History; Smithsonian Institution
Callithrix_penicillata_AMNH133692	*Callithrix penicillata*	*Callithrix*	Extant	Cebidae	Callithrichinae	Female	National Museum of Natural History; Smithsonian Institution
Callithrix_sp_AMNH17574	*Callithrix sp.*	*Callithrix*	Extant	Cebidae	Callithrichinae	Female	American Museum of Natural History
Callithrix_sp_AMNH22994	*Callithrix sp.*	*Callithrix*	Extant	Cebidae	Callithrichinae	?	American Museum of Natural History
Callithrix_sp_AMNH95127	*Callithrix sp.*	*Callithrix*	Extant	Cebidae	Callithrichinae	Male	American Museum of Natural History
Cebuella_pygmaea_USNM303037	*Cebuella pygmaea*	*Cebuella*	Extant	Cebidae	Callithrichinae	Male	National Museum of Natural History; Smithsonian Institution

Specimen	Species	Genus		Family	Subfamily	Sex	Institution
Cebuella_pygmaea_USNM336325	*Cebuella pygmaea*	*Cebuella*	Extant	Cebidae	Callithrichinae	Male	National Museum of Natural History; Smithsonian Institution
Leontopithecus_rosalia_AMNH137279	*Leontopithecus rosalia*	*Leontopithecus*	Extant	Cebidae	Callithrichinae	?	American Museum of Natural History
Leontopithecus_rosalia_USNM588152	*Leontopithecus rosalia*	*Leontopithecus*	Extant	Cebidae	Callithrichinae	Male	National Museum of Natural History; Smithsonian Institution
Leontopithecus_rosalia_USNM588176	*Leontopithecus rosalia*	*Leontopithecus*	Extant	Cebidae	Callithrichinae	Female	National Museum of Natural History; Smithsonian Institution
Leontopithecus_rosalia_USNM588334	*Leontopithecus rosalia*	*Leontopithecus*	Extant	Cebidae	Callithrichinae	Female	National Museum of Natural History; Smithsonian Institution
Leontopithecus_rosalia_USNM597831	*Leontopithecus rosalia*	*Leontopithecus*	Extant	Cebidae	Callithrichinae	Female	National Museum of Natural History; Smithsonian Institution
Saguinus_fuscicollis_AMNH147433	*Saguinus fuscicollis*	*Saguinus*	Extant	Cebidae	Callithrichinae	?	American Museum of Natural History
Saguinus_leucopus_AMNH148322	*Saguinus leucopus*	*Saguinus*	Extant	Cebidae	Callithrichinae	Female	American Museum of Natural History
Saguinus_midas_AMNH77693	*Saguinus midas*	*Saguinus*	Extant	Cebidae	Callithrichinae	?	American Museum of Natural History
Saguinus_midas_AMNH148453	*Saguinus midas*	*Saguinus*	Extant	Cebidae	Callithrichinae	?	American Museum of Natural History

Specimen	Genus species	Genus	Status	Family	Subfamily	Sex	Institution
Saguinus_midas_AMNH266480		Saguinus	Extant	Cebidae	Callithrichinae	Female	American Museum of Natural History
Saguinus_mystax_AMNH180091	Saguinus mystax	Saguinus	Extant	Cebidae	Callithrichinae	?	American Museum of Natural History
Saguinus_mystax_AMNH188171	Saguinus mystax	Saguinus	Extant	Cebidae	Callithrichinae	Male	American Museum of Natural History
Saguinus_mystax_AMNH188178	Saguinus mystax	Saguinus	Extant	Cebidae	Callithrichinae	Female	American Museum of Natural History
Saguinus_mystax_AMNH188179	Saguinus mystax	Saguinus	Extant	Cebidae	Callithrichinae	Male	American Museum of Natural History
Carlocebus_carmenensis_MACN-271_M7305-8171	Carlocebus carmenensis	Carlocebus	Extinct	?	?	?	Museo Argentino de Ciencias Naturales, Buenos Aires
Carlocebus_carmenensis_MACN-304_M7306-8172	Carlocebus carmenensis	Carlocebus	Extinct	?	?	?	Museo Argentino de Ciencias Naturales, Buenos Aires
Carlocebus_carmenensis_MACN-368_M7307-8173	Carlocebus carmenensis	Carlocebus	Extinct	?	?	?	Museo Argentino de Ciencias Naturales, Buenos Aires
Carlocebus_carmenensis_MACN-396_M7308-8174	Carlocebus carmenensis	Carlocebus	Extinct	?	?	?	Museo Argentino de Ciencias Naturales, Buenos Aires
Soriacebus_ameghinorum_MACN-397_M7309-8175	Soriacebus ameghinorum	Soriacebus	Extinct	?	?	?	Museo Argentino de Ciencias Naturales, Buenos Aires
Cacajao_calvus_USNM302626	Cacajao calvus	Cacajao	Extant	Pithecidae	Pitheciinae	Male	National Museum of Natural History; Smithsonian Institution

Cacajao_calvus_USNM302627	*Cacajao calvus*	*Cacajao*	Extant	Pitheciidae	Pitheciinae	Female	National Museum of Natural History; Smithsonian Institution
Cacajao_calvus_USNM302627	*Cacajao calvus*	*Cacajao*	Extant	Pitheciidae	Pitheciinae	Female	National Museum of Natural History; Smithsonian Institution
Cacajao_calvus_USNM319516	*Cacajao calvus*	*Cacajao*	Extant	Pitheciidae	Pitheciinae	Male	National Museum of Natural History; Smithsonian Institution
Cacajao_calvus_USNM395027	*Cacajao calvus*	*Cacajao*	Extant	Pitheciidae	Pitheciinae	Female	National Museum of Natural History; Smithsonian Institution
Cacajao_calvus_USNM519570	*Cacajao calvus*	*Cacajao*	Extant	Pitheciidae	Pitheciinae	Female	National Museum of Natural History; Smithsonian Institution
Callicebus_cupreus_AMNH130361	*Callicebus cupreus*	*Callicebus*	Extant	Pitheciidae	Callicebinae	Female	American Museum of Natural History
Callicebus_cupreus_AMNH136208	*Callicebus cupreus*	*Callicebus*	Extant	Pitheciidae	Callicebinae	Male	American Museum of Natural History
p_Callicebus_cupreus_AMNH136217_M_astR_ctA	*Callicebus cupreus*	*Callicebus*	Extant	Pitheciidae	Callicebinae	Male	American Museum of Natural History
p_Callicebus_donacophilus_AMNH211487_M_astR_ctA	*Callicebus donacophilus*	*Callicebus*	Extant	Pitheciidae	Callicebinae	Male	American Museum of Natural History

162

Specimen	Species	Genus	Status	Family	Subfamily	Sex	Institution
p_Callicebus_donacophilus_AMNH211489_F_astR_ctA	*Callicebus donacophilus*	*Callicebus*	Extant	Pithecidae	Callicebinae	Female	American Museum of Natural History
p_Callicebus_donacophilus_AMNH211492_M_astR_ctA	*Callicebus donacophilus*	*Callicebus*	Extant	Pithecidae	Callicebinae	Male	American Museum of Natural History
p_Callicebus_moloch_AMNH161806_astL_NI_ctA	*Callicebus moloch*	*Callicebus*	Extant	Pithecidae	Callicebinae	?	American Museum of Natural History
p_Callicebus_torquatus_USNM398212_F_astR_NI_ctD	*Callicebus torquatus*	*Callicebus*	Extant	Pithecidae	Callicebinae	Female	National Museum of Natural History; Smithsonian Institution
p_Chiropotes_satanas_USNM339661_F_astR_ctD	*Chiropotes satanas*	*Chiropotes*	Extant	Pithecidae	Pithecinae	Female	National Museum of Natural History; Smithsonian Institution
Proteropithecia_neuquenensis_MLP_91-IX-1-119	*Proteropithecia neuquenensis*	*Proteropithecia*	Extinct	?	?	?	Museo de la Plata, La Plata, Argentina
Ateles_belzebuth_AMNH-M-259_M3368-3050	*Ateles belzebuth*	*Ateles*	Extant	Atelidae	Atelinae	Female	Morphosource (http://morphosource.org/)
Cacajao_calvus_AMNH-M-70192_M3692-3359	*Cacajao calvus*	*Cacajao*	Extant	Pithecidae	Pithecinae	Male	Morphosource (http://morphosource.org/)
Callicebus_moloch_AMNH-M-94977_M3712-3376	*Callicebus moloch*	*Callicebus*	Extant	Pithecidae	Callicebinae	Male	Morphosource (http://morphosource.org/)
Chiropotes_satanas_irrorata_AMNH-M-95760_M3715-3379	*Chiropotes satanas*	*Chiropotes*	Extant	Pithecidae	Pithecinae	Male	Morphosource (http://morphosource.org/)

Specimen	Species	Genus	Status	Family	Subfamily	Sex	Repository
Chiropotes_satanas_satanas_AMNH-M-96123_M3718-3382	*Chiropotes satanas*	*Chiropotes*	Extant	Pitheciidae	Pitheciinae	Male	Morphosource (http://morphosource.org/)
Saguinus_midas_AMNH-M-97316_M3531-3207	*Saguinus midas*	*Saguinus*	Extant	Cebidae	Callithrichinae	Male	Morphosource (http://morphosource.org/)
Callithrix_jacchus_penicillata_AMNH-M-133698_M3476-3153	*Callithrix jacchus*	*Callithrix*	Extant	Cebidae	Callithrichinae	Female	Morphosource (http://morphosource.org/)
Callithrix_jacchus_penicillata_AMNH-M-133702_M3481-3159	*Callithrix jacchus*	*Callithrix*	Extant	Cebidae	Callithrichinae	Female	Morphosource (http://morphosource.org/)
AMNH-M-183289_M3460-3137_Callimico_goeldii_Astragalus	*Callimico goeldii*	*Callimico*	Extant	Cebidae	Callithrichinae	?	Morphosource (http://morphosource.org/)
Ateles_fusciceps_AMNH-M-188140_M3374-3056	*Ateles fusciceps*	*Ateles*	Extant	Atelidae	Atelinae	Male	Morphosource (http://morphosource.org/)
Lagothrix_lagotricha_poepiggi_AMNH-M-188142_M3445-3124	*Lagothrix lagotricha*	*Lagothrix*	Extant	Atelidae	Atelinae	?	Morphosource (http://morphosource.org/)
AMNH-M-188156_M3448-3128_Lagothrix_lagotricha_Astragalus	*Lagothrix lagotricha*	*Lagothrix*	Extant	Atelidae	Atelinae	Female	Morphosource (http://morphosource.org/)

Specimen	Species	Genus	Status	Family	Subfamily	Sex	Source
Saguinus_mystax_AMNH-M-188174_M3547-3224	Saguinus mystax	Saguinus	Extant	Cebidae	Callithrichinae	Male	Morphosource (http://morphosource.org/)
Saguinus_mystax_AMNH-M-188177_M3536-3213	Saguinus mystax	Saguinus	Extant	Cebidae	Callithrichinae	Male	Morphosource (http://morphosource.org/)
Cacajao_calvus_AMNH-M-201122_M3688-3356	Cacajao calvus	Cacajao	Extant	Pitheciidae	Pitheciinae	?	Morphosource (http://morphosource.org/)
Aotus_trivirgatus_AMNH-M-201647_M3266-2980	Aotus trivirgatus	Aotus	Extant	Cebidae	Cebinae	?	Morphosource (http://morphosource.org/)
Pithecia_pithecia_AMNH-M-202373_M3722-3384	Pithecia pithecia	Pithecia	Extant	Pitheciidae	Pitheciinae	Female	Morphosource (http://morphosource.org/)
Saguinus_midas_AMNH-M-207726_M3522-3199	Saguinus midas	Saguinus	Extant	Cebidae	Callithrichinae	?	Morphosource (http://morphosource.org/)
Saimiri_boliviensis_AMNH-M-209934_M3605-3276	Saimiri boliviensis	Saimiri	Extant	Cebidae	Cebinae	Male	Morphosource (http://morphosource.org/)
Callicebus_moloch_AMNH-M-210393_M3709-3373	Callicebus moloch	Callicebus	Extant	Pitheciidae	Callicebinae	?	Morphosource (http://morphosource.org/)
Aotus_azarae_AMNH-M-211482_M3259-2976	Aotus azarae	Aotus	Extant	Cebidae	Cebinae	Male	Morphosource (http://morphosource.org/)
Callicebus_donacophilus_AMNH-M-211490_M3695-3360	Callicebus donacophilus	Callicebus	Extant	Pitheciidae	Callicebinae	Female	Morphosource (http://morphosource.org/)

Specimen	Species	Genus	Status	Family	Subfamily	Sex	Source
Callicebus_donacophilus_AMNH-M-211491_M3699-3308	Callicebus donacophilus	Callicebus	Extant	Pitheciidae	Callicebinae	Male	Morphosource (http://morphosource.org/)
Alouatta_caraya_AMNH-M-211513_M3278-2990	Alouatta caraya	Alouatta	Extant	Atelidae	Alouattinae	Male	Morphosource (http://morphosource.org/)
Alouatta_caraya_AMNH-M-211525_M3281-2992	Alouatta caraya	Alouatta	Extant	Atelidae	Alouattinae	Male	Morphosource (http://morphosource.org/)
Alouatta_caraya_AMNH-M-211585_M3286-2995	Alouatta caraya	Alouatta	Extant	Atelidae	Alouattinae	Female	Morphosource (http://morphosource.org/)
Saimiri_boliviensis_AMNH-M-211650_M4110-3753	Saimiri boliviensis	Saimiri	Extant	Cebidae	Cebinae	Female	Morphosource (http://morphosource.org/)
Saimiri_boliviensis_AMNH-M-211651_M3617-3286	Saimiri boliviensis	Saimiri	Extant	Cebidae	Cebinae	Male	Morphosource (http://morphosource.org/)
Aotus_azarae_AMNH-M-215056_M3272-2983	Aotus azarae	Aotus	Extant	Cebidae	Cebinae	Female	Morphosource (http://morphosource.org/)
Aotus_nancymaae_AMNH-M-239851_M3275-2987	Aotus nancymaae	Aotus	Extant	Cebidae	Cebinae	Male	Morphosource (http://morphosource.org/)
Callithrix_pygmaea_AMNH-M-244101_M3516-3193	Cebuella pygmaea	Cebuella	Extant	Cebidae	Callithrichinae	Female	Morphosource (http://morphosource.org/)
Callicebus_moloch_AMNH-M-244363_M3705-3367	Callicebus moloch	Callicebus	Extant	Cebidae	Callicebinae	?	Morphosource (http://morphosource.org/)

Specimen	Species	Genus		Family	Subfamily	Sex	Institution
Saguinus_midas_AMNH-M-266481_M3528-3204	*Saguinus midas*	*Saguinus*	Extant	Cebidae	Callithrichinae	Female	Morphosource (http://morphosource.org/)
Aotus_infulatus_AMNH-M-94992_M3263-2978	*Aotus infulatus*	*Aotus*	Extant	Cebidae	Cebinae	Female	Morphosource (http://morphosource.org/)
Alouatta_caraya_AMNH211526	*Alouatta caraya*	*Alouatta*	Extant	Atelidae	Alouattinae	Male	Morphosource (http://morphosource.org/)
Alouatta_caraya_AMNH215061	*Alouatta caraya*	*Alouatta*	Extant	Atelidae	Alouattinae	Female	American Museum of Natural History
Alouatta_seniculus_AMNH211527	*Alouatta seniculus*	*Alouatta*	Extant	Atelidae	Alouattinae	Female	American Museum of Natural History
Alouatta_seniculus_AMNH211528	*Alouatta seniculus*	*Alouatta*	Extant	Atelidae	Alouattinae	Male	American Museum of Natural History
Alouatta_seniculus_AMNH211532	*Alouatta seniculus*	*Alouatta*	Extant	Atelidae	Alouattinae	Male	American Museum of Natural History
Alouatta_seniculus_AMNH211540	*Alouatta seniculus*	*Alouatta*	Extant	Atelidae	Alouattinae	Female	American Museum of Natural History
Alouatta_seniculus_AMNH211543	*Alouatta seniculus*	*Alouatta*	Extant	Atelidae	Alouattinae	Female	American Museum of Natural History
Ateles_marginatus_AMNH95038	*Ateles marginatus*	*Ateles*	Extant	Atelidae	Atelinae	Female	American Museum of Natural History
Aotus_azarae_AMNH215048	*Aotus azarae*	*Aotus*	Extant	Cebidae	Cebinae	Female	American Museum of Natural History
Cebus_albifrons_AMNH211587	*Cebus albifrons*	*Cebus*	Extant	Cebidae	Cebinae	Male	American Museum of Natural History

Specimen	Species	Genus		Family	Subfamily	Sex	Institution
Cebus_albifrons_AMNH211590	Cebus albifrons	Cebus	Extant	Cebidae	Cebinae	Male	American Museum of Natural History
Cebus_apella_AMNH133654	Cebus apella	Cebus	Extant	Cebidae	Cebinae	Male	American Museum of Natural History
Cebus_apella_AMNH133674	Cebus apella	Cebus	Extant	Cebidae	Cebinae	Female	American Museum of Natural History
Cebus_olivaceus_AMNH30197	Cebus olivaceus	Cebus	Extant	Cebidae	Cebinae	Female	American Museum of Natural History
Cebus_olivaceus_AMNH30198	Cebus olivaceus	Cebus	Extant	Cebidae	Cebinae	Male	American Museum of Natural History
Saimiri_boliviensis_AMNH211606	Saimiri boliviensis	Saimiri	Extant	Cebidae	Cebinae	Male	American Museum of Natural History
Saimiri_boliviensis_AMNH211614	Saimiri boliviensis	Saimiri	Extant	Cebidae	Cebinae	Female	American Museum of Natural History
Saimiri_boliviensis_AMNH211624	Saimiri boliviensis	Saimiri	Extant	Cebidae	Cebinae	Male	American Museum of Natural History
Saimiri_sp_AMNH188096	Saimiri sp.	Saimiri	Extant	Cebidae	Cebinae	Female	American Museum of Natural History
Saimiri_sp_AMNH188101	Saimiri sp.	Saimiri	Extant	Cebidae	Cebinae	Female	American Museum of Natural History
Callithrix_santaremensis_AMNH188164	Mico humeralifer	Callithrix	Extant	Cebidae	Callithrichinae	?	American Museum of Natural History
Cebuella_pygmaea_USNM337948	Cebuella pygmaea	Cebuella	Extant	Cebidae	Callithrichinae	Male	National Museum of Natural History; Smithsonian Institution

Specimen	Species	Genus	Status	Family	Subfamily	Sex	Institution
Saguinus_oedipus_AMNH200882	*Saguinus oedipus*	*Saguinus*	Extant	Cebidae	Callithrichinae	Female	American Museum of Natural History
Saguinus_sp_AMNH239875	*Saguinus sp.*	*Saguinus*	Extant	Cebidae	Callithrichinae	Female	National Museum of Natural History; Smithsonian Institution
Callicebus_personatus_USNM240088	*Callicebus personatus*	*Callicebus*	Extant	Pitheciidae	Callicebinae	Female	National Museum of Natural History; Smithsonian Institution
Chiropotes_satanas_USNM361016	*Chiropotes satanas*	*Chiropotes*	Extant	Pitheciidae	Pitheciinae	Female	National Museum of Natural History; Smithsonian Institution
Ateles_fusciceps_USNM338112	*Ateles fusciceps*	*Ateles*	Extant	Atelidae	Atelinae	Male	National Museum of Natural History; Smithsonian Institution
Ateles_fusciceps_USNM338116	*Ateles fusciceps*	*Ateles*	Extant	Atelidae	Atelinae	Female	National Museum of Natural History; Smithsonian Institution
Ateles_geoffroyi_USNM244863	*Ateles geoffroyi*	*Ateles*	Extant	Atelidae	Atelinae	Female	National Museum of Natural History; Smithsonian Institution
Ateles_geoffroyi_USNM276657	*Ateles geoffroyi*	*Ateles*	Extant	Atelidae	Atelinae	Female	National Museum of Natural History; Smithsonian Institution

Specimen	Genus	Status	Family	Subfamily	Sex	Source
Cebuella_pygmaea_USNM464994	*Cebuella*	Extant	Cebidae	Callithrichinae	Male	National Museum of Natural History; Smithsonian Institution
Cebus_apella_AMNH-M-133606_M3589-3260	*Cebus*	Extant	Cebidae	Cebinae	Male	Morphosource (http://morphosource.org/)
Pithecia_pithecia_AMNH-M-149149_M3728-3391	*Pithecia*	Extant	Pithecidae	Pitheciinae	Male	Morphosource (http://morphosource.org/)
Pithecia_monachus_AMNH-M-187978_M3725-3388	*Pithecia*	Extant	Pithecidae	Pitheciinae	?	Morphosource (http://morphosource.org/)
Saimiri_sciureus_Astragalus_AMNH-M-188090_M36610-3281	*Saimiri*	Extant	Cebidae	Cebinae	Male	Morphosource (http://morphosource.org/)
Aotus_azarae_AMNH211483	*Aotus*	Extant	Cebidae	Cebinae	Male	American Museum of Natural History
Cebus_albifrons_AMNH211562	*Cebus*	Extant	Cebidae	Cebinae	Male	American Museum of Natural History
Cebus_nigritus_USNM518478	*Cebus*	Extant	Cebidae	Cebinae	Male	National Museum of Natural History; Smithsonian Institution
Saimiri_boliviensis_AMNH211592	*Saimiri*	Extant	Cebidae	Cebinae	Male	American Museum of Natural History

Specimen	Species	Genus	Status	Cebidae	Callithrichinae	Male	Source
Callimico_goeldii_USNM583199	*Callimico goeldii*	*Callimico*	Extant	Cebidae	Callithrichinae	Male	National Museum of Natural History; Smithsonian Institution
Neosaimiri fieldsi_IGMKU_89030	*Neosaimiri fieldsi*	*Neosaimiri*	Extinct	?	?	?	cast from Alfred Rosenberger (CUNY)
Neosaimiri fieldsi_IGMKU_89031	*Neosaimiri fieldsi*	*Neosaimiri*	Extinct	?	?	?	cast from Alfred Rosenberger (CUNY)
Neosaimiri fieldsi_IGMKU_89199	*Neosaimiri fieldsi*	*Neosaimiri*	Extinct	?	?	?	cast from Alfred Rosenberger (CUNY)
Aotus_dindensis_IGMKU_8802	*Aotus dindensis*	*Aotus*	Extinct	?	?	?	cast from Alfred Rosenberger (CUNY)
Paralouatta_marianae_MNHNCu_76.3059	*Paralouatta marianae*	*Paralouatta*	Extinct	?	?	?	cast from Ross MacPhee (American Museum of Natural History)
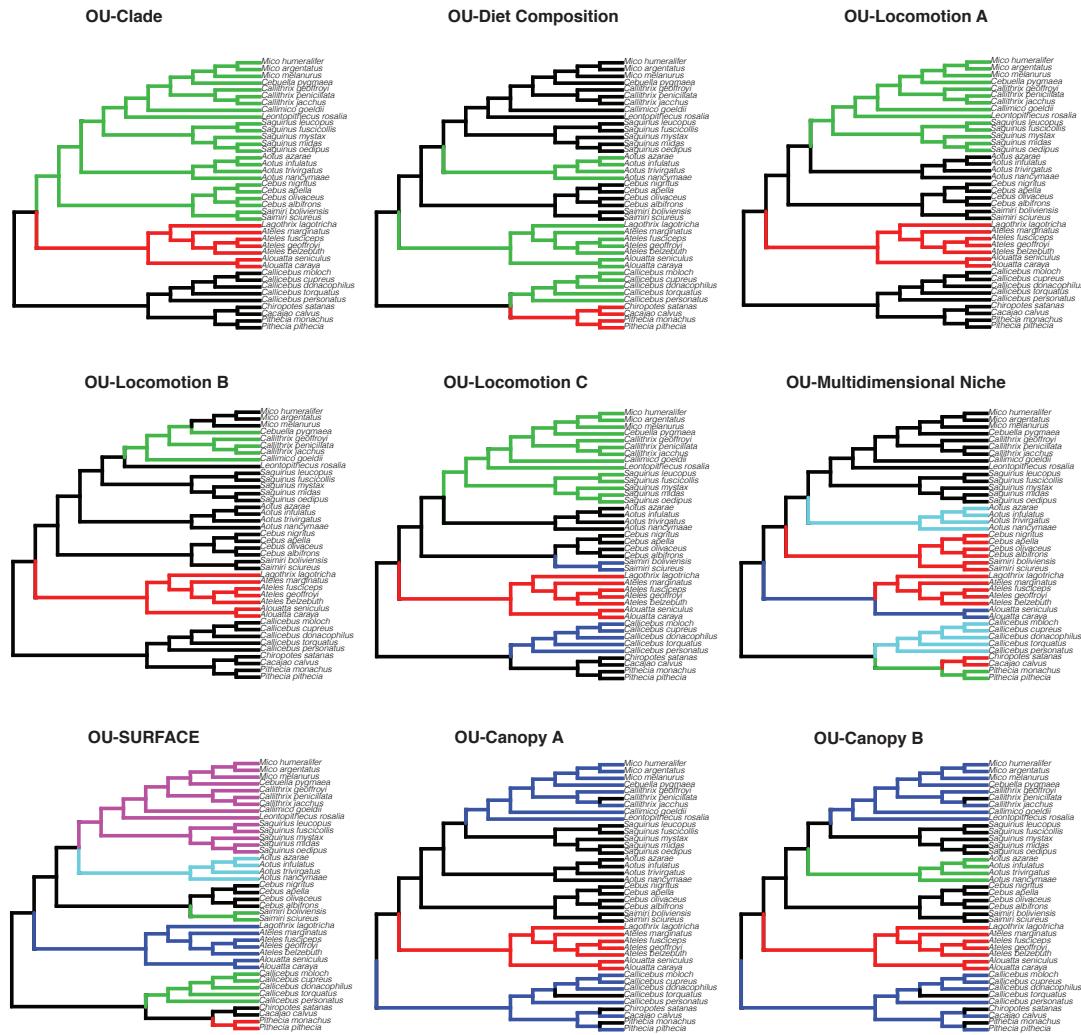
4.8.2 Supporting Information 2. Table 4.8 Missing landmarks of the fossil sample

Id	Species/Specimen	Missing landmarks
MACN 362	*Dolichocebus gaimanensis*	3,25,28,29,27,26
MUSM 2024	Madre de Dios	
SGO.PV 974	Río Cisnes	12,13,14,15,16,17
UCMP 38762	*Cebupithecia sarmientoi*	
MACN 271	*Carlocebus carmenensis*	6, 16,17
MACN 304	*Carlocebus carmenensis*	
MACN 368	*Carlocebus carmenensis*	4,7,,8,9,12,13,14,15,17,27
MACN 396	*Carlocebus carmenensis*	5,12,13,14,15, 17,20,21,22
MACN 397	*Soriacebus ameghinorum*	16,17,18,19,20,21,22,23,24
MLP 91-IX-1-119	*Proteropithecia neuquenensis*	
IGMKU 89030	*Neosaimiri fieldsi*	20,21,22
IGMKU 89031	*Neosaimiri fieldsi*	
IGMKU 89199	*Neosaimiri fieldsi*	13,15,16,17
IGMKU 8802	*Aotus dindensis*	
MNHNCu 76.3059	*Paralouatta marianae*	27

4.8.3 Supporting information 3. Phylogeny used in the comparative analyses in Newick format

((((Pithecia_pithecia:1,Pithecia_monachus:1):1,(Cacajao_calvus:1,Chiropotes_satanas:1):1):3,(Callicebus_personatus:4,(Callicebus_torquatus:3,(Callicebus_donacophilus:2,(Callicebus_cupreus:1,Callicebus_moloch:1):1):1):1):1):6,(((Alouatta_caraya:1,Alouatta_seniculus:1):4,(((Ateles_belzebuth:2,(Ateles_geoffroyi:1,Ateles_fusciceps:1):1):1,Ateles_marginatus:3):1,Lagothrix_lagotricha:4):1):5,(((Saimiri_sciureus:1,Saimiri_boliviensis:1):2,((Cebus_albifrons:1,Cebus_olivaceus:1):1,(Cebus_apella:1,Cebus_nigritus:1):1):1):6,((Aotus_nancymaae:3,(Aotus_trivirgatus:2,(Aotus_infulatus:1,Aotus_azarae:1):1):1):5,(((((Saguinus_oedipus:1,Saguinus_midas:1):1,Saguinus_mystax:2):1,(Saguinus_fuscicollis:1,Saguinus_leucopus:1):2):4,(Leontopithecus_rosalia:6,(Callimico_goeldii:5,(((Callithrix_jacchus:1,Callithrix_penicillata:1):1,Callithrix_geoffroyi:2):2,(Cebuella_pygmaea:3,(Mico_melanurus:2,(Mico_argentatus:1,Mico_humeralifer:1):1):1):1):1):1):1):1):1):1):1);

4.8.4 Supporting information 4.

Figure 4.10 Alternative multivariate OU hypotheses for the evolution of platyrrhine talar shape and size. The phylogenetic trees represent the different multi-regime OU hypotheses included in the model selection analyses carried out in 'mvMORPH'. Additionally to these multi-regime OU models, a single-peak OU (OU1), Brownian motion (BM), and early-burst (EB) models were also fitted.

4.8.5 Supporting Information 5. Table 4.9 Mass regression sample with surface area measurements

Genus	Species	Museum	Specimen	Ectal area (mm²)	Navicular area (mm2)	Sustentacular area (mm2)	Trochlear area (mm2)
Alouatta	*caraya*	AMNH	211510	82.67	131.78	51.16	173.76
	caraya	AMNH	211512	60.66	113.42	50.29	148.90
	caraya	AMNH	211517	60.66	90.51	61.58	128.26
	caraya	AMNH	211519	67.68	127.47	66.90	142.25
	caraya	AMNH	211522	56.04	97.63	56.34	128.61
	seniculus	AMNH	23549	70.20	98.98	61.72	155.41
	seniculus	AMNH	42316	64.15	96.55	76.27	138.13
	seniculus	AMNH	132790	86.09	115.57	95.71	187.97
	seniculus	AMNH	188006	69.04	100.89	113.79	141.36
Ateles	*belzebuth*	AMNH	259	91.07	130.35	96.64	243.53
	belzebuth	AMNH	30192	124.54	196.09	176.89	324.31
	belzebuth	AMNH	188126	97.64	97.30	132.88	206.79
	belzebuth	AMNH	201294	78.36	109.92	69.53	174.28
	fusciceps	AMNH	188140	121.77	107.75	160.85	255.07
	fusciceps	AMNH	388112	105.74	130.02	96.13	270.13
	fusciceps	AMNH	388116	103.80	110.37	98.67	226.51
	geoffroyi	AMNH	28420	130.36	130.43	107.41	276.31
	geoffroyi	USNM	244863	103.16	115.40	97.33	239.14
	geoffroyi	USNM	276657	98.25	135.40	65.78	202.36
	marginatus	AMNH	95038	111.85	129.41	119.99	228.32
	marginatus	AMNH	95040	134.51	132.55	117.70	229.25
	marginatus	AMNH	95041	108.29	138.77	99.73	248.90
	marginatus	AMNH	95042	117.49	133.37	102.46	271.89
Lagothrix	*lagotricha*	AMNH	188153	77.72	118.95	76.24	155.27
	lagotricha	AMNH	188156	65.41	88.86	63.42	135.27
	lagotricha	AMNH	188162	56.62	98.07	67.04	148.07
	lagotricha	AMNH	238487	93.92	129.94	105.21	217.80
	lagotricha	USNM	538105	68.75	105.45	45.57	185.15
Aotus	*azarae*	AMNH	211458	25.49	38.51	27.51	55.97
	azarae	AMNH	211459	24.93	38.27	26.38	57.12
	azarae	AMNH	211478	28.39	42.61	28.57	63.44
	azarae	AMNH	211479	25.57	38.23	27.73	58.43
	azarae	AMNH	211486	29.26	39.18	30.75	60.35
	azarae	AMNH	215048	24.30	34.12	24.77	54.87
	infulatus	AMNH	94992	17.64	27.93	13.97	35.41
	nancymaae	AMNH	239851	21.54	31.79	22.84	47.61
	nancymaae	AMNH	239852	19.60	30.13	19.64	44.66
	trivirgatus	AMNH	187963	21.71	28.41	20.72	41.50
	trivirgatus	AMNH	187967	23.24	34.18	23.16	49.19

Cebus	*albifrons*	AMNH	188018	53.39	88.41	56.45	123.17
	albifrons	AMNH	209923	45.74	60.74	43.16	110.50
	albifrons	AMNH	209924	46.34	59.20	39.07	98.26
	albifrons	AMNH	211547	47.48	65.80	43.72	112.26
	apella	AMNH	133606	45.37	71.15	49.91	124.42
	apella	AMNH	133607	45.20	65.49	34.21	112.40
	apella	AMNH	133608	35.89	49.38	35.03	95.33
	apella	AMNH	133647	37.04	58.12	39.74	102.36
	apella	AMNH	133654	51.83	71.78	47.41	140.16
	apella	AMNH	133656	46.36	64.57	40.58	125.86
	apella	AMNH	133660	40.09	55.41	39.27	114.84
	apella	AMNH	133671	32.74	48.47	36.62	96.15
	apella	AMNH	133674	38.14	58.56	42.30	102.82
	apella	AMNH	133681	38.59	57.41	35.12	92.68
	apella	AMNH	133764	38.77	54.94	40.14	98.81
	apella	AMNH	133815	48.20	63.25	46.11	109.84
	apella	AMNH	133851	49.40	70.77	29.11	116.81
	nigritus	USNM	518478	50.19	72.54	38.82	121.72
	olivaceus	AMNH	30196	42.82	70.64	39.59	97.52
	olivaceus	AMNH	30197	53.72	74.20	50.41	105.61
	olivaceus	AMNH	30198	55.09	83.15	62.30	109.53
	olivaceus	AMNH	42873	44.15	85.02	51.02	122.03
Saimiri	*boliviensis*	AMNH	209934	24.17	28.22	20.56	53.41
	boliviensis	AMNH	211592	25.72	25.58	22.71	45.54
	boliviensis	AMNH	211606	17.10	23.20	16.43	52.26
	boliviensis	AMNH	211609	18.19	25.31	15.29	52.48
	sciureus	AMNH	136214	19.94	27.58	17.71	39.12
	sciureus	AMNH	188086	16.35	24.73	18.71	38.32
	sciureus	AMNH	188090	17.36	26.73	13.82	39.30
	sciureus	AMNH	188093	21.00	26.61	19.26	43.89
Callimico	*goeldii*	USNM	303323	10.90	10.24	19.42	23.37
	goeldii	USNM	395455	11.81	13.37	15.06	23.06
	goeldii	USNM	464991	11.35	14.36	18.89	26.56
	goeldii	USNM	575153	12.81	20.61	14.55	29.10
	goeldii	USNM	583199	11.86	16.75	19.34	29.07
Callithrix	*argentata*	USNM	399069	7.72	11.03	10.63	16.59
	geoffroyi	USNM	518553	8.17	11.62	7.98	19.24
	geoffroyi	USNM	582900	8.11	13.41	8.11	21.69
	jacchus	AMNH	133701	6.27	9.01	8.82	16.02
	jacchus	AMNH	133702	6.50	10.94	7.69	17.08
	jacchus	USNM	398848	5.79	10.25	6.97	13.66
	jacchus	USNM	399034	7.63	12.82	10.04	19.72
	jacchus	USNM	399036	7.06	11.95	7.80	15.83
	jacchus	USNM	399037	6.93	11.85	6.54	15.55
	penicillata	AMNH	133692	8.31	11.60	8.84	17.54
	penicillata	AMNH	133698	6.22	9.40	7.20	14.47

176

	sp.	AMNH	95127	8.55	13.99	10.94	22.00
Cebuella	*pygmaea*	USNM	336325	2.86	4.84	4.12	6.98
	pygmaea	USNM	337948	2.27	4.60	4.18	6.67
	pygmaea	USNM	464994	2.90	4.96	4.38	7.92
Leontopithecus	*rosalia*	USNM	588152	12.05	19.09	17.77	29.88
	rosalia	USNM	588334	10.53	19.20	15.30	25.03
	rosalia	USNM	597831	10.95	19.70	13.87	26.80
Saguinus	*leucopus*	AMNH	148322	10.74	18.75	10.85	27.90
	midas	AMNH	97316	11.24	18.51	10.53	24.08
	midas	AMNH	266480	15.30	21.49	16.14	32.48
	mystax	AMNH	188171	7.94	14.31	9.75	18.44
	mystax	AMNH	188177	6.89	10.27	8.82	17.01
	mystax	AMNH	188178	7.98	12.28	10.47	19.35
	mystax	AMNH	188179	7.88	12.74	8.92	17.93
	sp.	AMNH	239875	8.52	16.13	8.95	25.72
Cacajao	*calvus*	AMNH	70192	47.03	76.75	51.02	123.82
	calvus	USNM	302626	41.89	86.14	42.91	119.04
	calvus	USNM	302627	42.30	90.40	42.75	109.06
	calvus	USNM	319516	46.58	75.66	46.51	129.61
	calvus	USNM	395027	44.90	71.00	45.41	106.79
	calvus	USNM	519570	41.80	76.43	53.99	113.21
Callicebus	*cupreus*	AMNH	130361	24.16	34.21	21.23	48.33
	cupreus	AMNH	136208	21.69	35.06	25.16	46.16
	cupreus	AMNH	136217	22.07	33.95	22.60	50.53
	donacophilus	AMNH	211487	22.27	35.60	22.32	46.60
	donacophilus	AMNH	211489	24.53	37.84	22.60	47.59
	donacophilus	AMNH	211492	22.90	33.43	23.07	48.81
	torquatus	USNM	398212	28.81	38.09	29.24	55.66
Chiropotes	*satanas*	AMNH	95760	51.05	69.49	52.53	127.51
	satanas	AMNH	96123	38.89	63.26	34.85	93.89
	satanas	USNM	338961	39.79	71.34	46.42	101.12
	satanas	USNM	361016	44.00	62.60	46.05	96.52
	satanas	USNM	549519	27.87	50.90	32.55	68.77
Pithecia	*monachus*	USNM	395692	37.98	68.78	39.70	119.00
	pithecia	AMNH	149149	28.58	42.86	24.37	78.65
	pithecia	USNM	300794	31.36	50.26	27.71	89.08
	pithecia	USNM	339659	30.18	39.99	28.21	146.94
	pithecia	USNM	339660	25.11	41.74	25.97	68.37

4.8.6 Supporting information 6. Table 4.10 PC loadings and PLS singular vectors for the locomotor mode percentages

a) Loadings for each locomotor mode percentage on each PC axis

	PC1	PC2	PC3	PC4	PC5
Arboreal quadrupedal walk	0.027784	-0.80713	0.2824	-0.041281	0.51606
Clamber/vertical climb	0.55997	0.16756	-0.14009	0.71077	0.36543
Leap/drop/hop	-0.5171	0.093809	-0.66132	-0.020051	0.53485
Bridge/suspensory	0.54191	0.27444	-0.059066	-0.69691	0.37663
Clawed locomotion	-0.353	0.48616	0.67808	0.083772	0.41501
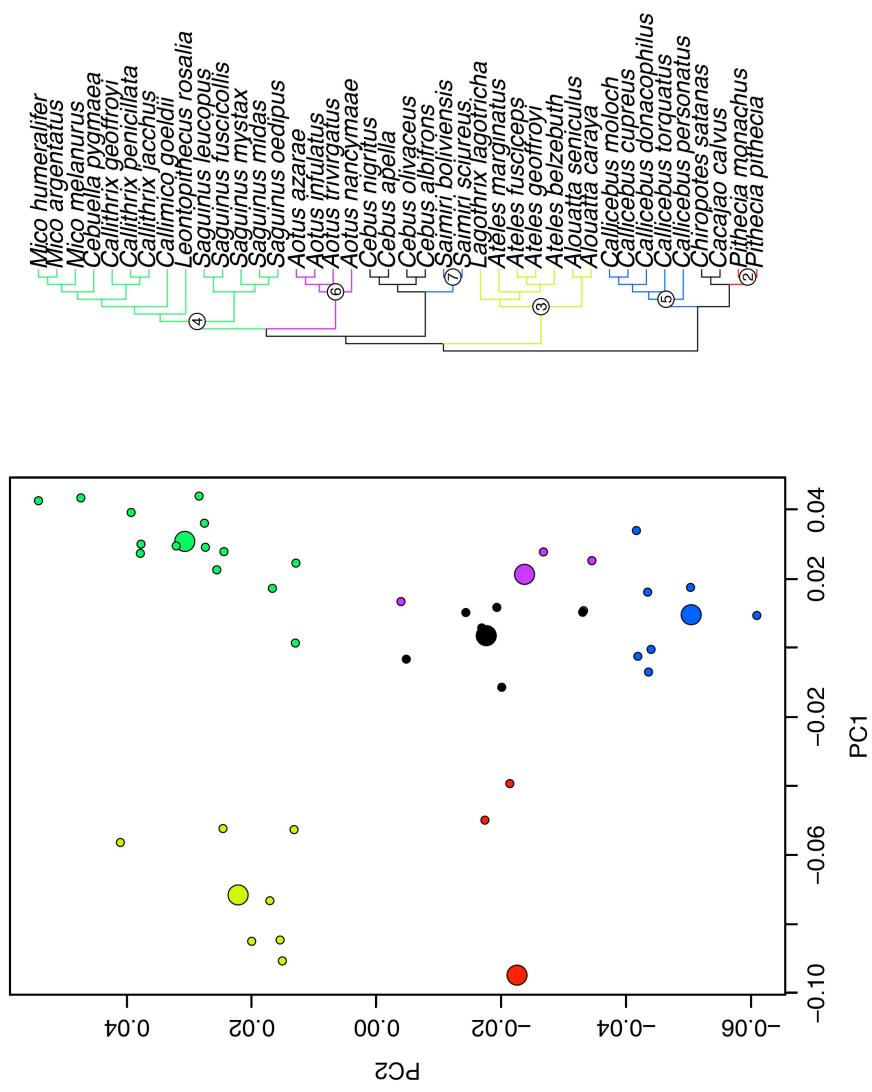
b) Singular vectors of the locomotor mode percentages (standard PLS)

	PLS1	PLS2	PLS3	PLS4	PLS5
Arboreal quadrupedal walk	-0.270810884	0.671027898	0.542299835	0.007371534	-0.426895274
Clamber/vertical climb	0.548720254	0.062800924	-0.107349203	-0.724451284	-0.398256968
Leap/drop/hop	-0.521669652	0.100056207	-0.726073579	-0.039820198	-0.434834497
Bridge/suspensory	0.5066767	-0.054348646	-0.097758637	0.679030785	-0.519312419
Clawed locomotion	-0.31097756	-0.729940124	0.397048416	-0.111568558	-0.447644261

c) Singular vectors of the locomotor mode percentages (phylogenetic PLS)

	PLS1	PLS2	PLS3	PLS4	PLS5
Arboreal quadrupedal walk	0.620457686	-0.536696357	0.099183885	-0.366574312	-0.427522059
Clamber/vertical climb	0.124705412	0.774548926	-0.06542545	-0.454107368	-0.417167269
Leap/drop/hop	-0.773329548	-0.307704175	0.03326438	-0.343454848	-0.433833839
Bridge/suspensory	0.000962255	0.12416053	0.655454615	0.564340431	-0.486294522
Clawed locomotion	0.037964531	-0.043969139	-0.745087106	0.472195317	-0.467442185

4.8.7 Supporting information 7.

Figure 4.11 Results of the SURFACE method: Adaptive regimes for the best-fitting model found by SURFACE are mapped on the a) morphospace defined by PC1 and PC2 and on the b) phylogeny. Large circles in a) represent the position of the estimated optima for each regime, while the small dots are the species values in the morphospace. Numbers at nodes in b) represent the different regimes found by the SURFACE method.

CHAPTER 5

Inferring locomotor behaviours in Miocene New World monkeys using Finite Element Analysis, Geometric Morphometrics and Machine-learning classification techniques applied to talar morphology

Inferring locomotor behaviours in Miocene New World monkeys using Finite Element Analysis, Geometric Morphometrics and Machine-learning classification techniques applied to talar morphology

Thomas A. Püschel[1*], Jordi Marcé-Nogué[2], Justin T. Gladman[3], René Bobe[4,5,], William I. Sellers[1]

1 School of Earth and Environmental Sciences, University of Manchester, M13 9PL, United Kingdom.
2 Center of Natural History (CeNak), Universität Hamburg, Martin-Luther-King-Platz 3, Hamburg, 20146, Germany.
3 Department of Engineering, Shared Materials Instrumentation Facility (SMIF), Duke University, Durham, NC, USA.
4 Departamento de Antropología, Universidad de Chile, Santiago, Chile.
5 Institute of Cognitive and Evolutionary Anthropology, School of Anthropology, University of Oxford, United Kingdom.

*Corresponding author: Thomas A. Püschel
E-mail: thomas.puschel@postgrad.manchester.ac.uk
Phone: +44 (0) 7476608464
Address: School of Earth and Environmental Sciences, University of Manchester, M13 9PL, United Kingdom.
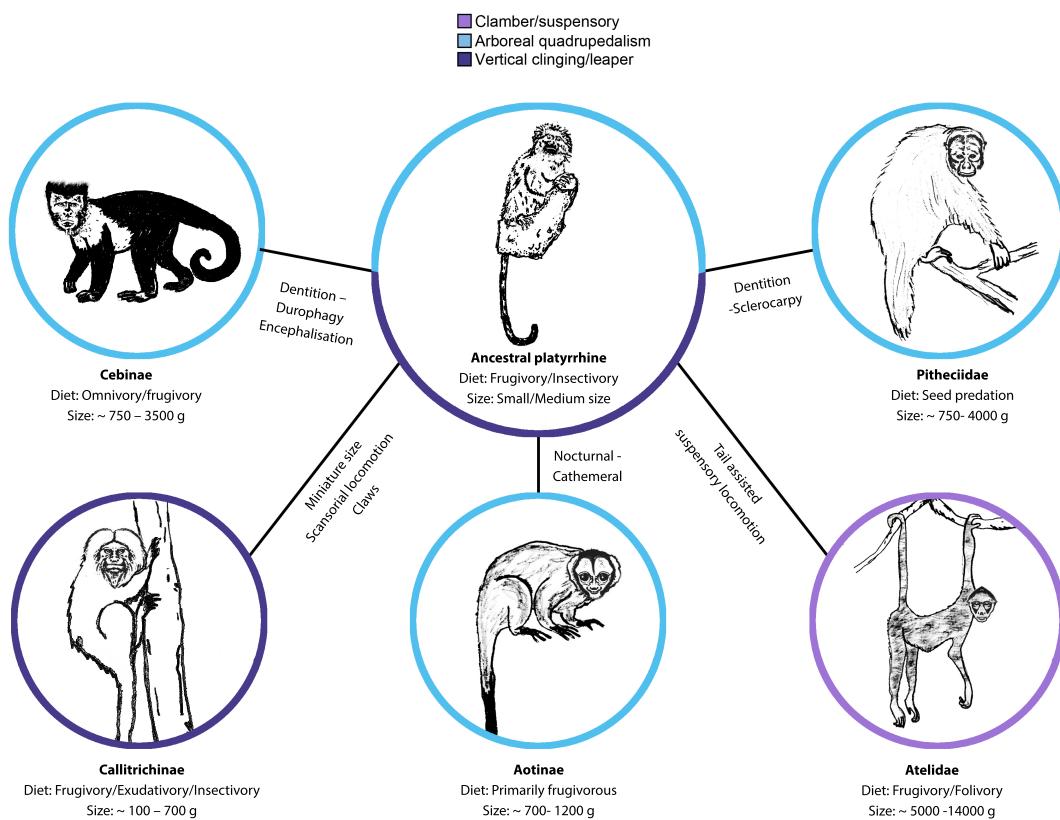
Abstract

The occupation of diverse niches by the New World Monkeys in the Americas has been accompanied by distinct locomotor, behavioural, morphological and ecological adaptations. The talus is the most commonly preserved post-cranial element in the platyrrhine fossil record, with several Miocene platyrrhine taxa having at least one conserved talus. Talus morphology can provide information about postural adaptations because it is the anatomical structure responsible for transmitting body mass forces from the leg to the foot, as well as providing stability and mobility throughout most postural and locomotor behaviours. The aim of this study was to see whether the locomotor behaviour of fossil plattyrhines could be inferred from their talus morphology. To test this possibility we first classified our extant sample into three different locomotor categories (clamber/suspensory, leaper/clawed and arboreal quadrupedalism) and then compared the talar strength in the different locomotion categories by simulating a static loading scenario using finite element analysis (FEA). Then we collected talar morphometric data and performed geometric morphometric analyses (GM) to distinguish between the main locomotor modes. The same morphometric data was used to evaluate if there was an association between talar shape and its strength by using partial least squares analysis (PLS). Finally, several machine-learning (ML) algorithms were trained using both the biomechanical and morphometric data from the extant sample in order to infer the possible locomotor behaviour of the Miocene fossil sample. The obtained results show that the different locomotor categories are distinguishable using either biomechanical or morphometric data. Clamber/suspensory specimens exhibit the weakest tali, while leaping species showed the strongest morphologies. The ML classification algorithm applied to both biomechanical and morphometric data categorised most of the fossil sample as arboreal quadrupeds. This study has shown that a combined approach using FEA, GM and ML algorithms can contribute in the understanding of platyrrhine talar morphology and its relationship with locomotion. In future this approach is likely to be beneficial for determining the locomotor habits in other primate taxa.

Keywords: Platyrrhini; Finite Element Analysis; Geometric Morphometrics; Talus; Machine Learning; Locomotor categories

5.1 Introduction

Extant platyrrhines or New World Monkeys (NWM) inhabit a diverse range of habitats in the Americas (Fleagle, 2013). The occupation of these niches has been coupled by distinct behavioural, locomotor, morphological and ecological adaptations in each one of the main platyrrhine clades (Ford and Davis, 1992; Rosenberger, 1992, 2002; Fleagle and Reed, 1996; Fleagle et al., 1999; Youlatos, 2004; Rosenberger et al., 2009), which can be summarised in broad ecophyletic groups (Fig 5.1).

Figure 5.1 Broad platyrrhine ecophyletic groups. Differences in diet strategies define the main separation between groups, while differences in locomotion further separate the different sub-groups. Colours represent different main locomotion modes. Illustration by Stephan A. Püschel.

Although the modern day success of this group is evident, the evolutionary history of platyrrhines is still commonly discussed (Youlatos and Meldrum, 2011). One of the main difficulties in NWM palaeobiology is the scarceness of fossils from the Eocene and Oligocene, with most NWM fossils dated to the Miocene or the

Pleistocene of the Caribbean and South America (Rímoli, 1977; Macphee and Woods, 1982; MacPhee et al., 2003; Kay and Cozzuol, 2006; Tejedor et al., 2006; Fleagle et al., 2012; Perkins et al., 2012), although it is important to notice that there have been outstanding but rare findings in Bolivia and Peru (Hoffstetter, 1969; Wolff, 1984; Rosenberger et al., 1991; Takai et al., 2000; Kay et al., 2002; Bond et al., 2015). Even though the fossil record of NWM has noticeably improved over the last decade (Kay, 2015a), the origin of the major modern clades is still highly disputed (Rosenberger and Tejedor, 2013; Kay, 2015b). It is particularly intriguing that the majority of the NWM fossil record for the Early Miocene has been found in Patagonia and central Chile, which are no longer areas occupied by any extant platyrrhine (Bordas, 1942; Fleagle et al., 1987; Fleagle and Kay, 1989; Fleagle, 1990; Meldrum, 1990; Flynn et al., 1995; Tejedor, 2002, 2003, 2005a, 2005b).

After teeth, the talus is probably the most commonly preserved anatomical element in the platyrrhine fossil record (Tejedor, 2008). Several Miocene platyrrhine taxa possess at least one conserved talus (i.e. *Carlocebus carmenensis*, *Soriacebus ameghinorum*, *Dolichocebus gaimanensis*, *Proteropithecia neuquenensis*, Río Cisnes, Madre de Dios, *Neosaimiri fieldsi*, *Aotus dindensis*, *Cebupithecia sarmientoi* and *Paralouatta marianae*) (Bordas, 1942; Fleagle et al., 1987; Fleagle and Kay, 1989; Daniel L. Gebo, 1990; Fleagle, 1990; Meldrum, 1990; Meldrum and Lemelin, 1991; Flynn et al., 1995; Nakatsukasa et al., 1997; Tejedor, 2002, 2003, 2005a, 2005b; MacPhee et al., 2003; Marivaux et al., 2012). Importantly, talar morphology can provide insight about postural adaptations due to its interconnection with other foot bones (Lisowski et al., 1974; Boyer et al., 2010, 2015; Yapuncich and Boyer, 2014; Yapuncich et al., 2015). The talus is also the principal mechanical connection between the leg and the foot and is responsible for transmitting the forces acting on the body mass, as well as providing stability and mobility throughout most locomotor behaviours (Boyer et al., 2015). The combination of its high occurrence and good preservation in the fossil record, and its functional role in the ankle joint make it a valuable element when hypothesizing the postural and locomotor behaviours of fossil primates (Gebo, 1986, 1988, 2011; Boyer and Seiffert, 2013).

There is strong and significant association between talar shape and locomotor behaviour (Püschel et al., 2017), and evidence shows that bone is functionally

adapted to the mechanical demands that are imposed during life (Wolff, 1892; Pearson and Lieberman, 2004). Therefore, it is logical to hypothesise that talar mechanical strength associated with biomechanical performance could also be used to distinguish and infer locomotor behaviours. Currently there is an absence of comparative biomechanical analyses that could provide important information about the usefulness of talar biomechanical performance as positional behaviour proxy. Consequently, we analysed the biomechanical performance of the extant platyrrhine talar morphological diversity by applying Finite Element Analysis (FEA). FEA is a technique that reconstructs deformation, strain and stress in material structures, and has become a standard technique of the virtual biomechanical toolkit (Rayfield, 2007; Bright, 2014). Currently there is an almost total absence of studies applying FEA to primate, let alone platyrrhine, talar biomechanics. To our knowledge, most of the studies analysing primate talar biomechanics using FEA have focused on human feet (Chen et al., 2001; Cheung and Zhang, 2005; Reggiani et al., 2006; Parr et al., 2013; Guiotto et al., 2014). Thus, the present contribution represents an important step in analysing an extensive non-human primate comparative sample using FEA. Since we were also interested in the relationship between talar biomechanical performance and its morphology, we used geometric morphometrics (GM) to collect shape data. GM is the quantitative analysis of coordinates representing form (i.e., shape and size) and how it covaries with other factors, such as biomechanics (Adams et al., 2013). In addition, since our objective was to classify the fossils into different locomotor categories, several machine-learning (ML) algorithms were trained using the extant biomechanical data to infer the locomotor categories of the Miocene fossil sample. Traditionally, most morphometric and also some of the FEA output analyses have been performed with reference to simple linear models (Fortuny et al., 2011; Zelditch et al., 2012). For instance, when dealing with classification problems most publications rely on linear discriminant analyses (or its more general extension, canonical variate analyses), in spite of the known limitations of these approaches (Feldesman, 2002; Klingenberg and Monteiro, 2005; Mitteroecker and Bookstein, 2011) and without even testing or comparing other possible techniques that might provide better classification results or that could be better suited for some research problems. Although the application of ML algorithms to tackle problems of specimen identification or group characterization has a vast literature in other biological fields

(Tarca et al., 2007), only recently have several ML methods been applied using morphometric or biomechanical data (Dobigny et al., 2002; Feldesman, 2002; Mendoza et al., 2002; Baylac et al., 2003; Bignon et al., 2005; MacLeod, 2007, 2017; Van Bocxlaer and Schultheiß, 2010; Brink and Bokma, 2011; Santos et al., 2014; Navega et al., 2015; Sonnenschein et al., 2015; Li et al., 2016; Hanot et al., 2017). While some of these techniques (e.g. support vector machines, random forests) are based on mathematical procedures, which are quite dissimilar to those regularly applied in standard morphometric studies, other approaches (e.g., logistic regression, Bayesian networks) are related to techniques that have been previously applied in morphometrics or in other related biological fields (MacLeod, 2017). Although there are available publications using ML methods to classify observations using morphometric data (Dobigny et al., 2002; Feldesman, 2002; Mendoza et al., 2002; Baylac et al., 2003; Bignon et al., 2005; MacLeod, 2007, 2017; Van Bocxlaer and Schultheiß, 2010; Brink and Bokma, 2011; Santos et al., 2014; Navega et al., 2015; Sonnenschein et al., 2015; Li et al., 2016; Hanot et al., 2017), most of them have not compared different approaches applied to the same problem. Therefore, some of these ML procedures were explored and their classification accuracy was assessed when applied to problem of classifying our Miocene fossil sample using morphometric and biomechanical data.

Consequently, the present study employed three basic approaches. 1) First, we classified our extant sample into broad locomotor categories and investigated whether there were significant differences in talar strength depending on locomotion category by simulating a static loading case using FEA. 2) Then we collected talar morphometric data to evaluate if there was an association between talar shape and stress by using partial least squares analysis (PLS). 3) Finally, several ML algorithms were trained and tested using the biomechanical and morphometric data and then used to infer the possible locomotor behaviour of the Miocene fossil sample.

5.2 Methods

5.2.1 Sample

The extant NWM sample included one talus from nearly every modern platyrrhine genus to capture the full morphological diversity of the extant crown group (40 species; Table 5.1). A total of nine tali were downloaded from the Morphosource (http://morphosource.org/) (Copes et al., 2016), as .ply surface models, while all the rest of the sample was μCT scanned at the Shared Materials Instrumentation Facility (SMIF) at Duke University or the Microscopy and Imaging Facility (MIF) at the American Museum of Natural History. The fossil sample considered one talus from most of the available Miocene platyrrhine tali (10 specimens; Table 5.2).

Table 5.1 Extant sample

Species	Subfamily	Locomotion	Sex	Average body mass (g) *	Accession number	Museum/Database
Alouatta caraya	Alouattinae	Clamber/Suspensory	Male	5375	AMNH211513	Morphosource (http:/morphosource.org/)
Alouatta seniculus	Alouattinae	Clamber/Suspensory	Male	5950	AMNH23549	American Museum of Natural History
Aotus azarae	Cebinae	Arboreal quadrupedalismism	Male	1205	AMNH211458	American Museum of Natural History
Aotus infulatus	Cebinae	Arboreal quadrupedalism	Female	1215	AMNH94992	Morphosource (http:/morphosource.org/)
Aotus nancymaae	Cebinae	Arboreal quadrupedalism	Male	787	AMNH239851	Morphosource (http:/morphosource.org/)
Aotus trivirgatus	Cebinae	Arboreal quadrupedalism	Female	786	AMNH187963	American Museum of Natural History
Ateles belzebul	Atelinae	Clamber/Suspensory	Male	8070	AMNH95040	American Museum of Natural History
Ateles fusciceps	Atelinae	Clamber/Suspensory	Male	9025	AMNH188140	Morphosource (http:/morphosource.org/)
Ateles geoffroyi	Atelinae	Clamber/Suspensory	Male	7535	AMNH28420	American Museum of Natural History
Ateles marginatus	Atelinae	Clamber/Suspensory	Male	10230	AMNH95040	American Museum of Natural History
Cacajao calvus	Pithecinae	Arboreal quadrupedalism	Male	3165	USNM319516	National Museum of Natural History; Smithsonian Institution
Callicebus cupreus	Callicebinae	Arboreal quadrupedalism	Male	1070	AMNH136208	American Museum of Natural History
Callicebus donacophilus	Callicebinae	Arboreal quadrupedalism	Male	950	AMNH211487	American Museum of Natural History
Callicebus moloch	Callicebinae	Arboreal quadrupedalism	?	988	AMNH210393	Morphosource (http:/morphosource.org/)
Callicebus personatus	Callicebinae	Arboreal quadrupedalism	Female	1325	USNM240088	National Museum of Natural History; Smithsonian Institution
Callicebus torquatus	Callicebinae	Arboreal quadrupedalism	Female	1325	USNM398212	National Museum of Natural History; Smithsonian Institution
Callimico goeldii	Callithrichinae	Vertical clinging/Leaper	Male	483.5	USNM395455	National Museum of Natural History; Smithsonian Institution
Callithrix geoffroyi	Callithrichinae	Vertical clinging/Leaper	Male	359	USNM582900	National Museum of Natural History; Smithsonian Institution
Callithrix jacchus	Callithrichinae	Vertical clinging/Leaper	Male	320.5	USNM399034	National Museum of Natural History; Smithsonian Institution
Callithrix penicillata	Callithrichinae	Vertical clinging/Leaper	Female	325.5	AMNH133692	American Museum of Natural History
Cebuella pygmaea	Callithrichinae	Vertical clinging/Leaper	Male	116	USNM303037	National Museum of Natural History; Smithsonian Institution
Cebus albifrons	Cebinae	Arboreal quadrupedalism	Male	2735	AMNH209924	American Museum of Natural History
Cebus apella	Cebinae	Arboreal quadrupedalism	Male	3085	AMNH133607	American Museum of Natural History
Cebus nigritus	Cebinae	Arboreal quadrupedalism	Male	2825	USNM518478	National Museum of Natural History; Smithsonian Institution

Species	Subfamily	Locomotion	Sex	Mass	Catalog	Source
Cebus olivaceus	Cebinae	Arboreal quadrupedalism	Male	2905	AMNH30197	American Museum of Natural History
Chiropotes satanas	Pitheciinae	Arboreal quadrupedalism	Male	2740	AMNH95760	Morphosource (http://morphosource.org/)
Lagothrix lagotricha	Atelinae	Clamber/Suspensory	Male	7150	AMNH188153	American Museum of Natural History
Leontopithecus rosalia	Callithrichinae	Vertical clinging/Leaper	Male	609	USNM588152	National Museum of Natural History; Smithsonian Institution
Mico argentatus	Callithrichinae	Vertical clinging/Leaper	Male	345	USNM399069	National Museum of Natural History; Smithsonian Institution
Mico humeralifer	Callithrichinae	Vertical clinging/Leaper	?	473.5	AMNH188164	American Museum of Natural History
Mico melanurus	Callithrichinae	Vertical clinging/Leaper	Female	350	USNM574137	National Museum of Natural History; Smithsonian Institution
Pithecia monachus	Pitheciinae	Arboreal quadrupedalism	Male	2360	USNM395692	National Museum of Natural History; Smithsonian Institution
Pithecia pithecia	Pitheciinae	Arboreal quadrupedalism	Male	1760	AMNH149149	Morphosource (http://morphosource.org/)
Saguinus fuscicollis	Callithrichinae	Vertical clinging/Leaper	?	350.5	AMNH147433	American Museum of Natural History
Saguinus leucopus	Callithrichinae	Vertical clinging/Leaper	Female	492	AMNH148322	American Museum of Natural History
Saguinus midas	Callithrichinae	Vertical clinging/Leaper	Male	545	AMNH97316	Morphosource (http://morphosource.org/)
Saguinus mystax	Callithrichinae	Vertical clinging/Leaper	Male	524.5	AMNH188171	Morphosource (http://morphosource.org/)
Saguinus oedipus	Callithrichinae	Vertical clinging/Leaper	Female	411	AMNH200882	American Museum of Natural History
Saimiri boliviensis	Cebinae	Arboreal quadrupedalism	Male	811	AMNH211596	American Museum of Natural History
Saimiri sciureus	Cebinae	Arboreal quadrupedalism	Male	720.5	AMNH188090	Morphosource (http://morphosource.org/)

* Aristide et al. 2015

Table 5.2 Fossil sample

Fossil	Age	Locality	Body mass estimates (g) **	Accession number	Museum
Dolichocebus gaimanensis	~ 20.0 Ma	Sarmiento, Chubut, Argentina	1601	MACN 362	Museo Argentino de Ciencias Naturales "Bernardino Rivadavia", Buenos Aires, Argentina.
Carlocebus carmenensis	17.5–16.5 Ma	Pinturas, Santa Cruz, Argentina	2914	MACN304	Museo Argentino de Ciencias Naturales "Bernardino Rivadavia", Buenos Aires, Argentina.
Soriacebus ameghinorum	17.5–16.5 Ma	Pinturas, Santa Cruz, Argentina	1721	MACN 397	Museo Argentino de Ciencias Naturales "Bernardino Rivadavia", Buenos Aires, Argentina.
Madre de Dios	~ 18.75–16.5 Ma	Atalaya, Cusco, Upper Madre de Dios Basin, Peru	352	MUSM 2024	Museo de Historia Natural de la Universidad Nacional Mayor San Marcos, Lima, Peru.
Río Cisnes	16.5 Ma	Alto Río Cisnes, Chile	1510	SGO.PV 974	Museo Nacional de Historia Natural, Santiago, Chile.
Proteropithecia neuquenensis	15.8 Ma	Collón Curá, Neuquén, Argentina	2006	MLP 91-IX-1-119	Museo de La Plata, La Plata, Argentina.
Aotus dindensis *	13.0–13.2 Ma	La Venta, Madgalena Valley, Colombia	874	IGMKU 8802	Museo Geológico, INGEOMINAS, Bogotá, Colombia.
Cebupithecia sarmientoi	13.5–11.8 Ma	La Venta, Madgalena Valley, Colombia	1825	UCMP 38762	University of California, Berkeley Museum of Paleontology, Berkeley, California, USA
Neosaimiri fieldsi *	12.0–13.2 Ma	La Venta, Madgalena Valley, Colombia	781	IGMKU 89031	Museo Geológico, INGEOMINAS, Bogotá, Colombia.
Paralouatta marianae *	~ 17.5–18.5 Ma	Domo de Zaza, Lagunitas Formation , Cuba	4709	MNHNCu 76.3059	Museo Nacional de Historia Natural de Cuba, La Habana, Cuba.

* Scans obtained from casts   ** Body mass estimates from Püschel et al. (2017)

Phylogeny

An updated platyrrhine phylogeny (Aristide et al., 2015) was modified slightly in R v.3.4.0 (https://www.r-project.org/) to include some species that were initially not present (i.e. *Ateles marginatus, Aotus infulatus, Chiropotes satanas, Mico melanurus,* and *Saguinus leucopus*) (Sena et al., 2002; Bonvicino et al., 2003; Araripe et al., 2008; Menezes et al., 2010) and to remove some species that were in the phylogeny but for which there was no talar data. This phylogeny (Supporting information 1 in this chapter) was used when necessary to carry out the described comparative analyses.

3D surface rendering

Surface models were imported into Geomagic Studio v. 12 (Geomagic, USA), where the irregularities that appeared due to the generation of the models when they were scanned were repaired using refinement and smoothing tools (Marcé-Nogué et al., 2015). The tali were aligned according to the standard anatomical position. In order to avoid possible problems when aligning different individuals according to the anatomical standard plane (due to inter-specific morphological differences), we selected one individual as a reference (i.e. *Chiropotes satanas*) to perform a best-fit alignment using Geomagic. This procedure was carried out prior to FEA to align all the models so that loads could be applied in the same axis and to allow an easier interpretation of the stress results. The procedure involved fitting two talar models at each time by measuring from point to point and adjusting the location of the target model to the stationary reference specimen until the average deviation was as low as possible using an iterative procedure (sample size: 9,999). The sums of squares of the distances between the sample pairs were minimized over all the rigid motions that could realign the two models to attain the best-fit alignment between them. This process was repeated for each one of the analysed specimens. After a CAD conversion, the models were imported into ANSYS 17.1 http://www.ansys.com/ software to perform the FEA modelling.

Fossil reconstruction

Some of the analysed fossils exhibit damage due to post-depositional processes. These missing anatomical regions were virtually reconstructed in order to generate models

suitable for FEA, because these specimens are key to understand the full range of variation in the available NWM fossil record. Different reconstruction approaches were applied depending on the specific preservation conditions of the fossils. The case-specific reconstruction methods that were applied are described in the Supporting information 2 of this chapter.

Locomotor categories

The analysed extant platyrrhine species were classified according to their main locomotion mode in three categories (i.e. Clamber/Suspensory, Leaper/Clawed and Arboreal quadrupedalism) based on the work of Youlatos and Meldrum (2011) in order to compare if there were differences due to different locomotion modes (Table 5.1).

5.2.2 Finite element analysis

Model properties

A structural static analysis to assess the biomechanical behaviour of the 40 extant tali were performed using the Finite Element Package ANSYS 17.1. The aim of this study was to carry out a structural comparative analysis using FEA, and so we were not interested in estimating the actual *in vivo* value of load forces or resulting stresses (Püschel and Sellers, 2016). Consequently, FEA was applied in a comparative manner rather than being used to validate the models against experimental data (Piras et al., 2013; Bright, 2014).
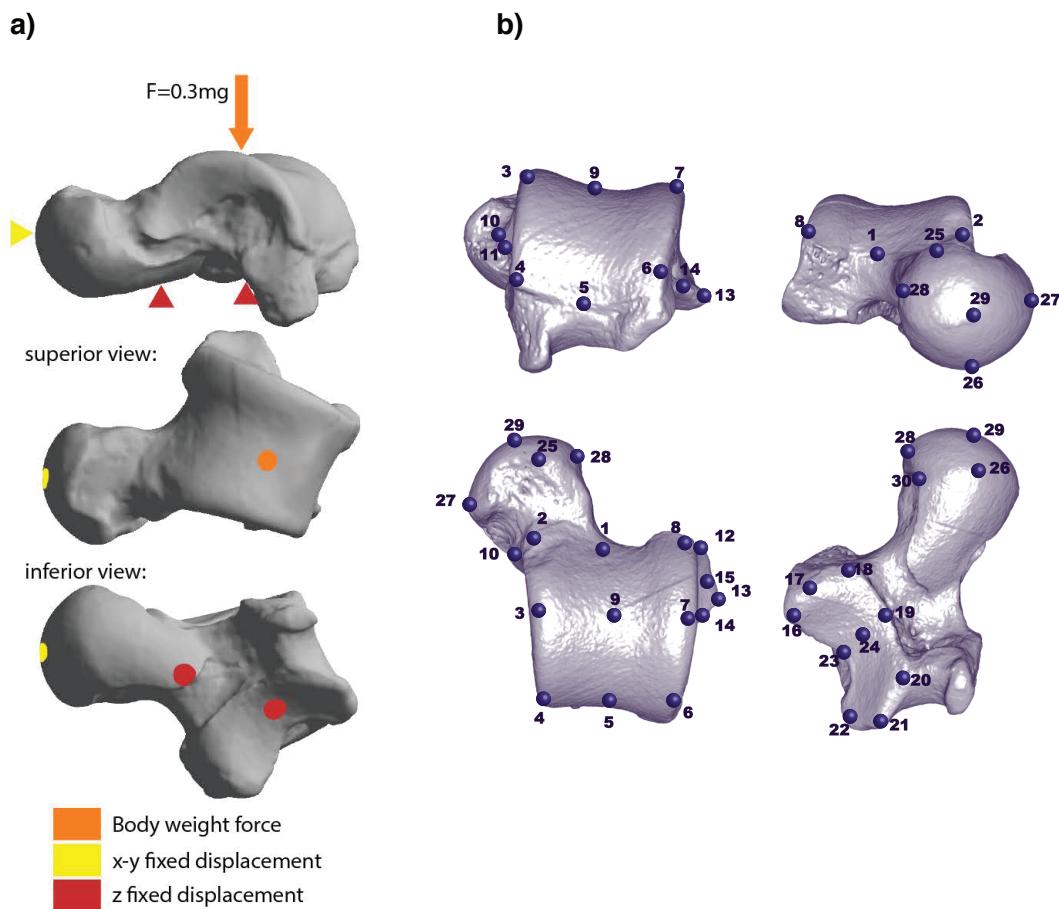
Homogeneous, linear and elastic material properties were assumed for the talar models. Unfortunately, there is almost a total absence of material property values for the platyrrhine talus, and certainly no information about whether it varies between taxa; hence the values applied for cortical bone in a human talar FEA simulation were used instead (Young's modulus: 20.7 GPa; Poisson's ratio 0.3) (Parr et al., 2013). However, it is important to notice that these values do not affect the comparative framework when computing stress in all the models (Gil et al., 2015).

In this study, we obtained the von Mises stress distribution in the talus under loading conditions. It has been shown that von Mises stress is the most accurate value used to predict fracture location when isotropic material properties are used to model cortical bone (Doblaré et al., 2004). The tali were modelled as solid models composed only of cortical bone in order to simplify the analyses and to limit the number of assumptions. Recent evidence has shown that FEA applied to specimens with unknown internal architecture can produce reliable results, even when the internal bone architecture cannot be modelled in detail (Fitton et al., 2015). The models were meshed with an adaptive mesh of hexahedral elements (Marcé-Nogué et al., 2015) meeting the conditions defined in Marcé-Nogué et al. (2016) to create a Quasi-Ideal Mesh (QIM), which allows statistical analysis of the values in the whole mesh. Further information about the FEA models can be found in the Supporting information 3 of this chapter.

Loading scenario and boundary conditions

Extant body mass data was obtained from Smith and Jungers (1997), while the fossil body mass prediction were obtained from Püschel et al. (2017) based on regressions of surface area measurements of the talar articular facets, which have been proven to be reliable and accurate predictors of body mass across primates (Yapuncich et al., 2015). Among living platyrrhine species, male and female body mass are highly correlated (Aristide et al., 2015), therefore average body mass were used in the subsequent analyses (Tables 5.1 and 5.2). Based on this information, we computed the Body Weight Force, which represents the applied load that was defined as the 30% of the average body mass of each species multiplied by gravitational acceleration g = 9.81 ms^{-2}. This load was applied on the trochlear surface of each talus, thus simulating a basic quadrupedal scenario (in most primates the hind limbs support more weight, hence the 30% [Raichlen et al., 2009]), which represents a common posture observed across platyrrhines families (Youlatos and Meldrum, 2011). This load was directed in the direction of the z-axis on the oriented tali to simulate the action of gravity and was located at the centre of the trochlear surface to simulate a compressive force. The talus was constrained on the areas comprising the sub-talar joint (i.e. anterior, medial and posterior calcaneal articular surfaces) as indicated in Figure 5.2a. Since the average mass of each species was used as the force applied in the models (via the use of the Body Weight Force), it was necessary to check that the observed differences in von Mises stress results between the different

platyrrhine taxa were not merely attributed to size-dependent effects. Therefore a multivariate phylogenetic regression (PGLS) of the stress percentile values on talar volume was performed taking into account the expected absence of independence across taxa due to the phylogenetic structure of the data. The obtained results indicate that allometry is not factor affecting our results when phylogenetic non-independence is considered (Supporting information 4 in this chapter).

Figure 5.2 a) Loading scenario tested in the FEA; b) the thirty landmarks used in the GM analyses.

Average Values and Quasi-Ideal Mesh

The von Mises stress distributions of the different tali were assessed using their average values and displayed using box-plots following previous suggestions (Farke, 2008). The application of box-plots for the stress and statistics derived from them (e.g. percentiles)

involves the generation of a quasi-ideal mesh (QIM), which corresponds to a mesh where all the elements have practically the same size, thus allowing the display of the obtained stress values as boxplots (Marcé-Nogué et al., 2016). Since a QIM is a non-uniform mesh (although its elements are almost identical), new statistics that consider this non-uniformity were calculated: 1) the mesh-weighted arithmetic mean (MWAM) and 2) the mesh-weighted median (MWM). Some data points contribute more than others depending on the size of the element in the MWAM, which is the sum of the value of the von Mises stress for each element multiplied by its own volume and divided by the total volume, whereas the MWM corresponds to the division of the median of the product of stress and volume by the median of the volume (Marcé-Nogué et al., 2016). These statistics (i.e. MWAM and MWM) are required to compute the percentage error of the arithmetic mean (PEofAM) and percentage error of the median (PEofM), which are values needed to ensure that the models were good-enough QIMs as described in Marcé-Nogué et al. (2016). By ensuring a QIM, we are able to use the stress values in the percentiles 25%, 50%, 75% and 95% of the von Mises stress distribution as talar strength proxies as well. The highest value of the boxplot was not considered since unusually high stresses appear where the boundary conditions are located. These stresses are artificially elevated, tending to infinity, by the constraints exerted on the model due to a numerical singularity (Marcé-Nogué et al., 2015). This numerical singularity results from the mathematical approach applied, and not to any meaningful biological process. Consequently the highest results from these areas were not considered, and instead we used the 95% percentile as a peak stress (Walmsley et al., 2013).

Analysis of the stress results

All statistical analyses were performed in R v.3.4.0 (R Core Team, 2017). A Mardia's multivariate normality test (i.e. Mardia's multivariate skewness and kurtosis coefficients) was applied to check the assumption of multivariate normality in the distribution of the stress percentiles. It was found that the stress percentile data was not multivariate normal (g1p: 5.48, skewness Chi-square: 36.53, p-value: 0.013; g2p: 28.61, kurtosis Z: 2.11, p-value: 0.035), therefore non-parametric statistics were preferred to analyse the stress data. First a PERMANOVA was calculated to test for differences between the groups considering all the stress percentiles together (Anderson, 2001). Then, pairwise PERMANOVA tests with a Holm correction for multiple comparisons were carried out

to test for differences in stress values between the three locomotor categories (the code for this test can be found in the Supplementary information 5 of this chapter). In both cases Euclidean distances were used as similarity index. The null hypothesis that there were no significant differences in talar strength between different locomotor categories was tested.

5.2.3 Geometric Morphometrics

The 3D models of all the analysed platyrrhines were used to perform GM analyses. Most of the specimens were right tali, but some of them were reflected when necessary to provide a uniformly right-sided dataset. First, a series of 30 Cartesian coordinates were collected on the surface of the models based on Turley and Frost (2013) (Fig. 5.2b). These coordinates were collected using Landmark editor v. 3.6 (Wiley et al., 2005) and then imported into R 3.4.0 to carry out the GM analyses using the 'geomorph' package (Adams and Otárola-Castillo, 2013). A Procrustes superimposition was performed on these coordinates to remove the differences due to scale, translation and rotation, leaving only variables directly related to shape. Then these shape variables were used to carry out a principal component analyses (PCA) in order to visualise morphological affinities. A broken-stick model was used to assess significance of variance (Jackson, 1993), which was applied to determine the number of PCs to be used in the subsequent analysis. This procedure was carried out to reduce the number of variables, produced by 40 taxa represented by 30 3D landmarks each. In order to visualize the structure of the data for both shape and stress variables, a consensus phylogeny was projected onto the space identified by the first two PCs obtained from the variance-covariance matrix of the shapes of the analysed modern taxa and the mesh-weighted median stress value (i.e., MWM) on the z-axis.

Then a standard PLS and a phylogenetic PLS analysis were carried out to examine the association between the shape variables and the percentile stress values (Rohlf and Corti, 2000). PLS computes the covariation level between the two blocks of data, while the phylogenetic PLS also takes into account the phylogenetic structure of data assuming a Brownian motion model of evolution (Adams and Felice, 2014). PLS does not assume that one block of variables is dependent on the other, hence being a valuable method

when assessing the relationship between blocks of data that could covary but for which there is no *a priori* directional relationship (Rohlf and Corti, 2000).

5.3.4 Fossil locomotor classification

A previous study has shown that using only talar shape it was possible to distinguish between these three main locomotion modes (Püschel et al., 2017), but it remains unexplored whether including stress information explain the differences in talar functional morphology between different locomotor modes or improve the locomotor resolution. Therefore, two different datasets were analysed and used to classify the fossil material: 1) biomechanical and 2) morphometric data.

In this case, the biomechanical data comprised a set of variables generated using the Intervals' method described in Marcé-Nogué et al. (2017a). This recently published methodology divides the values of stress of all the elements of the model into different N intervals, each one of them corresponding to the amount of volume of the original model having a specific range of stress values. These percentages are computed in relation with the total volume of the model of each specimen for standardisation. The number of intervals to be analysed (i.e. the number of biomechanical variables) was chosen following the convergence procedure proposed by Marcé-Nogué et al. (2017a), in which several PCAs are performed using a different number of intervals (in this case: 5, 10, 25, 50, 75 and 100) in order to establish the threshold in which the data converged (i.e. when adding more intervals yielded similar patterns in the PCAs and when the correlation between the respective first PCs was higher than 0.99). The obtained results from this procedure showed that convergence was easily obtained by using just 10 intervals (Supporting information 6 in this chapter). As a pre-processing procedure a Box-Cox transformation was performed in order to normalise the interval data. In addition, these 10 intervals were centred and scaled to improve the numerical stability of some subsequent calculations and to standardize their scale. As a result of centring, the variables have a zero mean, while scaling coerce the predictors to have a common standard deviation of one. These transformed interval values were subsequently used in the classification analyses.

The morphometric data consisted of the number of PCs obtained from the broken-stick model used to assess significance of variance (Jackson, 1993); this procedure was performed as a way to reduce the dimensionality of the dataset. This broken-stick model showed that only the first seven PCs had eigenvalues larger than the values randomly generated by the model. These seven PCs accounted for 63.6% of the total variance of the sample, thus providing a reasonable approximation of the total amount of talar shape variation. There was no need to perform any pre-processing procedure prior to the application of the ML classification methods given that the original raw coordinates were subjected to a Procrustes superimposition, which centred each configuration of landmarks at the origin, scaled them to unit centroid size and rotated them to optimal alignment on the average shape. In addition, a PCA was carried out using these shape coordinates to avoid any possible collinearity.

Six supervised algorithms were selected in order to represent a wide range of different classification models: Linear discriminant analysis (LDA); 2) classification and regression tree (CART); 3) k-nearest neighbours (kNN); 4) Naïve Bayes (NB); 5) support vector machine (SVM); and 6) Random Forest (RF). All the models were prepared and performed using the 'caret' package for R (Kuhn, 2008), which consist of a set of functions that help to streamline the generation of predictive models. A technical outline of these different algorithms is far beyond the scope of this study and several introductory books cover the topic (e.g. Kuhn and Johnson, 2013a; Hastie et al., 2017; James et al., 2017), along with the 'caret' package webpage https://topepo.github.io/caret/. This package also provides a grid search (automatic and manual) where it is possible to specify tuning parameters for the models. We first started with an automatic grid search by setting the 'tuneLength' option to indicate the number of different values to try for each algorithm parameter (we initially set this parameter to 10 in all the tested models). This only supports integer algorithm parameters, thus providing a quick first guess as to what values to try and which models are more promising. Then the models that were the most accurate for each one of the datasets (i.e. biomechanical and morphometric data) were further tuned by setting a manual grid search. In the grid, each algorithm parameter was specified as a vector of possible values. These vectors were combined to define all the possible combinations to further improve the performance of the model. Then using the best final model the fossil sample was

classified into the different locomotor categories by computing the class probabilities of belonging to each one the categories.
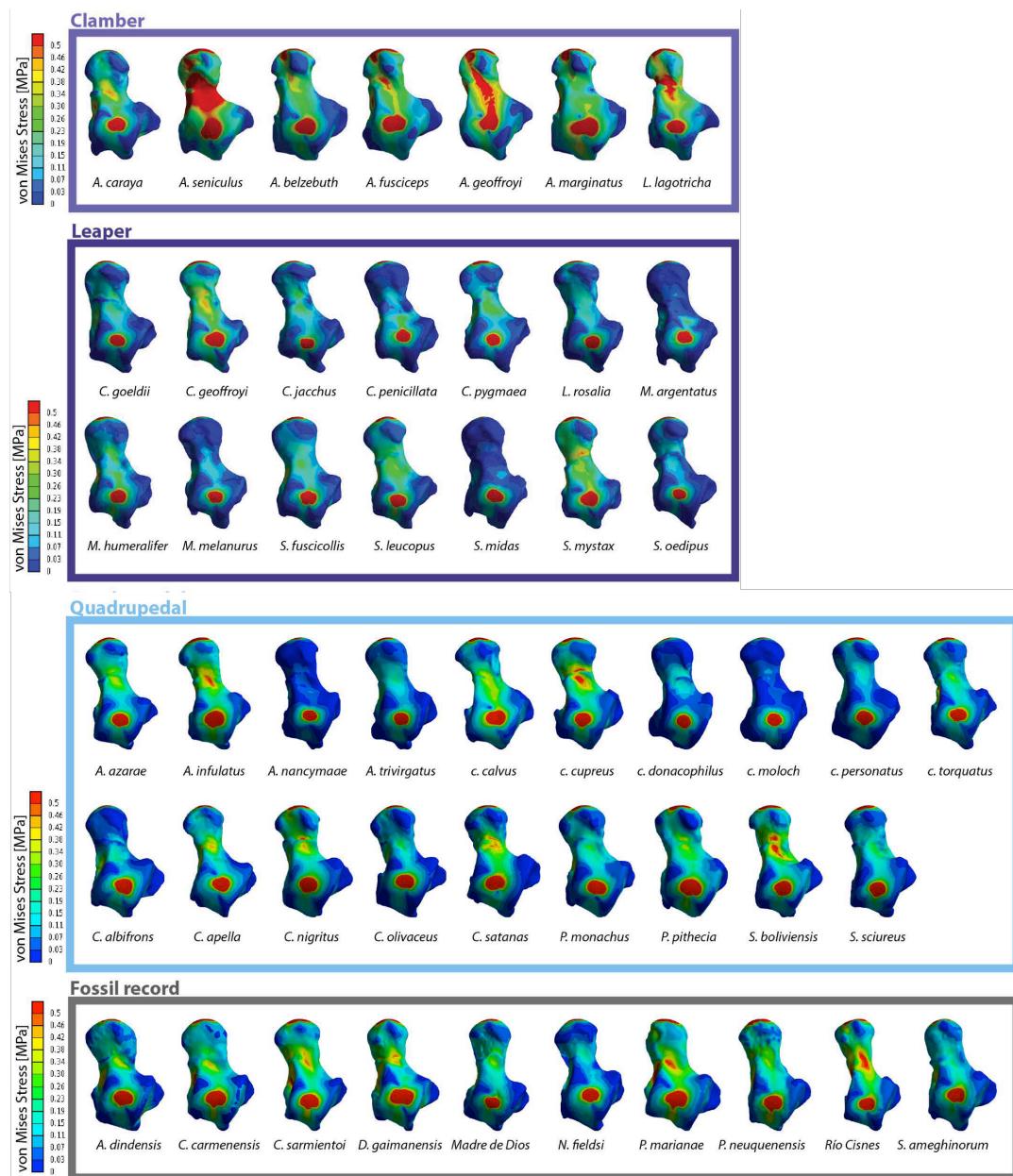
The performance of the classification models was quantified using the confusion matrix from which the overall classification accuracy (i.e. error rate) was computed. In addition, Cohen's Kappa was also calculated as a performance measurement. This statistic can range between −1 and 1, where a value of 0 means that there is no concordance between the observed and predicted classes, whilst a value of 1 would indicate perfect agreement of the model prediction and the observed classes (negative values are indicative that the prediction is in the opposite direction of the truth, but large negative values are rare when dealing with predictive models) (Kuhn and Johnson, 2013b). To assess the performance of the models, the complete dataset was resampled using a "leave-group-out" cross-validation, which is also known in the literature as "Monte Carlo" cross-validation or repeated training/test splits (Kuhn and Johnson, 2013c). This method simply generates multiple splits of the data into modelling and prediction sets. In this study this procedure was repeated 200 times and the data was divided into a modelling set containing 75% of randomly allocated observations, whilst the testing set contained the remaining 25%. The repetition number was selected to get stable estimates of performance and to reduce the uncertainty in these performance estimates. This procedure was preferred since is a much more efficient use of our reduced sample size than splitting the dataset into only one training and one testing subset. Finally, the best classification models obtained for the morphometric and biomechanical data were then used to infer the main locomotor mode of the Miocene fossil sample by computing their class probabilities to belong to each one of the locomotor categories.

5. 3 Results
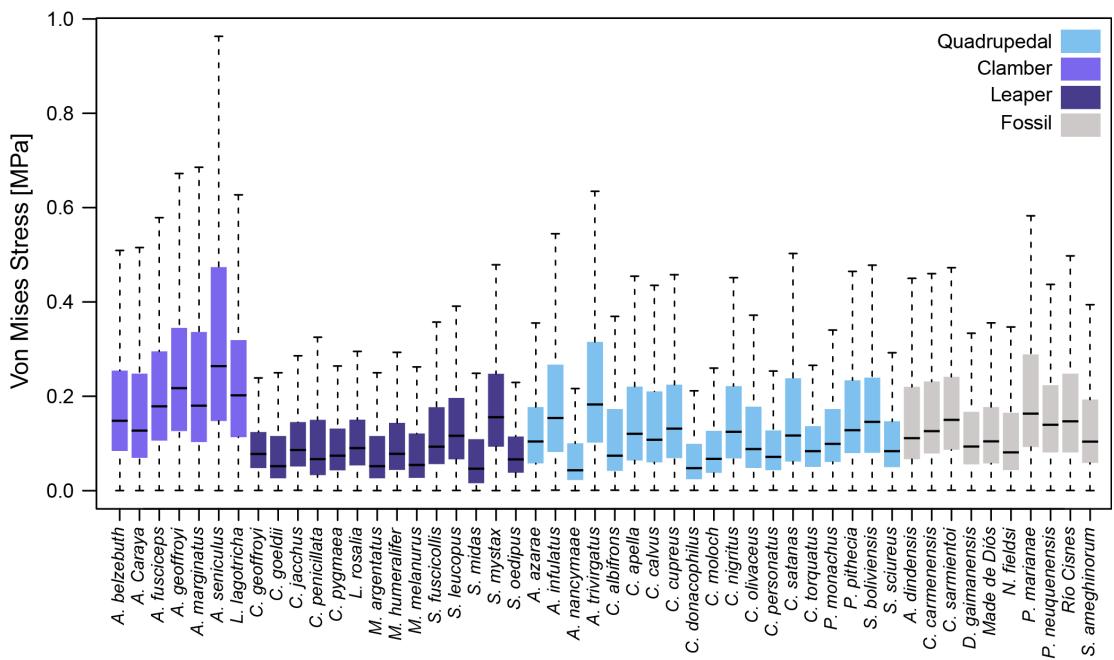
5.3.1 Finite element analysis

Figure 5.3 shows the maps of stress distribution for all the analysed species, while Figure 5.4 displays the stress distribution of the QIM in boxplots. These two figures help visualise the von Mises stress distribution on the models, as well as to quantitatively display the obtained stress results. The visual representation of the stress distribution for each talus is a useful indicator for comparative inference on their biomechanical

behaviour because these stress patterns can be interpreted as a sign of relative strength, with specimens with higher stresses being consequently weaker. The quantitative values of MWM, MWAM, the quartiles of the boxplots of stress, the PEofAM and the PEofM (i.e. percentages of error used to define the QIM) can be found in the Supporting information 3 of this chapter.

Figure 5.3 von Mises stress distribution for all the analysed specimens

Figure 5.4 Box-plots of von Mises stress distributions for all the analysed specimens.

Analysis of the stress results

Figure 5.4 shows that when comparing locomotor behaviours in extant species, the Clamber/Suspensory group exhibit the weakest tali, while the Arboreal quadrupedal taxa show intermediate values and Leaper/Clawed species present the strongest tali. There were significant differences between groups when comparing all the stress percentiles together using the PERMANOVA (F: 21.437; R^2:0.54; p-value: 1e-04; 9,999 permutations) (Table 5.3). Therefore, it is possible to distinguish these main locomotor behaviours using a biomechanical approach.
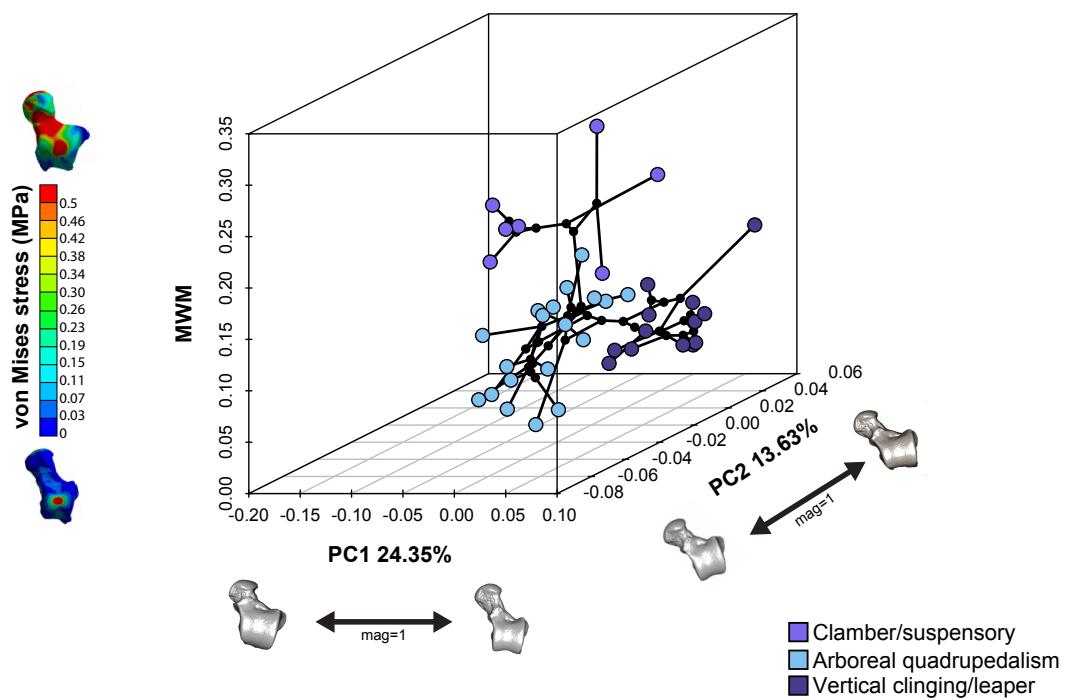
Table 3. Pairwise PERMANOVA results

Pairs	F	R^2	adjusted p-value (Holm)
Clamber/suspensory vs. arboreal quadrupedalism	18.84	0.44	0.003
Clamber/suspensory vs. vertical clinging/leaper	57.05	0.75	0.003
Arboreal quadrupedalism vs. vertical clinging/leaper	6.18	0.17	0.012
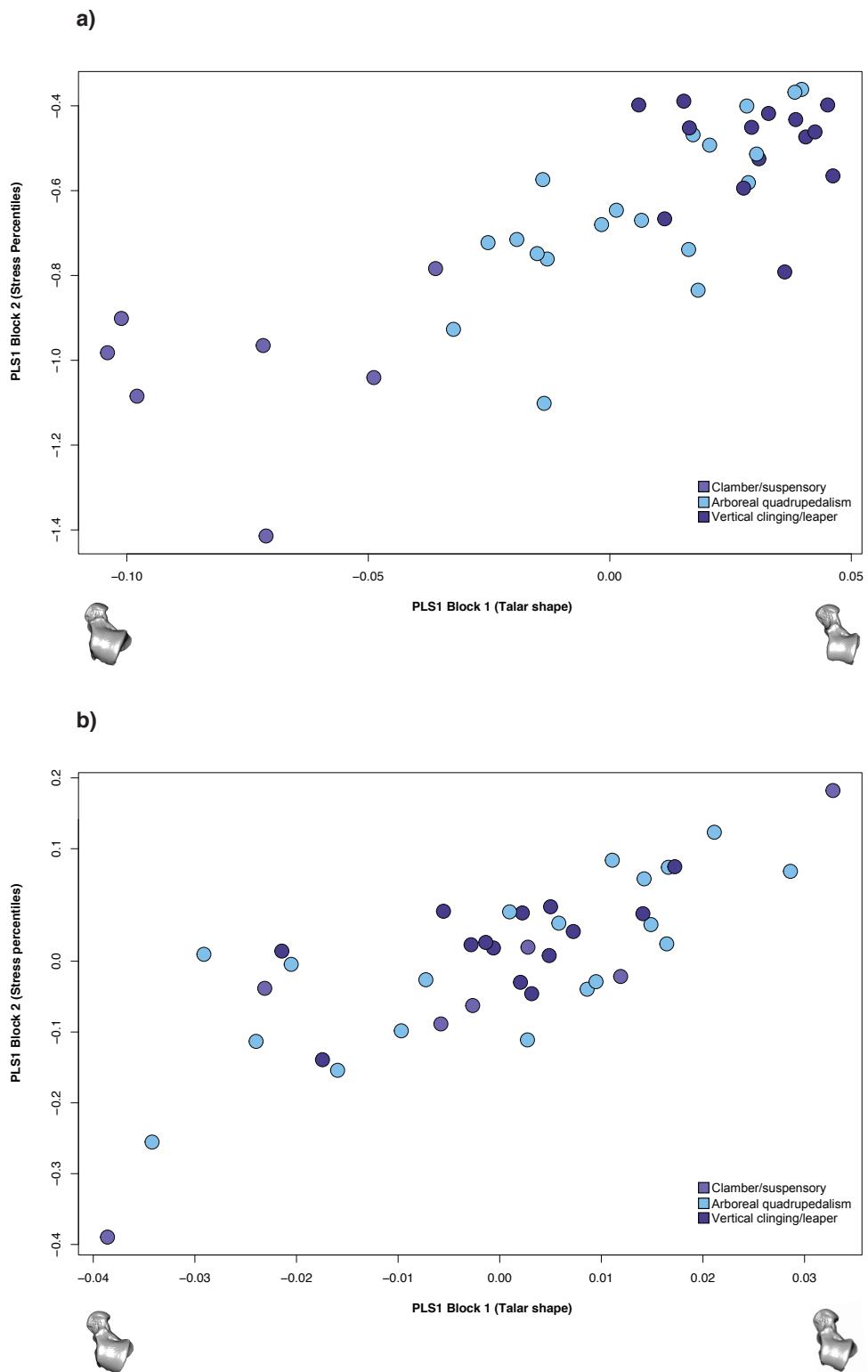
5.3.2 Geometric Morphometrics

The phylomorphospace of the first two PCs and the mesh-weighted median stress (i.e. MWM) as z-axis displays three main areas of occupied morphospace (Fig. 5.5), which broadly resemble the main NWM locomotor groups. PC1 mostly separates between the Atelidae on one extreme of the axis, which show clambering/climbing and suspensory behaviours, and the Callitrichinae, displaying claw-assisted clinging postures and higher frequency of leaping behaviour towards the opposite extreme of the axis. PC2 mostly distinguished between increasingly quadrupedal species from the other two locomotor categories. Finally, the MWM z-axis mostly separated between the clamber/climbing Atelidae (which show higher stress values) from all the rest of species.

The percentile stress values (i.e. M25, M50, M75, M95) showed significant covariation with talar shape (r-PLS: 0.8; p-value 2e-04; 9,999 permutations), as well as when considering the phylogenetic information (phylogenetic r-PLS: 0.78; p-value: 0.0018; 9,999 permutations) (Fig. 5.6a and 5.6b, respectively). This means that there is a strong association between talar shape and the biomechanical performance of the talus.

Figure 5.5 Phylomorphospace of the first two PCs and stress values (Mesh-weighted median) as vertical z-axis. One of the models closest to the mean shape was warped to match the multivariate mean using the thin plate spline method, and then the obtained average model was warped to represent the variation along the PC axes. In addition, the von Mises stress maps of two extreme models are displayed for reference to facilitate the understanding of the z-axis.
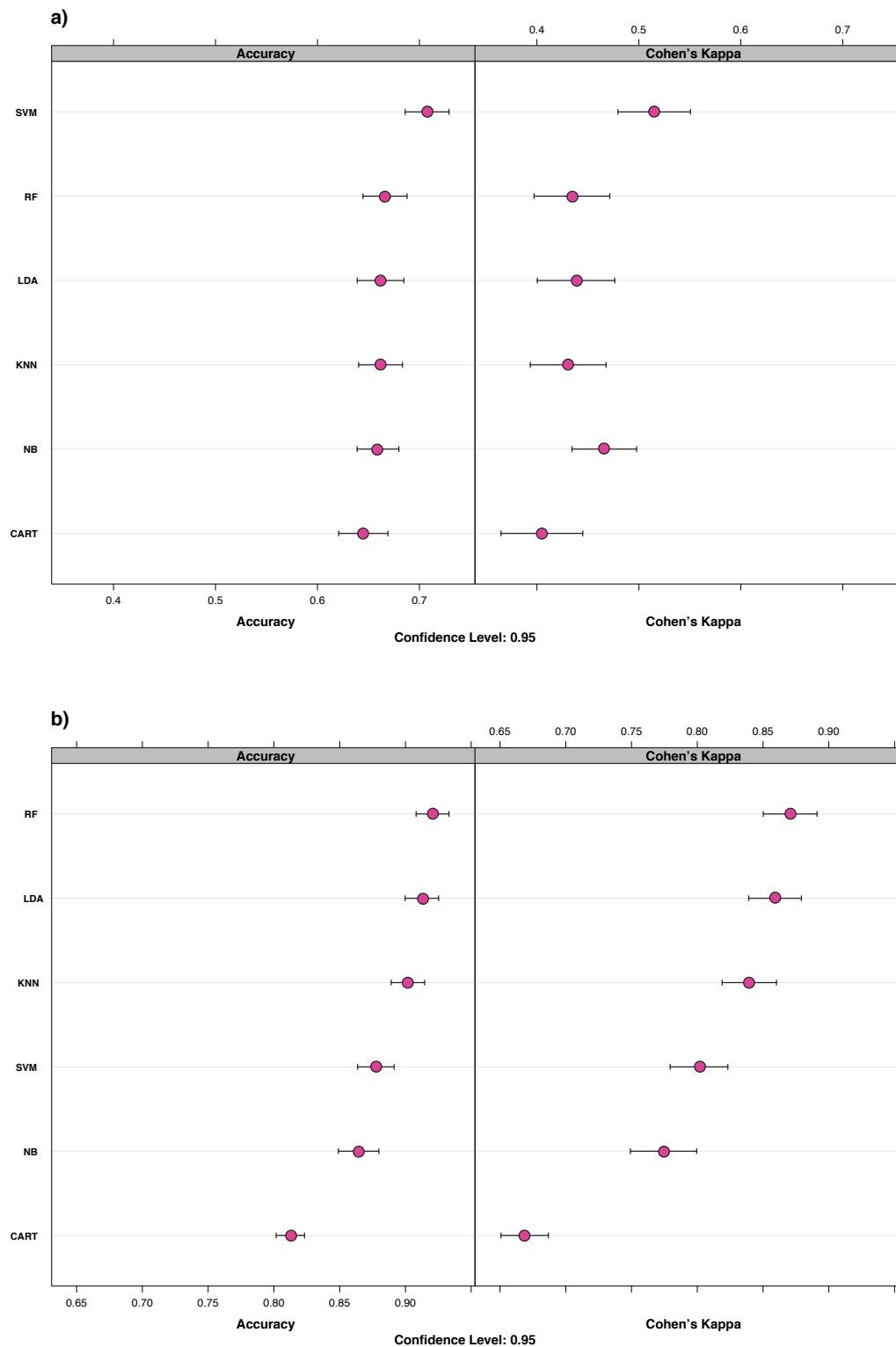
Figure 5.6 a) Standard partial least squares (PLS) and d) the phylogenetic PLS analysis of the shape variables and stress percentiles values. One of the models closest to the mean shape was warped to match the multivariate mean using the thin plate spline method, and then the obtained average model was warped to represent the covariation between the two blocks of data for PLS1.
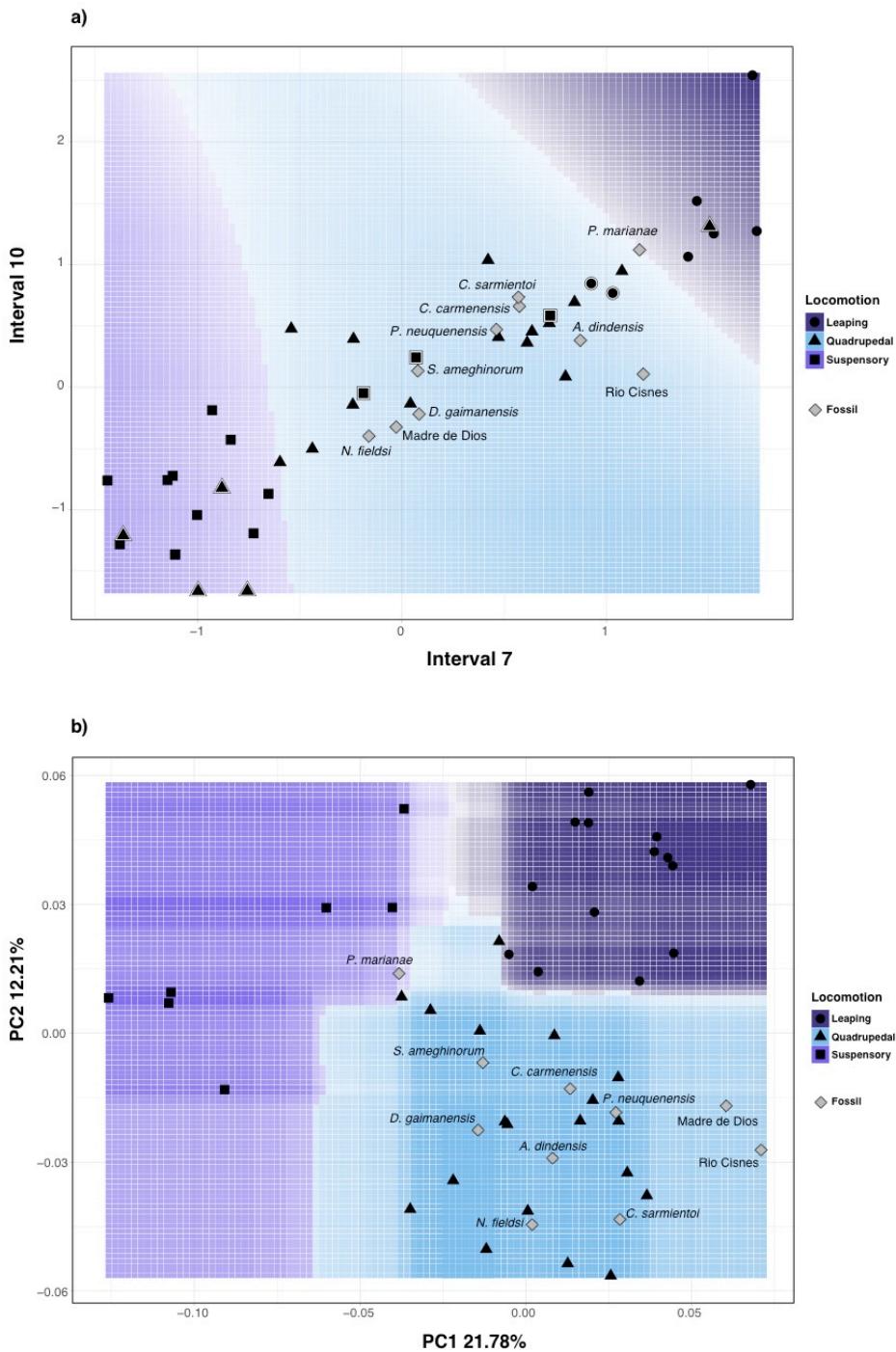
5.3.3 Fossil locomotor classification

Figure 5.7 shows the accuracy and Cohen's Kappa results for all the tested models for both the a) biomechanical and the b) morphometric data after performing the "leave-group-out" cross-validation and using the automatic grid search. In general shape data outperformed interval stress data when classifying according to locomotion in both accuracy and Cohen's Kappa values. The most accurate model for the biomechanical data was the support vector machine using a linear kernel (SVM), while in the case for the morphometric data the most accurate model was the Random Forest (RF). The only tuning parameter in the biomechanical SVM model using a linear kernel is 'cost', so we expanded the grid search to consider more values, however the best result was still achieved when cost = 2 (Average accuracy: 0.708; Average Cohen's Kappa: 0.515) (Fig 5.8a). A Cohen's Kappa value of ~0.5 represents a reasonable agreement (Kuhn and Johnson, 2013b); therefore we used the best obtained model to classify the fossil sample (Table 5.4a.). Using these interval data all the specimens were classified as arboreal quadrupeds.

The obtained RF model for the morphometric was further tuned using a manual grid search. Two parameters were tuned, the number of tress to grow (i.e. 100, 200, 500, 1000 and 2000) and number of variables randomly sampled as candidates at each split (i.e. 2,3,4,5 and 6). In general, the RF model was quite robust when changing these tuning parameters, showing similar classification accuracies. The final best RF model grew 200 trees and used five of variables randomly sampled as candidates at each split (Average accuracy: 0.925; Average Cohen's Kappa: 0.876) (Fig 5.8b). By applying the final RF model the fossil sample was classified (Table 5.4b), and all the specimens were categorised as arboreal quadrupeds excepting *Paralouatta marianae*, which was classified as a clamber/suspensory individual.

Figure 5.7 Dot-plot comparing the accuracy and Cohen's Kappa values of the different classification models applied to a) biomechanical (i.e., stress intervals) and b) morphometric data (i.e., seven PCs). The magenta dots represent the average accuracy and Cohen's Kappa values after performing the "leave-group-out" cross-validation (200 repeats), while the whiskers display their respective 0.95 confidence level.

Figure 5.8 Decision boundary plots for a) biomechanical and b) morphometric data. In a) only the seventh and tenth intervals are displayed because they contribute the most to class separation, while in b) only the first two PCs are shown. The colours represent the different locomotor category decision boundary, whilst transparency represents the probability for the predicted class in a particular graph area (i.e., darker colours imply higher probabilities of belonging to that class). Symbols surrounded by a white rim represent misclassified specimens.

Table 5.4 Prediction results for the fossil sample

Specimen	a) SVM model using Biomechanical data			b) Random Forest model using Morphometric data		
	Class probabilities			Class probabilities		
	Vertical clinging/leaper	Arboreal quadrupedalism	Clamber/suspensory	Vertical clinging/leaper	Arboreal quadrupedalism	Clamber/suspensory
Aotus dindensis	0.07	0.71	0.22	0.03	0.92	0.04
Carlocebus carmenensis	0.15	0.68	0.17	0.05	0.93	0.02
Cebupithecia sarmientoi	0.37	0.46	0.18	0.04	0.89	0.07
Dolichocebus guimanensis	0.13	0.79	0.08	0.02	0.97	0.01
Madre de Dios	0.32	0.59	0.09	0.15	0.74	0.11
Neosaimiri fieldsi	0.24	0.68	0.08	0.01	0.98	0.01
Paralouatta marianae	0.09	0.46	0.45	0.21	0.36	0.42
Proteropithecia neuquenensis	0.41	0.43	0.17	0.05	0.94	0.01
Río Cisnes	0.13	0.62	0.25	0.08	0.79	0.13
Soriacebus ameghinorum	0.22	0.68	0.10	0.01	0.99	0.00

5.4 Discussion

Studying the functional morphology of the platyrrhine talus is important because it represents one of the few post-cranial structures available in many of the oldest platyrrhine fossils (Youlatos and Meldrum, 2011), but also since its morphology has been shown to reflect locomotor behaviour (Püschel et al., 2017) and being associated with biomechanical performance (as shown in the present study). This study has shown that a combined approach using FEA, GM and ML algorithms can contribute in the understanding of platyrrhine talar morphology and its relationship with locomotion.

The biomechanical data obtained from the FEA modelling show that the clamber/suspensory species exhibit significantly higher stresses than the other two analysed locomotor categories, while the vertical clingers/leapers show the lowest stress values. This could be explained by the fact the leaping would be expected to exert higher forces on the lower extremities since the accelerations in primate leaping are generally high (for review see Crompton and Sellers, 2007), while suspensory behaviours would exert comparatively reduced bending forces on the limb bones (Swartz et al., 1989) and bending has been shown to be the loading pattern that most commonly leads to high stresses in limb bones (Brassey et al., 2013). In addition, it has also been shown that repetitive loading can cause bones to fail at much lower loads (Daffner, 1978; Buettmann and Silva, 2016). In order to avoid the possible damage caused by the effect of fatigue, it is plausible that talar morphologies that reduce stress would have been selected for in these groups. A recent study has shown that platyrrhine talar morphology seemed to evolve towards three different selective optima (Püschel et al., 2017), which are related to the main ecophylectic groups observed in extant NWM, and the three main locomotor groups analysed here.

The morphometric analysis clearly distinguished in PC1 between the species showing frequent leaping/vertical clinging from those with adaptions for suspensory/climbing behaviour, while PC2 distinguished the most quadrupedal species from the rest. The talar morphology of the species exhibiting leaping can be described as showing an anteroposteriorly shorter trochlea with more parallel medial and lateral rims and a longer anterior calcaneal facet. This morphology was the strongest one in the biomechanical analysis. On the other hand, the weakest talar morphology, which is associated with

clamber/suspensory behaviours, included characters such as a broader head, greater trochlear wedging, a lower trochlea and a shorter anterior and longer posterior calcaneal facet.

The PLS analyses showed that there is an association between talar shape and stress values. A previous study has shown that there is also a significant association between locomotor data and talar morphology (Püschel et al., 2017), therefore the present results contributes in the understanding about the relationship between talar morphology and locomotor behaviour by providing the link between these two factors: the biomechanical behaviour of talus during locomotion. The talus acts as the main mechanical link between the leg and the foot (Parr et al., 2013), transmitting not only the forces derived from an animal's body mass, but also providing stability and mobility for the lower limbs during diverse postural and locomotor behaviours (Boyer et al., 2015). It has been proposed that mechanical loading regulates trabecular remodelling (Turner, 1998; Zadpoor et al., 2012), and therefore different locomotor repertoires should exert differential loading regimes on the talus, thus gradually shaping its morphology. Although we only simulated a simplistic static biomechanical scenario, we were able to distinguish between main locomotor modes.

When comparing the two techniques (i.e. FEA and GM) in the classification task using several ML algorithms, the best performing approach was a RF model applied to GM data. Even though we were concerned with functional groupings, we found that shape outperforms FEA derived values when classifying according to locomotor groups. This is likely because morphological variation is influenced by diverse factors, including loading, diet, sex and evolutionary history, among others, all of which may be associated with differences in locomotion. A complex phenomenon such as the differences in locomotor behaviour reflected in talar morphology probably includes many factors that are only partially accounted when biomechanical analyses are performed. These kinds of analyses simply focus on more specific and constrained aspects of variation (e.g., loading resistance), whereas GM incorporates more diverse sources, although with the disadvantage of not always knowing what part of this variation is strictly related to function. General questions that ask what is the most likely locomotor behaviour of a fossil are probably best answered with statistical approaches that can include all the available information. The main value of biomechanical approaches is that they enable us

to test our ideas about the adaptive value of particular features of the fossils, in ways that purely associative statistical analysis alone cannot. This is when mechanical analyses such as FEA are required to test alternative functional hypotheses, making both approaches complementary. However, it is important to bear in mind that the load cases chosen only allow the FEA to consider specific aspects of function (e.g. stresses arising from specific loadings), and so may omit important functional differences that would require different measures of load resistance or different simulated load cases to characterise them. Therefore, it is possible that the functional analysis performed here failed to identify some functionally relevant differences between groups. It is still possible that a more detailed biomechanical scenario might yield better discriminating results when comparing locomotor groups, so future studies should test other loading scenarios that might improve discriminatory performance, including the possibility of generating load cases using multibody dynamic analysis as has been done with mastication (Moazen et al., 2008).

It is important to keep in mind that when reconstructing locomotor behaviours in fossil taxa, it is mostly the main locomotor modes that are reconstructed and not the entire repertoire of possible habits (MacPhee and Meldrum, 2006). This means that when the main locomotor mode is reconstructed in a certain species that does not imply that the animal was not capable of performing other locomotor behaviours, but rather that there was a predominant locomotor mode that is reflected in morphology. Both the biomechanical and morphometric based classifications categorised most of the fossil sample as arboreal quadrupeds, which is consistent with previous proposals based on morphological analyses, morphometric classifications and ancestral state reconstructions (Ford, 1988; Gebo et al., 1990; Tallman and Cooke, 2016; Püschel et al., 2017). It is interesting that in spite of the class imbalance that could affect our results, *Paralouatta* is still classified as a possible clamber/suspensory species using the morphometric data. Previous analyses have shown that its talar morphology is similar in its main aspects of variation to the Alouattinae (which are species that spend important amount of time exhibiting clamber/suspensory behaviours) and some of the oldest Patagonian fossils (i.e., *Dolichocebus*, *Carlocebus*, *Soriacebus*; which are specimens reconstructed as mostly quadrupedal) (Püschel et al., 2017). Based on the presence of a strong cotylar fossa, along with several other postcranial adaptations, it has been suggested that *Paralouatta* could even have been a semi-terrestrial species (MacPhee and Iturralde-Vinent, 1995; MacPhee

and Meldrum, 2006). The present analysis did not include this category so it not possible to rule out this possible locomotor specialisation, but the fact that our analysis indicate both clamber/suspensory and quadrupedal modes probably points to locomotor behaviours similar to *Alouatta* (i.e. showing variable degrees of arboreal quadrupedalism, climbing and clambering). It is also interesting that even though the Madre de Dios talus was classified as quadrupedal, its posterior probabilities suggest a variable degree of leaping behaviours as it has been previously proposed (Püschel et al., 2017). In addition the biomechanical results also suggests that *Proteropithecia* could have engaged in significant amount of leaping, which is also consistent with previous suggestions (Kay et al., 1998).

Several ecomorphological studies of diverse groups of animals have provided numerous morphological correlates of ecological, functional and/or locomotor categories (Püschel et al., 2017). Consequently, some of these morphological traits allow discrimination based on these kinds of categories, enabling us to make inferences about possible adaptations in extinct taxa. Nonetheless, absolute discrimination among such categories is rarely achieved by any single measurement or set of variables because these values normally show considerable overlap. This overlap is direct consequence of the covariation pattern observed in most morphological adaptations. This means that in many cases the way in which any morphological feature adapts might also be influenced by the changes occurring in other regions of an animal's morphology and by other environmental factors besides the one under analysis. The implication of this widespread covariation is that many ecomorphological adaptations might be better characterized by complex morphological patterns that can be better described in a multidimensional morphospace rather than defined by single variables or indices. These multidimensional spaces cannot be simply displayed in two dimensions, so traditionally multivariate techniques such as PCAs or LDAs have been commonly applied to deal with this sort of classification problems. However, more recently ML approaches have been used to tackle these sort of problems due to their inherent capabilities when it comes to uncover patterns, associations, and statistically significant structures in high dimensional data (MacLeod, 2007, 2017). The present study showed how using different ML algorithms is possible to successfully address problems of group analysis and classifications using morphometric and biomechanical data. The present findings have shown that the application of these algorithms to at least some types of morphometric and

biomechanical problems is a contribution that can improve the traditional way classification tasks have been undertaken in these fields. Some of the advantages are evident, such as the flexibility that allows the use of several different algorithms which can have dissimilar performance depending on the specific problem, rather than using only one classification approach (e.g., LDA) without comparing its performance against alternative approaches that might be more suitable for a particular task. The choice of algorithm is an active area of research within the ML field and depends on the characteristics of the dataspace being searched. Although further examples are needed to test how to apply ML classification techniques to functional morphology data, the potentialities are enormous. For example, the ability of some of these algorithms to deal with image identification could provide a complementary approach to traditional morphometrics that cannot typically deal with some visual information other than shape (e.g. texture, colour, etc.) that could provide highly useful when carrying out classification tasks. Incorporating the predictive modelling techniques derived from ML into the standard virtual functional morphology toolkit can prove to be a useful addition that could offer further flexibility and predictive power when analysing data and dealing with classification problems.

5.5 Acknowledgements

5.6 References

Adams, D.C., Felice, R.N., 2014. Assessing Trait Covariation and Morphological Integration on Phylogenies Using Evolutionary Covariance Matrices. PLOS ONE. 9, e94335.

Adams, D.C., Otárola-Castillo, E., 2013. geomorph: an r package for the collection and analysis of geometric morphometric shape data. Methods in Ecology and Evolution. 4, 393–399.

Adams, D.C., Rohlf, F.J., Slice, D.E., 2013. A field comes of age: geometric morphometrics in the 21st century. Hystrix the Italian Journal of Mammalogy. 21, 7–14.

Anderson, M.J., 2001. A new method for non-parametric multivariate analysis of variance. Austral Ecology. 26, 32–46.

Araripe, J., Tagliaro, C.H., Rêgo, P.S., Sampaio, I., Ferrari, S.F., Schneider, H., 2008. Molecular phylogenetics of large-bodied tamarins, Saguinus spp. (Primates, Platyrrhini). Zoologica Scripta. 37, 461–467.

Aristide, L., Rosenberger, A.L., Tejedor, M.F., Perez, S.I., 2015. Modeling lineage and phenotypic diversification in the New World monkey (Platyrrhini, Primates) radiation. Molecular Phylogenetics and Evolution. 82, Part B, 375–385.

Baylac, M., Villemant, C., Simbolotti, G., 2003. Combining geometric morphometrics with pattern recognition for the investigation of species complexes. Biological Journal of the Linnean Society. 80, 89–98.

Benítez, H.A., Püschel, T., Lemic, D., Čačija, M., Kozina, A., Bažok, R., 2014. Ecomorphological Variation of the Wireworm Cephalic Capsule: Studying the Interaction of Environment and Geometric Shape. PLoS ONE. 9, e102059.

Bignon, O., Baylac, M., Vigne, J.-D., Eisenmann, V., 2005. Geometric morphometrics and the population diversity of Late Glacial horses in Western Europe (Equus caballus arcelini): phylogeographic and anthropological implications. Journal of Archaeological Science. 32, 375–391.

Bond, M., Tejedor, M.F., Campbell Jr, K.E., Chornogubsky, L., Novo, N., Goin, F., 2015. Eocene primates of South America and the African origins of New World monkeys. Nature. 520, 538–541.

Bonvicino, C. r., Boubli, J. p., Otazú, I. b., Almeida, F. c., Nascimento, F. f., Coura, J. r., Seuánez, H. n., 2003. Morphologic, karyotypic, and molecular evidence of a new form of Chiropotes (primates, pitheciinae). American Journal of Primatology. 61, 123–133.

Bordas, A., 1942. Anotaciones sobre un "Cebidae" fósil de Patagonia. Physis. 19, 265–269.

Boyer, D.M., Seiffert, E.R., 2013. Patterns of astragalar fibular facet orientation in extant and fossil primates and their evolutionary implications. American Journal of Physical Anthropology. 151, 420–447.

Boyer, D.M., Seiffert, E.R., Simons, E.L., 2010. Astragalar morphology of Afradapis, a large adapiform primate from the earliest late Eocene of Egypt. American Journal of Physical Anthropology. 143, 383–402.

Boyer, D.M., Yapuncich, G.S., Butler, J.E., Dunn, R.H., Seiffert, E.R., 2015. Evolution of postural diversity in primates as reflected by the size and shape of the medial tibial facet of the talus. American Journal of Physical Anthropology. 157, 134–177.

Brassey, C.A., Margetts, L., Kitchener, A.C., Withers, P.J., Manning, P.L., Sellers, W.I., 2013. Finite element modelling versus classic beam theory: comparing methods for stress estimation in a morphologically diverse sample of vertebrate long bones. Journal of the Royal Society, Interface / the Royal Society. 10, 20120823.

Bright, J.A., 2014. A review of paleontological finite element models and their validity. Journal of Paleontology. 88, 760–769.

Brink, V. van den, Bokma, F., 2011. Morphometric shape analysis using learning vector quantization neural networks—an example distinguishing two microtine vole species. In: Annales Zoologici Fennici. BioOne, pp. 359–364.

Buettmann, E.G., Silva, M.J., 2016. Development of an in vivo bone fatigue damage model using axial compression of the rabbit forelimb. Journal of Biomechanics. 49, 3564–3569.

Chen, W.-P., Tang, F.-T., Ju, C.-W., 2001. Stress distribution of the foot during mid-stance to push-off in barefoot gait: a 3-D finite element analysis. Clinical Biomechanics. 16, 614–620.

Cheung, J.T.-M., Zhang, M., 2005. A 3-dimensional finite element model of the human foot and ankle for insole design. Archives of Physical Medicine and Rehabilitation. 86, 353–358.

Copes, L.E., Lucas, L.M., Thostenson, J.O., Hoekstra, H.E., Boyer, D.M., 2016. A collection of non-human primate computed tomography scans housed in MorphoSource, a repository for 3D data. Scientific Data. 3.

Crompton, R.H., Sellers, W.I., 2007. A Consideration of Leaping Locomotion as a Means of Predator Avoidance in Prosimian Primates. In: Gursky-Doyen, S.,

Nekaris, K.A.I. (Eds.), Primate Anti-Predator Strategies, Developments in Primatology: Progress and Prospects. Springer, Boston, MA, pp. 127–145.

Daffner, R.H., 1978. Stress fractures: Current concepts. Skeletal Radiology. 2, 221–229.

Daniel L. Gebo, M.D., 1990. New primate tali from La Venta, Colombia. Journal of Human Evolution. 19, 737–746.

Dobigny, G., Baylac, M., Denys, C., 2002. Geometric morphometrics, neural networks and diagnosis of sibling Taterillus species (Rodentia, Gerbillinae). Biological Journal of the Linnean Society. 77, 319–327.

Doblaré, M., García, J.M., Gómez, M.J., 2004. Modelling bone tissue fracture and healing: a review. Engineering Fracture Mechanics. 71, 1809–1840.

Farke, A.A., 2008. Frontal sinuses and head-butting in goats: a finite element analysis. Journal of Experimental Biology. 211, 3085–3094.

Feldesman, M.R., 2002. Classification trees as an alternative to linear discriminant analysis. American Journal of Physical Anthropology. 119, 257–275.

Fitton, L.C. , Prôa, M. , Rowland, C. , Toro-Ibacache, V. , O'Higgins, P. , 2015. The impact of simplifications on the performance of a finite element model of a Macaca fascicularis cranium. Anatomical Record . 298, 107–121.

Fleagle, J.G., 1990. New fossil platyrrhines from the Pinturas Formation, southern Argentina. Journal of Human Evolution. 19, 61–85.

Fleagle, J.G., 2013. Primate Adaptation and Evolution, 3rd edition. Academic Press, Amsterdam ; Boston.

Fleagle, J.G., Janson, C., Reed, K., 1999. Primate Communities. Cambridge University Press.

Fleagle, J.G., Kay, R.F., 1989. The Dental Morphology of Dolichocebus-Gaimanensis, a Fossil Monkey from Argentina. American Journal of Physical Anthropology. 78, 221–221.

Fleagle, J.G., Perkins, M.E., Heizler, M.T., Nash, B., Bown, T.M., Tauber, A.A., Dozo, M.T., Tejedor, M.F., 2012. Absolute and relative ages of fossil localities in the Santa Cruz and Pinturas Formations. In: Vizcaíno, S.F., Kay, R.F., Bargo S.M. (Eds.), Early Miocene Paleobiology in Patagonia. Cambridge University Press, pp 41-58.

Fleagle, J.G., Powers, D.W., Conroy, G.C., Watters, J.P., 1987. New fossil platyrrhines from Santa Cruz province, Argentina. Folia Primatologica. 48, 65–77.

Fleagle, J.G., Reed, K.E., 1996. Comparing primate communities: a multivariate approach. Journal of Human Evolution. 30, 489–510.

Flynn, J.J., Wyss, A.R., Charrier, R., Swisher, C.C., 1995. An Early Miocene anthropoid skull from the Chilean Andes. Nature. 373, 603–607.

Ford, S.M., 1988. Postcranial adaptations of the earliest platyrrhine. Journal of Human Evolution. 17, 155–192.

Ford, S.M., Davis, L.C., 1992. Systematics and body size: implications for feeding adaptations in New World monkeys. American Journal of Physical Anthropology. 88, 415–468.

Fortuny, J., Marcé-Nogué, J., De Esteban-Trivigno, S., Gil, L., Galobart, À., 2011. Temnospondyli bite club: ecomorphological patterns of the most diverse group of early tetrapods. Journal of Evolutionary Biology. 24, 2040–2054.

Gebo, D.L., 1986. Anthropoid origins—the foot evidence. Journal of Human Evolution. 15, 421–430.

Gebo, D.L., 1988. Foot morphology and locomotor adaptation in Eocene primates. Folia Primatologica; International Journal of Primatology. 50, 3–41.

Gebo, D.L., 2011. Vertical clinging and leaping revisited: vertical support use as the ancestral condition of strepsirrhine primates. American Journal of Physical Anthropology. 146, 323–335.

Gebo, D.L., Dagosto, M., Rosenberger, A.L., Setoguchi, T., 1990. New platyrrhine tali from La Venta, Colombia. Journal of Human Evolution. 19, 737–746.

Gil, L., Marcé-Nogué, J., Sánchez, M., 2015. Insights into the controversy over materials data for the comparison of biomechanical performance in vertebrates. Palaeontologia Electronica. 18.1.12A, 1–24.

Guiotto, A., Sawacha, Z., Guarneri, G., Avogaro, A., Cobelli, C., 2014. 3D finite element model of the diabetic neuropathic foot: A gait analysis driven approach. Journal of Biomechanics. 47, 3064–3071.

Hanot, P., Guintard, C., Lepetz, S., Cornette, R., 2017. Identifying domestic horses, donkeys and hybrids from archaeological deposits: A 3D morphological investigation on skeletons. Journal of Archaeological Science. 78, 88–98.

Hastie, T., Tibshirani, R., Friedman, J., 2017. The Elements of Statistical Learning: Data Mining, Inference, and Prediction, Second Edition, 2nd ed. 2009, Corr. 9th printing 2017 edition. ed. Springer, New York, NY.

Hoffstetter, R., 1969. Un primate de l'Oligocene inférieur sudamericain: Branisella boliviana gen. et sp. nov. CR Acad. Sci. Paris. 269, 434–437.

Jackson, D.A., 1993. Stopping Rules in Principal Components Analysis: A Comparison of Heuristical and Statistical Approaches. Ecology. 74, 2204–2214.

James, G., Witten, D., Hastie, T., Tibshirani, R., 2017. An Introduction to Statistical Learning: with Applications in R, 1st ed. 2013, Corr. 7th printing 2017 edition. ed. Springer, New York.

Kay, R.F., 2015a. New World monkey origins. Science. 347, 1068–1069.

Kay, R.F., 2015b. Biogeography in deep time – What do phylogenetics, geology, and paleoclimate tell us about early platyrrhine evolution? Molecular Phylogenetics and Evolution, Phylogeny and Biogeography of Neotropical Primates. 82, Part B, 358–374.

Kay, R.F., Cozzuol, M.A., 2006. New platyrrhine monkeys from the Solimões Formation (late Miocene, Acre State, Brazil). Journal of Human Evolution. 50, 673–686.

Kay, R.F., Johnson, D., Meldrum, D.J., 1998. A new pitheciin primate from the middle Miocene of Argentina. American Journal of Primatology. 45, 317–336.

Kay, R.F., Williams, B.A., Anaya, F., 2002. The Adaptations of Branisella boliviana, the Earliest South American Monkey. In: Plavcan, J.M., Kay, R.F., Jungers, W.L., Schaik, C.P. van (Eds.), Reconstructing Behavior in the Primate Fossil Record, Advances in Primatology. Springer US, pp. 339–370.

Klingenberg, C.P., Monteiro, L.R., 2005. Distances and Directions in Multidimensional Shape Spaces: Implications for Morphometric Applications. Systematic Biology. 54, 678–688.

Kuhn, M., 2008. Caret package. Journal of Statistical Software. 28, 1–26.

Kuhn, M., Johnson, K., 2013a. Applied Predictive Modeling, 2013 edition. ed. Springer, New York.

Kuhn, M., Johnson, K., 2013b. Measuring Performance in Classification Models. In: Applied Predictive Modeling. Springer, New York, NY, pp. 247–273.

Kuhn, M., Johnson, K., 2013c. Over-Fitting and Model Tuning. In: Applied Predictive Modeling. Springer, New York, NY, pp. 61–92.

Li, S.-F., Jacques, F.M.B., Spicer, R.A., Su, T., Spicer, T.E.V., Yang, J., Zhou, Z.-K., 2016. Artificial neural networks reveal a high-resolution climatic signal in leaf physiognomy. Palaeogeography, Palaeoclimatology, Palaeoecology. 442, 1–11.

Lisowski, F.P., Albrecht, G.H., Oxnard, C.E., 1974. The form of the talus in some higher primates: A multivariate study. American Journal of Physical Anthropology. 41, 191–215.

Losos, J.B., 1990. Ecomorphology, Performance Capability, and Scaling of West Indian Anolis Lizards: An Evolutionary Analysis. Ecological Monographs. 60, 369–388.

MacLeod, N., 2007. Automated Taxon Identification in Systematics: Theory, Approaches and Applications. CRC Press.

MacLeod, N., 2017. On the Use of Machine Learning in Morphometric Analysis. In: Lestrel, P.E. (Ed.), Biological Shape Analysis: Proceedings of the 4th International Symposium. pp. 134–171.

MacPhee, R.D.E., Iturralde-Vinent, M., Gaffney, E.S., 2003. Domo de Zaza, an Early Miocene Vertebrate Locality in South-Central Cuba: With Notes on the Tectonic Evolution of Puerto Rico and the Mona Passage. American Museum of Natural History.

MacPhee, R.D.E., Iturralde-Vinent, M.A., 1995. Earliest monkey from Greater Antilles. Journal of Human Evolution. 28, 197–200.

MacPhee, R.D.E., Meldrum, J., 2006. Postcranial Remains of the Extinct Monkeys of the Greater Antilles, with Evidence for Semiterrestriality in Paralouatta. American Museum Novitates. 16.

MacPhee, R.D.E., Woods, C.A., 1982. A new fossil cebine from Hispaniola. American Journal of Physical Anthropology. 58, 419–436.

Marcé-Nogué, J., De Esteban-Trivigno, S., Escrig, C., Gil, L., 2016. Accounting for differences in element size and homogeneity when comparing Finite Element models: Armadillos as a case study. Palaeontologia Electronica. 19, 1–22.

Marcé-Nogué, J., Esteban-Trivigno, S.D., Püschel, T.A., Fortuny, J., 2017a. The intervals method: a new approach to analyse finite element outputs using multivariate statistics. PeerJ. 5, e3793.

Marcé-Nogué, J., Fortuny, J., Gil, L., Sánchez, M., 2015. Improving mesh generation in Finite Element Analysis for functional morphology approaches. Spanish Journal of Palaeontology. 31, 117–132.

Marcé-Nogué, J., Püschel, T.A., Kaiser, T.M., 2017b. A biomechanical approach to understand the ecomorphological relationship between primate mandibles and diet. Scientific Reports. 7, 8364.

Marivaux, L., Salas-Gismondi, R., Tejada, J., Billet, G., Louterbach, M., Vink, J., Bailleul, J., Roddaz, M., Antoine, P.-O., 2012. A platyrrhine talus from the early Miocene of Peru (Amazonian Madre de Dios Sub-Andean Zone). Journal of Human Evolution. 63, 696–703.

Meldrum, D.J., 1990. New fossil platyrrhine tali from the early miocene of Argentina. American Journal of Physical Anthropology. 83, 403–418.

Meldrum, D.J., Lemelin, P., 1991. Axial skeleton of Cebupithecia sarmientoi (Pitheciinae, Platyrrhini) from the middle miocene of La Venta, Colombia. American Journal of Primatology. 25, 69–89.

Mendoza, M., Janis, C.M., Palmqvist, P., 2002. Characterizing complex craniodental patterns related to feeding behaviour in ungulates: a multivariate approach. Journal of Zoology. 258, 223–246.

Menezes, A.N., Bonvicino, C.R., Seuánez, H.N., 2010. Identification, classification and evolution of Owl Monkeys (Aotus, Illiger 1811). BMC Evolutionary Biology. 10, 248.

Mitteroecker, P., Bookstein, F., 2011. Linear Discrimination, Ordination, and the Visualization of Selection Gradients in Modern Morphometrics. Evolutionary Biology. 38, 100–114.

Moazen, M., Curtis, N., Evans, S.E., O'Higgins, P., Fagan, M.J., 2008. Combined finite element and multibody dynamics analysis of biting in a Uromastyx hardwickii lizard skull. Journal of Anatomy. 213, 499–508.

Nakatsukasa, M., Takai, M., Setoguchi, T., 1997. Functional morphology of the postcranium and locomotor behavior of Neosaimiri fieldsi, a Saimiri-like Middle Miocene platyrrhine. American Journal of Physical Anthropology. 102, 515–544.

Navega, D., Vicente, R., Vieira, D.N., Ross, A.H., Cunha, E., 2015. Sex estimation from the tarsal bones in a Portuguese sample: a machine learning approach. International Journal of Legal Medicine. 129, 651–659.

Parr, W.C.H., Chamoli, U., Jones, A., Walsh, W.R., Wroe, S., 2013. Finite element micro-modelling of a human ankle bone reveals the importance of the trabecular network to mechanical performance: New methods for the generation and comparison of 3D models. Journal of Biomechanics. 46, 200–205.

Pearson, O.M., Lieberman, D.E., 2004. The aging of Wolff's "law": Ontogeny and responses to mechanical loading in cortical bone. American Journal of Physical Anthropology. 125, 63–99.

Perkins, M.E., Fleagle, J.G., Heizler, M.T., Nash, B., Bown, T.M., Tauber, A.A., Dozo, M.T., 2012. Tephrochronology of the Miocene Santa Cruz and Pinturas Formations, Argentina. In: Vizcaíno, S.F., Kay, R.F., Bargo, S.M. (Eds.), Early Miocene Paleobiology in Patagonia. Cambridge University Press.

Piras, P., Maiorino, L., Teresi, L., Meloro, C., Lucci, F., Kotsakis, T., Raia, P., 2013. Bite of the Cats: Relationships between Functional Integration and Mechanical Performance as Revealed by Mandible Geometry. Systematic Biology. 62, 878–900.

Püschel, T.A., Gladman, J.T., Bobe, R., Sellers, W.I., 2017. The evolution of the platyrrhine talus: A comparative analysis of the phenetic affinities of the Miocene platyrrhines with their modern relatives. Journal of Human Evolution. 111, 179–201.

Püschel, T.A., Sellers, W.I., 2016. Standing on the shoulders of apes: Analyzing the form and function of the hominoid scapula using geometric morphometrics and finite element analysis. American Journal of Physical Anthropology. 159, 325–341.

R Core Team, 2017. R: A Language and Environment for Statistical Computing. R Foundation for Statistical Computing, Vienna, Austria.

Raichlen, D.A., Pontzer, H., Shapiro, L.J., Sockol, M.D., 2009. Understanding hind limb weight support in chimpanzees with implications for the evolution of primate locomotion. American Journal of Physical Anthropology. 138, 395–402.

Rayfield, E.J., 2007. Finite Element Analysis and Understanding the Biomechanics and Evolution of Living and Fossil Organisms. Annual Review of Earth and Planetary Sciences. 35, 541–576.

Reggiani, B., Leardini, A., Corazza, F., Taylor, M., 2006. Finite element analysis of a total ankle replacement during the stance phase of gait. Journal of Biomechanics. 39, 1435–1443.

Rímoli, R.O., 1977. Una nueva especie de monos (Cebidae: Saimirinae: Saimiri) de la Hispaniola. Universidad Autónoma de Santo Domingo.

Rohlf, F.J., Corti, M., 2000. Use of Two-Block Partial Least-Squares to Study Covariation in Shape. Systematic Biology. 49, 740–753.

Rosenberger, A.L., 1992. Evolution of feeding niches in new world monkeys. American Journal of Physical Anthropology. 88, 525–562.

Rosenberger, A.L., 2002. Platyrrhine paleontology and systematics: the paradigm shifts. In: Hartwig, W.C. (Ed.), The Primate Fossil Record. Cambridge University Press.

Rosenberger, A.L., Hartwig, W.C., Wolff, R.G., 1991. Szalatavus attricuspis, an early platyrrhine primate. Folia Primatologica. 56, 225–233.

Rosenberger, A.L., Tejedor, M.F., 2013. The misbegotten: long lineages, long branches and the interrelationships of Aotus, Callicebus and the saki-uacaris. In: Veiga,

L.M., Barnett, A.A., Ferrari, S.F., Norconk, M.A. (Eds.), Evolutionary Biology and Conservation of Titis, Sakis and Uacaris, Cambridge Studies in Biological and Evolutionary Anthropology. Cambridge University Press, Cambridge.

Rosenberger, A.L., Tejedor, M.F., Cooke, S.B., Pekar, S., 2009. Platyrrhine Ecophylogenetics in Space and Time. In: Garber, P.A., Estrada, A., Bicca-Marques, J.C., Heymann, E.W., Strier, K.B. (Eds.), South American Primates, Developments in Primatology: Progress and Prospects. Springer New York, pp. 69–113.

Santos, F., Guyomarc'h, P., Bruzek, J., 2014. Statistical sex determination from craniometrics: Comparison of linear discriminant analysis, logistic regression, and support vector machines. Forensic Science International. 245, 204.e1-204.e8.

Sena, L., Vallinoto, M., Sampaio, I., Schneider, H., Ferrari, S.F., Cruz Schneider, M.P., 2002. Mitochondrial COII Gene Sequences Provide New Insights into the Phylogeny of Marmoset Species Groups (Callitrichidae, Primates). Folia Primatologica. 73, 240–251.

Serrano-Fochs, S., De Esteban-Trivigno, S., Marcé-Nogué, J., Fortuny, J., Fariña, R.A., 2015. Finite Element Analysis of the Cingulata Jaw: An Ecomorphological Approach to Armadillo's Diets. PLOS ONE. 10, e0120653.

Smith, R.J., Jungers, W.L., 1997. Body mass in comparative primatology. Journal of Human Evolution. 32, 523–559.

Sonnenschein, A., VanderZee, D., Pitchers, W.R., Chari, S., Dworkin, I., 2015. An image database of Drosophila melanogaster wings for phenomic and biometric analysis. GigaScience. 4, 25.

Swartz, S.M., Bertram, J.E.A., Biewener, A.A., 1989. Telemetered in vivo strain analysis of locomotor mechanics of brachiating gibbons. Nature. 342, 270–272.

Takai, M., Anaya, F., Shigehara, N., Setoguchi, T., 2000. New fossil materials of the earliest new world monkey, Branisella boliviana, and the problem of platyrrhine origins. American Journal of Physical Anthropology. 111, 263–281.

Tallman, M., Cooke, S.B., 2016. New endemic platyrrhine humerus from Haiti and the evolution of the Greater Antillean platyrrhines. Journal of Human Evolution. 91, 144–166.

Tarca, A.L., Carey, V.J., Chen, X., Romero, R., Drăghici, S., 2007. Machine Learning and Its Applications to Biology. PLOS Computational Biology. 3, e116.

Tejedor, M.F., 2002. Primate canines from the early Miocene Pinturas Formation, Southern Argentina. Journal of Human Evolution. 43, 127–141.

Tejedor, M.F., 2003. New fossil primate from Chile. Journal of Human Evolution. 44, 515–520.

Tejedor, M.F., 2005a. New fossil platyrrhine from Argentina. Folia Primatologica. 76, 146–150.

Tejedor, M.F., 2005b. New specimens of Soriacebus adrianae Fleagle, 1990, with comments on pitheciin primates from the Miocene of Patagonia. Ameghiniana. 42, 249–251.

Tejedor, M.F., 2008. The origin and evolution of Neotropical Primates. Arquivos do Museu Nacional, Rio de Janeiro. 66, 251–269.

Tejedor, M.F., Tauber, A.A., Rosenberger, A.L., Swisher, C.C., Palacios, M.E., 2006. New primate genus from the Miocene of Argentina. Proceedings of the National Academy of Sciences. 103, 5437–5441.

Turley, K., Frost, S.R., 2013. The Shape and Presentation of the Catarrhine Talus: A Geometric Morphometric Analysis. The Anatomical Record. 296, 877–890.

Turner, C.H., 1998. Three rules for bone adaptation to mechanical stimuli. Bone. 23, 399–407.

Van Bocxlaer, B., Schultheiß, R., 2010. Comparison of morphometric techniques for shapes with few homologous landmarks based on machine-learning approaches to biological discrimination. Paleobiology. 36, 497–515.

Walmsley, C.W., Smits, P.D., Quayle, M.R., McCurry, M.R., Richards, H.S., Oldfield, C.C., Wroe, S., Clausen, P.D., McHenry, C.R., 2013. Why the Long Face? The Mechanics of Mandibular Symphysis Proportions in Crocodiles. PLoS ONE. 8, e53873.

Wiley, D.F., Amenta, N., Alcantara, D.A., Ghost, D., Kil, Y.J., Delson, E., Harcourt-Smith, W., Rohlf, F.J., St John, K., Hamann, B., 2005. Evolutionary morphing. In: EEE Visualization, 2005. VIS 05.

Wolff, J., 1892. Das Gesetz der Transformation der Knochen. Hirschwald, Berlin.

Wolff, R.G., 1984. New specimens of the primate Branisella boliviana from the early oligocene of Salla, Bolivia. Journal of Vertebrate Paleontology. 4, 570–574.

Yapuncich, G.S., Boyer, D.M., 2014. Interspecific scaling patterns of talar articular surfaces within primates and their closest living relatives. Journal of Anatomy. 224, 150–172.

Yapuncich, G.S., Gladman, J.T., Boyer, D.M., 2015. Predicting euarchontan body mass: A comparison of tarsal and dental variables. American Journal of Physical Anthropology. 157, 472–506.

Youlatos, D., 2004. Multivariate analysis of organismal and habitat parameters in two neotropical primate communities. American Journal of Physical Anthropology. 123, 181–194.

Youlatos, D., Meldrum, J., 2011. Locomotor Diversification in New World Monkeys: Running, Climbing, or Clawing Along Evolutionary Branches. The Anatomical Record: Advances in Integrative Anatomy and Evolutionary Biology. 294, 1991–2012.

Zadpoor, A.A., Campoli, G., Weinans, H., 2012. Neural network prediction of load from the morphology of trabecular bone. arXiv:1201.6044 [physics, q-bio].

Zelditch, M.L., Swiderski, D.L., Sheets, H.D., 2012. Geometric Morphometrics for Biologists, Second Edition: A Primer, 2 edition. Academic Press, Amsterdam.

5.7 Supporting information

(S1) Phylogeny used in the comparative analyses

(S2) Fossil reconstruction procedures

(S3) Further information about the FEA models

(S4) Results of the phylogenetic multiple regression of stress percentile values on volume

(S5) Code for pairwise PERMANOVA test with Holm correction

(S6) Convergence results for the stress interval data.

5.7.1 Supporting information 1. Phylogeny used in the comparative analyses in Newick format

((((Pithecia_pithecia:1,Pithecia_monachus:1):1,(Cacajao_calvus:1,Chiropotes_satanas:1):1):3,(Callicebus_personatus:4,(Callicebus_torquatus:3,(Callicebus_donacophilus:2,(Callicebus_cupreus:1,Callicebus_moloch:1):1):1):1):1):6,(((Alouatta_caraya:1,Alouatta_seniculus:1):4,(((Ateles_belzebuth:2,(Ateles_geoffroyi:1,Ateles_fusciceps:1):1):1,Ateles_marginatus:3):1,Lagothrix_lagotricha:4):1):5,(((Saimiri_sciureus:1,Saimiri_boliviensis:1):2,((Cebus_albifrons:1,Cebus_olivaceus:1):1,(Cebus_apella:1,Cebus_nigritus:1):1):1):6,((Aotus_nancymaae:3,(Aotus_trivirgatus:2,(Aotus_infulatus:1,Aotus_azarae:1):1):1):5,(((((Saguinus_oedipus:1,Saguinus_midas:1):1,Saguinus_mystax:2):1,(Saguinus_fuscicollis:1,Saguinus_leucopus:1):2):4,(Leontopithecus_rosalia:6,(Callimico_goeldii:5,(((Callithrix_jacchus:1,Callithrix_penicillata:1):1,Callithrix_geoffroyi:2):2,(Cebuella_pygmaea:3,(Mico_melanurus:2,(Mico_argentatus:1,Mico_humeralifer:1):1):1):1):1):1):1):1):1):1):1);

5.7.2 Supporting information 2. Fossil reconstruction procedures

Madre de Dios: This specimen exhibited some minor cracks on its surface and a relatively small hole on its trochlear surface. Hence, it was manually repaired using the 'sculpt knife' in Geomagic v. 12 (Geomagic, USA) in order to correct these minor defects (sculpt knife parameters: width: 0.1 mm; offset: 0.01 mm; smoothness: 30; shape: 0).

Dolichocebus gainamensis: This fossil talus showed an eroded talar head, along a noticeable missing portion of the trochlear surface. Manually reconstructing these missing portions would have been particularly subjective, due to the size of the damaged areas; hence it was decided to avoid that approach. Therefore a reference-based geometric reconstruction tactic was preferred instead (Zollikofer and Ponce de León, 2005; Gunz et al., 2009; Weber and Bookstein, 2011). The consensus shape of the comparative extant sample was estimated and then the 3D surface of a *Chiropotes satanas* specimen was warped to match this multivariate mean configuration using the thin plate spline interpolation function (Bookstein, 1991).

This specimen was selected because a previous analysis of 203 platyrrhine tali (Püschel et al., 2017) has shown that this species exhibits one of the closest morphologies to the talar consensus configuration, and also due to its high resolution that allowed us to carry out the different proposed reconstruction approaches. This consensus surface model was then warped to match the coordinates of *Dolichocebus gainamensis*. In this way, missing data was estimated by mapping this consensus configuration to the fossil specimen with missing landmarks (Gunz et al., 2009) by applying again the thin plate spline interpolation function based on the subset of observable landmarks (the landmarks 3, 4 and 25-29 were not used because they were absent in the fossil individual). These warping procedures were carried out in Landmark v. 3.6 (Wiley et al., 2005). Subsequently, the obtained model was imported into Geomagic v. 12 (Geomagic, USA) and scaled to the same volume as *Dolichocebus gainamensis*. Then it was aligned with respect to it, using a best-fit alignment (sample size: 10,000; tolerance: 0.17699). Then the damaged portions were removed from the fossil and the reconstructed areas were trimmed from the warped model and used to patch the removed areas. Finally, the patched areas were slightly smoothed by using the 'sand paper' tool in the same software.

Soriacebus ameghinorum: This specimen was entirely missing the posterior calcaneal articular surface. The same procedure outlined above for the *Dolichocebus gainamensis* specimen was performed in order to reconstruct the missing anatomical portion using the *Chiropotes* surface file already described. The subset of landmarks used to perform the thin plate spline warpings considered all the original coordinates except for landmarks 19-24. Additionally, using the warped model some areas of the talar neck and medial tubercle were reconstructed.

Río Cisnes: This fossil talus did not exhibit any extremely broken areas, however its whole surface was noticeably eroded. For that reason it was not possible to apply any of the previously described reconstruction approaches. In this case, it was decided that instead of manually and subjectively reconstructing the eroded surfaces, it was better to simply use the already described consensus surface model and warp it to match the available landmarks for this specimen.

References

Gunz, P., Mitteroecker, P., Neubauer, S., Weber, G.W., Bookstein, F.L., 2009. Principles for the virtual reconstruction of hominin crania. Journal of Human Evolution. 57, 48–62.

Püschel, T.A., Gladman, J.T., Bobe, R., Sellers, W.I., 2017. The evolution of the platyrrhine talus: A comparative analysis of the phenetic affinities of the Miocene platyrrhines with their modern relatives. Journal of Human Evolution. 111, 179–201.

Weber, G.W., Bookstein, F.L., 2011. Virtual anthropology: a guide to a new interdisciplinary field. Springer, Wien; London.

Wiley, D.F., Amenta, N., Alcantara, D.A., Ghost, D., Kil, Y.J., Delson, E., Harcourt-Smith, W., Rohlf, F.J., St John, K., Hamann, B., 2005. Evolutionary morphing. In: EEE Visualization, 2005. VIS 05.

Zollikofer, C.P., Ponce de León, M.P. de, 2005. Virtual Reconstruction: A Primer in Computer-Assisted Paleontology and Biomedicine, 1 edition. ed. Wiley-Liss, Hoboken, N.J.

5.7.3 Supporting Information 3. Table 5.5 Further details about the FEA models

Specimen	Average Body Mass (g)	Body Weight Force [N]	Volume of the model [mm3]	Elements of the Mesh	AM	MWAM	PeofAM	M	MWM	PEofM	M25	M50	M75	M95
Alouatta Caraya	5375.00	15.82	1702.80	345230	0.2525	0.2490	1.4127	0.1274	0.1265	0.7486	0.0698	0.1274	0.2480	0.7300
Alouatta seniculus	5950.00	17.51	1186.53	382757	0.4715	0.4679	0.7750	0.2641	0.2615	1.0042	0.1477	0.2641	0.4739	1.2979
Aotus azarae	1205.00	3.55	303.08	331074	0.1874	0.1866	0.4545	0.1042	0.1019	2.1892	0.0579	0.1042	0.1770	0.5408
Aotus infulatus	1215.00	3.58	161.55	416393	0.2700	0.2671	1.0685	0.1540	0.1515	1.6225	0.0821	0.1540	0.2671	0.7716
Aotus nancymaae	787.00	2.32	225.21	336589	0.0985	0.0981	0.3469	0.0432	0.0431	0.1531	0.0228	0.0432	0.1003	0.3459
Aotus trivirgatus	786.00	2.31	205.17	321450	0.3243	0.3213	0.9549	0.1826	0.1809	0.9412	0.1021	0.1826	0.3151	1.0366
Ateles belzebuth	8070.00	23.75	2532.46	344673	0.2760	0.2731	1.0557	0.1482	0.1464	1.2493	0.0843	0.1482	0.2543	0.8496
Ateles fusciceps	9025.00	26.56	2594.97	352527	0.3167	0.3152	0.4891	0.1787	0.1771	0.9044	0.1062	0.1787	0.2953	0.9139
Ateles geoffroyi	7535.00	22.18	2561.37	348531	0.3587	0.3556	0.8948	0.2172	0.2151	0.9552	0.1266	0.2172	0.3449	0.8671
Ateles marginatus	10230.00	30.11	2362.84	321892	0.3446	0.3417	0.8554	0.1801	0.1794	0.3737	0.1032	0.1801	0.3362	1.0111
Cacajao calvus	3165.00	9.31	868.94	281534	0.2283	0.2252	1.4134	0.1080	0.1074	0.5831	0.0601	0.1080	0.2102	0.6821
Callicebus cupreus	1070.00	3.15	251.27	206752	0.2207	0.2181	1.2019	0.1316	0.1290	2.0369	0.0692	0.1316	0.2246	0.5876
Callicebus donacophilus	950.00	2.80	248.24	328852	0.0990	0.0992	0.1416	0.0478	0.0474	1.0252	0.0245	0.0478	0.0993	0.3523
Callicebus moloch	988.00	2.91	302.23	382235	0.1255	0.1251	0.3220	0.0673	0.0670	0.4810	0.0378	0.0673	0.1266	0.3723
Callicebus personatus	1325.00	3.90	352.63	288735	0.1405	0.1398	0.4920	0.0717	0.0716	0.1675	0.0434	0.0717	0.1275	0.4708
Callicebus torquatus	1325.00	3.90	299.06	299368	0.1476	0.1458	1.2394	0.0838	0.0826	1.4374	0.0506	0.0838	0.1366	0.4376
Callimico goeldii	483.50	1.42	85.30	269334	0.1096	0.1092	0.3615	0.0519	0.0513	1.1182	0.0264	0.0519	0.1158	0.3781
Mico argentatus	345.00	1.02	53.24	269334	0.1096	0.1092	0.3615	0.0519	0.0513	1.1182	0.0264	0.0519	0.1158	0.3781
Callibrix geoffroyi	359.00	1.06	59.25	299573	0.1414	0.1405	0.6357	0.0778	0.0765	1.7240	0.0479	0.0778	0.1243	0.4491
Callibrix jacchus	320.50	0.94	57.96	293129	0.1632	0.1612	1.2146	0.0863	0.0848	1.7154	0.0513	0.0863	0.1452	0.4954
Callithrix penicillata	325.50	0.96	51.57	259924	0.1300	0.1294	0.5250	0.0667	0.0656	1.7045	0.0330	0.0667	0.1500	0.3838
Mico humeralifer	473.50	1.39	62.54	370120	0.1465	0.1459	0.3918	0.0782	0.0773	1.0748	0.0439	0.0782	0.1437	0.4179
Cebuella pygmaea	116.00	0.34	14.61	371370	0.1315	0.1308	0.5047	0.0742	0.0737	0.7535	0.0433	0.0742	0.1317	0.4031
Cebus albifrons	2735.00	8.05	622.74	347017	0.1804	0.1797	0.3853	0.0742	0.0746	0.5862	0.0421	0.0742	0.1730	0.6474
Cebus apella	3085.00	9.08	790.96	440087	0.2191	0.2174	0.8000	0.1206	0.1183	1.9745	0.0641	0.1206	0.2204	0.6289
Cebus nigritus	2825.00	8.31	822.11	457220	0.2303	0.2272	1.3496	0.1249	0.1232	1.3432	0.0685	0.1249	0.2217	0.6653
Cebus olivaceus	2905.00	8.55	921.47	512797	0.1770	0.1762	0.4511	0.0883	0.0878	0.5834	0.0484	0.0883	0.1778	0.5373

Chiropotes satanas	2740.00	8.06	810.20	451582	0.2446	0.2420	1.0637	0.1169	0.1153	1.4213	0.0619	0.1169	0.2382	0.7121
Lagothrix lagotricha	7150.00	21.04	2096.07	286851	0.3426	0.3373	1.5735	0.2022	0.1967	2.8054	0.1136	0.2022	0.3190	0.9634
Leontopithecus rosalia	609.00	1.79	113.30	293964	0.1764	0.1747	0.9497	0.0903	0.0888	1.6731	0.0537	0.0903	0.1503	0.5365
Mico melanurus	350.00	1.03	54.69	475595	0.1272	0.1267	0.4274	0.0544	0.0543	0.1993	0.0272	0.0544	0.1212	0.4448
Pithecia monachus	2360.00	6.95	509.08	202919	0.2104	0.2060	2.1329	0.0992	0.0982	1.0368	0.0609	0.0992	0.1728	0.7253
Pithecia pithecia	1760.00	5.18	233.14	597809	0.2612	0.2609	0.1341	0.1281	0.1280	0.0480	0.0799	0.1281	0.2339	0.8896
Saguinus fuscicollis	350.50	1.03	40.59	204460	0.1776	0.1772	0.2091	0.0931	0.0929	0.2869	0.0564	0.0931	0.1768	0.5576
Saguinus leucopus	492.00	1.45	70.17	277957	0.2076	0.2055	1.0094	0.1163	0.1141	1.9756	0.0665	0.1163	0.1964	0.6233
Saguinus midas	545.00	1.60	82.20	213317	0.1135	0.1119	1.4226	0.0465	0.0454	2.4518	0.0160	0.0465	0.1091	0.4418
Saguinus mystax	524.50	1.54	56.63	285421	0.2588	0.2571	0.6862	0.1558	0.1526	2.0722	0.0933	0.1558	0.2476	0.7298
Saguinus oedipus	411.00	1.21	99.06	256323	0.1217	0.1202	1.2060	0.0664	0.0657	1.0104	0.0381	0.0664	0.1147	0.3642
Saimiri boliviensis	811.00	2.39	168.67	434947	0.2433	0.2397	1.5014	0.1458	0.1429	2.0381	0.0804	0.1458	0.2394	0.6788
Saimiri sciureus	720.50	2.12	162.75	419785	0.1566	0.1563	0.1739	0.0838	0.0832	0.6675	0.0499	0.0838	0.1469	0.4834
Fossil specimen														
Aotus dindensis	873.50	2.57	131.94	340928	0.2190	0.2180	0.4620	0.1112	0.1106	0.4783	0.0670	0.1112	0.2202	0.6508
Carlocebus carmenensis	2913.52	8.57	684.40	740230	0.2471	0.2440	1.2946	0.1263	0.1267	0.3615	0.0788	0.1263	0.2314	0.7320
Cebupithecia sarmientoi	1825.11	5.37	366.87	398090	0.2677	0.2667	0.3711	0.1500	0.1476	1.6750	0.0867	0.1500	0.2411	0.7498
Dolichocebus gaimanensis	1600.59	4.71	377.15	409623	0.1758	0.1750	0.4278	0.0935	0.0932	0.2898	0.0558	0.0935	0.1669	0.5296
Madre de Dios	352.18	1.04	57.24	463393	0.1806	0.1793	0.7108	0.1045	0.1033	1.1956	0.0580	0.1045	0.1770	0.5128
Neosaimiri fieldsi	781.47	2.30	131.94	145794	0.1582	0.1567	0.9630	0.0811	0.0803	1.0568	0.0438	0.0811	0.1651	0.4996
Paralouatta marianae	4708.85	13.86	1242.39	400195	0.2956	0.2938	0.6158	0.1632	0.1624	0.5279	0.0928	0.1632	0.2888	0.8327
Proteropithecia neuquenensis	2006.40	5.90	482.90	524490	0.2353	0.2336	0.7291	0.1398	0.1371	1.9436	0.0812	0.1398	0.2236	0.6523
Río Cisnes	1509.87	4.44	407.05	441230	0.2377	0.2358	0.8002	0.1470	0.1440	2.0530	0.0813	0.1470	0.2479	0.5874
Soriacebus ameghinorum	1720.95	5.06	415.48	451422	0.1961	0.1952	0.4738	0.1040	0.1032	0.8005	0.0590	0.1040	0.1931	0.5896

5.7.4. Supporting information 4. Table 5.6 Results of the phylogenetic multiple regression of stress percentile values on volume (9,999 iterations)*

	Df	SS	MS	R^2	F	Z	Pr(>F)
Volume	1	0.023	0.023	0.043	1.703	1.129	0.116
Residuals	38	0.518	0.014				
Total	39	0.541					

5.7.5 Supporting information 5. R function for pairwise PERMANOVA with Holm correction

```
#pairwise PERMANOVA with Holm correction
# adapted from https://github.com/pmartinezarbizu/pairwiseAdonis

pairwise_permanova <- function(x,factors, sim.function = 'vegdist', sim.method =
'euclidean', p.adjust.m ='holm')
{
  require(vegan)

  co = combn(unique(as.character(factors)),2)
  pairs = c()
  F_Model =c()
  R_squared = c()
  p_value = c()

  for(elem in 1:ncol(co)){
    if(sim.function == 'vegdist'){
      x1 = vegdist(x[factors %in% c(co[1,elem],co[2,elem]),],method=sim.method)}

    ad = adonis(x1 ~ factors[factors %in% c(co[1,elem],co[2,elem])] );
    pairs = c(pairs,paste(co[1,elem],'vs',co[2,elem]));
    F_Model =c(F_Model,ad$aov.tab[1,4]);
    R_squared = c(R_squared,ad$aov.tab[1,5]);
    p_value = c(p_value,ad$aov.tab[1,6])
  }
  p_adjusted = p.adjust(p_value,method=p.adjust.m)
  sig = c(rep('',length(p_adjusted)))
  sig[p_adjusted <= 0.05] <-'.'
  sig[p_adjusted <= 0.01] <-'*'
  sig[p_adjusted <= 0.001] <-'**'
  sig[p_adjusted <= 0.0001] <-'***'

  pairw.res = data.frame(pairs,F_Model,R_squared,p_value,p_adjusted,sig)
  print("Signif. codes:  0 '***' 0.001 '**' 0.01 '*' 0.05 '.' 0.1 ' ' 1")
  return(pairw.res)
}
```

5.7.6 Supporting information 6. Table 5.7 Convergence results for the stress interval data.

	R² for PC1	R² for PC2
PCA 5 vs. PCA 10	0.9974458	0.6029997
PCA 10 vs. PCA 25	0.9983928	0.996538
PCA 25 vs. PCA 50	0.9997889	0.9995826
PCA 50 vs. PCA 75	0.9999801	0.9999799
PCA 75 vs. PCA 100	0.9999948	0.9999771

CHAPTER 6

Discussion

DISCUSSION

The fundamental issue addressed in this dissertation can be summarised as being the analysis of the relationship between form and function in different primate skeletal elements taking into account phylogenetic relatedness. Diverse methodologies including 3D GM, FEA, PCMs, and ML classification algorithms were employed to address bone form and function in different ecomorphological contexts, using shape and biomechanical stress data obtained from both extant and extinct anthropoids.

The main aims of each chapter can be summarised as follows:

- **Chapter 1:** To review the central issues required to understand of the different chapters of this dissertation, including a definition of ecomorphology, a brief primate evolutionary history, and a review of the applied methodologies and how to combine them.

- **Chapter 2:** To perform an analysis of the relationship between scapular form and function in hominoids using GM and FEA, and taking into account the phylogenetic structuration of the data.

- **Chapter 3:** To address the issue of whether there is a sclerocarpic specialization gradient in the mandibular morphology of pitheciids (i.e. if *Callicebus–Pithecia–Chiropotes-Cacajao* represent a morphocline or not), and to test whether mandibular shape is associated with mandibular strength.

- **Chapter 4:** To analyse the phenetic affinities of extant platyrrhine tali and their Miocene counterparts by using GM. To assess if locomotor mode percentages (i.e. LMPs) were associated with talar shape in order to allow locomotor inferences. To test if there was convergence in talar morphology, as well as to test different models that could explain the evolution of talar shape and size in platyrrhines by using PCMs. To compute body mass predictions for the fossil sample using the available articular surfaces and to

reconstruct the ancestral platyrrhine condition considering body mass, locomotion and talar shape.

- **Chapter 5:** To test if talar shape is related to biomechanical performance. To infer the locomotor behaviour of Miocene fossil plattyrhines using shape and stress data obtained from GM and FEA, respectively. To introduce several ML classification algorithms that can be applied in functional morphology and to compare their performance when classifying the fossil sample according to locomotor groups. To show that a combined approach using FEA, GM and ML algorithms is likely to be beneficial for the determination of locomotor habits in primates.

The results of each one of the analytical chapters (i.e. 2-5) are summarised as follows:

- **Chapter 2:** Although it has been suggested that primate scapular morphology is mainly a product of function rather than phylogeny, the obtained results showed that scapular shape exhibits a significant phylogenetic signal. A significant relationship was found between scapular shape and its biomechanical performance; hence, at least part of the scapular shape variation can be explained due to non-phylogenetic factors, probably related to functional demands. This chapter has shown that a combined approach using GM and FEA is able to cast some light on the functional and phylogenetic contributions in hominoid scapular morphology.

- **Chapter 3:** There is indeed a relative specialization continuum in the pitheciid mandible for some aspects of shape as expected for the morphocline hypothesis, although from a biomechanical perspective *Cacajao* and *Chiropotes* showed a similar performance, thus not exhibiting the expected gradient. This is consistent with some previous studies, which suggest that *Chiropotes* shows a more robust mandibular morphology. Additionally, it was found that there is a significant association between mandibular shape and stress values. This chapter expected to contribute to a

better insight regarding the ecomorphological relationship between mandibular morphology and mechanical performance among pitheciids.

- **Chapter 4:** The results of this chapter show that most analysed Miocene fossils exhibit a generalized morphology that is similar to some 'generalist' modern species. It was found that talar shape covaries with locomotor data (i.e. LMPs), thus allowing the inference of locomotion from talar morphology. The results further suggest that talar shape diversification can be explained by invoking a model of shifts in adaptive peak to three peaks representing a phylogenetic hypothesis in which each platyrrhine family occupied a separate adaptive optimum. The analyses indicate that platyrrhine talar centroid size diversification was characterized by an early differentiation related to a multidimensional niche model. New body mass predictions for all the analysed Miocene platyrrhines were provided, which show that at that time there was already a noticeable size variation. In addition, body mass predictions for *Paralouatta marianae* and the Río Cisnes talus were provided for the first time. Finally, the ancestral platyrrhine condition was reconstructed as a medium-sized, generalized, arboreal, quadruped.

- **Chapter 5:** The results obtained in this chapter show that the different locomotor categories are distinguishable using either biomechanical or morphometric data. Clamber/suspensory specimens exhibit the weakest tali, while leaping species showed the strongest morphologies. The ML classification algorithm applied to both biomechanical and morphometric data categorised most of the fossil sample as arboreal quadrupeds, which is consistent with previous studies that used other methodologies. This study has shown that a combined approach using FEA, GM, and ML algorithms can contribute in the understanding of platyrrhine talar morphology and its relationship with locomotion.

Each chapter presented here is a discrete body of work, either already peer-reviewed, or written to be submitted for peer review in the near future. As such, every chapter contains its own discussion on how that piece of work fits into the

broader context of primate ecomorphology. Nevertheless, there are two key topics, which run through chapters and will be discussed in depth. The first one relates to the question of how to combine FEA and GM, while the second addresses the issue of the application of PCMs when combining these two methods. Additionally, some future research possibilities are also discussed.

6.1 Combining Finite Element Analysis and Geometric Morphometrics

Currently, both GM and FEA are an important part of the virtual morpho-functional toolkit which is being applied to study problems in functional, ecological, and evolutionary morphology (Polly et al., 2016), and that can be successfully applied to provide new insights about fossil taxa (e.g. Chapter 5 in this dissertation). Although GM and FEA are undeniably productive in their own, questions have been raised regarding whether they could be more comprehensively integrated (Weber et al., 2011). In fact, the way in which the different specimens are compared and how GM and FEA are combined, is still a developing area and therefore subject of debate (Bookstein, 2013). In broad terms, it is possible to say that GM enables the quantification of form as well as the comparison of morphological differences across a sample, whilst FEA provides a way in which to simulate biomechanical scenarios, obtaining stress and strain results of individual biological structures (Parr et al., 2012).

However, when combined, a problem arises derived from the fact that most current FEA applications were developed in engineering contexts that did not consider a population perspective (Zienkiewicz et al., 2005). This means that while GM was developed to compare several specimens, in most cases FEA was used to exclusively analyse a single individual (even nowadays, most comparative FEA studies analyse only a handful of individuals, and in most of them only one specimen per species). Organismal biology emphasises comparing specimens, which by contrast is not really common in engineering applications of FEA, which leads to a need to develop methods that enable meaningful comparison between the FEA results from models that differ in geometry (O'Higgins et al., 2011). In part, this can be explained due to the limitations associated with the generations of FE models,

which make it difficult to generate comparable models. For example, one limitation concerns how to scale the models to carry out meaningful comparisons (Dumont et al., 2009). Diverse proposals have been advanced (see section 1.3.1 for some examples), but in most cases models are scaled to achieve the same volume or area depending on whether they are tri or bi-dimensional and if strain or stress are being compared (Dumont et al., 2009).

Another associated problem is how to compare strains/stress results between different individuals (or even different meshes of the same structure) under, for example, similar loadings. This problem has been tackled by applying different methodologies that allow us to obtain quantitative data that can be subsequently used to compare diverse specimens (Marcé-Nogué et al., 2017). All of these approaches require either calculating a global performance measure (e.g. median or mean) or the satisfactory collection of equivalent coordinates between models from which to extract stress/strain values, which is known to be a non-trivial task when comparing dissimilar geometries (Oxnard and O'Higgins, 2009). One possibility is to simply compute the arithmetic mean of the von Mises stress values for each one of the specimens under analysis and then carry out statistical comparisons (e.g. McHenry et al., 2007; Farke, 2008; Figueirido et al., 2014; Lautenschlager, 2017). Nevertheless, as several authors have pointed out (e.g. Bright and Rayfield, 2011; Tseng and Flynn, 2015; Marcé-Nogué et al., 2016) this approach is problematic because it assumes that all the elements of the model are identical, while in reality and in most cases there will be size differences. To avoid this limitation some corrections that take into account the existing size differences between the elements of a FE mesh have been proposed (e.g. weighting stress by the size of the element prior to estimating the global arithmetic mean) (Marcé-Nogué et al., 2016), as it was done in Chapters 3 and 5. Another applied option is to compare stress values from dissimilar models is to use box-plots or other similar approaches to display distributions (e.g. histograms, density, violin, or bean plots, among others) to visually compare whether one specimen shows more or less stress than another one (e.g. Farke, 2008; Figueirido et al., 2014; Fortuny et al., 2017), as was also done in Chapters 3 and 5. A further possibility is to simply collect von Misses stress/strain values at particular coordinates and/or slices to compare the performance between

different individuals (e.g. Piras et al., 2015; Serrano-Fochs et al., 2015; Püschel and Sellers, 2016), as done in Chapter 2.

In spite of the convenience of all the above-mentioned proposals, these approaches still represent rough measurements that do not make the most of the results obtained from FEA. This is because the latter provides as output an immense amount of quantitative data (i.e. many kinds of stress and strain at hundreds of thousands or millions of elements, as well as nodal displacements at the nodes) (Zienkiewicz et al., 2005), which in most cases is understudied. Consequently, there is still a need for quantitative variables derived from FEA that could effectively summarise the vast amount of data derived from FEA, as well as allowing the use of multivariate statistical analyses. This is particularly true if we consider that most multivariate analyses using stress values have been carried out by exclusively comparing a limited number of points (e.g. 101 coordinates along a meaningful anatomical slice in Chapter 2) (Marcé-Nogué et al., 2015; Fortuny et al., 2016; Püschel and Sellers, 2016).

A recently published method which was applied in the ML section of Chapter 5 has attempted to solve some of the mentioned limitations (Marcé-Nogué et al., 2017). This new methodology has been named as 'the intervals' method', and in brief terms involves generating a new set of variables, each one of them defined by an interval of stress values from the models under analysis (Marcé-Nogué et al., 2017). Each variable is expressed as a percentage of the area of the model showing a certain range of stress values, which can be then used in multivariate procedures, such as PCAs (Marcé-Nogué et al., 2017). In Chapter 5, it is shown that this method can be effectively applied to generate useful variables to be used in several classification tasks. The 'intervals' method' is an improved option when compared to global performance measures (e.g. stress means), because it allows the application of multivariate procedures. It is also a better option than collecting a limited number of points that supposedly represent all the stress or strain variation of a model (e.g. Marcé-Nogué et al., 2015; Fortuny et al., 2016; Püschel and Sellers, 2016). Although this method is evidently a contribution, there is still a large amount of information in FEA outputs that can be used (e.g. stress/strains directions, nodal displacements) and have not been tested using this methodology. In addition, the

statistical properties of the variables generated by the 'intervals' method' have to be studied in more detail. Consequently, there are still a considerable number of areas, which have to be researched in the future. In fact, there has been some controversy regarding the discrepancy between FEA's basis in deterministic computations (i.e. given a particular input, the same output will be always produced) and GM's focus on variability and uncertainty (i.e. a statistical population perspective) (Weber et al., 2011). However, by carrying out an appropriate scaling that enables meaningful comparisons, it possible to conciliate these perspectives. The obtained differences in stress or strain between different models would be strictly due to differences in shape (Dumont et al., 2009). Therefore, the differences in the geometries of the models under analysis (i.e. shape), would necessarily result in differences in stress and strain, since FEA is a deterministic method (Zienkiewicz et al., 2005). In addition, some advances have been made in the field of stochastic FEA, so that the uncertainty of a system that occurs as result of variations in initial conditions (e.g. different materials or geometries) are considered (Arregui-Mena et al., 2016). However these novel methods have not been yet widely adopted in the organismal biology community. Additionally, it is true that to the date there are no available methods that preserve the spatial information of resulting stress or strain that allow pattern comparisons between geometrically dissimilar models. Although useful as a multivariate measure of the performance of a whole model, the 'intervals' method' does not preserve the spatial information of the obtained patterns of stress or strain (Marcé-Nogué et al., 2017).

A proposed solution combining GM and FEA that preserves the spatial information of the obtained patterns is the approach described in the Introduction (1.3.3) as 'GM as a tool to analyse deformations after FEA analysis'. As explained there, this approach consists in applying GM to analyse global deformation before and after FEA (O'Higgins et al., 2017). Even though this method certainly preserves information about form and its variation by analysing nodal displacements due to applied loadings, there are serious concerns regarding its biomathematical foundations (Bookstein, 2013). From a mathematical perspective, GM has almost nothing to do with FEA at the level of their underlying formalisms and equations (Weber et al., 2011). The essential deformations of GM, is incompatible with those of FEA, since in GM the quantity being minimized in the thin plane spline method

is the integral of the squared second derivatives (i.e. this integral is computed over all the space, thus considering where the biological object is located but also where it is not), while in elastic analyses the minimised quantity derives from sum of squared deviations of the first derivatives from unity (i.e. the integral considers only the region occupied by the actual object) (Bookstein, 2013). Furthermore, GM does not consider differences in material properties, which are of vital importance in FEA (Weber et al., 2011). Consequently, this approach combining the two methods manifestly requires further developments. It is evident that more work, particularly in the underlying statistics, mathematics, and informatics is required if a combined biomathematical theory joining FEA and GM is desired. Yet this is not strictly necessary if each method is kept in its own respective domain and the combination of the two occurs via the analyses of the obtained results, as it was done in the present dissertation and many previous studies (see Introduction 1.3.3).

GM and FEA are powerful on their own, both providing interesting insights about the functional morphology of a given structure. For example when analysing adaptation in ecomorphological contexts, it is possible to approach the questions from different angles. FEA allows addressing this issue from a mechanics point of view, while GM provides information about the influence of shape differences. However, if combined in the context of evolutionary theory (e.g. by applying PCMs), a new framework is generated that enables testing hypotheses regarding the relative contribution of a specific function or morphology in the evolution of a particular clade. For example, it is possible to estimate the ancestral states of biomechanical performance or morphologies, or to test different evolutionary scenarios that could explain the observed diversity in particular group (Püschel et al., 2017). Although some of these results can be approached using either FEA or GM separately, the evolutionary framework provided by PCMs allows linking the two methods in a particularly powerful manner, thus allowing quantitative testing of the ecological and evolutionary consequences of a particular morphology. Furthermore, GM and FEA can quantify shape variation and biomechanical performance in extinct taxa (e.g. Chapter 5) and compare those results against related modern taxa (Stayton, 2009; Piras et al., 2015; Polly et al., 2016). The role of dissimilar morphologies on functional performance in particular clades has been previously studied (e.g. Tseng, 2013; Dumont et al., 2014). However, it is only when

modern PCMs are included that it is possible to profit from the powerful tools provided by these methods (Paradis, 2014). PCMs enable a formidable way of testing the evolutionary implications of functional performance in morphological evolution, as well as considering the role of evolutionary factors such as drift, or selection (Pennell and Harmon, 2013). For these reasons the following subsection deals with the implications of applying PCMs to complex multivariate datasets such as those provide by FEA and GM.

6.2 Phylogenetic comparative methods when combining finite element analysis and geometric morphometrics

A central issue in the analysis of the connection between form and function is how to actually carry out that objective when dealing with several species (i.e. non-independence due to the phylogenetic structuration of the data). Several approaches have been applied such as the use of phylogenetic generalized least squares models (PGLS) to fit regressions between matrices of functional/ecological variables and shape variables. Other approaches are the use of phylogenetic independent contrasts (PICs) estimated for each shape variable before associating them with contrasts derived from functional/ecological variables by applying either partial least squares (PLS) (Klingenberg and Ekau, 1996) or multivariate regressions (Figueirido et al., 2010), as well as the correlation between morphometric, functional/ecological, and phylogenetic distance matrices (Harmon et al., 2005; Young et al., 2007; Astúa, 2009; Monteiro and Nogueira, 2011).

Even though the second chapter of this thesis applied regressions to link shape and biomechanical performance in the same way as previous studies (e.g. ordinary regressions of shape on functional performance, PICs or PGLS; Pierce et al., 2008; Pierce et al., 2009; Piras et al., 2013), the following chapters applied an improved approach by using PLS (Adams and Felice, 2014). In the context of analyses investigating the relationship between form and function, this technique has certain clear advantages when compared to regressions. Although previous studies have used PLS to research the covariation between shape and function in comparative contexts, they simply performed PLS using blocks of data comprising PICs of the original variables (Klingenberg and Marugán-Lobón, 2013). Although initially useful

(Felsenstein, 1985), PICs are now evidently outdated. It has been shown that PICs and PGLS provide identical results when assuming a BM mode of evolution (Blomberg et al., 2012), however PGLS approaches have certain advantages which make them a better option (Garland and Ives, 2000; Rohlf, 2001). Firstly, PICs are differences between sister nodes (Felsenstein, 1985), therefore when plotted they do not represent the original species under analysis but these differences, while PGLS do not suffer this limitation. Secondly, PIC assumes completely bifurcating phylogenetic trees, whilst PGLS can be applied with phylogenies exhibiting polytomies (Adams, 2014a). Thirdly, while PICs are restricted to assume BM, PGLS approaches can be applied under several evolutionary models such as OU models (Hansen, 1997; Butler and King, 2004). Since PGLS in its simple formulation is equivalent to PICs and because PGLS is more broadly applicable in other contexts, there is no obvious reason to keep using PICs other than familiarity.

Nowadays, PLS has been extended to take into account the phylogenetic relationships between taxa based on a PGLS-based algorithm (Adams and Felice, 2014). In addition, PLS has the advantage over standard and PGLS regressions, as it assesses patterns of covariation between blocks of data without assuming that one block of data is dependent on the other (Rohlf and Corti, 2000; Bookstein et al., 2003). The advantage of this is clear in functional morphology studies of skeletal elements, because both form and function interact with each other (i.e. a certain shape has a particular functional performance, but due the bone functional adaptation that shape changes to accommodate function, and so on). Consequently, this makes PLS a particularly useful tool when analysing the association between blocks of data that are expected to covary but for which there is no *a priori* directional relationship established between them (Rohlf and Corti, 2000).

Another way in which the present dissertation differs from previous approaches that combine FEA and GM data is that it applies evolutionary modelling techniques derived from the PCMs toolkit. Polly et al. (2016) proposed a similar approach, however their proposal is inserted within the quantitative genetics tradition rather than in the modern PCMs framework. In brief terms, Polly et al. (2016) suggest that a good approach is to carry out multivariate regressions or polynomial surface fitting to estimate a performance surface by fitting the performance indices of the

taxa under analysis (derived from FEA) to their spacing in morphospace. Then, these performance indices can be mapped onto phylogenies to estimate evolutionary changes from empirical data in order to generate performance surfaces representing functional scenarios that can be combined into adaptive landscapes used to simulate the outcomes of selection (assuming that the morphologies under analysis are being selected for functional performance) (Polly et al., 2016). Although highly valuable and interesting, their proposal is based on Lande's quantitative genetic models (Lande, 1976), which can pose problems when analysing multiple species at macroevolutionary scales, most strikingly in deep-time (Pennell and Harmon, 2013). The problem arises because there is still a serious disconnection between Lande's quantitative genetics models and macroevolutionary analyses (Pennell and Harmon, 2013). The rates of phenotypic evolution inferred from the fossil record seem to be extremely slow at macroevolutionary scales (Eldredge and Gould, 1972; Gingerich, 1983; Gould, 2007), which is known as the 'paradox of stasis' (Hansen and Houle, 2004). However, at a microevolutionary scale it has been observed that both wild and experimental populations commonly exhibit strong selection (Hendry and Kinnison, 1999; Kingsolver et al., 2001; Hereford et al., 2004), and that there is usually plenty of additive genetic variation for selection to act upon (Futuyma, 2010; Hansen et al., 2011). Therefore, the 'paradox of stasis' implies that most likely over long timescales (i.e. macroevolutionary scales, which is the time scale used in many comparative studies), simple evolutionary models based on Lande's quantitative genetics models are almost undoubtedly incorrect (Pennell and Harmon, 2013). This means that due to this disconnection between macro- and microevolutionary processes and associated models, the simplified quantitative genetic interpretations of macroevolutionary models will probably lead to erroneous conclusions (Uyeda et al., 2011). Different proposals have been advanced to try to connect these two evolutionary scales. For instance, it has been suggested that randomly varying selection (in both strength and direction) from one generation to the next will result in a BM model of evolution (Felsenstein, 1973). Other mechanisms that might explain (at least partially) the observed macroevolutionary stasis are ephemeral divergence (i.e. common phenotypic changes that do not last for long time periods) (Futuyma, 2010), constraints due to multivariate selection (e.g. integration between traits) (Hansen and Houle, 2004) and depletion of additive

genetic variance (i.e. reduction of the genetic variation for selection to act upon) (Turelli et al., 1988).

It is in part because of this decoupling between the methods analysing macro- and microevolution that the present dissertation used PCMs instead of quantitative genetic models as proposed by Polly et al. (2016). Most macroevolutionary models used in PMCs do not consider quantitative genetics and are rather heuristic in their functioning (Pennell, 2015). PCMs allow us to coherently model macroevolutionary processes and to test the causes and consequences of large-scale patterns of biodiversity (e.g. tempo and mode of evolution) (Smaers et al., 2016), without presenting the above mentioned limitations regarding the application of quantitative genetic models at a macroevolutionary scale (Pennell and Harmon, 2013). As a result, the approach advanced in this dissertation, which analyses data derived from GM and FEA in an evolutionary context using PCMs seems to be more coherent with current techniques and their known limitations. As outlined above, Lynch (1990) showed that Lande's (1976) models using BM and OU to generate quantitative genetic predictions for trait evolution over many generations are most likely wrong (i.e. their are too fast, since variation among species is too small compared to the potential of selection and drift to modify traits) (Uyeda et al., 2011). This does not necessarily mean that Polly et al.'s (2016) approach is not valuable, but rather that it has to be applied with caution at either a microevolutionary level or when comparing species that have only recently evolved. In fact, there is no doubt that developing further quantitative genetic models that can be applied to comparative data would be an extremely useful addition when analysing trait evolution (e.g. morphological or biomechanical data) at macroevolutionary scales. The combination of both quantitative genetic models and PCMs would make possible the generation of a consistent framework to model long-term evolution considering drift, stasis on an adaptive peak, peak climbing, and peak shift models, which in return might help solving the 'paradox of stasis' (Estes and Arnold, 2007; Hadfield and Nakagawa, 2010). However, this is currently an active area of research with no fully developed methods (Estes and Arnold, 2007; Uyeda et al., 2011), so to the date if analysing comparative data from several species at a macroevolutionary scale, it is still recommended to follow the approach proposed in this dissertation. Perhaps future approaches trying to model

comparative trait evolution with quantitative genetics parameters could profit from the phylogenetic mixed model literature (Lynch, 1991; Housworth et al., 2004; Hadfield and Nakagawa, 2010), since it represents the natural connection between multivariate approaches in quantitative genetics and PCMs, by applying the traditional 'animal model' (Henderson, 1976).

Nevertheless, by applying PCMs to multivariate data from GM or FEA there are still some limitations that need to be addressed. For instance, most comparative studies are either univariate or consider several traits, in which case they just analyse one at a time (Pennell and Harmon, 2013). However, making the most of the GM or FEA toolkit necessarily implies applying fully multivariate approaches. During the last ten years there has been a rising interest in applying trait-evolution PCMs to multivariate datasets (many of them highly multidimensional) (e.g. Rüber and Adams, 2001; Revell and Collar, 2009; Bastir et al., 2010; Monteiro, 2013; Polly et al., 2013; Sherratt et al., 2016). Several methods have been advanced to deal with multivariate data in phylogenetic contexts, yet to the date there is no consensus regarding how to carry out these procedures and there are areas which have to be further developed (Adams and Collyer, 2017).

One approach assesses evolutionary models through log-likelihood estimation across single trait dimensions treated separately (i.e. one at a time), and then sums these to achieve a best-fitting evolutionary model for the data given a phylogeny (e.g. the SURFACE method), thus not representing a fully multivariate approach (dimensions are considered separately) (Ingram and Mahler, 2013; Moen et al., 2015). Unfortunately, these sets of techniques are defective as it is impossible for multivariate trait dimensions to be independent with respect to each other under evolutionary models (i.e. the evolutionary covariance matrix cannot contains nonzero off-diagonal elements, since evolutionary correlation is naturally expected) (Adams and Collyer, 2017). This was the reason underlying the decision to translate the obtained SURFACE scenario in Chapter 4 into a fully multivariate OU hypothesis that was tested along other possible scenarios.

Another recently published approach (i.e. pairwise composite likelihood for high-dimensional comparative models or PCL) uses a pseudo-likelihood estimated from

all (or a portion) of the possible pairwise combinations of the variables under analysis, as well as phylogenetic simulation to compare the fit of the multivariate dataset to the phylogeny (Goolsby, 2016, 2017). This method was developed to deal with some of the limitation of distance-based PCMs. Among the shortcomings of distance-based methods that this approach attempts to solve is that they require the eigen-decomposition and inversion of the phylogenetic covariance matrix, which are enormously time-consuming and inefficient for large phylogenetic tress (Goolsby, 2016). In addition, distance-based methods still lack a proper likelihood function, thus being forced to be computed using closed-form solutions, which in turn implies that parameters for many possible models that lack these sort of solutions cannot be calculated (e.g., non-BM processes, missing data, within species variation, etc.) (Goolsby, 2016). In spite of the caveats exhibit by the distance-based approaches, PCL itself shows other limitations that seriously diminish its applicability, thus not really solving the multidimensional problem. For one, it has been observed that levels of trait covariation, as well as the orientation of the multivariate dataspace largely influence the obtained statistical estimates (Adams and Collyer, 2017). This is a serious matter because PCL does not only show a strong support for incorrect models as trait covariation increased, but also it is not invariant with respect to the orientation of the dataspace. This means that if the data is rotated as done when performing a PCA, then the statistical summaries of the data will not be identical (Adams and Collyer, 2017).

Finally, another group of methods, which are distance-based, apply test statistics obtained from the traces of the same covariance matrices used for log-likelihood estimation to assess macroevolutionary scenarios using high-dimensional datasets (Adams, 2014a, 2014b; Adams and Felice, 2014; Denton and Adams, 2015). These methods started with a multivariate extensions of Blomberg's K (Blomberg et al., 2003; Adams, 2014b), but they have been extended to also include PGLS (Adams, 2014a), evolutionary rates comparisons (Denton and Adams, 2015), as well as phylogenetic PLS (Adams and Felice 2014). These methods are based on a phylogenetic transformation of the data, which is subsequently analysed using distance-based methods (Q-mode), rather than more traditional covariance-based tests (R-mode) (Legendre and Legendre, 2012). This allows these methods to analyse high-dimensional datasets by avoiding the problem of dealing with non-

invertible maximum likelihood trait covariance matrices, which arise when analysing a large number of variables (i.e. dimensions) that equals or exceeds the number of taxa under analysis (Adams, 2014a). Although highly useful, distance-based approaches show the above mentioned problems of being comparatively inefficient when dealing with large phylogenies and that they lack a proper likelihood function, which limits the scenarios to which they can be applied (Goolsby, 2016). Nonetheless, they are probably among the most robust methods when comparing evolutionary models for multivariate data since they are rotation invariant and resistant to levels of trait covariation (Adams and Collyer, 2017). It is for this reason that they were applied in the present dissertation when estimating phylogenetic signal (i.e. K-mult) (Adams, 2014b), and associating form and function (i.e. both PGLS and phylogenetic PLS) (Adams, 2014a; Adams and Felice, 2014).

However, these distance-based methods are currently limited to exclusively assume a BM mode of evolution (Goolsby, 2016). Therefore, in the present dissertation other solutions were applied when testing different possible evolutionary scenarios that could explain the observed phenotypic diversity as it was done in Chapter 4. In order to deal with the problem of analysing multidimensional datasets, a dimensionality reduction approach was used (i.e. a PCA) and the number of dimensions to be analysed was selected using a broken-stick model (Püschel et al., 2017). This data simplification solution using only a subset of summary axes has been previously proposed and applied in other publications (e.g. Monteiro and Nogueira, 2011; Monteiro, 2013; Aristide et al., 2016). Although it represents a simple solution to multidimensional problem that currently exists in PCMs, it has been shown that it has certain caveats that it is necessary to be aware of. At least for datasets simulated under the BM process, it seems that the first few PCs incorrectly support more complex scenarios such as early-burst models when the first few PCs are treated as univariate traits (Uyeda et al., 2015), thus effectively examining a biased sample of a multivariate pattern (Mitteroecker et al., 2004). However, it is has to be noted that the approach applied in Chapter 4 differs from the above criticism in that a fully multivariate approach that considered all PCs together was applied (i.e. the PCs were not considered as univariate traits and were not analysed separately) (Clavel et al., 2015). Furthermore, the best-supported model was neither the most complex one, nor the early burst model, which means that the applied approach did

not exhibit the problems that arise when using PCs as univariate traits. Nonetheless, the limitations of the proposed approach remain unknown and further investigations are required to understand the limitations of using PCA to study macroevolutionary patterns and processes.

6.3 Future work

Future research addressing evolutionary and ecomorphological hypotheses focused on primate skeletal elements should address several methodological questions, which are still unsolved and under development. When using GM, FEA and PCMs to study the evolution of morphological traits, it is necessary to tackle the known limitations of these techniques, as well as to defining explicitly the way in which they are combined.

Currently GM represents perhaps the most popular and robust tools used to quantify morphology (Adams et al., 2004, 2013). Nevertheless, it is evident that there is an important compromise involved when representing complex morphologies as just sets of landmark and/or semi-landmark configurations (i.e. there is more morphological information available, including not only non-landmarked areas, but also variables such as texture or colour). For instance, it has been argued that arbitrary choice of which exact biological features to collect data from (i.e. the anatomical loci represented by landmarks or semi-landmarks) can have a significant effect on the results obtained, which can be in some cases as important as the composition of the sample (Bookstein, 1997; Zelditch et al., 2004; MacLeod, 2008). In fact, there are several situations in which either linear or GM approaches would fail to properly describe changes in shape/form. For example, a change in outline but not in landmark position would probably lead to an underestimated shape variation, or a pronounced outline variation between specimens would cast doubts on semi-landmark homology (Oxnard and O'Higgins, 2009). In addition, current GM procedures require that all specimens display all the same landmarks/semi-landmarks, so if one or more coordinates are missing most analyses become impossible unless a missing data imputation procedure is carried out (O'Higgins, 2000; Klingenberg, 2008; Oxnard and O'Higgins, 2009).

A possible solution to this problem is to develop landmark-free methods to characterise morphological variation. Several techniques have been advanced, but none of them is widely adopted (e.g. Bookstein, 1997; Joshi et al., 2011; Laga et al., 2014; Pomidor et al., 2016; Carlson et al., 2017). This is probably due to some specific limitations of these methods, but also because GM is well-rooted in traditional multivariate statistics (Bookstein, 1997; Dryden and Mardia, 1998; Zelditch et al., 2012), which are widely used in biology (Legendre and Legendre, 2012), while the statistical properties of some of these methods have not been yet extensively studied. Another possibility of analysing complex morphologies without a need to rely on landmark data would be the application of ML algorithms to classify morphological structures such as those employed in Chapter 5. Even though in this Chapter both landmark and stress data were used to train ML techniques, it would also possible also apply these techniques (many of them specifically developed for pattern recognition tasks) directly on image data (MacLeod, 2017) or other sorts of variables such as vertex coordinates from 3D surfaces (Pomidor et al., 2016) (previously homologized and superimposed using some algorithmic procedure) to address in particular problems of group characterization and/or specimen identification.

In fact, the same sort of ML methods could be used to also describe FEA differences between specimens based on the traditional heat-maps used to represent strain/stress levels. Recent approaches have been proposed to study FEA-derived data to be applied in statistical analyses, such as the Intervals' method which was also used in Chapter 5 (Marcé-Nogué et al., 2017). This method was in part developed due to the traditional limitations when describing differences between models after FEA (Marcé-Nogué et al., 2017). Results obtained from FEA are generally displayed as colour maps where warmer colours (i.e., orange, red) correspond to high levels of stress, whereas colder colours (i.e., blue) represent lower levels (although this colour palette is arbitrary and can be easily modified). These colour maps obtained from FEA have been shown to be useful in biomechanics, particularly when the key goal is to detect which regions of the structure under analysis are most affected by the simulated loading scenario (Rayfield, 2007). Despite the convenience of these colour maps (i.e. it is possible to locate the strongest or weakest area of a structure by mere visual inspection), no

quantitative performance comparison is possible. This leads to imprecise and subjective interpretation, because these colour maps are visually interpreted (e.g. more "bluish" specimens are stronger when compared to those more "reddish") (Marcé-Nogué et al., 2017), which is particularly accentuated when comparing similar specimens (e.g. closely related species). However, as discussed above, it would be possible to characterise the differences in colour map patterns by using ML classification algorithms developed for pattern recognition and computer vision, which have been proven to be powerful when dealing with this sort of tasks (Chen et al., 1993; Bishop, 2007; Prince, 2012).

It has also been suggested that comparative organismal FEA can be improved by increasing the complexity of the model under analysis (Toro-Ibacache et al., 2016). In the present dissertation FEA was applied in a comparative rather than validative way (i.e. since the objective was to simply compare the mechanical performance of different species in the context of their phylogenetic relationships). It has been shown that in comparative analyses material property values are not necessarily crucial (see Gil et al., 2015 for discussion) and that specimens with unknown internal architecture can still produce reliable results (Fitton et al., 2015). Nonetheless, the question of whether models that are more complex would increase our insight of function in comparative studies remains open. Structural FEA relies on underlying models of how the different simulated materials behave, and these are not physical laws, but simply convenient approximations (Zienkiewicz et al., 2005). FEA models do not achieve more accurate results when more elements beyond a certain threshold are considered because the underlying approximation for each material has certain flaws (Smith et al., 2013). These flaws become more evident when analyses further depart from simply linear elastic models, tending to fail when simulating problems at meso and nano scales (Wriggers and Hain, 2007). Therefore, modelling muti-scale models and/or using diverse non-linear materials (e.g. certain soft-tissues) is still an area under development, which constraints the possible complexity of an FE model. In spite of these limitations, many studies have generated more complex FE models by incorporating detailed information or parameters such as muscle activation data, anisotropic material properties, numerous different tissues with dissimilar material attributes, among other factors (e.g. Ross et al., 2005; Strait et al., 2005; Kupczik et al., 2007; Chalk et al., 2011;

Gröning et al., 2011; Rayfield, 2011). These kinds of analyses have shown that when this sort of information is considered the correlation between simulations and experimental data is frequently increased (although validation is required when dealing with these more complex models due to the uncertainty associated with higher number of unknowns and variables, thus limiting its applicability). Generating FE models by collecting data from real individuals (e.g. reaction forces from *in vivo* experiments and muscle PCSA from dissections) represents a further step towards more realistic and complex models, which could result in increased robustness of functional analyses. All FEA carried out in this dissertation could be re-elaborated in the future considering extra information, particularly from soft tissues such as muscles, ligaments, tendons, etc. (Püschel and Sellers, 2016). Furthermore, FEA loading scenarios could be derived from either experiments or other computer simulations. For instance, multibody dynamics software (e.g. GaitSym, Opensim) could be used to simulate different dynamic scenarios representing particular movements or locomotor modes, and based on the results obtained from these simulations, loading scenarios can be exported to be subsequently analysed using FEA (Sellers et al., 2017). Therefore, future work should perhaps generate more complex models when assessing ecomorphological questions. The increasing availability in 3D models and accessibility of FEA software would probably allow the generation of numerous models in a comparatively inexpensive way in the following years, which would have the effect of simplifying some of the current constraints (Cunningham et al., 2014; Davies et al., 2017).

Another aspect that could be beneficial in FEA studies would be to perform preliminary studies of intra-specific variation, which is something still lacking in most publications. Comparing specimens of the same species could improve the understanding of the biomechanical behaviour of the structure under analysis, particularly from an evolutionary perspective. It would be relevant to compare the existing differences between the intra and inter-specific levels, because if they are similar, then the interpretation of FEA results would significantly change. One study compared the FEA outputs from several chimpanzee crania showing that intraspecific cranial variation is associated with quantitatively high levels of variation in strain magnitudes, but qualitatively reduced variation in the distribution of strain

concentrations (Smith et al., 2015). However, this study did not compare within species variation levels against the intra-specific variation of other related taxa, so that information is still absent. As pointed out above, it is clear that more studies considering both intra and inter-specific levels of variation are required in comparative FEA studies.

Another aspect worth discussing derived from the results obtained in Chapters 5, is that it seems that shape (measured using GM) is better in predicting ecological context (in this case locomotion) than biomechanical data (measured using FEA). Although further studies are required to test if this methodological result is consistent (i.e. if other studies have found that shape is better than biomechanical data in predicting ecological factors/locomotion/diet), there are underlying biological factors that might explain the observed result. Morphological variation is influenced by varied factors, including loading, diet, sex and evolutionary history, etc., all of which may relate to differences in locomotion. The differences in locomotor behaviour that are reflected in morphology possibly comprise many factors that are just partly considered when biomechanical analyses are carried out (Pearson and Lieberman, 2004; Barak et al., 2011). A possible explanation could be that biomechanical analyses seem to focus on more specific aspects of variation (e.g. loading resistance), while GM incorporates other factors that could be involved in bone morphology (although without explicitly separating them). Nevertheless, the key importance of biomechanical analyses is that they allow testing specific and well-defined adaptive hypotheses regarding particular traits, in ways that associative statistical analysis cannot (e.g. GM). As discussed in Chapter 5, further research is required to test the discriminatory capabilities of both GM and FEA to properly understand their role in classification task, as well as when generating ecological and behavioural interpretations from morphological data.

Another area that requires development is the application of PCMs to highly multivariate data as explained before. Even though the present dissertation does not provide definitive answers regarding this question, some basic requirements about the properties these methods should posses can be advanced. Any novel method developed for trait-evolution inference at a macroevolutionary scale has to satisfy some fundamental requirements (Adams and Collyer, 2017). Firstly, the newly

developed methods must be rotation invariant and resistant to trait covarition (i.e. not like methods such as PCL) in order to respect the geometric principles of the multidimensional space under study (Goolsby, 2016). Secondly, any approach dealing with multivariate macroevolutionary inference has to display adequate statistical properties (i.e. appropriate Type I error levels and statistical power) (Pennell and Harmon, 2013). Thirdly, a proper multivariate approach should be capable of dealing with highly multidimensional datasets (e.g. comparative genomic data, complex phenotypic data, 3D morphometrics, tissue expression levels, biomechanical stress data, etc.) either directly or via dimensionality reduction, since these types of datasets are becoming ubiquitous in many areas of biology with the advent of Big Data (Marx, 2013). In any case, the properties of these methods have to be fully assessed through simulations and/or empirical dataset testing to avoid limitations when applied to different case studies. In addition to all of these, much can be gained if methods combining quantitative genetics and PCMs are fully developed (Pennell and Harmon, 2013). They could provide a more comprehensive perspective to future studies of form and function under an evolutionary approach linking microevolutionary mechanisms with macroevolutionary patterns. Finally, PCMs could also benefit from incorporating information from the fossil record, because paleontological materials can provide direct information about temporal ranges, whereas molecular phylogenies are less affected by the sampling bias of the fossil record (Pennell and Harmon, 2013). Although not performed in the present dissertation, it certainly represents a path worth following (Slater et al., 2012).

6.4 Conclusions

Understanding the structure and function of organisms is perhaps one of the oldest areas within organismal biology, and yet it is still a highly active research area (Wainwright and Reilly, 1994). It is now clear that ecomorphological investigations combining organismal biology, functional morphology, and biomechanics (Thorpe, 2016) are required to understand the ecological and evolutionary consequences of an organism's form. In order to contribute with this objective the present dissertation showed how to apply diverse modern analytical tools to generate an integrative ecomorphological approach. Consequently, this thesis investigated how to combine FEA, GM and PCMs in the context of primate skeletal ecomorphology,

since understanding the diversity and associated ecologies of complex organisms such as primates is a multifaceted problem that requires an interdisciplinary perspective (Thorpe, 2016).

The results obtained in the frame of this dissertation have shown that it is possible to associate form and function using multivariate data blocks (i.e. landmark and stress data) while taking into account the phylogenetic relatedness of the analysed species by using both PGLS and phylogenetic PLS. All chapters either associated biomechanical data with shape (Chapters 2, 3 and 5), or with locomotor data (Chapter 4). In addition, it was shown that it is possible estimate multivariate phylogenetic signal from biomechanical and shape data (Chapters 2 and 4). By using the proposed framework, explicit ecomorphological hypotheses were tested (e.g. Chapter 3), and also competing macroevolutionary scenarios that could explain the observed phenotypic diversity were analysed (Chapter 4). Furthermore, body mass predictions for extinct taxa were also provided (Chapter 4). Finally, by applying ML classification algorithms to morphometric and FEA-derived data it was possible to infer locomotor behaviour in fossil primates, as well as showing that traditional classifications techniques (e.g. linear discriminant analysis) are not always the best available option (Chapter 5). To summarise, the different chapters of the present dissertation provide examples that display how a combined approach using state-of-the-art *in silico* techniques can shed some light upon the way in which primate skeletal morphology, biomechanical performance, ecology and evolution interact.

6.5 References

Adams, D.C., 2014a. A Method for Assessing Phylogenetic Least Squares Models for Shape and Other High-Dimensional Multivariate Data. Evolution. 68, 2675–2688.

Adams, D.C., 2014b. A Generalized K Statistic for Estimating Phylogenetic Signal from Shape and Other High-Dimensional Multivariate Data. Systematic Biology. 63(5), 685-697.

Adams, D.C., Collyer, M.L., 2018. Multivariate Phylogenetic Comparative Methods: Evaluations, Comparisons, and Recommendations. Systematic Biology. 67(1), 14-31.

Adams, D.C., Felice, R.N., 2014. Assessing Trait Covariation and Morphological Integration on Phylogenies Using Evolutionary Covariance Matrices. PLOS ONE. 9, e94335.

Adams, D.C., Rohlf, F.J., Slice, D.E., 2004. Geometric morphometrics: Ten years of progress following the 'revolution.' Italian Journal of Zoology. 71, 5–16.

Adams, D.C., Rohlf, F.J., Slice, D.E., 2013. A field comes of age: geometric morphometrics in the 21st century. Hystrix the Italian Journal of Mammalogy. 21, 7–14.

Aristide, L., Reis, S.F. dos, Machado, A.C., Lima, I., Lopes, R.T., Perez, S.I., 2016. Brain shape convergence in the adaptive radiation of New World monkeys. Proceedings of the National Academy of Sciences. 113, 2158–2163.

Arregui-Mena, J.D., Margetts, L., Mummery, P.M., 2016. Practical Application of the Stochastic Finite Element Method. Archives of Computational Methods in Engineering. 23, 171–190.

Astúa, D., 2009. Evolution of Scapula Size and Shape in Didelphid Marsupials (didelphimorphia: Didelphidae). Evolution. 63, 2438–2456.

Barak, M.M., Lieberman, D.E., Hublin, J.-J., 2011. A Wolff in sheep's clothing: Trabecular bone adaptation in response to changes in joint loading orientation. Bone. 49, 1141–1151.

Bastir, M., Rosas, A., Stringer, C., Cuétara, J.M., Kruszynski, R., Weber, G.W., Ross, C.F., Ravosa, M.J., 2010. Effects of brain and facial size on basicranial form in human and primate evolution. Journal of Human Evolution. 58, 424–431.

Bishop, C.M., 2007. Pattern Recognition and Machine Learning, Newer. ed. Springer, New York.

Blomberg, S.P., Garland, T., Ives, A.R., 2003. Testing for Phylogenetic Signal in Comparative Data: Behavioral Traits Are More Labile. Evolution. 57, 717–745.

Blomberg, S.P., Lefevre, J.G., Wells, J.A., Waterhouse, M., 2012. Independent contrasts and PGLS regression estimators are equivalent. Systematic Biology. 61, 382–391.

Bookstein, F.L., 1997. Landmark methods for forms without landmarks: morphometrics of group differences in outline shape. Medical Image Analysis. 1, 225–243.

Bookstein, F.L., 2013. Allometry for the Twenty-First Century. Biological Theory. 7, 10–25.

Bookstein, F.L., Gunz, P., Mitteroecker, P., Prossinger, H., Schaefer, K., Seidler, H., 2003. Cranial integration in Homo: singular warps analysis of the midsagittal plane in ontogeny and evolution. Journal of Human Evolution. 44, 167–187.

Bright, J.A., Rayfield, E.J., 2011. The Response of Cranial Biomechanical Finite Element Models to Variations in Mesh Density. The Anatomical Record: Advances in Integrative Anatomy and Evolutionary Biology. 294, 610–620.

Butler, M.A., King, A.A., 2004. Phylogenetic Comparative Analysis: A Modeling Approach for Adaptive Evolution. The American Naturalist. 164, 683–695.

Carlson, C., Gutman, B., Sotiriostetradis, A.J., Moon, W., 2017. Landmark-Free Three-dimensional Quantification of Morphological Variation and Shape Change in the Mouse Mandible: Methodological Development and Application. In: Lestrel, P.E. (Ed.), Biological Shape Analysis: Proceedings of the 4th International Symposium. pp. 332–367.

Chalk, J., Richmond, B.G., Ross, C.F., Strait, D.S., Wright, B.W., Spencer, M.A., Wang, Q., Dechow, P.C., 2011. A finite element analysis of masticatory stress hypotheses. American Journal of Physical Anthropology. 145, 1–10.

Chen, C.H., Pau, L.F., Wang, P.S.P., 1993. Handbook of Pattern Recognition and Computer Vision. World Scientific Pub Co Inc, Singapore.

Clavel, J., Escarguel, G., Merceron, G., 2015. mvmorph: an r package for fitting multivariate evolutionary models to morphometric data. Methods in Ecology and Evolution. 6, 1311–1319.

Cunningham, J.A., Rahman, I.A., Lautenschlager, S., Rayfield, E.J., Donoghue, P.C.J., 2014. A virtual world of paleontology. Trends in Ecology & Evolution. 29, 347–357.

Davies, T.G., Rahman, I.A., Lautenschlager, S., Cunningham, J.A., Asher, R.J., Barrett, P.M., Bates, K.T., Bengtson, S., Benson, R.B.J., Boyer, D.M., Braga, J., Bright, J.A., Claessens, L.P.A.M., Cox, P.G., Dong, X.-P., Evans, A.R., Falkingham, P.L., Friedman, M., Garwood, R.J., Goswami, A., Hutchinson, J.R., Jeffery, N.S., Johanson, Z., Lebrun, R., Martínez-Pérez, C., Marugán-Lobón, J., O'Higgins, P.M., Metscher, B., Orliac, M., Rowe, T.B., Rücklin, M., Sánchez-Villagra, M.R., Shubin, N.H., Smith, S.Y., Starck, J.M., Stringer, C., Summers, A.P., Sutton, M.D., Walsh, S.A., Weisbecker, V., Witmer,

L.M., Wroe, S., Yin, Z., Rayfield, E.J., Donoghue, P.C.J., 2017. Open data and digital morphology. Proc. R. Soc. B. 284, 20170194.

Denton, J.S.S., Adams, D.C., 2015. A new phylogenetic test for comparing multiple high-dimensional evolutionary rates suggests interplay of evolutionary rates and modularity in lanternfishes (Myctophiformes; Myctophidae). Evolution. 69, 2425–2440.

Dryden, I.L., Mardia, K.V., 1998. Statistical Shape Analysis. Wiley-Blackwell, Chichester ; New York.

Dumont, E.R., Grosse, I.R., Slater, G.J., 2009. Requirements for comparing the performance of finite element models of biological structures. Journal of Theoretical Biology. 256, 96–103.

Dumont, E.R., Samadevam, K., Grosse, I., Warsi, O.M., Baird, B., Davalos, L.M., 2014. Selection for Mechanical Advantage Underlies Multiple Cranial Optima in New World Leaf-Nosed Bats. Evolution. 68, 1436–1449.

Eldredge, N., Gould, S.J., 1972. Punctuated equilibria: an alternative to phyletic gradualism Assumptions and interpretations of biological models. In: Schopf, T. (Ed.), Models in Paleobiology. Freeman, Cooper & Co., San Francisco, pp. 82–115.

Estes, S., Arnold, S.J., 2007. Resolving the paradox of stasis: models with stabilizing selection explain evolutionary divergence on all timescales. The American Naturalist. 169, 227–244.

Farke, A.A., 2008. Frontal sinuses and head-butting in goats: a finite element analysis. Journal of Experimental Biology. 211, 3085–3094.

Felsenstein, J., 1973. Maximum-likelihood estimation of evolutionary trees from continuous characters. American Journal of Human Genetics. 25, 471–492.

Felsenstein, J., 1985. Phylogenies and the Comparative Method. The American Naturalist. 125, 1–15.

Figueirido, B., Serrano-Alarcón, F.J., Slater, G.J., Palmqvist, P., 2010. Shape at the cross-roads: homoplasy and history in the evolution of the carnivoran skull towards herbivory. Journal of Evolutionary Biology. 23, 2579–2594.

Figueirido, B., Tseng, Z.J., Serrano-Alarcón, F.J., Martín-Serra, A., Pastor, J.F., 2014. Three-dimensional computer simulations of feeding behaviour in red and giant pandas relate skull biomechanics with dietary niche partitioning. Biology Letters. 10, 20140196.

Fitton, L.C., Prôa, M., Rowland, C., Toro-Ibacache, V., O'higgins, P., 2015. The impact of simplifications on the performance of a finite element model of a Macaca fascicularis cranium. Anatomical Record. 298, 107–121.

Fortuny, J., Marcé-Nogué, J., Konietzko-Meier, D., 2017. Feeding biomechanics of Late Triassic metoposaurids (Amphibia: Temnospondyli): a 3D finite element analysis approach. Journal of Anatomy. 230, 752–765.

Fortuny, J., Marcé-Nogué, J., Steyer, J.-S., Esteban-Trivigno, S. de, Mujal, E., Gil, L., 2016. Comparative 3D analyses and palaeoecology of giant early amphibians (Temnospondyli: Stereospondyli). Scientific Reports. 6, srep30387.

Futuyma, D.J., 2010. Evolutionary Constraint and Ecological Consequences. Evolution. 64, 1865–1884.

Garland, T., Ives, A.R., 2000. Using the past to predict the present: confidence intervals for regression equations in phylogenetic comparative methods. The American Naturalist. 155, 346–364.

Gil, L., Marcé-Nogué, J., Sánchez, M., 2015. Insights into the controversy over materials data for the comparison of biomechanical performance in vertebrates. Palaeontologia Electronica. 18.1.12A, 1–24.

Gingerich, P.D., 1983. Rates of evolution: effects of time and temporal scaling. Science. 222, 159–161.

Goolsby, E.W., 2016. Likelihood-Based Parameter Estimation for High-Dimensional Phylogenetic Comparative Models: Overcoming the Limitations of "Distance-Based" Methods. Systematic Biology. 65, 852–870.

Goolsby, E.W., 2017. Rapid maximum likelihood ancestral state reconstruction of continuous characters: A rerooting-free algorithm. Ecology and Evolution. 7, 2791–2797.

Gould, S.J., 2007. Punctuated Equilibrium, 1st edition. Harvard University Press, Cambridge, Mass.

Gröning, F., Liu, J., Fagan, M.J., O'Higgins, P., 2011. Why do humans have chins? Testing the mechanical significance of modern human symphyseal morphology with finite element analysis. American Journal of Physical Anthropology. 144, 593–606.

Hadfield, J.D., Nakagawa, S., 2010. General quantitative genetic methods for comparative biology: phylogenies, taxonomies and multi-trait models for

continuous and categorical characters. Journal of Evolutionary Biology. 23, 494–508.

Hansen, T.F., 1997. Stabilizing selection and the comparative analysis of adaptation. Evolution. 51, 1341–1351.

Hansen, T.F., Houle, D., 2004. Evolvability, stabilizing selection, and the problem of stasis. In: Pigliucci, M., Preston, K.A. (Eds.), Phenotypic Integration: Studying the Ecology and Evolution of Complex Phenotypes. Oxford University Press, Oxford, pp. 130–150.

Hansen, T.F., Pélabon, C., Houle, D., 2011. Heritability is not Evolvability. Evolutionary Biology. 38, 258.

Harmon, L.J., Kolbe, J.J., Cheverud, J.M., Losos, J.B., 2005. Convergence and the multidimensional niche. Evolution; International Journal of Organic Evolution. 59, 409–421.

Henderson, C.R., 1976. A simple method for computing the inverse of a numerator relationship matrix used in prediction of breeding values. Biometrics. 69–83.

Hendry, A.P., Kinnison, M.T., 1999. Perspective: The pace of modern life: measuring rates of contemporary microevolution. Evolution; International Journal of Organic Evolution. 53, 1637–1653.

Hereford, J., Hansen, T.F., Houle, D., 2004. Comparing strengths of directional selection: how strong is strong? Evolution; International Journal of Organic Evolution. 58, 2133–2143.

Housworth, E.A., Martins, E.P., Lynch, M., 2004. The phylogenetic mixed model. The American Naturalist. 163, 84–96.

Ingram, T., Mahler, D.L., 2013. SURFACE: detecting convergent evolution from comparative data by fitting Ornstein-Uhlenbeck models with stepwise Akaike Information Criterion. Methods in Ecology and Evolution. 4, 416–425.

Joshi, S.H., Prieto-Márquez, A., Parker, W.C., 2011. A landmark-free method for quantifying biological shape variation. Biological Journal of the Linnean Society. 104, 217–233.

Kingsolver, J.G., Hoekstra, H.E., Hoekstra, J.M., Berrigan, D., Vignieri, S.N., Hill, C.E., Hoang, A., Gibert, P., Beerli, P., 2001. The strength of phenotypic selection in natural populations. The American Naturalist. 157, 245–261.

Klingenberg, C.P., 2008. Novelty and "Homology-free" Morphometrics: What's in a Name? Evolutionary Biology. 35, 186–190.

Klingenberg, C.P., Ekau, W., 1996. A combined morphometric and phylogenetic analysis of an ecomorphological trend: pelagization in Antarctic fishes (Perciformes: Nototheniidae). Biological Journal of the Linnean Society. 59, 143–177.

Klingenberg, C.P., Marugán-Lobón, J., 2013. Evolutionary Covariation in Geometric Morphometric Data: Analyzing Integration, Modularity, and Allometry in a Phylogenetic Context. Systematic Biology. 62, 591–610.

Kupczik, K., Dobson, C.A., Fagan, M.J., Crompton, R.H., Oxnard, C.E., O'Higgins, P., 2007. Assessing mechanical function of the zygomatic region in macaques: validation and sensitivity testing of finite element models. Journal of Anatomy. 210, 41–53.

Laga, H., Kurtek, S., Srivastava, A., Miklavcic, S.J., 2014. Landmark-free statistical analysis of the shape of plant leaves. Journal of Theoretical Biology. 363, 41–52.

Lande, R., 1976. Natural selection and random genetic drift in phenotypic evolution. Evolution. 30, 314–334.

Lautenschlager, S., 2017. Functional niche partitioning in Therizinosauria provides new insights into the evolution of theropod herbivory. Palaeontology. 60, 375–387.

Legendre, P., Legendre, L.F.J., 2012. Numerical Ecology, 3 edition. Elsevier, Amsterdam.

Lynch, M., 1990. The Rate of Morphological Evolution in Mammals from the Standpoint of the Neutral Expectation. The American Naturalist. 136, 727–741.

Lynch, M., 1991. Methods for the analysis of comparative data in evolutionary biology. Evolution. 45, 1065–1080.

MacLeod, N., 2008. Understanding morphology in systematic contexts: 3D specimen ordination and 3D specimen recognition. The New Taxonomy. CRC Press, Taylor & Francis Group, London. 143–210.

MacLeod, N., 2017. On the Use of Machine Learning in Morphometric Analysis. In: Lestrel, P.E. (Ed.), Biological Shape Analysis: Proceedings of the 4th International Symposium. pp. 134–171.

Marcé-Nogué, J., De Esteban-Trivigno, S., Escrig, C., Gil, L., 2016. Accounting for differences in element size and homogeneity when comparing Finite Element models: Armadillos as a case study. Palaeontologia Electronica. 19, 1–22.

Marcé-Nogué, J., Esteban-Trivigno, S.D., Püschel, T.A., Fortuny, J., 2017. The intervals method: a new approach to analyse finite element outputs using multivariate statistics. PeerJ. 5, e3793.

Marcé-Nogué, J., Fortuny, J., Esteban-Trivigno, S.D., Sánchez, M., Gil, L., Galobart, À., 2015. 3D Computational Mechanics Elucidate the Evolutionary Implications of Orbit Position and Size Diversity of Early Amphibians. PLOS ONE. 10, e0131320.

Marx, V., 2013. Biology: The big challenges of big data. Nature. 498, 498255a.

McHenry, C.R., Wroe, S., Clausen, P.D., Moreno, K., Cunningham, E., 2007. Supermodeled sabercat, predatory behavior in Smilodon fatalis revealed by high-resolution 3D computer simulation. Proceedings of the National Academy of Sciences. 104, 16010–16015.

Mitteroecker, P., Gunz, P., Bernhard, M., Schaefer, K., Bookstein, F.L., 2004. Comparison of cranial ontogenetic trajectories among great apes and humans. Journal of Human Evolution. 46, 679–698.

Moen, D.S., Morlon, H., Wiens, J.J., 2015. Testing convergence versus history: convergence dominates phenotypic evolution for over 150 million years in frogs. Systematic biology. 65, 146–160.

Monteiro, L.R., 2013. Morphometrics and the comparative method: studying the evolution of biological shape. Hystrix, the Italian Journal of Mammalogy. 24, 25–32.

Monteiro, L.R., Nogueira, M.R., 2011. Evolutionary patterns and processes in the radiation of phyllostomid bats. BMC Evolutionary Biology. 11, 137.

O'Higgins, P., 2000. The study of morphological variation in the hominid fossil record: biology, landmarks and geometry. Journal of Anatomy. 197, 103–120.

O'Higgins, P., Cobb, S.N., Fitton, L.C., Gröning, F., Phillips, R., Liu, J., Fagan, M.J., 2011. Combining geometric morphometrics and functional simulation: an emerging toolkit for virtual functional analyses. Journal of Anatomy. 218, 3–15.

262

O'Higgins, P., Fitton, L.C., Godinho, R.M., 2017. Geometric morphometrics and finite elements analysis: Assessing the functional implications of differences in craniofacial form in the hominin fossil record. Journal of Archaeological Science.

Oxnard, C., O'Higgins, P., 2009. Biology Clearly Needs Morphometrics. Does Morphometrics Need Biology? Biological Theory. 4, 84–97.

Paradis, E., 2014. An introduction to the phylogenetic comparative method. In: Modern Phylogenetic Comparative Methods and Their Application in Evolutionary Biology. Springer, pp. 3–18.

Parr, W.C.H., Wroe, S., Chamoli, U., Richards, H.S., McCurry, M.R., Clausen, P.D., McHenry, C., 2012. Toward integration of geometric morphometrics and computational biomechanics: New methods for 3D virtual reconstruction and quantitative analysis of Finite Element Models. Journal of Theoretical Biology. 301, 1–14.

Pearson, O.M., Lieberman, D.E., 2004. The aging of Wolff's "law": Ontogeny and responses to mechanical loading in cortical bone. American Journal of Physical Anthropology. 125, 63–99.

Pennell, M.W., 2015. Modern Phylogenetic Comparative Methods and Their Application in Evolutionary Biology: Concepts and Practice. — Edited by László Zsolt Garamszegi. Systematic Biology. 64, 161–163.

Pennell, M.W., Harmon, L.J., 2013. An integrative view of phylogenetic comparative methods: connections to population genetics, community ecology, and paleobiology. Annals of the New York Academy of Sciences. 1289, 90–105.

Pierce, S.E., Angielczyk, K.D., Rayfield, E.J., 2008. Patterns of morphospace occupation and mechanical performance in extant crocodilian skulls: A combined geometric morphometric and finite element modeling approach. Journal of Morphology. 269, 840–864.

Pierce, S.E., Angielczyk, K.D., Rayfield, E.J., 2009. Shape and mechanics in thalattosuchian (Crocodylomorpha) skulls: implications for feeding behaviour and niche partitioning. Journal of Anatomy. 215, 555–576.

Piras, P., Maiorino, L., Teresi, L., Meloro, C., Lucci, F., Kotsakis, T., Raia, P., 2013. Bite of the Cats: Relationships between Functional Integration and Mechanical Performance as Revealed by Mandible Geometry. Systematic Biology. 62, 878–900.

Piras, P., Sansalone, G., Teresi, L., Moscato, M., Profico, A., Eng, R., Cox, T.C., Loy, A., Colangelo, P., Kotsakis, T., 2015. Digging adaptation in insectivorous subterranean eutherians. The enigma of Mesoscalops montanensis unveiled by geometric morphometrics and finite element analysis. Journal of Morphology. 276, 1157–1171.

Polly, D.P., Lawing, M.A., Fabre, A.-C., Goswami, A., 2013. Phylogenetic Principal Components Analysis and Geometric Morphometrics. Hystrix the Italian Journal of Mammalogy. 24.

Polly, P.D., Stayton, C.T., Dumont, E.R., Pierce, S.E., Rayfield, E.J., Angielczyk, K.D., 2016. Combining geometric morphometrics and finite element analysis with evolutionary modeling: towards a synthesis. Journal of Vertebrate Paleontology. 0, e1111225.

Pomidor, B.J., Makedonska, J., Slice, D.E., 2016. A Landmark-Free Method for Three-Dimensional Shape Analysis. PLOS ONE. 11, e0150368.

Prince, D.S.J.D., 2012. Computer Vision: Models, Learning, and Inference, 1 edition. ed. Cambridge University Press, New York.

Püschel, T.A., Gladman, J.T., Bobe, R., Sellers, W.I., 2017. The evolution of the platyrrhine talus: A comparative analysis of the phenetic affinities of the Miocene platyrrhines with their modern relatives. Journal of Human Evolution. 111, 179–201.

Püschel, T.A., Sellers, W.I., 2016. Standing on the shoulders of apes: Analyzing the form and function of the hominoid scapula using geometric morphometrics and finite element analysis. American Journal of Physical Anthropology. 159, 325–341.

Rayfield, E.J., 2007. Finite Element Analysis and Understanding the Biomechanics and Evolution of Living and Fossil Organisms. Annual Review of Earth and Planetary Sciences. 35, 541–576.

Rayfield, E.J., 2011. Strain in the ostrich mandible during simulated pecking and validation of specimen-specific finite element models. Journal of anatomy. 218, 47–58.

Revell, L.J., Collar, D.C., 2009. Phylogenetic analysis of the evolutionary correlation using likelihood. Evolution. 63, 1090–1100.

Rohlf, F.J., 2001. Comparative methods for the analysis of continuous variables: geometric interpretations. Evolution. 55, 2143–2160.

Rohlf, F.J., Corti, M., 2000. Use of Two-Block Partial Least-Squares to Study Covariation in Shape. Systematic Biology. 49, 740–753.

Ross, C.F., Patel, B.A., Slice, D.E., Strait, D.S., Dechow, P.C., Richmond, B.G., Spencer, M.A., 2005. Modeling masticatory muscle force in finite element analysis: sensitivity analysis using principal coordinates analysis. The Anatomical Record. Part A, Discoveries in Molecular, Cellular, and Evolutionary Biology. 283, 288–299.

Rüber, L., Adams, D.C., 2001. Evolutionary convergence of body shape and trophic morphology in cichlids from Lake Tanganyika. Journal of Evolutionary Biology. 14, 325–332.

Sellers, W.I., Pond, S.B., Brassey, C.A., Manning, P.L., Bates, K.T., 2017. Investigating the running abilities of Tyrannosaurus rex using stress-constrained multibody dynamic analysis. PeerJ. 5, e3420.

Serrano-Fochs, S., De Esteban-Trivigno, S., Marcé-Nogué, J., Fortuny, J., Fariña, R.A., 2015. Finite Element Analysis of the Cingulata Jaw: An Ecomorphological Approach to Armadillo's Diets. PLOS ONE. 10, e0120653.

Sherratt, E., Alejandrino, A., Kraemer, A.C., Serb, J.M., Adams, D.C., 2016. Trends in the sand: Directional evolution in the shell shape of recessing scallops (Bivalvia: Pectinidae). Evolution. 70, 2061–2073.

Slater, G.J., Harmon, L.J., Alfaro, M.E., 2012. Integrating Fossils with Molecular Phylogenies Improves Inference of Trait Evolution. Evolution. 66, 3931–3944.

Smaers, J.B., Mongle, C.S., Kandler, A., 2016. A multiple variance Brownian motion framework for estimating variable rates and inferring ancestral states. Biological Journal of the Linnean Society. 118, 78–94.

Smith, A.L., Benazzi, S., Ledogar, J.A., Tamvada, K., Pryor Smith, L.C., Weber, G.W., Spencer, M.A., Dechow, P.C., Grosse, I.R., Ross, C.F., Richmond, B.G., Wright, B.W., Wang, Q., Byron, C., Slice, D.E., Strait, D.S., 2015. Biomechanical Implications of Intraspecific Shape Variation in Chimpanzee Crania: Moving Toward an Integration of Geometric Morphometrics and Finite Element Analysis. The Anatomical Record. 298, 122–144.

Smith, I.M., Griffiths, D.V., Margetts, L., 2013. Programming the Finite Element Method, 5th Edition edition. John Wiley & Sons, Chichester, West Sussex, United Kingdom.

Stayton, C.T., 2009. Application of Thin-Plate Spline Transformations to Finite Element Models, or, How to Turn a Bog Turtle into a Spotted Turtle to Analyze Both. Evolution. 63, 1348–1355.

Strait, D.S., Wang, Q., Dechow, P.C., Ross, C.F., Richmond, B.G., Spencer, M.A., Patel, B.A., 2005. Modeling elastic properties in finite-element analysis: How much precision is needed to produce an accurate model? The Anatomical Record Part A: Discoveries in Molecular, Cellular, and Evolutionary Biology. 283A, 275–287.

Thorpe, S.K.S., 2016. Symposium on Primate Ecomorphology: introduction. Journal of Anatomy. 228, 531–533.

Toro-Ibacache, V., Fitton, L.C., Fagan, M.J., O'Higgins, P., 2016. Validity and sensitivity of a human cranial finite element model: implications for comparative studies of biting performance. Journal of Anatomy. 228, 70–84.

Tseng, Z.J., 2013. Testing Adaptive Hypotheses of Convergence with Functional Landscapes: A Case Study of Bone-Cracking Hypercarnivores. PLoS ONE. 8, e65305.

Tseng, Z.J., Flynn, J.J., 2015. Convergence analysis of a finite element skull model of Herpestes javanicus (Carnivora, Mammalia): Implications for robust comparative inferences of biomechanical function. Journal of Theoretical Biology. 365, 112–148.

Turelli, M., Gillespie, J.H., Lande, R., 1988. Rate Tests for Selection on Quantitative Characters During Macroevolution and Microevolution. Evolution. 42, 1085–1089.

Uyeda, J.C., Caetano, D.S., Pennell, M.W., 2015. Comparative Analysis of Principal Components Can be Misleading. Systematic Biology. 64, 677–689.

Uyeda, J.C., Hansen, T.F., Arnold, S.J., Pienaar, J., 2011. The million-year wait for macroevolutionary bursts. Proceedings of the National Academy of Sciences. 108, 15908–15913.

Wainwright, P.C., Reilly, S.M., 1994. Ecological morphology: integrative organismal biology. University of Chicago Press.

Weber, G.W., Bookstein, F.L., Strait, D.S., 2011. Virtual anthropology meets biomechanics. Journal of Biomechanics. 44, 1429–1432.

Wriggers, P., Hain, M., 2007. Micro-Meso-Macro Modelling of Composite Materials. In: Computational Plasticity, Computational Methods in Applied Sciences. Springer, Dordrecht, pp. 105–122.

Young, R.L., Haselkorn, T.S., Badyaev, A.V., 2007. Functional equivalence of morphologies enables morphological and ecological diversity. Evolution; International Journal of Organic Evolution. 61, 2480–2492.

Zelditch, M.L., Swiderski, D.L., Sheets, H.D., 2012. Geometric Morphometrics for Biologists, Second Edition: A Primer, 2 edition. ed. Academic Press, Amsterdam.

Zelditch, M.L., Swiderski, D.L., Sheets, H.D., Fink, W.L., 2004. Geometric Morphometrics for Biologists: A Primer, 1 edition. ed. Academic Press.

Zienkiewicz, O.C., Taylor, R.L., Zhu, J.Z., 2005. The finite element method its basis and fundamentals. Elsevier Butterworth-Heinemann, Amsterdam; Boston.